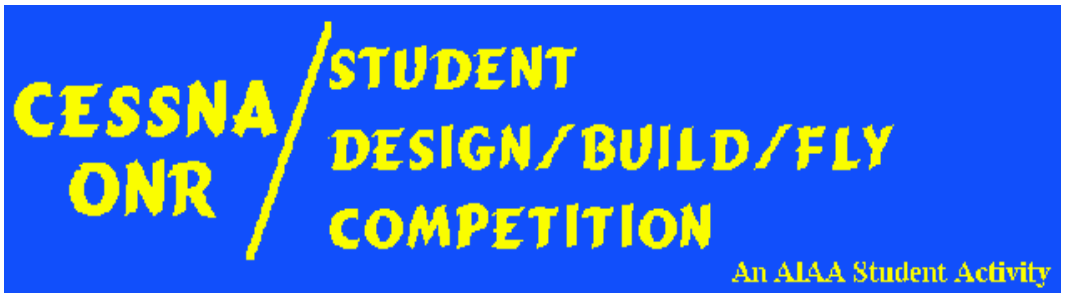

The 2003 Cessna/ONR Student Design/Build/Fly competition was held at the Ridgely Airpark in Ridgely Maryland over the weekend of 25-27 April. In all, 33 teams from the United States, Canada, Italy and Turkey attended the fly-off portion of the contest. Of the 33 teams attending the fly-off competition, 19 made at least one successful scoring flight attempt, with many teams completing the maximum allowed 5 flights during the two days of competition.

The contest was moved from it's traditional east coast home, Webster Field, due to the increased security at military installations resulting from the Iraq war. Mr. Tracy Coleman volunteered the use of Ridgely Airpark so that the contest could continue it's 7-year history without interruption. The facilities at Ridgely provided an excellent contest site with ample setup and flying area. The managers, sponsors, and teams of the DBF competition would like to express their thanks to Mr. Coleman for his generosity.

The competition spanned two days of flying, with the flight queue filled with aircraft waiting for their turn to make a competition flight. A number of the flights on Saturday had to dodge the rain drops, while Sunday provided near perfect flying weather.

The design objective for this year's competition was to create an airplane that could be rapidly assembled from a 2 x 4 x 1 foot shipping container and then complete two of the three specified simulated UAV missions: Missile EW Decoy; Sensor Deployment; or Communications Repeater. Each mission was assigned it's own Degree of Difficulty multiplier factor.

The total score for each team was comprised of their flight performance on their best two flights, their score on a written report documenting their aircraft design and selection, and a "Rated Aircraft Cost" representing the complexity and manufacturing costs of their design.

The final results showed a close battle between teams from the San Diego State University and California Polytechnic State University at San Luis Obispo. One of the Italian teams from Università degli studi "La Sapienza" di Roma placed a close third. The highest score obtained on the written report portion of the competition was from Utah State University with 96.5 of a possible 100 points awarded. The fastest assembly time was for Mississippi State at 9 seconds.

The final positions and scores for all of the competing teams are listed in the table below.

More details on the 2003 competition objectives and rules can be found at the contest web site at http://www.aae.uiuc.edu/aiaadbf

Position	School	Team	Paper	RAC	Flight	Score
1	San Diego State University	Spirit of Monty	84.5	8.28	1.16	11894.80
2	Calif Poly State Univ SLO	Bareback	85.5	7.91	1.09	11736.63

3	La Sapienza	Galileo IV	89.5	7.99	0.95	10609.09
4	Univ of Southern California	SCyRaider	93.5	10.90	0.97	8365.98
5	Oklahoma State University	OSU Black	91.6	9.86	0.89	8228.28
6	Oklahoma State University	OSU Orange	90.5	10.24	0.83	7331.55
7	USNA	Severn Discomfort	86.0	13.04	1.03	6775.88
8	Mississippi State University	SWAG	90.0	12.09	0.89	6605.70
9	USNA	Yeager Chasers	89.7	12.25	0.86	6263.12
10	Middle East Technical University	Anatolian-Craft	87.0	12.21	0.80	5699.88
11	Univ of California San Diego	Aerodrone F8273	80.5	9.15	0.61	5380.84
12	Istanbul Technical University	Ucakcilar	74.8	11.24	0.80	5301.99
13	University of Illinois UC	Gas Guzzler	72.0	9.35	0.65	5009.39
14	Washington State University	CAT	46.0	10.01	0.59	2692.87
15	Utah State University	Nyx	96.5	13.34	0.35	2563.83
16	Univ of Texas Austin	7700	93.4	8.70	0.23	2490.02
17	Univ of California San Diego	Furious Flier	74.0	9.22	0.31	2473.78
18	University of Colorado	Bellwether	68.4	8.41	0.28	2279.43
19	La Sapienza	Leonardo	79.5	6.69	0.19	2264.63
20	Georgia Tech	Buzzweiser	89.0	7.30	0.01	121.95
21	University of Maryland	The Stop and Go	89.5	9.71	0.01	92.17
22	Ohio Northern University	It's Supposed to Fly	59.0	8.08	0.01	73.05
23	Case Western Reserve	Marsupial Falcon X	61.3	8.92	0.01	68.69
24	Virginia Polytechnic University	Draggin Fly	77.3	11.81	0.01	65.40
25	W. Virginia University	Lock-N-Load	79.0	12.65	0.01	62.46
26	University at Buffalo	Bull Ship	71.0	11.86	0.01	59.87
27	Queen's University	Some Assembly Required	79.2	13.28	0.01	59.61
28	Wichita State University	WU Flyer	74.3	12.79	0.01	58.05

29	Univ California LA	Bruin Bud-E	58.9	10.58	0.01	55.62
30	Calif Poly State Univ Pomona	Pegasus	47.5	8.78	0.01	54.13
31	Western Michigan University	Western Flyer	59.3	11.83	0.01	50.17
32	University of Arizona	AirCat 2003	47.9	10.08	0.01	47.51
33	Univ of Texas Arlington	Spirit of Arlington	65.0	13.70	0.01	47.45
34	Turkish Air Force Academy	Haberci	90.0	100.00	0.01	9.00
35	Syracuse University	The Judge Chaser	73.8	100.00	0.01	7.38
36	Clarkson University	Knight Riders	73.3	100.00	0.01	7.33
37	University of Central Florida	K-03 Pegasus	69.9	100.00	0.01	6.99
38	University at Buffalo	Frier Fly	66.5	100.00	0.01	6.65

The success of the competition required the efforts of many individuals. A special thanks goes to the judges who assisted in the operation, technical inspections and scoring of the flight competition; and to the many judges who evaluated and scored the teams written proposal reports. Thanks also go to the Applied Aerodynamics, Aircraft Design, Design Engineering, and Flight Test Technical committees of the AIAA who organized and manage the competition, and the AIAA Foundation for their administrative support. Special thanks is due to the competitions corporate supporters, the Cessna Aircraft Company and the Office of Naval Research.

Overall the 2003 Cessna/ONR Student Design/Build/Fly competition marked another very successful event, allowing the participating students to mix a highly enlightening educational experience with a good dose of fun. Congratulations goes to all the teams for their great enthusiasm and achievement.

See you next year - Greg Page: Contest Director

4/29/03

[Top] [AIAA Student Design/Build/Fly Competition homepage] [AIAA Homepage]
Webmaster *m-selig@uiuc.edu*

Highest Report Score

2002/2003 AIAA Foundation Cessna/ONR Student Design Build Fly Competition

DESIGN REPORT

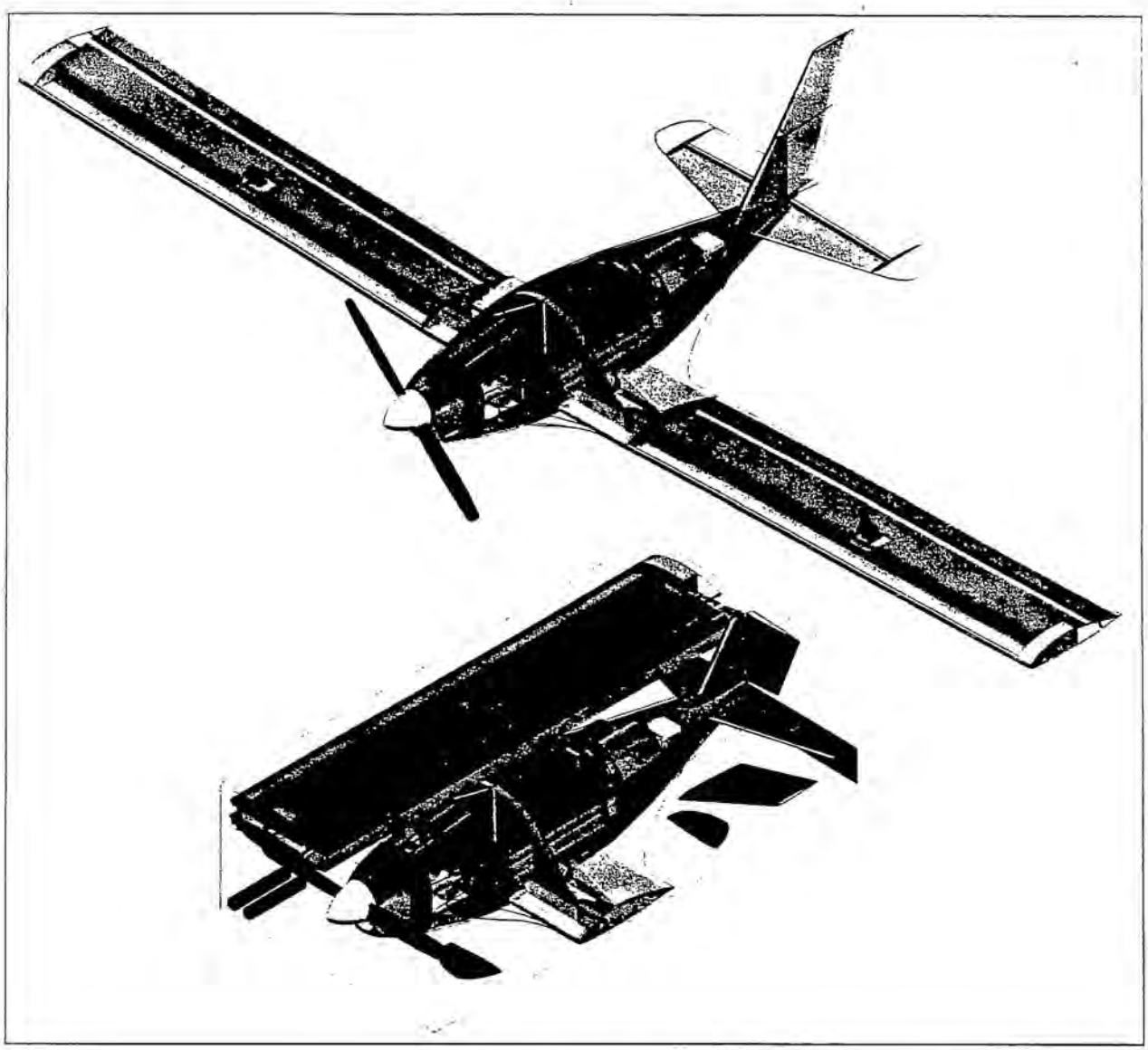

"Zephyr"

Utah State University

March 2003

TABLE OF CONTENTS

1. EXECUTIVE SUMMARY

This report provides an overview of the design, manufacturing, and testing procedures used in the development of the Utah State University entry in the 2003 Design, Build, and Fly competition. The aircraft was designed to complete two of three predefined missions; the "Missile Decoy Mission" (MDM), the "Sensor Deployment Mission" (SDM), and/or the "Communication Repeater Mission" (CRM).

1.1. Overview of the Design Development

During the conceptual design phase of the development process, energy approximations and Figures of Merit (FOM), based on mission requirements, were used to identify the two most cost-effective missions and narrow the range of design parameters to be studied in later design phases. Over 5,000 aircraft configurations were studied by varying critical design parameters. Computer code was written to analyze mission profiles and predict FOM. Some important conclusions were drawn from the results. First, the CRM always results in scores that are lower than the SDM or MDM. Second, there are possible optimums in battery weight, turn load factor, and aspect ratio.

In the preliminary design phase, more detailed analysis and experimental testing were used to further investigate potential optimums revealed during conceptual design. A computer program was written to iterate through millions of configurations and compute flight times, airspeeds, and Rated Aircraft Cost (RAC), and total score. The parameters that were investigated were wing area, wingspan, turn load factor, number of battery cells, and motor/propeller combinations. Tests were also performed to get better estimates for important aircraft parameters. This analysis and testing verified many of the trends discovered during conceptual design. High aspect ratio gave improved mission-effectiveness, despite the higher RAC. High load factors were verified to increase mission scores. In contrast to conceptual design results, it was found that including more battery cells in the power plant increased the maximum total score and speed capabilities of the aircraft, despite the higher RAC for increased weight and power.

During the detail design phase, computational aerodynamics, finite element structural analysis, dynamic stability analysis, mission flight simulation, and additional experimental testing were used to finalize geometry, component selection, system architecture, and mission performance predictions. Since overall score is inversely proportional to the flight time, the performance was enhanced by structural analysis and testing to produce an airplane that could perform high-g turns. The lift-to-drag ratio was also an area of focus and was dramatically improved by the use of full-span twisting flaps. Additional analysis and testing also aided in power plant selection and performance prediction. The final result was a stable, high-performance aircraft, which is quick to assemble and should score well.

1.2. Design Alternatives Investigated

Many different aircraft configurations and individual components were considered and evaluated. Three general aircraft configurations were examined early in the design process. These were the conventional aft tail, V-tail, and canard configurations. The conventional tail configuration was chosen based on takeoff, mission effectiveness, and RAC. The dimensions of the payload required a teardrop shaped fuselage instead of a lifting body. Retractable landing gear with brakes were chosen over fixed gear. To accommodate the gear, a low wing, instead of mid or high wing was chosen. The wing was constructed of a foam core and carbon fiber spar covered with balsa, after considering both a foam core with a composite skin and a balsa build-up method. This choice was based on manufacturability and weight constraints. Two antenna mount configurations were considered for the MDM. Based on trim considerations, a top mount was chosen over a bottom mount. One and two-motor designs were analyzed, resulting in a single-motor solution. An air cooling system was chosen, because tests showed

that complex liquid cooling is not beneficial. Two battery types were also considered, 36-cell, 2400-mAhr and 48-cell, 1700-mAhr packs. The latter was chosen based on power versus total energy tradeoffs.

1.3. Highlights of the Development Process

Since the design competition rules only allow two of the three missions to count toward the final team score, it was important to identify the two most cost-effective missions. By creating energy models for all three missions and comparing the resulting scores for thousands of different aircraft configurations, it was discovered that the CRM always generates the lowest scores. Therefore, design efforts were directed toward optimizing an aircraft for the MDM and SDM.

Antenna drag in the MDM was found to have a very significant effect on mission performance. Thus, a full-scale PVC model of the antenna was built and tested in a wind tunnel to obtain an improved estimate for the antenna drag coefficient. Results from this test indicate antenna drag that is 67% higher than that predicted by the relation for finite cylinders presented by White (1999). The measured value was used in all subsequent optimization studies, so that more realistic results would be obtained.

It was found in past years that manufacturer-published efficiency for DC motors does not match the realized efficiency. For the power plants tested, it was found that motor efficiency was at best 70%, whereas manufacturer's published values were 78-80%. Measured battery resistance per cell was found to be 0.015 ohms, compared with a published value of 0.005 ohms. Measured values were used for analysis.

During preliminary design, an effort was made to verify results found in conceptual design dealing with the possibility of an optimum wing aspect ratio. The analysis software written partly for this purpose iterated on different combinations of wing area and wingspan. It was found that an aspect ratio of approximately 11 produced the best mission scores, in spite of the increased RAC.

The effect of maximum load factor in the turns was studied during the conceptual and preliminary design phases. Conceptual design revealed a trend for increasing score with increasing load factor. This was verified using methods developed for preliminary design. A design load factor of 7 was found to be a near optimum solution based on the tradeoff between wing weight and mission flight times.

A static stability analysis was performed to optimize the size and placement of the tail surfaces on the aircraft. Optimum placement of the tail was found to be relatively close to the wing. Another advantage of the short tail was that it made possible a one-piece fuselage that is the length of the 4-ft long box. Overall score increases with decreased aircraft assembly time. Thus, speed and ease of assembly are of high merit and out of the box assembly is greatly simplified with a one-piece fuselage design.

Full-span twisting flaps called *twisterons*, Phillips, Alley, and Goodrich, (2003) were introduced on the aircraft. Twisterons are flaps used to produce variable aerodynamic washout. This reduces induced drag and overall pitching moment produced by the wing. The use of twisterons instead of ailerons and flaps showed improvements in the lift-to-drag ratio of 10 to 20%, in some mission phases. This significantly decreased mission flight times and increased mission effectiveness as measured by total score.

In order to characterize the handling qualities of the aircraft more accurately, a complete dynamic stability analysis was performed. All calculations included the contribution of the propeller and fuselage to the stability derivatives. It was found that the aircraft had divergent spiral and phugoid modes. The spiral mode had a short doubling time of about 2.5 seconds on takeoff. This was initially a concern, but it was decided that a pilot in visual reference flight should be able to easily handle the aircraft. However, the dynamic stability analysis revealed possible problems with the sizing of the vertical stabilizer. The chosen solution was a vertical surface that could be modified during the flight-testing phase of development.

2. MANAGEMENT SUMMARY

The Utah State University design team for this year's competition is composed of eleven Mechanical and Aerospace Engineering students. In order to efficiently utilize the teams various skills and produce a quality aircraft on time, an effective management plan was devised.

2.1. Architecture of the Design Team

In order to ensure that each design task was accomplished and that the workload was distributed as evenly as possible among the team members, the team was divided into three sub-groups; aerodynamics, propulsion, and structures. The aerodynamics team was responsible for generating the aerodynamic models and iterating through various aircraft configurations to be studied. They were also responsible for the stability and control analysis of the aircraft. The propulsion team was responsible for investigating possible motor/battery/propeller combinations. They also studied the effects of battery resistance and motor heating on power plant performance. The structures team was charged with the structural design and analysis of the aircraft. This included the structural testing and finite element analysis of the major aircraft components.

A project manager was chosen along with three sub-team leaders. The project manager addressed concerns that affected the team as a whole and was responsible for making sure the team stayed on schedule. The sub-team leaders were responsible for delegating work to their team members. Three other team members were chosen to keep track of the team's budget, order necessary materials and testing equipment, and arrange the shipping and travel accommodations for the competition. Table 2.1.1 lists the design personnel and their assignment areas.

Project manager: Nick Alley		
Treasurer: Mark Anderson;	*Procurement:* Tristan Young;	*Logistics:* Mike Oksness
Aerodynamics	**Propulsion**	**Structures**
Leader: Wayne Goodrich	*Leader:* Nate Bunderson	*Leader:* Adam Spinner
Mark Anderson	Mike Oksness	Tristan Young
Kyle Barton	Underclassmen	Nick Alley
Mike Oksness		Underclassmen

Table 2.1.1. Team architecture, design personnel and their assignment areas.

Table 2.1.2 shows how each team member was involved in the design, analysis, and construction of the airplane. A rating of 5 indicates that 100% of that team member's work time was devoted to the given phase and a 0 indicates no involvement.

2.2. Configuration and Schedule Control

Early in the design process, the team identified the major design milestones and the dates by which they were to be achieved (see Fig. 2.2.1). Each week thereafter the team met with faculty advisor Dr. W.F. Phillips to discuss the progress and setbacks of the previous week and set goals for the following week. At other times during the week the sub-teams met individually to discuss design goals or to work on tasks as a group.

	Nick Alley	Mark Anderson	Kyle Barton	Nate Bunderson	Wayne Goodrich	Mike Oksness	Adam Spinner	Tristan Young	Underclassmen
3. Conceptual Design									
3.1 Mission Requirements	1	5	5	0	5	5	0	0	1
3.2 Study of Aircraft Requirements	1	5	5	0	5	5	0	0	1
3.3 Screening of Numerical FOM	0	5	5	0	5	5	0	0	1
3.4 Mission Modeling and Analysis	5	5	5	0	5	5	0	0	0
3.3.1-3 Aircraft Weight and Drag	5	5	5	0	5	5	0	0	0
3.3.4-5 Takeoff, Climb, Steady-Level Flight	5	5	5	0	5	5	0	0	0
3.3.6-7 Turning, Descent, and Landing	5	5	5	0	5	5	0	0	0
3.3.8 Uncertainty	0	0	5	0	0	0	0	0	0
4. Preliminary Design									
4.1 Study of Design Parameter and Sizing Trades	1	5	5	1	5	5	4	0	1
4.2 Improved Mission Modeling and Optimization	1	5	5	5	5	5	0	0	1
4.2.2-5 Weight, Drag, Lift and Thrust Estimation	1	5	5	5	5	5	0	0	1
4.2.6 Stability Analysis	1	5	5	0	5	5	0	0	1
4.2.7-10 Takeoff, Landing, Turning, Flight Analysis	0	5	5	0	5	5	0	0	1
5. Final Design									
5.2 Component Selection/System Architecture	2	5	5	5	5	3	5	0	5
5.2.1 Main Wing (Airfoil, *Twisterons*, Flaps)	0	5	1	0	5	1	0	0	0
5.2.2 Stability and Control Surface Sizing	1	1	5	0	5	0	0	0	0
5.2.3 Propulsion (Motor/Battery/Prop Tests)	0	0	0	5	0	2	0	0	5
5.2.4 Structural Design	2	0	0	0	0	0	5	5	0
5.2.5 Payload Support and Deployment	2	0	0	0	0	2	5	5	0
5.3 Final Aircraft Specifications	0	5	5	3	5	5	5	5	0
5.3.1-3 Aircraft Geometry/Weight and Balance	0	5	5	3	5	5	5	5	0
5.4 Final Aircraft performance Analysis	0	5	5	3	5	5	0	0	1
5.4.1 Aerodynamic Coefficients and Derivatives	0	0	0	0	5	5	0	0	0
5.4.2 Static Stability	0	5	5	0	2	5	0	0	0
5.4.3 Dynamic Stability	0	0	1	0	5	5	0	0	0
5.4.1 Predicted Mission Performance	0	5	5	4	5	5	0	0	1
A. Documentation of Design									
A.1 Journal	1	5	5	4	2	2	2	2	1
A.2 Letter of Intent	0	0	0	0	5	0	0	0	0
A.3 Final Report	3	5	5	5	5	0	0	5	2
6. Manufacturing									
6.2 Manufacturing Process Detail	5	0	1	0	0	0	5	5	0
6.3 Manufacturing Processes Selection	5	0	1	0	0	0	5	5	0
6.3 Detail Manufacturing Plan	5	0	1	0	0	0	5	5	0
Final Airplane Construction	5	5	5	5	5	5	5	5	2
B. Drafting Package	0	0	0	0	5	0	5	2	0

Table 2.1.2. List of design personnel and assignment areas. This table summarizes the major design phases and each member's contribution to those phases. A rating of 5 indicates 100% of design time devoted to a given phase and a rating of 0 indicates no involvement.

Task Name	Start	Finish
USU Design Build Fly	**Aug 13**	**Apr 22**
Conceptual Design Phase	**Aug 13**	**Oct 1**
Design Program Preparation	Aug 13	Sep 3
-Actual-	Aug 13	Sep 17
Data Collection and Documenting	Sep 4	Oct 1
-Actual-	Sep 18	Oct 15
Preliminary Design Phase	**Sep 17**	**Dec 13**
Design Program Preparation	Oct 3	Nov 12
-Actual-	Oct 17	Dec 5
Powerplant Analysis and Testing	Sep 17	Oct 16
-Actual-	Sep 18	Oct 30
Data Collection and Documenting	Nov 13	Dec 16
-Actual-	Dec 6	Jan 6
Detail Design	**Dec 6**	**Feb 4**
Refinement and Stability Analysis	Dec 17	Jan 21
-Actual-	Dec 17	Feb 11
Structural Analysis and Testing	Dec 6	Jan 21
-Actual-	Dec 6	Feb 10
Drawing Package	Jan 21	Feb 4
-Actual-	Jan 7	Feb 25
Manufacturing	**Jan 27**	**Feb 28**
Component/Aircraft Construction	Jan 27	Feb 28
Flight Evaluation	**Mar 1**	**Apr 14**
Documentation	**Aug 14**	**Apr 14**
Design Journal	Aug 14	Apr 14
Letter of Intent	Oct 31	Oct 31
Report Preparation	Feb 4	Mar 10
-Actual-	Oct 1	Mar 10
Contest	**Apr 25**	**Apr 27**

Figure 2.2.1. Project Schedule/Milestone Chart. This schedule illustrates the project milestones and time periods designated for each design phase. The blue bars represent the planned schedule while the pink bars show the time periods over which the events actually occurred.

3. CONCEPTUAL DESIGN

An aircraft was to be designed to complete two of three predefined missions. The goal for the conceptual design process was to eliminate one of the three mission sorties and allow a more focused approach to the design process by narrowing the range of design parameters to be studied in the later design phases. Energy approximations were used along with estimated aircraft parameters to determine the rated aircraft cost and mission flight time, for each aircraft configuration studied. Figures of merit, based on mission requirements, made the best missions and aircraft configurations discernable.

3.1. Mission Requirements

The three possible competition missions were named "Missile Decoy", "Sensor Deployment", and "Communications Repeater". Each mission flown will be scored using a degree of difficulty factor divided by the sum of the mission flight time and the aircraft assembly time. The required mission tasks for each of these three missions are described below.

3.1.1. Aircraft Storage and Timed Assembly. It was required that the aircraft be disassembled and fit into a 4 ft x 2 ft x 1 ft box. One task in the competition will be the timed assembly. This assembly will take place directly from the box and the time required to make the aircraft flight ready will be measured and recorded. The assembly time will be added to the flight time for each mission. This requirement placed certain limitations on the design of the aircraft. However, it was decided that consideration of this requirement would be left for the later phases of design, because the focus of conceptual design was on choosing the most effective missions and narrowing general aircraft parameters, not on specific aircraft structure and construction. An assembly time of 30 seconds was assumed for conceptual design.

3.1.2. Takeoff. For all missions there is a maximum takeoff distance requirement of 120 feet. The wheels must be off the runway within this distance. If the aircraft is unable to meet this constraint, a zero score will result for that sortie.

3.1.3. Missile Decoy Mission (MDM). For this mission, the aircraft must carry a five-pound rectangular payload, 6 inches in width and height, and 12 inches long. A simulated cylindrical antenna created from a 3-inch tall, 6-inch diameter PVC pipe section must be attached to the aircraft and suspended at least three inches from any other aircraft structure. The aircraft must fly four laps with a 360-degree turn on the downwind leg of each lap. This mission was given a difficulty factor of 2.0.

3.1.4. Sensor Deployment Mission (SDM). This mission requires the aircraft to carry the same five-pound payload box as the MDM. The aircraft must land after the second lap, stop completely, remotely deploy the payload, then takeoff again and complete two more laps. Each lap has one 360-degree turn on its downwind leg. This difficulty factor for this mission is 1.5.

3.1.5. Communication Repeater Mission (CRM). This mission requires the aircraft to carry the same five-pound payload box as the MDM, while completing four laps with three 360-degree turns on the downwind leg of each lap. A difficulty factor of 1.0 was assigned to this mission.

3.1.6. Aircraft Cost-Effectiveness. The final competition score will depend on a Rated Aircraft Cost (RAC), which is a function of the complexity and technology of the design. It is essential that the RAC be as low as possible, since the competition score is inversely proportional to RAC. Rated Aircraft Cost is discussed further in Sec. 3.3.5.

3.2. Aircraft Configurations Studied

Aircraft design parameters were selected based on experience and general aircraft knowledge. These were used as a basis for selecting the aircraft configurations studied. Parameters such as

empennage configuration, wing design, battery weight and landing gear were considered in the conceptual design phase. Initial configuration parameters were analyzed to limit the number of aircraft configuration to be studied in detail. The critical configuration parameters were then further analyzed to optimize the aircraft for each mission.

3.2.1. Initial Configuration Parameters Studied. In order to narrow the range of aircraft configuration parameters to be considered for further study, three different main configurations were investigated in the initial phase of conceptual design. These were the conventional aft tail, V-tail, and canard configurations. The method of Phillips and Snyder (2000) was used to compare the mission suitability of the three configurations. All three aircraft configurations were analyzed using the same weight, speed, wing area, planform, aspect ratio and fuselage length. The conventional aircraft configuration was found to have the most efficient distribution of lift, while the V-tail produced counteracting lift, which decreased tail performance. The canard's downwash and upwash on the main wing disrupted the lift distribution, thereby increasing the shed vorticity and induced drag. The canard also had a longer takeoff distance. Based on these results, the conventional configuration was found to have the best overall L/D and a shorter takeoff distance. This configuration was chosen for further analysis.

Mission flight time is a major contributor to total score and shorter mission flight times give higher scores. This meant that drag minimization was critical. For this reason, retractable landing gear was chosen for all aircraft configurations investigated in the critical configuration parameter study. This eliminated a major component of drag.

3.2.2. Critical Configuration Parameters Studied. For the purpose of conceptual design, the aircraft parameters considered to be critical to mission effectiveness were wing area, wingspan, battery weight, and turn load factor. Remaining parameters were estimated through functional relations with these parameters. Over 5,000 conventional aircraft configurations were studied by varying the critical parameters within ranges and by increments shown in Table 3.2.1.

Critical Parameter	Minimum	Maximum	Increment
Wing Area, S_w (ft^2)	2	10	1
Wingspan, b_w (ft)	4	10	1
Battery Weight, W_b (lbf)	1	5	0.5
Turn Load Factor, n_t (g)	2	10	1

Table 3.2.1. Critical aircraft configuration parameters used for conceptual design.

3.3. Numerical Figures of Merit (FOM) used for Screening

A numerical rating system based on FOM, described below, was developed to evaluate each aircraft's performance with respect to critical mission requirements. For each mission, 30 seconds were added to the flight time to account for the timed assembly.

3.3.1. Takeoff Distance Rating (TDR). If the airplane is not able to takeoff within the required distance of 120 ft, the sortie will be disqualified. However, there is no significant advantage to shorter takeoff distances. For this reason, TDR was defined by the relation

$$\text{TDR} = (0.0, \text{if estimated takeoff} > 120\ \text{ft}) \text{ or } (1.0, \text{if estimated takeoff} < 120\ \text{ft}) \qquad (3.3.1)$$

3.3.2. Missile Decoy Rating (MDR). This FOM reflects the weighted score for the Missile Decoy Mission. This mission has a difficulty factor of 2.0 and is defined as

$$MDR = 2.0/(\text{estimated mission flight time} + 30\ \text{sec}) \tag{3.3.2}$$

3.3.3. Sensor Deployment Rating (SDR). This FOM was used to rate aircraft effectiveness for the Sensor Deployment Mission using its difficulty factor of 1.5. Thus, SDR was

$$SDR = 1.5/(\text{estimated mission flight time} + 30\ \text{sec}) \tag{3.3.3}$$

3.3.4. Communication Repeater Rating (CRR). Suitability for the Communication Repeater Mission was rated based on the mission difficulty factor of 1.0, so CRR was defined as

$$CRR = 1.0/(\text{estimated mission flight time} + 30\ \text{sec}) \tag{3.3.4}$$

3.3.5. Rated Aircraft Cost (RAC). This FOM was specified by the contest rules and is used to estimate the cost of the aircraft based on its components and structures. The RAC was included both as a contest requirement and as a method of quantifying the cost of the concepts studied. It is defined as

$$RAC = (100 * MEW + 1500 * REP + 20 * MFHR)/1000 \tag{3.3.5}$$

where MEW is the Manufacturers Empty Weight, defined as the actual airframe weight with all flight and propulsion batteries but without payload; REP is the Rated Engine Power defined by

$$REP = [(1 + 0.25 * (\#\ \text{engines} - 1)] * (\text{total battery weight}) \tag{3.3.6}$$

and MFHR is the Manufacturing Man Hours, defined as

$$\begin{aligned} MFRH = {} & 8\ \text{hr} * [\text{wingspan (ft)} + \text{maximum exposed wing chord (ft)}] \\ & + 3\ \text{hr} * (\#\ \text{wing control surfaces}) + 10\ \text{hr} * [\text{maximum body length (ft)}] \\ & + 5\ \text{hr} * (\#\ \text{vertical surfaces without control}) + 10\ \text{hr} * (\#\ \text{vertical surfaces with control}) \\ & + 10\ \text{hr} * (\#\ \text{horizontal surfaces}) + 5\ \text{hr} * (\#\ \text{servo/controllers} + \#\ \text{engines} + \#\ \text{propellers}) \end{aligned} \tag{3.3.7}$$

3.3.6. Total Figure of Merit (TFM). The TFM was calculated from the best two mission scores, the TDR, and the RAC according to the relation

$$TFM = TDR * \text{max2}(MDR, SDR, CRR)/RAC \tag{3.3.8}$$

where max2 is a function that returns the sum of the largest two of three arguments.

3.3.7. Relation between Mission Requirements and FOM. Table 3.3.1 describes how the mission requirements are related to the FOM used for conceptual design. Note that aircraft storage and timed assembly were not considered in the conceptual design phase. It was decided that consideration of this requirement would be left for the later phases of design.

Mission Requirement	FOM
Aircraft Storage and Timed Assembly	Not Considered in Conceptual Design
Takeoff	TDR
Missile Decoy Mission	MDR
Sensor Deployment Mission	SDR
Communication Repeater Mission	CRR
Aircraft Cost-Effectiveness	RAC

Table 3.3.1. Relation between mission requirements and figures of merit used for conceptual design.

3.4. Mission Modeling and Analysis

In order to analyze each mission, a program was designed from fundamental equations that were derived to be functions of wing area, wingspan, battery weight, load factor, and payload weight. It was desired to obtain the FOM for all three missions for a range of these characteristic parameters. Over each segment of flight, the total energy available was used to determine the maximum flight velocity attainable, and from this, the time required to complete the mission was estimated.

3.4.1. Total Aircraft Weight. To estimate the weight of the aircraft, every component was assigned a specific weight and summed into an overall weight. Where possible, actual components were weighed. Equations had to be formed for the empennage and main wing weight estimates. A list of the measured component weights and equations is listed in Table 3.4.1.

Main Wing Weight. The weight of the main wing was estimated by finding an average wing weight per area for typical RC aircraft and multiplying by the wing area of the aircraft.

Fuselage Weight. For the conceptual analysis it was assumed that the entire fuselage would be constructed out of balsa. The fuselage was assumed to have 5 cross-sections; 3 in the center section, 1 in the nose, and 1 in the tail. The nose and tail cross-sections were assumed to be half the diameter of the center sections. The skin (outer covering) was assumed to be 1/16 inch thick while the cross-sections were assumed to be 1/4 inch thick. The density of the balsa was found to be 10 pounds per cubic foot. A pound was added for extras, including motor mounts, control rods, epoxy resin, covering, and payload mounting system.

Landing Gear Weight. To determine a reasonable weight for landing gear, Robart Mfg. Incorporated was contacted for weight estimates. For tricycle landing gear rated for a 12-24 pound aircraft, a weight range of 1.6 to 1.8 lbf was given. The weight of the three wheels was 0.31 lbf. A conservative total weight of the gear was used.

Empennage Weight. The main purpose of an empennage is to stabilize the forward pitching moment inherent of any cambered wing. For this reason the empennage was sized according to the main wing area. The 2001 Design Build Fly report was consulted to get a ratio between the weight of the empennage and the area of the main wing.

Component	Weight (lbf)
Motor (lbf) , W_m	0.93
Propeller (lbf), W_p	0.44
Speed Controller (lbf), W_{sc}	0.12
Servo (lbf/servo), W_s	0.1
Fuselage (lbf) W_f	1.62
Landing Gear (lbf)	1.7
Propulsion Battery (lbf)	Input Variable
Receiver (lbf), W_r	0.058
Receiver Battery (lbf) , W_{rb}	0.31
Cylinder (lbf) W_{cyl}	1.75
Empennage (lbf), W_{emp}	$W_{emp} = 0.255*(lbf/ft^2)*S_w$
Main Wing (lbf), W_w	$W_w = 0.238*(lbf/ft^2)*S_w$

Table 3.4.1. Aircraft weight estimates.

Final Weight Equation. Assuming a design requiring 5 servos and 1 motor controller, the total weight of the aircraft was estimated as

$$W = W_m + W_p + W_{sc} + 5W_s + W_b + W_r + W_{rb} + W_{cyl} + W_{emp} + W_w \quad (3.4.1)$$

3.4.2. Parasitic Drag. As with the weight, the drag of the aircraft depended on its many drag components. These components were analyzed and combined into an overall drag equation. For conceptual design, the zero-lift drag slope, $C_{Do,L}$, was assumed to be zero in all calculations.

Tail Boom Drag. Turbulent, axial flow with no separation was assumed, so the drag associated with the tail boom was only due to skin friction and was approximated using an equation for drag on a flat plate. As depicted in White (1999) the skin friction drag coefficient is defined as

$$C_{Dotb} = 0.031/(\mathrm{Re}_L^{1/7}) \quad (3.4.2)$$

The tail boom length was a function of wing area since the size and location of the empennage combine to stabilize the main wing. As the wing area increases, the tail boom must be lengthened for the aircraft to remain stable. To find a relation for the tail boom length as a function of wing area another ratio was developed based on the DBF2001 aircraft. Using this relation the tail boom length is defined as

$$L_{tb} = 0.627 * (1/ft) * S_w \quad (3.4.3)$$

This length was used in calculating the Reynolds Number, thus making the drag coefficient for the tail boom a function of the main wing area.

The equation for tail boom drag was based on the area of a flat plate, so the reference area used to predict the drag created by the tail boom was its surface area. To get this surface area another ratio based on the DBF2001 aircraft was developed in order to find an estimate for the diameter of the tail boom. With this ratio, the diameter of the tail boom is defined as

$$d_{tb} = 0.0147 * (1/ft) * S_w \quad (3.4.4)$$

Equations (3.4.2)-(3.4.4) can be combined with the equation for the surface area of a cylinder to give an area relation based on the wing area.

$$S_{tb} = \pi d_{tb} L_{tb} \quad (3.4.5)$$

Tail Feather Parasitic Drag. The tail feathers were assumed to have NACA 0009 airfoil cross-sections, giving them a parasitic drag coefficient of 0.005, according to Abbot and Von Doenhoff (1959). To estimate the reference planform area, a ratio of the area of the tail feathers to the main wing was found based on the DBF2001 aircraft. Using this ratio the tail feather area was estimated as

$$S_{tf} = 0.0825 * S_w \quad (3.4.6)$$

Main Wing Drag. For conceptual design purposes, the main wing was assumed to have a NACA 2412 airfoil cross-section. These airfoils have a parasitic drag coefficient, obtained from Abbot and Von Doenhoff (1959), of C_{Dow}= 0.006. The reference area for this drag coefficient was the planform wing area.

Fuselage Drag. A streamline teardrop shape was chosen for the fuselage in order to accommodate the payload and operational equipment while creating the least possible amount of drag. This fuselage had a parabolic shaped nose, a cylindrical center section, and a parabolic shaped tail. The center section was sized to 8.5 inches in diameter and 12 inches long so the rectangular payload would easily fit inside. The nose and tail sections were sized according to a percentage of the remaining length with the nose containing 25% and the tail 75%. The fineness ratio (d / l) of the complete fuselage was considered to be the largest diameter of 8.5 inches divided by the total length.

An empirical equation from Hoerner (1965) was used to estimate the parasitic drag of the fuselage from the fineness ratio and skin friction coefficient. It is defined by

$$C_{Dwet} = C_f\left(1 + 1.5(d/l)^{3/2} + 7(d/l)^3\right) \tag{3.4.7}$$

where d is the maximum diameter of the fuselage and l is the total length of the fuselage. The skin friction coefficient C_f is defined by Hoerner (1965) to be

$$C_f = 0.427/(\log(R_e) - 0.407)^{2.64} \tag{3.4.8}$$

For any given diameter there exists a fuselage length that will produce the minimum amount of drag. With a diameter of 8.5 inches, the minimum drag length was 2.835 feet.

Substituting a Reynolds number based on the length of the fuselage into equation (3.4.8) gave a skin friction coefficient that was substituted into Eq. (3.4.7) along with the fineness ratio to produce a parasitic drag coefficient. When the optimum fineness ratio and a conservative Reynolds number of 2.5×10^6 was used, a parasitic drag coefficient of $C_{Dof} = 0.0049$ based on the fuselage surface area was calculated.

Cylinder Drag. The MDM required the addition of an antenna. A conservative estimate of $C_{Dcyl} = 1.0$. The reference area for the cylinder was estimated as the fontal area to be $S_{cyl} = 0.375$ ft^2.

Landing Gear Drag. The drag on the gear is mainly due to pressure drag. The frontal area of the struts, S_s, came from detailed drawings on Robart Mfg. Inc.'s website. The struts have a diameter of 0.5 inches and a length of 5.4 inches. The wheels had a diameter of 3.0 inches and a thickness of 1.0 inch. The coefficient of drag for the strut was approximated for a finite cylinder with an aspect ratio of 10. This was found in White (1999) to be $C_{Dos} = 0.82$ based on frontal area for laminar flow at Reynolds numbers above 10000. From Hoerner (1965), the wheels could be approximated as supercritical spheres for their drag coefficient. This coefficient (based on frontal area) had a value of $C_{Dowh} = 0.1$.

Final Coefficient of Drag Equation. When the product of all the previous drag coefficients and areas are summed, the resulting drag coefficient is defined by

$$C_{Do} = \frac{C_{Dotb}S_{tb} + C_{Dotf}S_{tf} + C_{Dow}S_w + C_{Dof}S_f + C_{Dos}S_s + C_{Dowh}S_{wh} + C_{cyl}S_{cyl}}{S_w} \tag{3.4.9}$$

where C_{Do} is the coefficient of drag on takeoff and rotation. It was important to note that the landing gear chosen for conceptual design was retractable. Therefore, during flight, the drag coefficients of the struts and the wheels were set to zero. For missions other than the MDM, the cylinder drag is neglected.

3.4.3. Induced Drag. It was decided to estimate the aircraft's Oswald efficiency factor to predict induced drag. For an aircraft with elliptical wings, a conservative approximation for the Oswald efficiency factor was given by using the span efficiency factor for a rectangular wing with the same planform area and aspect ratio as the elliptical wing. Data for the span efficiency factor of a rectangular wing were computed using a numerical lifting-line method and fit by a least squares polynomial equation.

3.4.4. Takeoff and Accelerated Climb. The total energy required to accelerate from a standing start to the liftoff velocity was the sum of the change in kinetic energy and the energy dissipated by drag and rolling friction divided by the efficiency of the power plant. The equation for takeoff energy used an approximation that neglects the change in net force with airspeed. All forces were evaluated at 70% of the liftoff airspeed as recommended by Phillips (2003) for initial estimates for takeoff.

The total energy required to rotate the aircraft to the takeoff angle of attack was the sum of the energy dissipated by drag and rolling friction divided by the efficiency of the power plant. The equation for rotation energy used an approximation that neglected the change in net force with angle of attack.

The energy required to climb to altitude and accelerate to flight velocity was the sum of the change in kinetic and potential energy and the energy dissipated by drag divided by an average efficiency of the power plant between liftoff and cruise velocity. The drag during accelerated climb was approximated with the induced drag evaluated at the average lift coefficients of the start and finish velocities.

The ground distance of the accelerated climb (s_{ac}) was calculated using an effective net force (F_{ac}) during transition, which was an average of the thrust available and thrust required at the liftoff (V_{LO}) and cruise velocities (V_C). This relation is found in Phillips (2003) to be defined as

$$s_{ac} = W / F_{ac}\left(h + (V_C^2 - V_{LO}^2)/(2g)\right) \tag{3.4.10}$$

where

$$F_{ac} = 0.5 * (T_{ALO} - T_{RLO} + T_{Ac} - T_{Rc}) \tag{3.4.11}$$

$$T_{ALO} = P_A / V_{LO} * (\eta_{ac} / \eta_c) \tag{3.4.12}$$

$$T_{Ac} = P_A / V_C * (\eta_{ac} / \eta_c) \tag{3.4.13}$$

$$T_{RLO} = D_{LO} \tag{3.4.14}$$

$$T_{Rc} = D_C \tag{3.4.15}$$

T_{ALO}, T_{Ac} are the thrust available at liftoff and cruise velocity, respectively. T_{RLO}, T_{Rc}, D_{LO}, and D_C are the thrust required and drag at liftoff and cruise velocity, respectively.

The propulsive efficiency ratio, η_{ac}/η_c, was defined to be the ratio of the efficiency at an instantaneous speed divided by the efficiency at the cruise speed. The power available (P_A) throughout the accelerated climb was assumed to be the greater of either the power required at the cruise velocity or at takeoff. The total time required for the accelerated climb was computed using the average velocity of the climb.

3.4.5. Steady Level Flight. The total energy required for cruising flight was the energy dissipated by drag divided by the efficiency of the power plant at cruise velocity given by

$$E_f \cong s_f \, D_f / \eta_f \tag{3.4.16}$$

where s_f is the flight distance not used in takeoff, climbing, turning, landing or braking over the four laps. η_f is the efficiency computed at the cruise airspeed. D_f is the induced drag given by

$$D_f = \tfrac{1}{2}\rho V^2 S_w C_{D_f} = \tfrac{1}{2}\rho V^2 S_w \left(C_{Do} + C_{Do,L}\, C_L + C_{Wf}^2 / \pi e R_A\right) \tag{3.4.17}$$

3.4.6. Turning. The total energy required for a steady, level coordinated turn was estimated to be the energy dissipated by drag divided by the efficiency of the power plant. The equation is defined by

$$E_t \cong s_t \, D_t / \eta_t \tag{3.4.18}$$

where s_t is the distance the aircraft flies during a 360 degree turn calculated by

$$s_t = 2\pi \frac{{V_C}^2}{g\,Tan(\phi)} \tag{3.4.19}$$

and η_t is the efficiency computed at the turning airspeed, which was assumed to be the cruise airspeed. D_t is found in Phillips (2003) to be the total drag as a function of the bank angle, ϕ, and is given by

$$D_t = \tfrac{1}{2}\rho V^2 S_w C_{D_t} = \tfrac{1}{2}\rho V^2 S_w \left(C_{Do} + C_{Do,L}\, C_L + (C_{Wt} / Cos(\phi))^2 / (\pi e R_A)\right) \tag{3.4.20}$$

Three different bank angles were considered for the turning analysis; the stall limited, load limited, and minimum energy bank angle. The smallest bank angle of the three was used to compute the total energy of the turn. The stall limited, minimum energy, and load limited bank angles are defined by

$$\phi_{Stall} = ArcCos\left(2W/(\rho V_C^2 S_w C_{L\max})\right) \tag{3.4.21}$$

$$\phi_{MinE} = ArcTan\left(\sqrt{1+(e\pi(\rho V_C^2)^2 S_w^2 R_A^2 C_{D_0})/(2W^2)}\right) \tag{3.4.22}$$

$$\phi_{ll} = ArcCos(1/n_{\max}) \tag{3.4.23}$$

3.4.7. Descent and Landing. The total energy required for descending flight is the energy dissipated by drag divided by the efficiency of the power plant. In the case where the energy required was negative, a value of zero was assumed since energy cannot be returned to the batteries. The energy required to descend is defined to be

$$E_D \equiv (\sqrt{s_D^2 + h^2}\, D_D + \Delta KE_D + \Delta PE_D)/\eta_D \tag{3.4.24}$$

where ΔKE_D is the change in kinetic energy defined as

$$\Delta KE_D = \tfrac{1}{2} W/g(V_{LO}{}^2 - V^2) \tag{3.4.25}$$

and ΔPE_D is the change in potential energy defined by

$$\Delta PE_D = W h \tag{3.4.26}$$

D_D is drag during decent, which is given by

$$D_D = \tfrac{1}{2}\rho V^2 S_w C_{DD}/2 \equiv \tfrac{1}{2}\rho V^2 S_w\left(C_{Do} + C_{Do,L}C_L + (C_{W_C}^2 + C_{W_{TD}}^2)/(2*\pi e R_A)\right) \tag{3.4.27}$$

and η_D is the efficiency during decent evaluated at the average airspeed between cruise and touchdown. The length s_D is the distance from the exit of the last turn to the finish line less the distance needed for braking. Where the braking distance s_b is defined as

$$s_b \equiv V_{TD}^2/(2\,g\,\mu_r) \tag{3.4.28}$$

where V_{TD} is the touchdown velocity and assuming the special case of the lift coefficient being equal to the drag coefficient divided by the coefficient of rolling friction. This is a valid, simplifying assumption in the case of no wind and no thrust reversal. The total energy required for stopping was assumed zero because the motor was off. The time required to come to a complete stop is defined by

$$t_b = 2s_b/V_{TD} \tag{3.4.29}$$

3.4.8. Uncertainty. Initially the maximum lift-to-drag ratios for the SDM and CRM were above 35. This was a concern since manufacturing an aircraft with this high of a lift-to-drag ratio would be difficult. It was decided that a "worst case" lift-to-drag ratio would be 20. The drag coefficient for the fuselage was increased until the maximum lift-to-drag ratio of the airplane for these two missions was approximately 20.

The main uncertainty in the mission model was associated with the power plant. It was assumed that there was always enough power to perform the required maneuvers for any given configuration and flight pattern. This assumption was justified in that the main objective in this phase of design was to observe trends that would help in determining which missions would produce the best overall score.

3.5. Results

Due to the number of aircraft configurations studied, it is not possible to show all of the results here. Instead, a representative set was chosen for depicting some general trends. Table 3.5.1 gives the critical configuration parameters for the representative aircraft along with the computed FOM. For every

configuration, the MDR and SDR are always higher than the CRR. Low wing areas, battery weights, and RAC ratings as well as high load factors typically produce larger TFM values.

S_w (ft^2)	W_b (lbf)	n_t	b_w (ft)	TDR	MDR	SDR	CRR	RAC	TFM
4	2	7	6	1	0.9	0.6	0.3	7	0.07
4	2	2	8	1	0.9	0.6	0.3	8	0.07
4	2	7	8	1	0.9	0.6	0.4	8	0.07
6	2	7	6	1	0.9	0.6	0.3	8	0.07
6	2	7	8	1	0.9	0.6	0.4	8	0.07
4	2	7	12	1	0.9	0.6	0.4	8	0.07
6	2	7	12	1	0.9	0.6	0.4	9	0.06
10	2	7	8	1	0.9	0.6	0.4	9	0.06
10	2	7	12	1	0.9	0.6	0.4	9	0.06
10	5	7	6	1	0.9	0.6	0.3	13	0.04
10	2	7	6	1	0.9	0.4	0.4	9	0.04
4	5	7	6	1	0.9	0.6	0.3	15	0.03
6	2	2	8	1	0.5	0.4	0.2	8	0.02
4	2	2	12	1	0.5	0.4	0.2	8	0.02
6	2	2	12	1	0.5	0.4	0.2	9	0.02
10	2	2	8	1	0.5	0.4	0.2	9	0.02

Table 3.5.1. Select random sample of aircraft configurations and example FOM calculation.

3.6. Conclusions

After considering results from conceptual design, some important conclusions were drawn. First, the CRM results in scores that are lower than both the SDM and MDM. For this reason, future design efforts will not consider the CRM. Second, as the battery weight is reduced, the score improves due to the reduction of RAC. Third, as the maximum load factor of the wing increases, the overall score increases due to the aircraft being able to turn at larger bank angles and thus lower turn times. These trends will be taken into consideration in future design phases.

The airplane configuration at the end of conceptual design is summarized in Table 3.6.1. Because of power plant inaccuracies, critical parameter ranges were left fairly large and will be narrowed down in the preliminary design phase.

Geometry	Value	Performance	Value	Weight Statement	Value
S_w (ft^2)	4 ~ 10	C_{Lmax}	1.6	Airframe (lbs)	3.5 ~ 4.7
b_w (ft)	6 ~ 12	$(L/D)_{max}$	20 ~ 35	Propulsion System (lbs)	5.4
W_b (lbs)	1~ 5	Stall Speed (mph)	29 ~ 37	Control System (lbs)	0.5
n_t (g)	3 ~ 10	Max Speed (mph)	105 ~ 135	Payload (lbs)	5 ~ 6.75
		Take-off Field Length (empty) (ft)	80	Empty Weight (lbs)	9.4 ~ 10.6
		Take-off Field Length (Gross Weight) (ft)	110	Gross Weight (lbs)	14.4 ~ 16.35

Table 3.6.1. Aircraft data summary.

4. PRELIMINARY DESIGN

The focus of preliminary design was to determine approximate dimensions, weight, power, load limit, and other physical characteristics for an optimum aircraft, which would best meet objectives for the two missions selected in conceptual design, namely MDM and SDM. The main areas of concern were wing area and span, empennage size, battery weight, motor/propeller combination, and wing strength. The entire aircraft flight routine was modeled more accurately than in the conceptual design phase and motor/propeller performance was modeled in much greater detail. For empennage optimization, the stability of the aircraft was estimated with algorithms that computed static margin and the yaw stability derivative.

4.1. Critical Design Parameters and Sizing Trades

Based on results obtained in the conceptual design phase, the critical design parameters were revised to reflect the performance parameters considered most influential to the overall score. These included main wing dimensions, power plant, empennage dimensions, battery weight, and load factor.

4.1.1. Wing Area. Trends found in conceptual design indicated that an optimum wing area may exist. For a fixed gross weight, decreasing wing area increases wing loading and raises the minimum drag airspeed. This results in higher flight speeds and reduced mission flight times. However, increasing wing loading also increases the stall speed, which increases takeoff distance. Since mission requirements call for short takeoff and high flight speed, wing loading must be a compromise.

4.1.2. Wingspan. The wing contribution to RAC is proportional to the sum of the wingspan and the maximum chord. Thus, minimum RAC per unit wing area is realized with a rectangular wing of aspect ratio 1. This places a penalty on high aspect ratio wings and an even greater penalty on efficient wing planforms, such as elliptic and tapered wings. For a given wing area, a higher wingspan produces a more efficient, faster wing while increasing the RAC. This means that wingspan must be a compromise between cost and efficiency. Other limitations on wingspan were manufacturability, storage of the wing in the aircraft storage box, and speed of assembly.

4.1.3. Overall Aircraft Length and Empennage Size. The main goal in designing an empennage for any aircraft is to stabilize the aircraft both statically and dynamically as efficiently as possible. For the purposes of preliminary design, efficiency was defined in terms of RAC and total drag. Due to the interaction and influence of these parameters, an optimum empennage was known to exist. The RAC increases with overall aircraft length and weight. For a very short aircraft, the total drag can usually be decreased by increasing the empennage length and decreasing empennage area. Thus, aircraft length and empennage size will also be a compromise between cost and efficiency.

4.1.4. Motor Size and Number. Motor selection was based on several criteria; the effect of motor weight and number on the RAC, the power output of the motor, and the maximum current draw. An increase in motor size or increase in the number of motors will increase the power output thereby decreasing takeoff distance. A more powerful motor can produce higher rpm's for a given propeller, which increases the maximum possible velocity. Increasing motor size increases the RAC due to increased weight. Using multiple motors induces a double penalty by increasing weight and rated engine power. Here again, motor selection must be a compromise between cost and mission effectiveness.

4.1.5. Propeller Pitch and Diameter. It is known that for best overall propulsive efficiency, a large air mass should be accelerated over a small incremental velocity. This warrants a large diameter propeller. However, ground clearance and compressibility effects limit allowable propeller diameters. Furthermore, propellers with low pitch-to-diameter ratios have greatest propulsive efficiency at low airspeeds, while

high pitch-to-diameter ratios result in greater propulsive efficiency at higher airspeeds. Since variable-pitch propellers are not available in the sizes required, a fixed-pitch propeller must be used. Due to the large range of velocities encountered in the missions, propeller pitch must be a compromise between takeoff performance and maximum airspeed.

4.1.6. Battery Weight and Number of Cells. As noted in conceptual design, the weight of batteries carried in the aircraft contributes to the RAC, the maximum airspeed, and the maximum time the aircraft can remain in flight. According to trends from conceptual design, there is possibly an optimum battery weight that would maximize the overall score attained by the aircraft. As more batteries are carried the aircraft has the potential to complete a mission in less time. On the other hand, as battery weight increases, the RAC and induced drag increase. Using lower capacity batteries allows more cells to be used within the weight constraint, which produces higher voltage and rpm. The tradeoff for decreasing battery capacity is reduced total available energy.

4.1.7. Load Factor Limit. The conceptual design phase also revealed a potential optimum load factor for the aircraft well above the competition's required 2.5 g's. As the design load factor increases the maximum allowable bank angle increases, thereby reducing the turning radius to use less energy and time in the turns. However, this requires increased power, wing strength, and wing weight, resulting in higher RAC.

4.1.8. Range of Critical Design Parameters Studied. In an attempt to optimize an aircraft for mission cost-effectiveness, a very large number of aircraft configurations were analyzed in greater detail using a computer program written by the design team. Each of the critical design parameters was varied over some range in an attempt to expose the optimum aircraft configuration. Table 4.1.1 shows the range and increments for each of the critical design parameters studied.

In addition to the iterations listed in Table 4.1.1, a data file of approximately 100 Astroflight motors was created along with each motor's associated critical constants. These were iterated through one at a time for each of the possible combinations of critical design parameters defined by Table 4.1.1. The largest horizontal stabilizer span allowed by the RAC was also the most efficient and was fixed at a constant 25% of the main wingspan.

Critical Design Parameter	Minimum	Maximum	Increment
Wing Area (S_w), ft^2	4	10	0.25
Wingspan (b_w), ft	6	12	0.25
Horizontal Stabilizer Area (S_h), ft^2	0.8	2.2	0.2
Vertical Stabilizer Area (S_v), ft^2	0.8	2.2	0.2
Empennage Horizontal Offset (l_h), ft	0.5	4.5	0.4
Motor Number	1	2	1
Propeller Diameter (d_p), in	8	26	1
Propeller Pitch (λ), in	8	24	1
Battery Cells	24	48	1
Battery Capacity (b_c), mAh	1700	2400	700
Turn Load Factor (n_t), g's	3	10	1

Table 4.1.1. Critical design parameters studied during the preliminary design phase.

4.2. Improved Mission Modeling and Optimization Analysis

The preliminary design phase focused on the development and use of computer programs called DBF2002 and DBFEMP. The purpose of these programs was to iterate through the critical design parameters listed in Table 4.1.1. The programs' outputs were the important aerodynamic properties, RAC, and total score. This made it possible to determine which range of aircraft would attain the best overall score and directed detail design efforts toward an optimum range of aircraft.

4.2.1. Overview of Mission Modeling and Optimization Programs. Figure 4.2.1 is a block diagram of the DBF2002 program operation. First, the variables were initialized and data files opened for reading and writing. The data files contained the motor database along with limits and increments for each aircraft parameter. The thrust and power curves of the motor were then calculated. The program iterated through all combinations of motors, battery cells, and propellers that drew a maximum current less than 50 amps. An airplane was then modeled using the geometric parameters listed in Table 4.1.1. along with the chosen power plant. Approximations for the drag, lift, and weight were then computed. Each aircraft configuration was cycled through the two mission flights at the slower of either the maximum possible flight velocity or the velocity that would fully deplete the battery energy. If, at some point during the flight routine, the program determined that the aircraft and mission combination was impossible, a new aircraft was drafted and the cycle repeated. If the missions were completed, the RAC, mission scores, and overall score were then calculated and sent with other important parameters to an output file. The entire process was repeated until all critical design parameters had been stepped through and the results recorded in the output file.

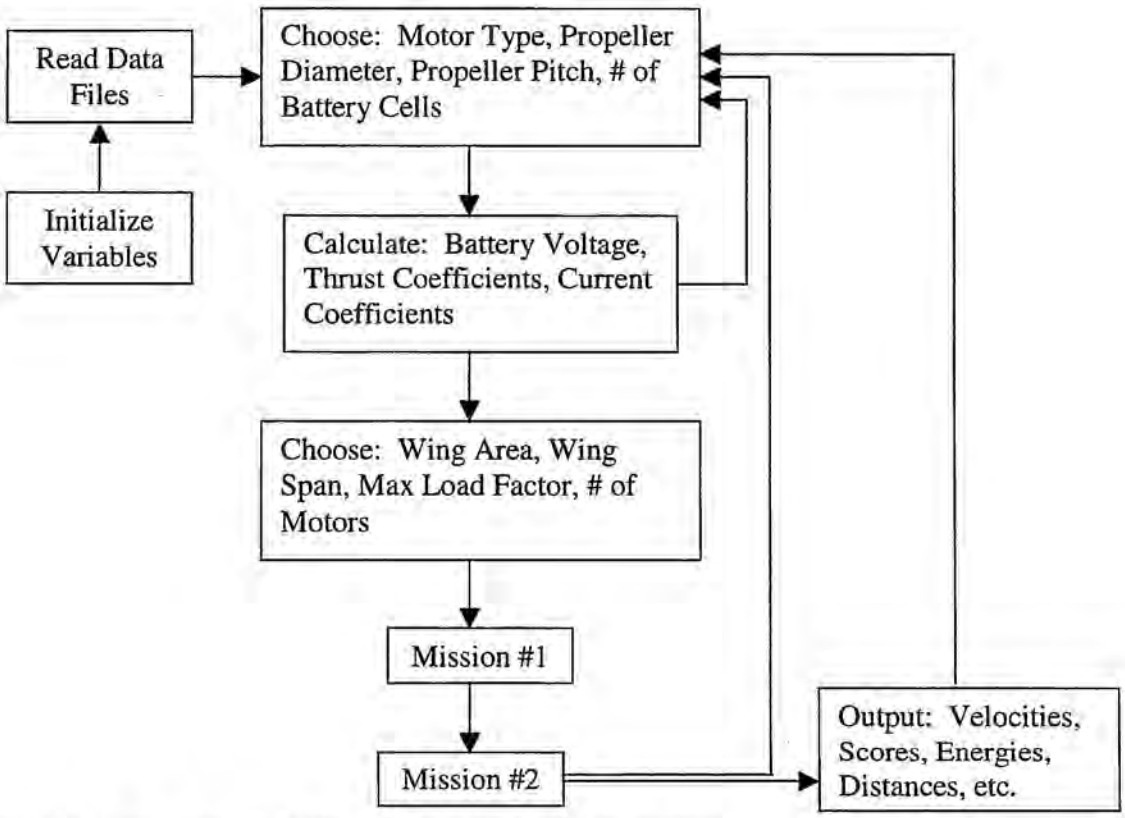

Figure 4.2.1. Block diagram of the DBF2002 optimization program.

After initial runs of the program, data files were created containing many thousands of aircraft configurations along with their respective scores and other characteristics. A spreadsheet program was used to sort the data with respect to score to determine where the maximums occurred. Based on the highest scoring aircraft configurations, a more polished range of aircraft parameters was chosen with higher resolutions set to narrow the search for an optimum aircraft. This refinement process was repeated many times and thus millions of aircraft configurations were simulated.

The DBFEMP program was written to determine the empennage needed to stabilize the aircraft by iterating on the critical empennage parameters located in Table 4.1.1. Stability was quantified by specifying a static margin and a yaw stability derivative. Based on rule of thumb values obtained for conventional aircraft, these were chosen to be 10% and 0.06 respectively. Once a stable configuration was found, the program calculated the RAC of the entire aircraft with the new empennage. The program then simulated the tail being flown through critical flight conditions that the aircraft would encounter such as takeoff, steady flight, and turning. For each flight condition, the program iterated on elevator size and computed the elevator deflection needed to trim the aircraft. It then computed the drag associated with that deflection.

4.2.2. Estimating Aircraft Gross Weight. Several approximations were refined to produce a better model of the overall aircraft weight. The predicted wing weight is not only a function of the wing area, but also a function of the wing design load factor. Wing weight increases proportionally with wing area, span, and design load factor. The model considered the dimensions and weight of a wing spar needed to withstand bending forces, ribs and webbing needed for torsion loads, and non-structural weight. The weights of the empennage surfaces were based on the same formula used for the main wing. The manufacturer's listed weight was used for each motor considered.

4.2.3. Estimating Aircraft Drag. The source of parasitic drag that was of most concern during the preliminary design phase was that of the mock antenna for the MDM. This mission required that a simulated cylindrical antenna be attached to the exterior of the aircraft. Contest rules state that the cylinder must be mounted 3 inches away from any aircraft surface and be entirely exposed to the free stream. Since this structure will create a significant drag force, an accurate prediction of this force was desired. Figure 4.2.2 shows a full-scale model of the cylinder, constructed of competition materials, that was tested in a wind tunnel. A force measurement device was designed and known weights were used to calibrate the setup. Strain and pressure differential data were recorded for velocities up to 80 ft/s. The resultant drag coefficient was found to be a constant for velocities between 30 and 80 ft/s. In this region, the drag coefficient was 0.9 ± 0.15 for a confidence level of 95%. As shown in Fig. 4.2.3, this is significantly higher than the value predicted from the relation presented by White (1999). Drag estimates from conceptual design were used for the other aircraft components.

4.2.4. Estimating Aircraft Maximum Lift Coefficient. For the purposes of preliminary design, the estimate of the aircraft maximum lift coefficient was taken to be the maximum lift coefficient of a NACA 2412 airfoil. This gave a resulting maximum lift coefficient of 1.6.

4.2.5. Estimating Power Plant Performance. The motor-propeller combinations were modeled in a subroutine called GPROPS, which uses principles from Phillips (2002). This program uses Goldstein's vortex theory along with electric motor theory to predict the thrust and current draw for a particular motor-propeller combination. It also uses the propeller geometry of a particular propeller manufacturer to further increase the accuracy of the results.

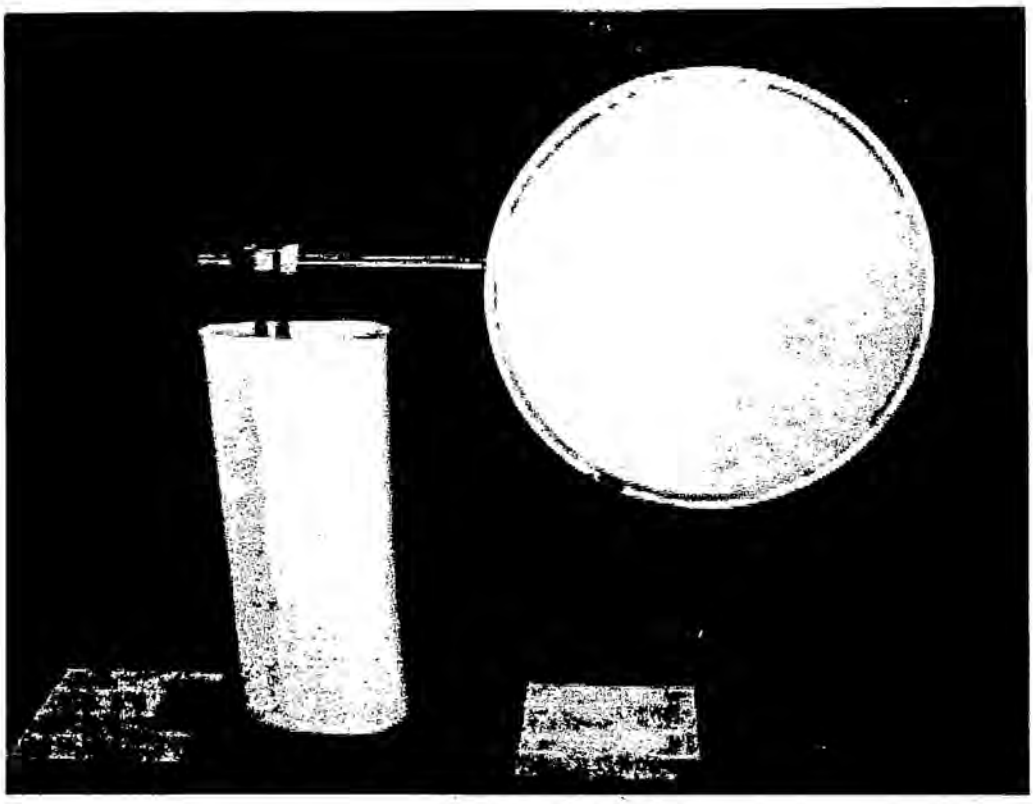

Figure 4.2.2. Wind tunnel setup for cylinder drag measurements.

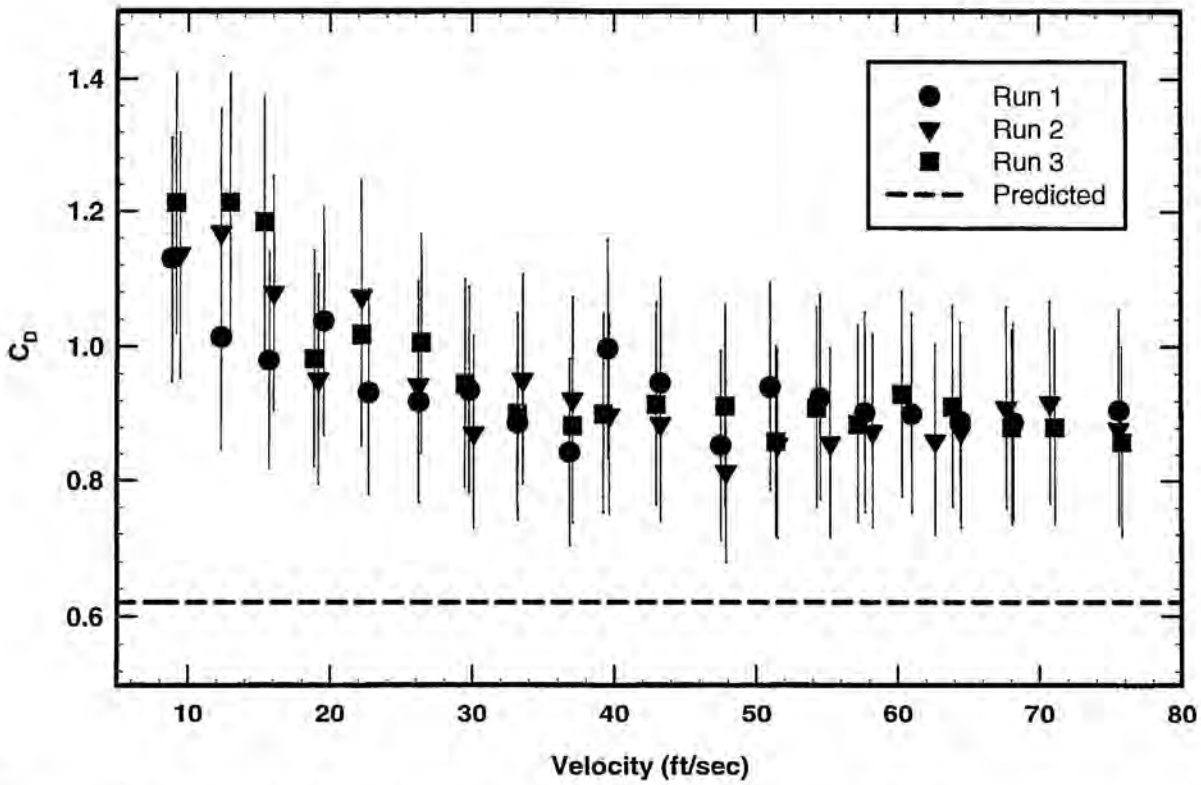

Figure 4.2.3. Results of cylinder wind tunnel testing with confidence level of 95%.

Given a motor and propeller, the GPROPS subroutine would sample thrust data points at six different velocities for each of six different throttle settings. Velocities ranged from 0 to 200 ft/sec in steps of 40 ft/sec while throttle settings ranged from 0.5 to 1 in steps of 0.1. The same was done for current draw. A quadratic least squares fit was used to approximate thrust and current as a function of velocity at each throttle setting. Once these coefficients were obtained another least squares fit was used to fit quadratic functions to these sets of coefficients as functions of throttle setting to yield two 9X9 matrices of coefficients. These two matrices represented the thrust and current as a quadratic function of both throttle setting and velocity. This was done so that the computationally intensive GPROPS subroutine needed only to be called once for each motor and propeller combination thereby greatly reducing the run time of the main program.

It is common to overestimate the performance of batteries and motors by using efficiencies and energy capacities given by the manufacturers of these products. Manufacturers often use the best-case test scenarios and not actual flight conditions. To remedy this problem, tests were designed to monitor power plant component characteristics based upon the conditions that would be expected during an actual flight. These tests gave an estimate of the expected energy output of a possible competition motor and battery pack. These estimates were used in the GPROPS subroutine to aid in the determination of an accurate optimal aircraft range.

Figure 4.2.4 shows general trends in battery voltage, current and motor speed. However, due to the large uncertainty in the torque measurement, a new load cell had to be obtained. Also due to errors in the current measurement, large sections of data had to be removed to provide an accurate picture. Still, sufficient information was gathered for the GPROPS subroutine as seen in Table 4.2.1.

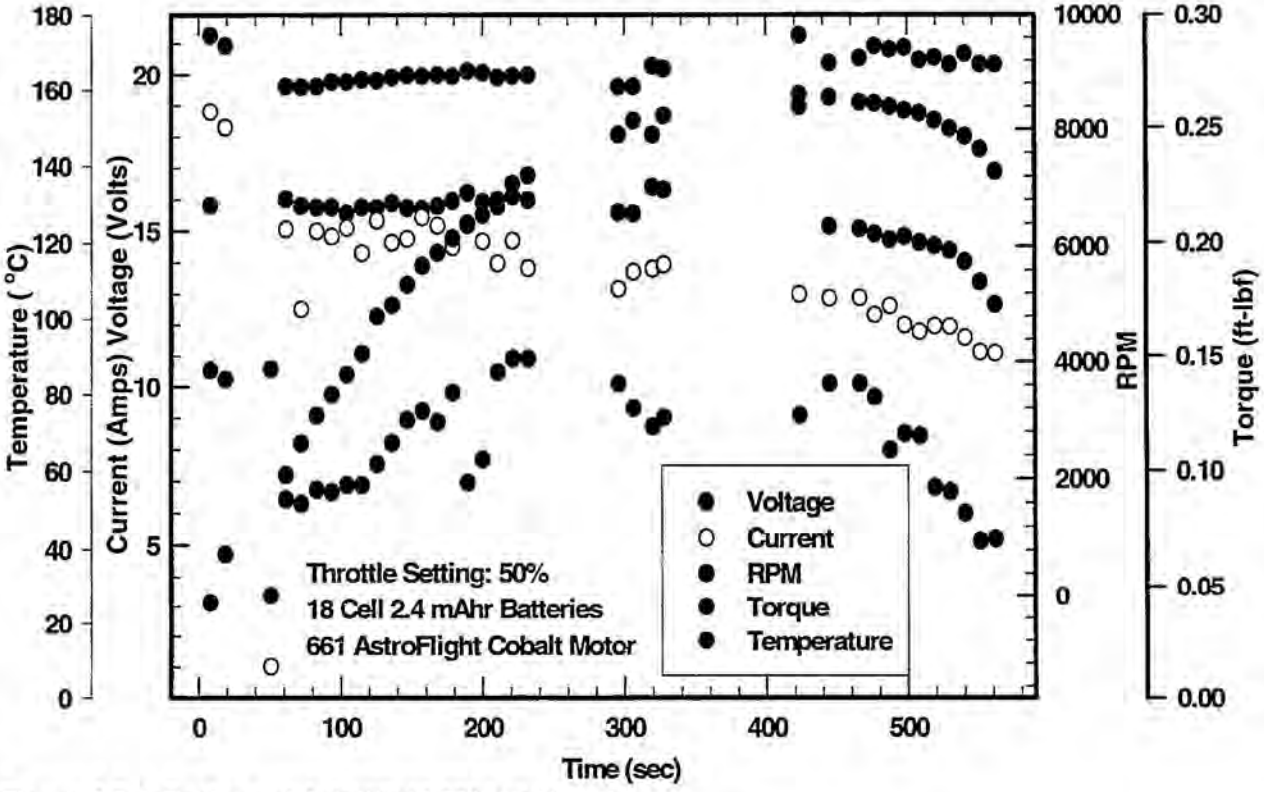

Figure 4.2.4. Test run of AstroFlight 661 cobalt motor.

	Battery Resistance	Battery Capacity	Torque	Speed	Efficiency
Manufacturer	0.005 ohms	2400 mAhrs	0.26 ft-lbf	8400 rpm	80%
Test	0.015 ohms	1800 mAhrs	0.15 ft-lbf	8500 rpm	75%

Table 4.2.1. Comparison between actual tests and manufacturer's battery specifications.

4.2.6. Static Stability Analysis. Both the static margin and yaw stability derivative equations that were used in the DBFEMP program were based on the moment distribution of the aircraft along the fuselage reference line. The aerodynamic centers of all surfaces and the thrust line were allowed to be offset and rotated from the fuselage reference line. Main wing flap, and elevator deflections, along with the destabilizing effects of a tractor propeller and fuselage were accounted for, along with downwash and sidewash effects from the main wing on the stabilizer surfaces.

4.2.7. Mission Modeling Equations. Conceptual design predicted cruise speeds well above takeoff speeds. This meant that a considerable portion of each mission would be spent in accelerating flight. Three options were available to model the accelerated portions of flight; full numerical integration using time steps, closed form approximations assuming a linear change in force and small climb angles, or a closed form integral solution with an approximation for the thrust, drag, and current distributions. Since minimal program run times were critical due to a tight design schedule, the first option was not feasible. The second option used assumptions that were inaccurate due to the nature of the missions, which exaggerate nonlinearities in drag and lift forces. The thrust and current draw curves are well behaved and closely follow the form of a quadratic curve. It was therefore possible to develop, in closed form, the integrals of the time, distance, and energy equations, with respect to velocity. These equations are respectively defined

$$t = \int_{V_o}^{V} \frac{m}{c_1 + c_2 V + c_3 V^2} dV \tag{4.2.1}$$

$$s = \int_{V_o}^{V} \frac{V m}{c_1 + c_2 V + c_3 V^2} dV \tag{4.2.2}$$

$$Energy = E \int_{V_o}^{V} \frac{m(i_1 + i_2 V + i_3 V^2)}{c_1 + c_2 V + c_3 V^2} dV \tag{4.2.3}$$

where t, and s, are the values of time and distance respectively, m is the mass, E is the battery pack voltage. V_o and V are the initial and final velocities, and i and c are the coefficients for the quadratic functions.

The classical form of the drag equation made a closed form solution to the integral impossible. To overcome this, the best approximation theorem, Greenberg (1998), was used to find a quadratic equation that accurately modeled the drag over the velocity interval from liftoff to cruise velocity. There were two advantages associated with using the best approximation theorem as opposed to a curve fit of the data. First, the resulting equation was robust enough to be used for any aircraft configuration and second, it was only necessary to recalculate the coefficients for each V^2 term to acquire the three coefficients for a quadratic. This was faster computationally than having to use a curve fit routine coupled with a Gaussian matrix solver. Figure 4.2.5. shows the original function and the best approximation function curves for the optimal aircraft configuration.

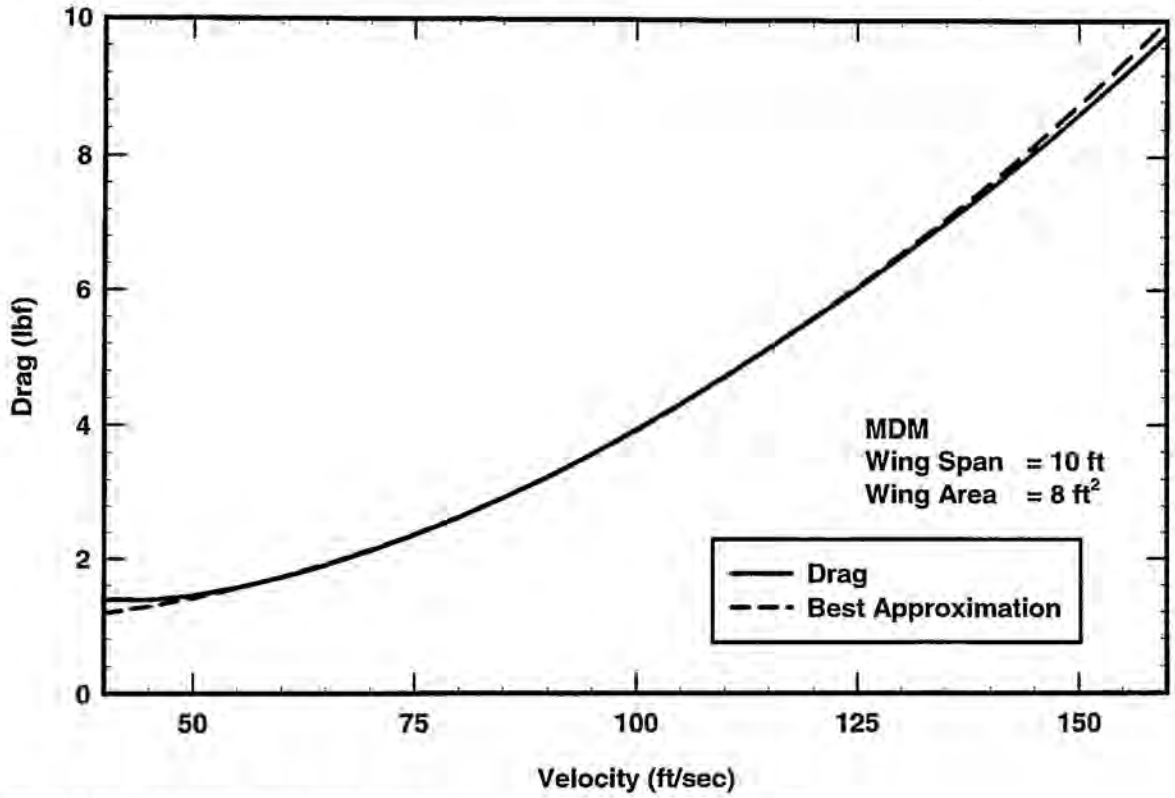

Figure 4.2.5. Aircraft drag and best approximation quadratic function.

4.2.8. Takeoff Analysis. The takeoff portion of the flight routine used the acceleration model along with a rotation time estimate of one second and a liftoff speed equal to 110% of the aircraft's stall speed. The time, energy and distance needed to accelerate to takeoff speed and rotate at a constant velocity were then obtained and sent back to the main routine. Aircraft configurations that exceeded a 120 ft takeoff distance were discarded.

4.2.9. Accelerated Climb Analysis. Given a height to climb, initial velocity, and velocity objective, the accelerating climb portion of the flight was modeled with the same equations developed in Sec. 4.2.7. The required horizontal distance was calculated from the flight distance obtained from Eq. 4.2.2. The climb angle was the tangent of the height to climb and the available horizontal distance of each straight section of the lap. If the required distance exceeded the available distance before the upcoming turn, the velocity that could be attained was evaluated with a root finder and returned to the flight routine. If the distance required to reach the velocity objective was less than that available, then a steady climb, which is a special case of the acceleration equations, was used over the remaining distance.

4.2.10. Steady Level Flight Analysis. The steady level flight portions of the missions were modeled using the same equations of acceleration, but without elevation or velocity change.

4.2.11. Turning Analysis. Accelerated turning was prohibited by the high induced drag caused by large load factors. Instead, a constant speed turn was used that allowed for a loss in altitude to balance the kinetic energy lost due to drag being greater than thrust. The time, energy, and height loss during the turn were computed and returned to the flight routine.

4.2.12. Descent and Landing Analysis. Descent and landing were modeled using the same algorithms but assumed zero thrust or power usage from the motor. A bisection method was used to

determine the point in the last lap of the sortie at which the motor should be shut off to allow the aircraft to touchdown and stop at the start/finish line of the course. This method used decelerating forms of the time and distance equations to calculate losses in potential and kinetic energy of the aircraft through level decelerating turns, the downwind leg straightaway, the decelerating decent from the end of the last turn to touchdown and the ground roll.

4.3. Optimization Results

Data obtained from the optimization programs was sorted and maximum overall scores identified. It was found that an optimum score is given for high aspect ratio wings, despite the fact that RAC increases with aspect ratio. Figure 4.3.1 shows how score is affected by the aspect ratio of the main wing for the MDM and SDM missions. The MDM score increases with aspect ratio while the SDM score decreases. The combined total score has an optimum with an aspect ratio of approximately 11 (see Fig 4.3.2).

High load factor limits also gave better scores due to the ability to turn at higher bank angles, producing higher turns rates. The tradeoff is increased aircraft weight and the associated increase in RAC and induced drag.

Increasing the number of battery cells was found to increase the score despite the penalty of added weight. This results from putting a higher voltage drop across the motor, which increases the power output and maximum flight velocity.

4.3.1. Configuration Parameters for Optimized Aircraft. After analysis of the program outputs, the 10 best airplanes were selected. Table 4.3.1 shows the parameter ranges for these 10 aircraft. These were approximate values to be finalized in detail design with more accurate models and analysis.

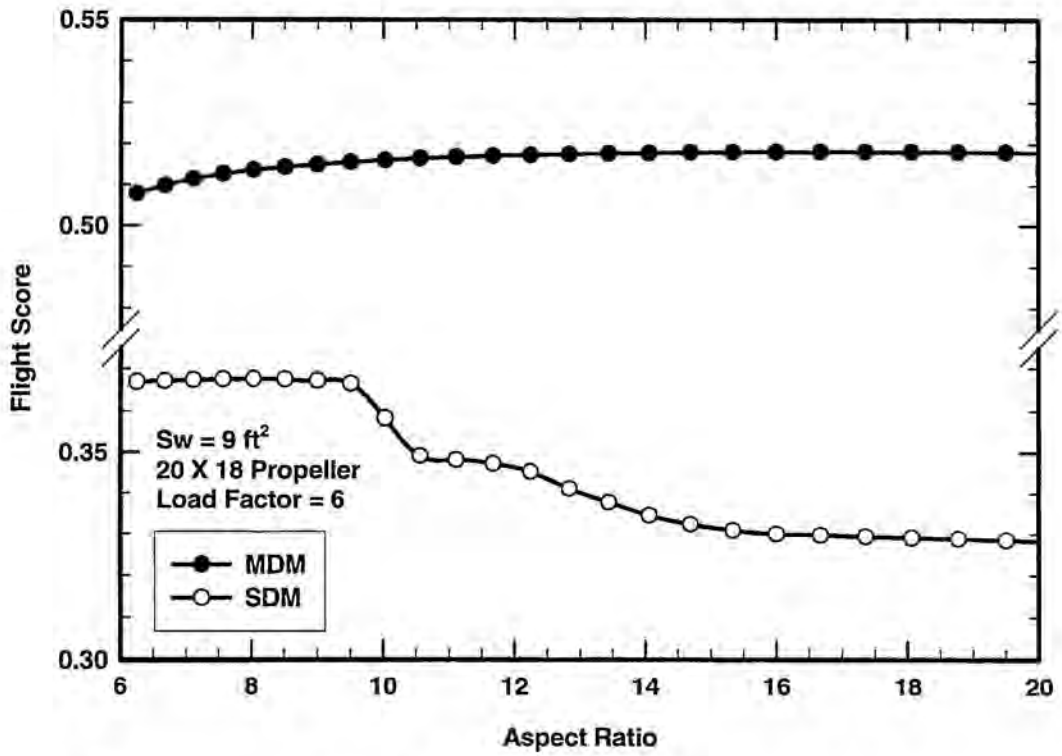

Figure 4.3.1. Flight score with respect to aspect ratio.

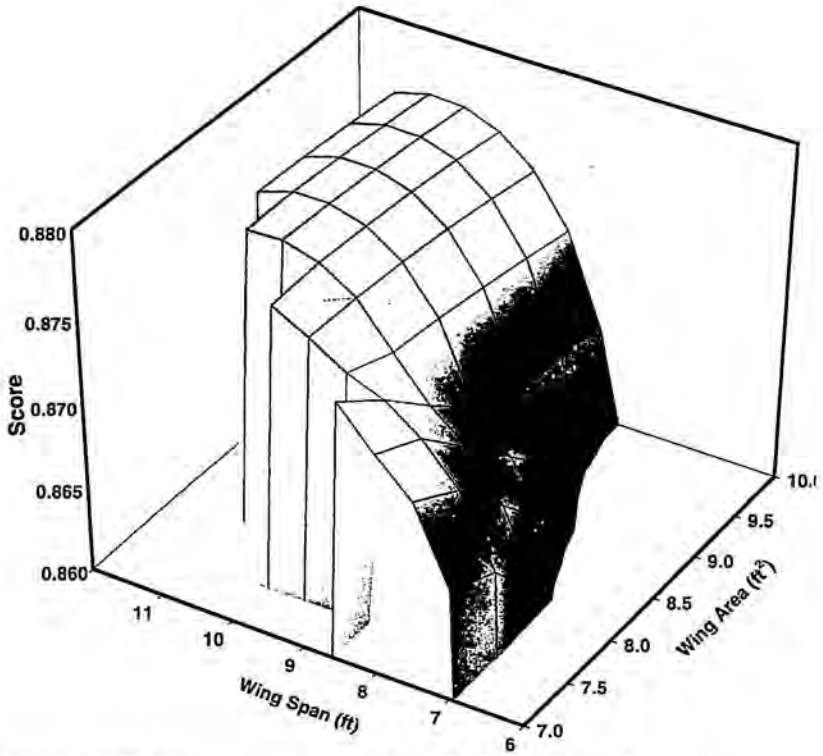

Figure 4.3.2. Combined flight scores as a function of wing area and span.

Design Parameter	Approximate Value
Wing Area (S_w), ft^2	8~9
Wingspan (b_w), ft	9~10
Horizontal Stabilizer Area (S_h), ft^2	1.5707~1.7
Horizontal Stabilizer Span (b_h), ft	2.5
Vertical Stabilizer Area (S_v), ft^2	1.5707~1.7
Vertical Stabilizer Span (S_v), ft	2.5
Elevator Width (% chord)	40~50
Empennage Horizontal Offset (l_h), ft	1.6~1.7
Battery Weight (W_b), lbf	5
Turn Load Factor (n_t), g's	7~8
Number of Motors	1
Motor	Astroflight 691
Propeller Pitch and Diameter (MDM) (λ_p) (d_p), in	21X19 ~ 17X19
Propeller Pitch and Diameter (SDM) (λ_p) (d_p), in	21X19 ~ 17X19
Rated Aircraft Cost (RAC), k$	13.5

Table 4.3.1. Optimized ranges of aircraft design parameters.

4.3.2. Aerodynamic and Stability Characteristics of Optimized Aircraft. Plots were made to evaluate the performance characteristics of aircraft in the optimal range. Figure 4.3.2 is an example of one these plots. They were analyzed to determine the best performance characteristics. This evaluation aided in further narrowing the optimal configuration ranges. Table 4.3.2 gives approximate values for the predicted performance.

The empennage was sized according to a static margin of 10% and a yaw stability derivative of 0.06 at mission flight velocity. These stability derivatives were then plotted over a range of lift coefficients to ensure stability for all operating conditions to be encountered. Figure 4.3.3 shows an example of one of these plots. These plots helped the team decide which aircraft configurations would not only be the most efficient, but also be the most stable through the range of operating conditions.

Performance Parameter	Approximate Values
Maximum Lift Coefficient (C_{Lmax})	1.6
Maximum Lift-To-Drag Ratio (*L/D*)	20
Maximum Takeoff Distance, ft	115
Maximum Takeoff Distance (Loaded), ft	100
Maximum Takeoff Distance (Empty), ft	75
Static Margin, %	10
Yaw Stability Derivative	0.06

Table 4.3.2. Predicted performance characteristics.

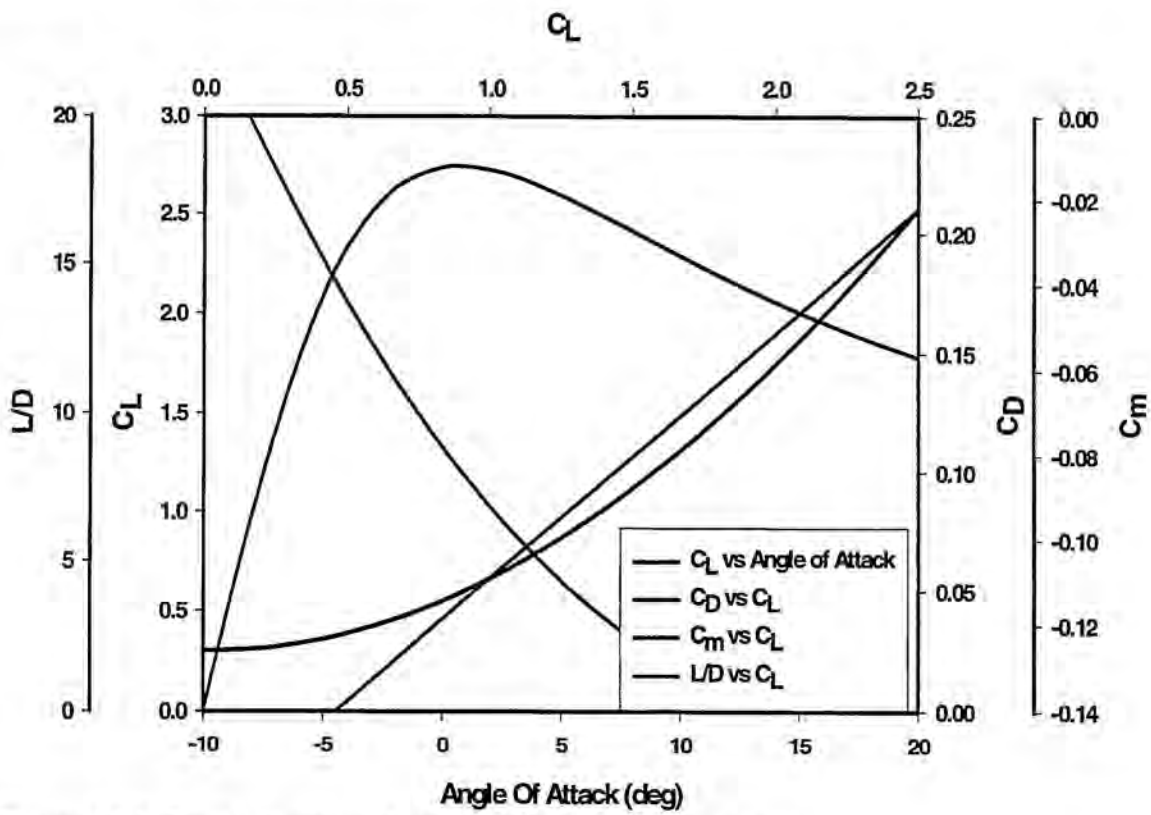

Figure 4.3.2. Graph of some performance parameters at 110 ft/sec.

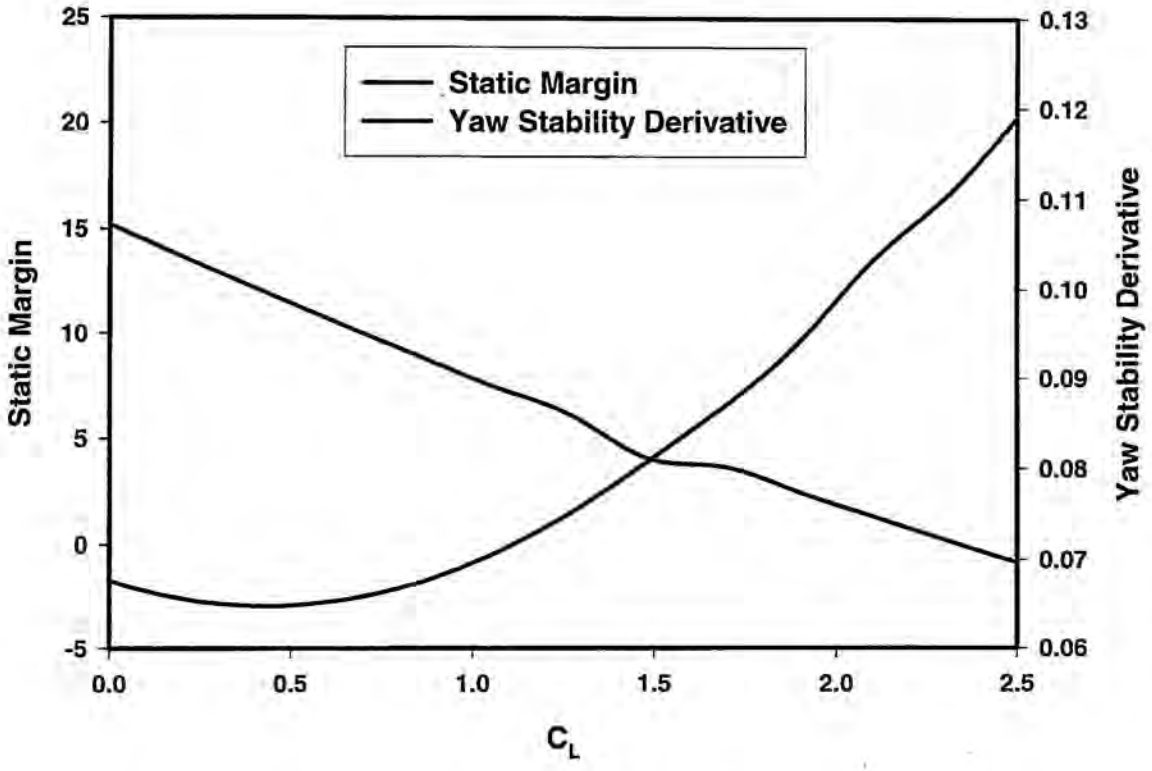

Figure 4.3.3. Graph of stability parameters at 110 ft/sec.

4.3.3. Predicted Mission Performance for Optimized Aircraft. Table 4.3.3 shows the approximate mission performance values typical of the 10 best aircraft, selected from thousands of configurations that were considered during preliminary design.

Performance Parameter	Approximate Value
RAC, k$	13.5
Time MDM, min	2.15
Time SDM, min	2.38
Score MDM	0.482
Score SDM	0.342

Table 4.3.3. Predicted mission performance for the optimized aircraft.

4.4. Conclusions

The results predicted from the preliminary design program showed significant differences from optimal velocities and aircraft sizes predicted during the conceptual design phase. This was due to the introduction of improved estimates for power plant efficiencies, current limits, and more accurate algorithms for predicting drag and thrust. Some trends found in conceptual design were verified, such as the increase in score with aspect ratio and load factor. Unlike results predicted during conceptual design, the preliminary design program predicted that adding cells to the battery pack would increase the total score, up to battery weights beyond the 5-lbf limit.

5. DETAIL DESIGN

With the major aircraft components determined in preliminary design, the final task before manufacturing was to maximize design performance. This was accomplished by shaving off weight and reducing drag while still meeting the stringent demands of strength and stability. This final optimization was done by detailed analysis and design of the airframe's aerodynamics, power plant, and structure.

5.1. Engineering Requirements

The final aircraft design has basic engineering requirements that must be met to guarantee safe and successful flying. These requirements fall under three major categories; contest rules, strength, and flight performance. Most requirements have basic values that must be met or the aircraft design is not viable. The requirements for the detail design phase are listed in Table 5.1.1. All aspects of detail design are aimed at meeting or exceeding these requirements.

Engineering requirements	Required	Goal
Mission Rules		
Gross Weight (lbf)	< 55	< 22
Takeoff Distance (ft)	< 120	110 ~ 120
Flight Time (min)	< 10	2 ~ 3
Radio Fail Safe Mode	Yes	Yes
Disassembled Dimensions (ft)	4 X 2 X 1	4 X 2 X 1
Assembly Time (sec)		15
Rated Aircraft Cost ($1000)		13
Strength		
Load Factor Limit (g)	>7	9
Lift Limit (lbf)	>154	198
Payload Support (lbf)	35	45
Flight Performance		
Maximum Lift Coefficient	1.6	2
Maximum Lift-To-Drag Ratio	20	30
Maximum Speed Empty (ft/sec)	110	140
Stability (Static & Dynamic)		
Static Margin (%)	5 ~ 20	12
Divergent Mode Doubling Time (s)	>1	>3

Table 5.1.1. Engineering requirements for final aircraft configuration.

5.2. Component Selection and Systems Architecture

To optimize the aircraft and meet engineering requirements, the aircraft was divided into subsystems that were analyzed in greater detail. These subsystems were the main wing, empennage, flight control system, propulsion system, structural system, payload support and deployment system, and the takeoff and landing system. The main wing and empennage were optimized with the use of numerical programs such as JAVAFOIL, Hepperle (2002), and code developed by the team. These codes computed the lift, drag, and stability characteristics among other mission performance parameters. The flight control system was chosen to meet the complex flight operations encountered in the different mission profiles. Due to the high structural loadings predicted during flight, high strength-to-weight materials and structures were used. Structures were analyzed using SDRC I-DEAS finite element analysis package and tested to

failure in a laboratory. In order to support and deploy the payload, the mechanism and support structure were optimized for weight, reliability and strength. The takeoff and landing system was optimized to reduce drag, weight, and mission flight time while maintaining good ground handling characteristics, and strength.

5.2.1. The Main Wing. Throughout the conceptual and preliminary phase of the aircraft design, all wing performance was based on the NACA 2412 airfoil section. In order to improve upon the NACA 2412 and the main wing performance, a new airfoil and the use of washout were investigated.

Airfoil. In an effort to improve on the overall performance of the wing, extensive analysis was done on over 200 different airfoils using an application based on the well-used PROFIL code developed by Eppler, called JAVAFOIL, Hepperle (2002). This program uses basic boundary layer theory to predict the viscous drag over an airfoil, the transition from laminar to turbulent flow, and stall of the airfoil based on laminar and turbulent flow separation. Of the over 200 airfoils analyzed, 150 of them were based on various combinations of the NACA 5 and 6 digit camber lines. The remaining 50 airfoils were taken from the University of Illinois, Urbana Champagne 1500+ airfoil database. The airfoils selected were based on their application and thickness greater than 12%, to make room for the retractable landing gear.

The criteria to select the "best" airfoil out of the 200 analyzed, were based upon the following parameters for both the takeoff and cruise speeds; maximum lift coefficient > 1.6 without flaps, maximum lift coefficient > 2.0 with flaps, maximum L/D > 40 without flaps, maximum L/D > 50 with flaps, and moment coefficient about quarter-chord > -0.1 without flaps. The airfoil that had the best overall performance based on these criteria is the Eppler 584, originally designed as a low Reynolds number airfoil for sailplanes (Eppler, 1990). The airfoil polars are plotted in Fig. 5.2.1 for the cruise Reynolds number.

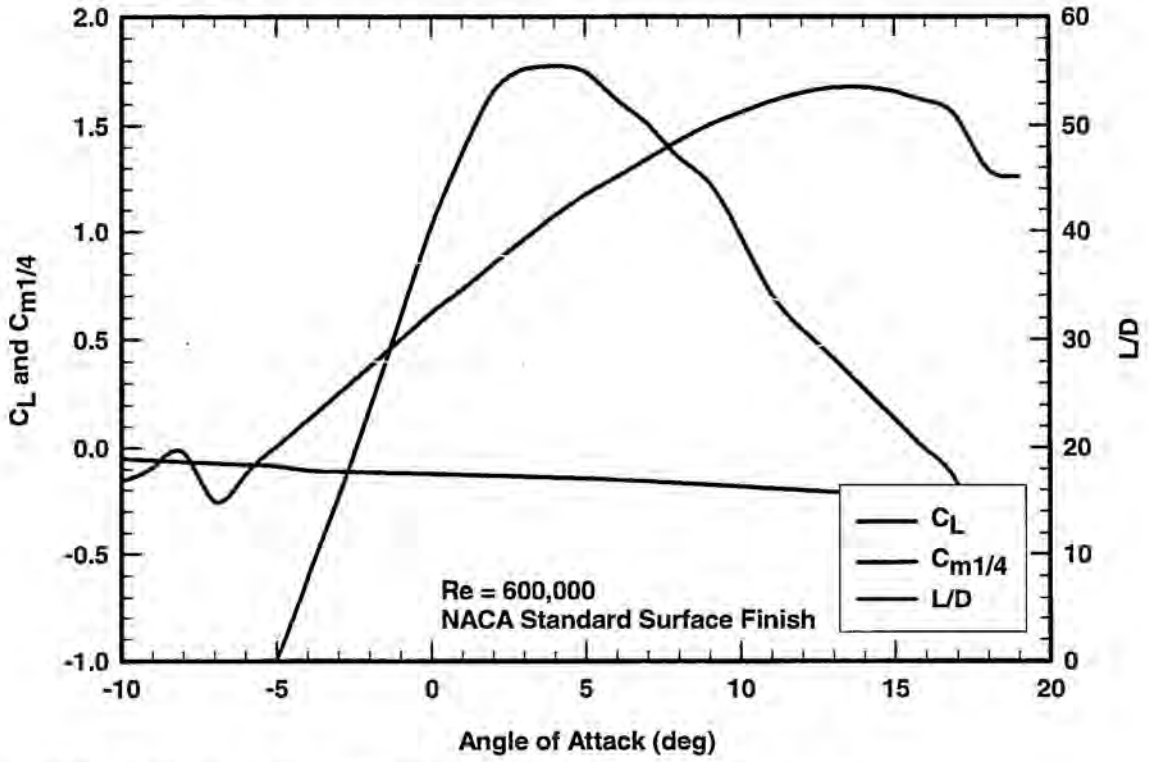

Figure 5.2.1. Polars for Eppler 584 airfoil at a Reynolds number of 600,000.

Washout. With an airfoil and planform shape decided upon, the next option considered was that of using washout to reduce the induced drag of the wing. With the use of an elliptic washout distribution the induced drag of a wing can be reduced to that of an elliptic planform for a given lift coefficient, Phillips (2003). A wing with optimum washout will always produce less induced drag than that of a wing without washout at all lift coefficients above one-half the design lift coefficient. Using the numerical solution for optimum washout presented by Phillips (2003) the effects of washout for a finite wing were studied. Figure 5.2.2 shows the maximum decrease in induced drag that can be obtained for a finite wing for a given aspect ratio. All values are calculated for the Eppler 584 airfoil. For the wing chosen in this design with an aspect ratio of 10.9, the potential performance increase is 8%.

With two possible means of implementing washout, geometric or aerodynamic twist, the simplest is to use geometric twist. To determine the amount of twist needed at the wingtip a program was written using the aforementioned algorithm to iterate on design lift coefficients and compare the reduction in induced drag across the entire range of expected lift coefficients. Figure 5.2.3 shows the optimum drag reduction over the lift coefficient range. One disadvantage of using this fixed twist is shown by the narrow peak at low lift coefficients with reduction in benefit at higher lift coefficients. Since nearly half of the flying will be at the high end of the lift coefficient range due to takeoffs, landings, and high load factor turns, a fixed twist gives relatively little advantage. Other difficulties encountered in using this type of washout were the problems in manufacturing. The washout presented in Fig. 5.2.3 represents only 1.5 degrees of maximum twist at the wingtip. Considering the relatively crude manufacturing methods used in building R/C aircraft, the quality control for such a small amount of twist would be prohibitive to the cost and time required to complete the design.

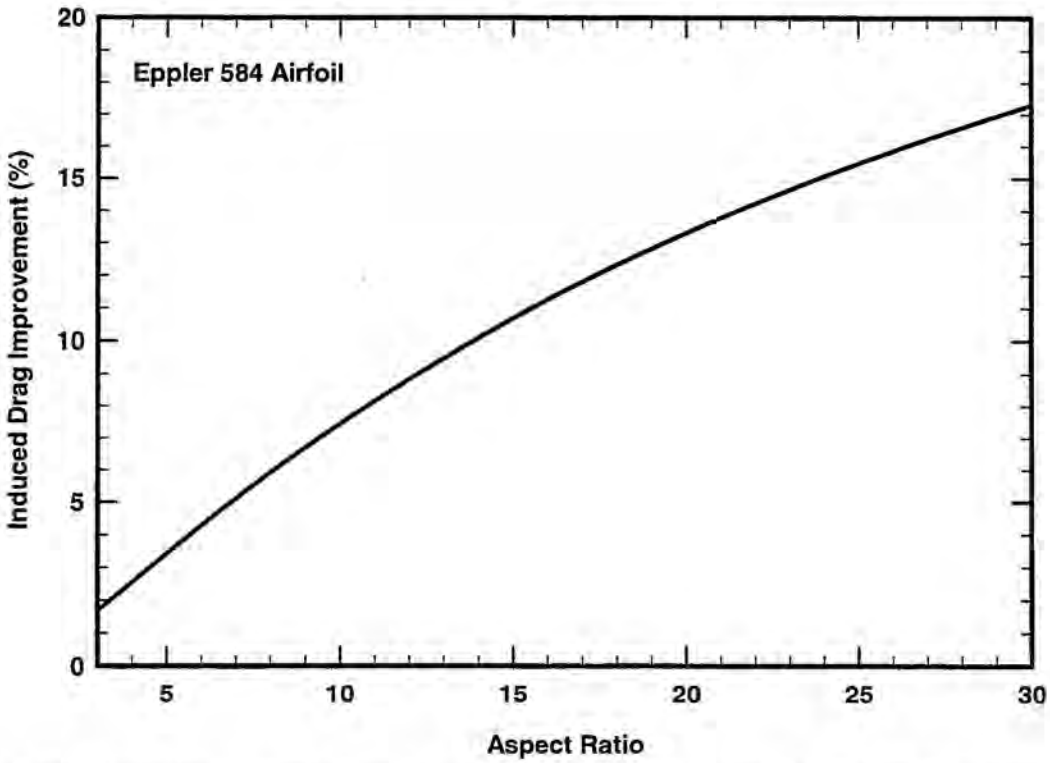

Figure 5.2.2. Reduction of induced drag versus aspect ratio for a wing with optimum washout.

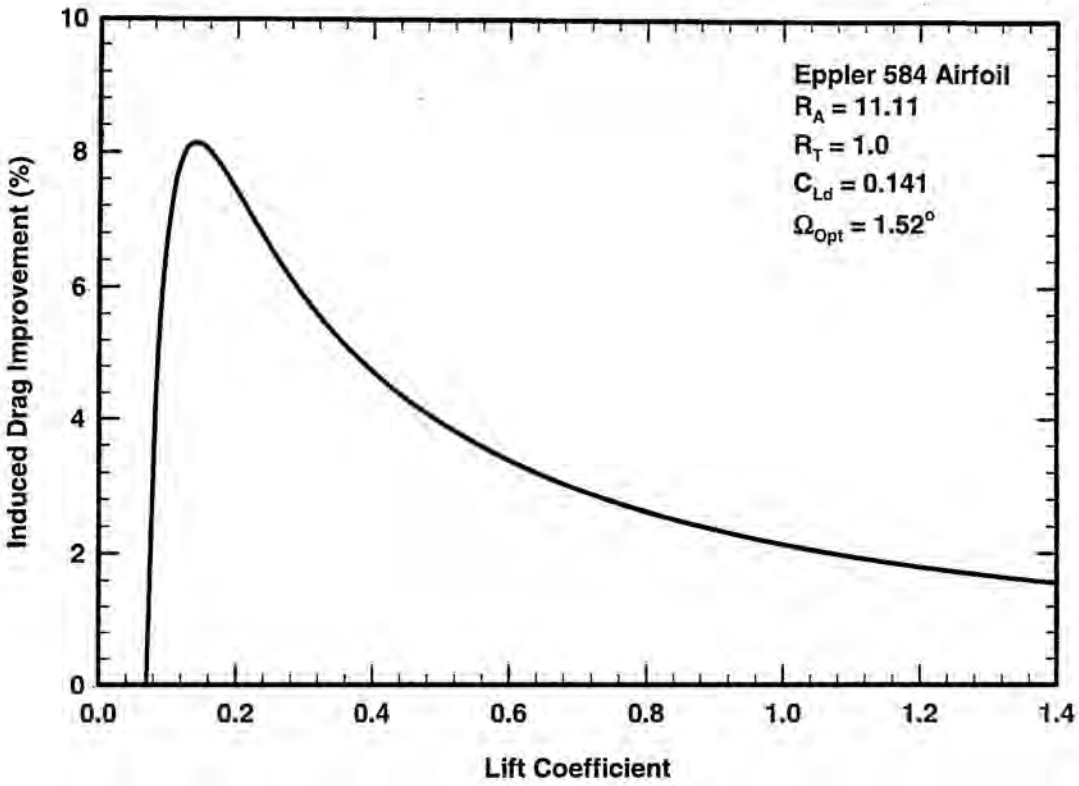

Figure 5.2.3. Reduction of induced drag versus lift coefficient for a wing with optimum washout.

The use of aerodynamic twist presented a more complex problem than that of geometric twist since the washout is implemented by twisting the local zero lift angle of attack along the wing. This would require a very time intensive manufacturing process that uses numerous different airfoil templates, each with the correct zero lift angle of attack. The design of a minimum number of modified airfoils alone would prove too daunting for the time and manpower available. For these reasons, the use of fixed aerodynamic twist was not considered further.

A third option for introducing wing twist is the use of *twisterons*, Phillips, Alley, and Goodrich (2003). This idea utilizes the flaps to produce aerodynamic twist in the wing. The greatest single advantage of using the flaps to produce aerodynamic washout is that the optimum washout can be maintained over the entire range of lift coefficients. Another potential advantage of using flap washout is the reduction in overall pitching moment produced by the wing. This would reduce the negative lift produced on the conventional aft tail in trimmed flight. Because of its potential influence on other surfaces of the aircraft, the method of Phillips and Snyder (2000) was used to analyze the effects of flap washout, or twisterons, on the aircraft lift-to-drag ratio. Since the benefit of twisterons would be best realized in the high-g turns, all computations were done for a lift coefficient of 1.4. Parameters iterated on were; the width of the flaps in percent chord, deflection of flaps in degrees, and twist angle of the flaps at the tip.

Figure 5.2.4 depicts the elliptical twist generated on the flaps along the span. In order to determine which flap percentage should be used for the final design, several more performance criteria were considered. The first considered was the total L/D improvement that the flap washout could produce for the aircraft. Based on these results shown in Fig. 5.2.5, the range of flaps considered for further analysis were the 25, 30 and 35% flap widths.

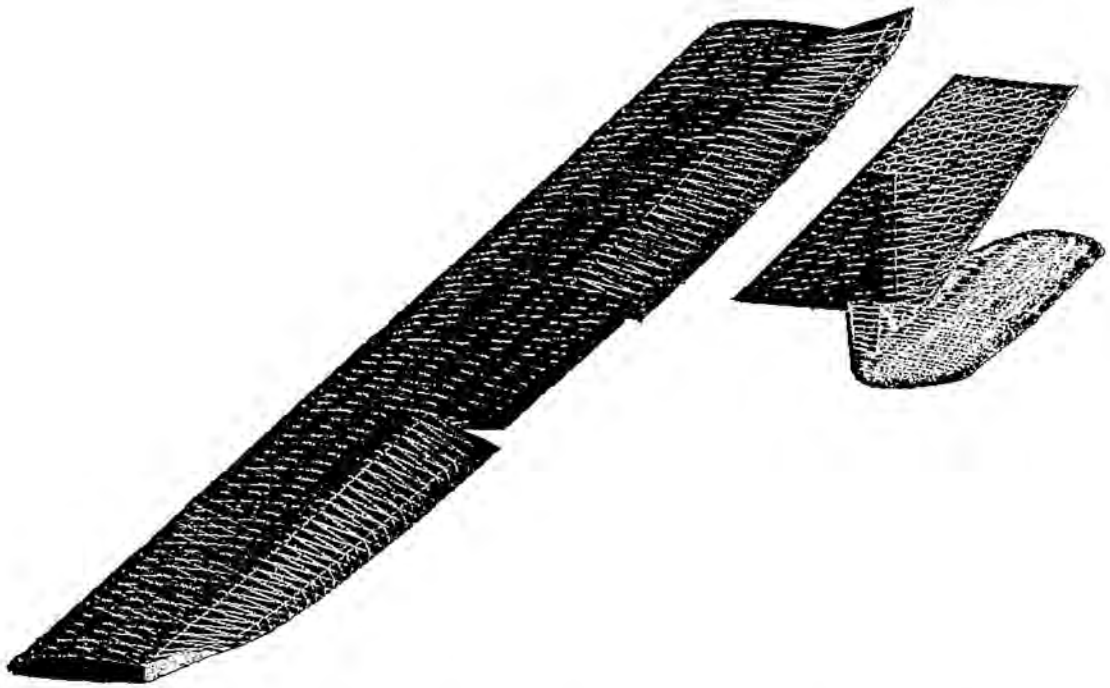

Figure 5.2.4. Representation of twisteron deflection with elliptic washout distribution.

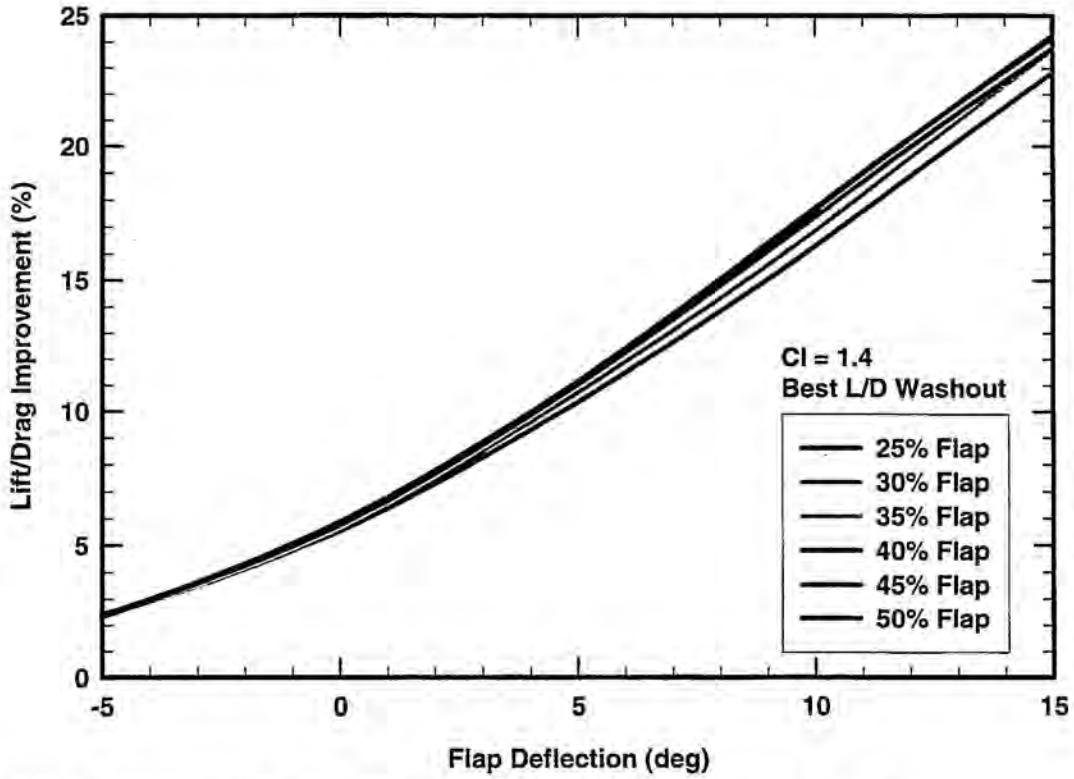

Figure 5.2.5. Best possible lift-to-drag ratio improvement as a function of flap width.

The effect of flap width on the maximum lift coefficient for a given flap deflection was analyzed using JAVAFOIL. Figure 5.2.6 shows the maximum lift coefficient for the three flap percentages. With the 25 and 30% flaps having very similar characteristics, the final criterion considered was that of manufacturability. The 25% flaps are the best choice considering that it would be easier to twist a shorter and thinner flap while sacrificing very little performance over the range of flight conditions to be encountered. Figure 5.2.7 shows the improvement in lift-to-drag ratio that the use of flap washout can provide, for the 25% flaps. As shown in Fig. 5.2.7, increases in lift-to-drag ratio from 10 to 20% can be realized with this flap modification. An improvement of this magnitude with a single modification is unheard of beyond the fairing of bluff bodies. Based on these results, the best configuration is a wing with 25% flaps. The flaps would be deflected 15 degrees with 35 degrees of washout at the tip for turning and takeoff, and the flaps would be deflected –1.5 degrees with 6.5 degrees of washout at the tip for level flight.

In order to address the problem of manufacturing this design, the use of multiple control points along the span are necessary. This can be accomplished with the use of one servo per wing attached to three bellcrank/control horn assemblies and one stationary control point. In order to create the elliptic washout distribution on the flap, the control points are clustered toward the tip with a cosine distribution. Figure 5.2.8 shows the position of each control point along the span at both the cruise and turning flap deflections. With each dynamic control point needed different degrees of rotation and direction, the pushrods connecting each bellcrank assembly must have the correct lever arm length relative to the servo rotation. The servo is placed in the wing at the 60% semi-span with pushrods going to the bellcranks at the root and tip of the wing section. This arrangement minimizes the length of the pushrods

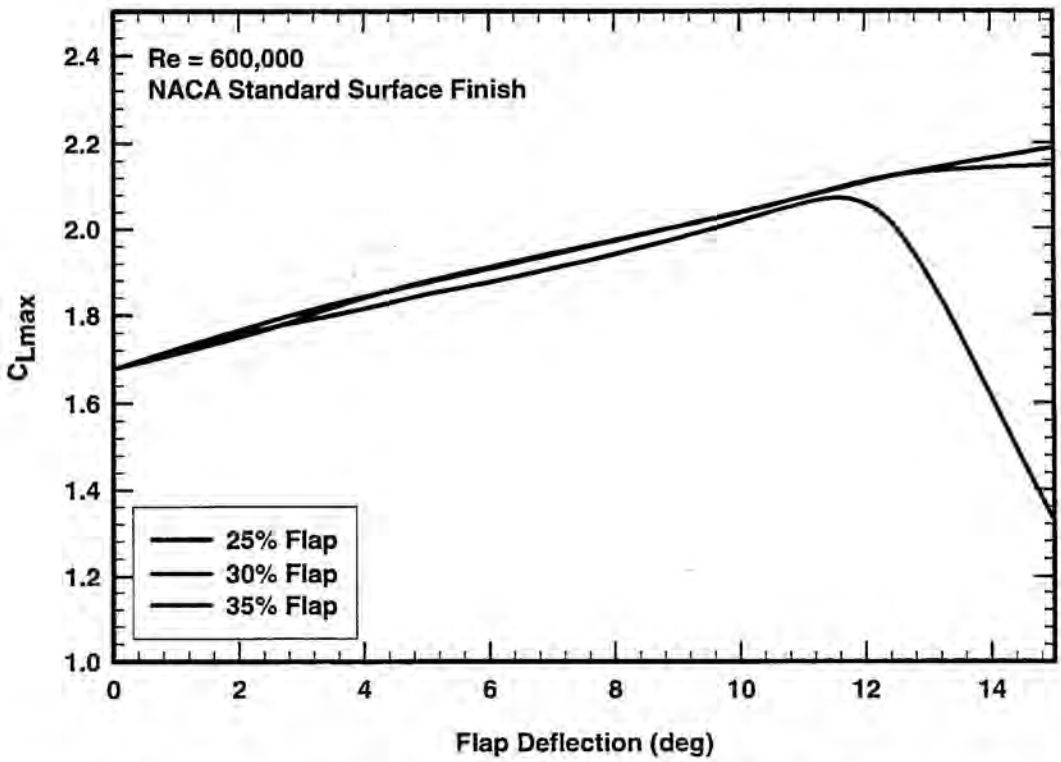

Figure 5.2.6. Maximum lift coefficient for a given flap deflection and flap width.

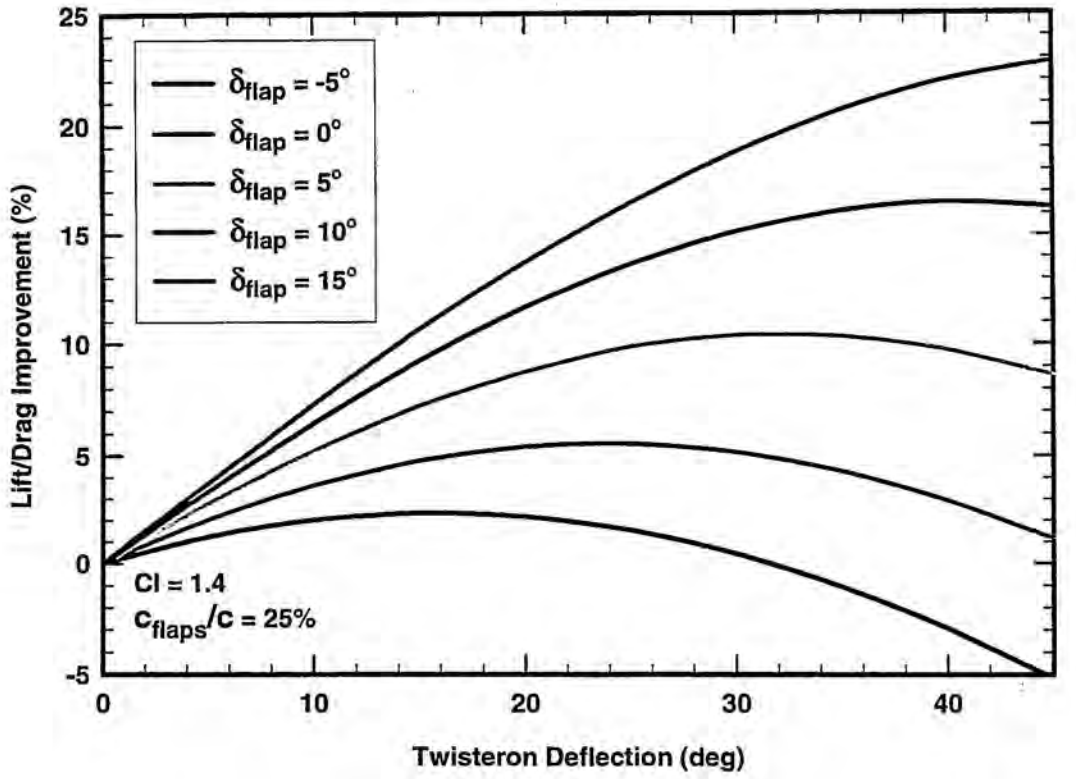

Figure 5.2.7. Lift-to-drag improvement as a function of twisteron deflection.

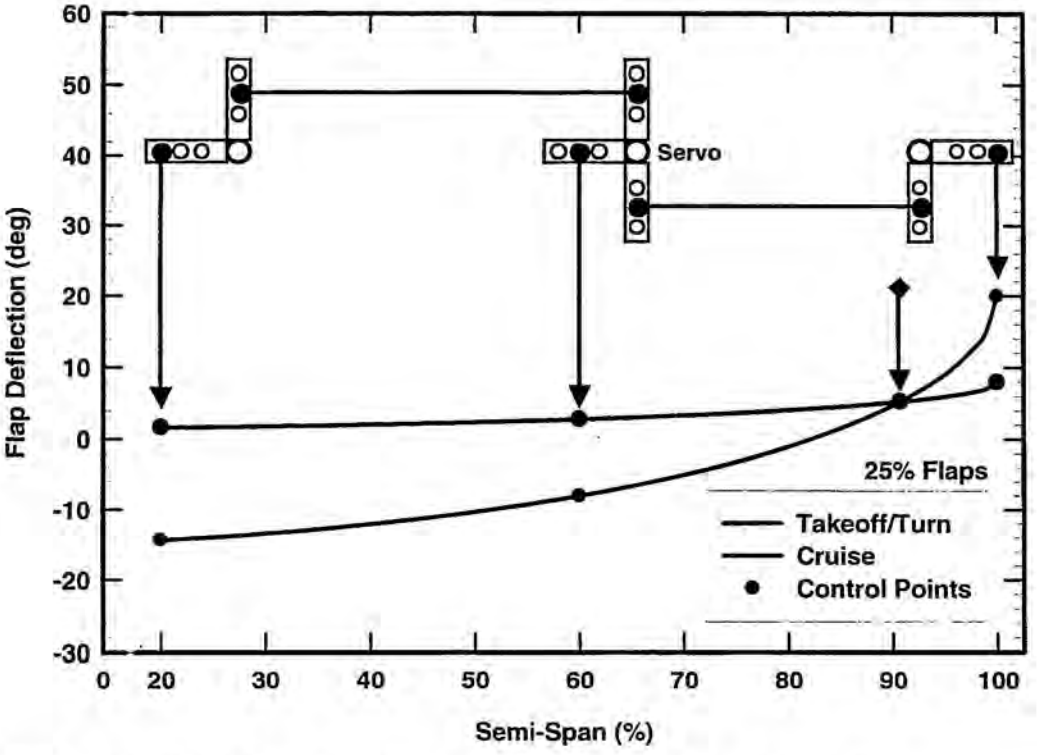

Figure 5.2.8. Flap washout over operating range with control linkage schematic.

and limits the amount of twist between the closest control points. For a flap 2.7 inches wide, the most severe relative twisting that would be experienced is 15 degrees over 6 inches. The rotation of the root bellcrank is 148% of the servo bellcrank and the tip rotation is –111% of the servo bellcrank. By implementing washout, the lift-to-drag ratio of the aircraft can potentially increase by 20%.

5.2.2. The Stability and Control System. The results that were obtained from preliminary design combined with the most recent wing properties, were used to finalize the design of the empennage and its control surfaces.

Empennage. In the detail design phase, more accurate models of the aerodynamic forces and moments were needed to finalize the design of the empennage. For this, the method of Phillips and Snyder (2000) was utilized. The first task was to model the optimal aircraft from preliminary design and analyze its stability. The results were within 5% of those found from the DBFEMP program, giving confidence in the results found in preliminary design. From this optimal empennage geometry it was noticed that the total length of the aircraft was close to the length of the aircraft storage box. This shifted the focus of the team to not only optimize the empennage in terms of RAC, drag, and manufacturability, but also in terms of assembly time. If the empennage could be made to fit into the box, this would greatly reduce assembly time.

Geometry. Elliptical planform lifting surfaces are the most efficient in terms of lift and drag. However, they are extremely difficult to manufacture. Due to the time constraints of this design process, it was decided that elliptical surfaces would not be feasible to manufacture. A tapered lifting surface is a good compromise between elliptical and rectangular shapes. A planform with a taper ratio of 0.4 and some degree of washout approximates an elliptic lift distribution reasonably well, however a planform with a taper ratio of 0.6 fitted with elliptical tips is more accurate. The tradeoff again was manufacturability, the wing with a taper ratio of 0.4 and washout would be easier to manufacture than the wing with a taper ratio of 0.6 fitted with elliptical tips. The final decision was that, because of the high lift carried on the tail during some mission phases, the aerodynamic advantages associated with the elliptic wingtips overcame the increase in manufacturing difficulty.

Control Surface Sizing, Location and Hinging. Once the possibility of storing the fuselage and empennage as one piece was recognized, design efforts were directed toward sizing the empennage to fit within the box. The empennage optimization problem iterated on the empennage parameters of horizontal offset, the tail feather size, and the hinge location.

It was determined that a tape hinge across the bottom of the horizontal stabilizer would facilitate an elevator deflection of 90 degrees. With total aircraft length constrained by the length of the box, an elevator deflection of 90 degrees would allow the empennage to be moved aft a distance equal to the elevator width less the airfoil thickness. This would slightly increase the RAC, while increasing stability and aircraft efficiency. The stability gain outweighed the increase in RAC. Results from preliminary design suggested that an elevator chord of 50% would be within the optimal range. Because the box is only 2 feet wide and the span of the horizontal stabilizer is 2.5 feet, it was decided that the elliptic tips would have to be attached during assembly. A 50% elevator would give a good mounting surface for these elliptical tips.

The same tradeoffs between efficiency and manufacturability were considered for the vertical stabilizer. The rudder was also hinged to deflect 90 degrees. This allowed for a larger vertical tail surface to fit inside the box. Since the vertical stabilizer carries little lift, manufacturability overcame the efficiency considerations and the vertical stabilizer was designed with a taper ratio of 0.4. To increase the

yaw stability for such a short aircraft, the vertical stabilizer was swept aft 41 degrees to increase its effective moment arm. This produced a slight increase in the RAC based on length.

The upper portion of the vertical stabilizer was designed to be removable in order to fit in the box. This removable section attaches to, and acts as an extension of the rudder. The rudder will be hinged on one side with a tape hinge giving it 90 degrees of travel in one direction. This hinge had to be perpendicular to the fuselage in order to fit it into the aircraft storage box.

A 50% elevator chord was in the optimal range from preliminary design. Having an elevator this size offered good control and allowed reasonable surface area to attach the tips. In designing the hinge line of the elevator, two possibilities were considered; one with a straight quarter-chord and one with a straight trailing edge. At cruise speeds, these two designs were modeled using the method of Phillips and Snyder (2000) and had lift-to-drag ratios of 5.9 and 6.1, respectively. Based on these results, the horizontal stabilizer has a swept quarter-chord and a straight trailing edge.

Flight Electronics. The electronic control system for the aircraft was chosen to be a 10 channel JR 10X radio and receiver package. Seven of the channels are used to power the Astroflight speed controller and 6 Hitec servos. To facilitate ease of assembly and allow a single control surface on each wing to serve as both flaps and ailerons, a separate servo was used in each wing. Three more servos were used for the rudder and nose gear, elevator, and retractable gear. One more servo was used to actuate both the wheel brakes and payload release mechanism. This arrangement of servos maximized aircraft control while minimizing the RAC.

5.2.3. The Propulsion System. Optimization of the propulsion system was focused on characterizing the motor and battery packs and implementing them into the power plant program to more accurately predict the best propeller for each mission.

Motor. Motor efficiency tests were performed in order to determine motor characteristics and optimize the motor and batteries with the specific mission requirements. The tests serve several purposes; they show the relationship between motor efficiency and temperature, provide an independent verification of the manufacturer's characteristic curves, and give accurate battery-life profiles under expected flight conditions. Efficiency tests required measurements of battery voltage, current, motor torque, and shaft speed. Measurements provided all the necessary data to effectively analyze the motor/battery combination. The temperature of the motor was also measured in order to monitor thermal effects. The measurements were sampled on a PC using a National Instruments 604xE board and LabVIEW data acquisition software. The test setup is shown in Fig. 5.2.9 with an early test motor. A hysteresis brake with a load cell serves as a dynamometer. Changing the current flow through the brake varies the load applied to the motor.

The uncertainty of the motor efficiency is a function of the uncertainty of each of the four measurements. An error propagation analysis was performed to quantify this uncertainty and was found to be 6% for nominal current, voltage, torque, and speed values. Figures 5.2.10 through 5.2.12 show test results using an Astroflight 691 Cobalt motor with a 24-cell, 1700-mAhr battery pack. This motor was chosen for the final aircraft configuration.

System efficiency. System efficiency is the power put into the motor from the batteries divided by the power output from the motor. The efficiency and temperature of the motor test are plotted in Fig. 5.2.10 with the computed uncertainty. As can be seen, efficiency is basically independent of temperature even after significant heating. This allowed the team to save the added weight of a complex cooling system, which was originally contemplated. A simple air intake was designed to cool the motor.

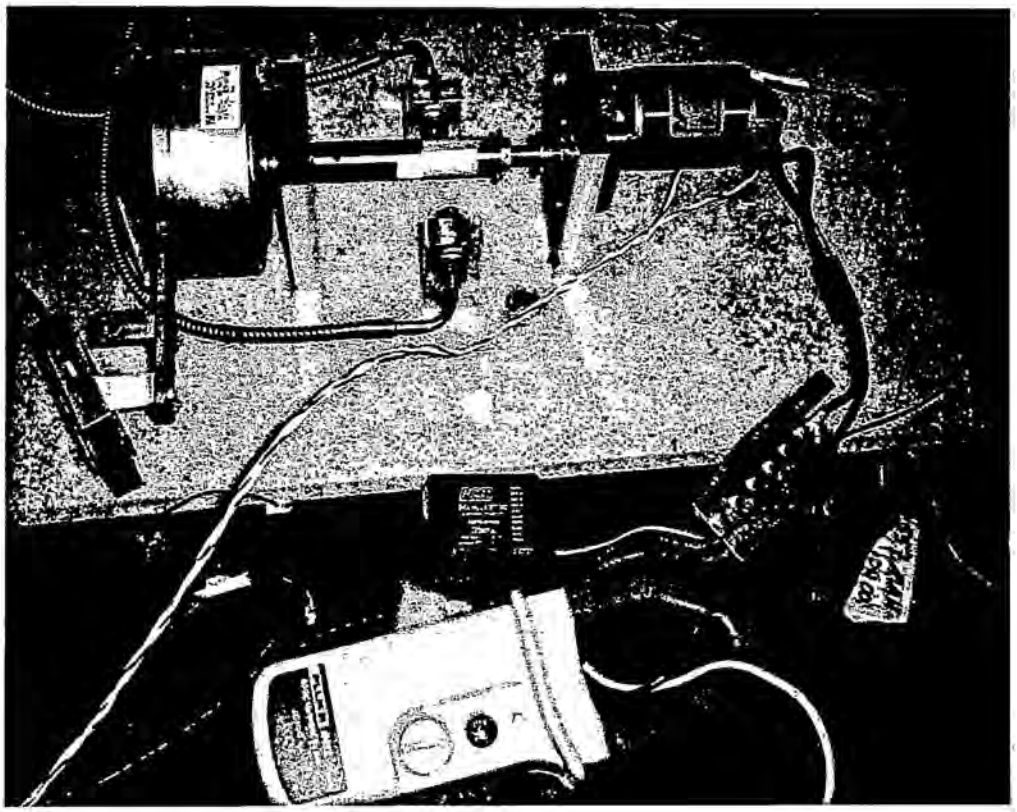

Figure 5.2.9. The motor test setup.

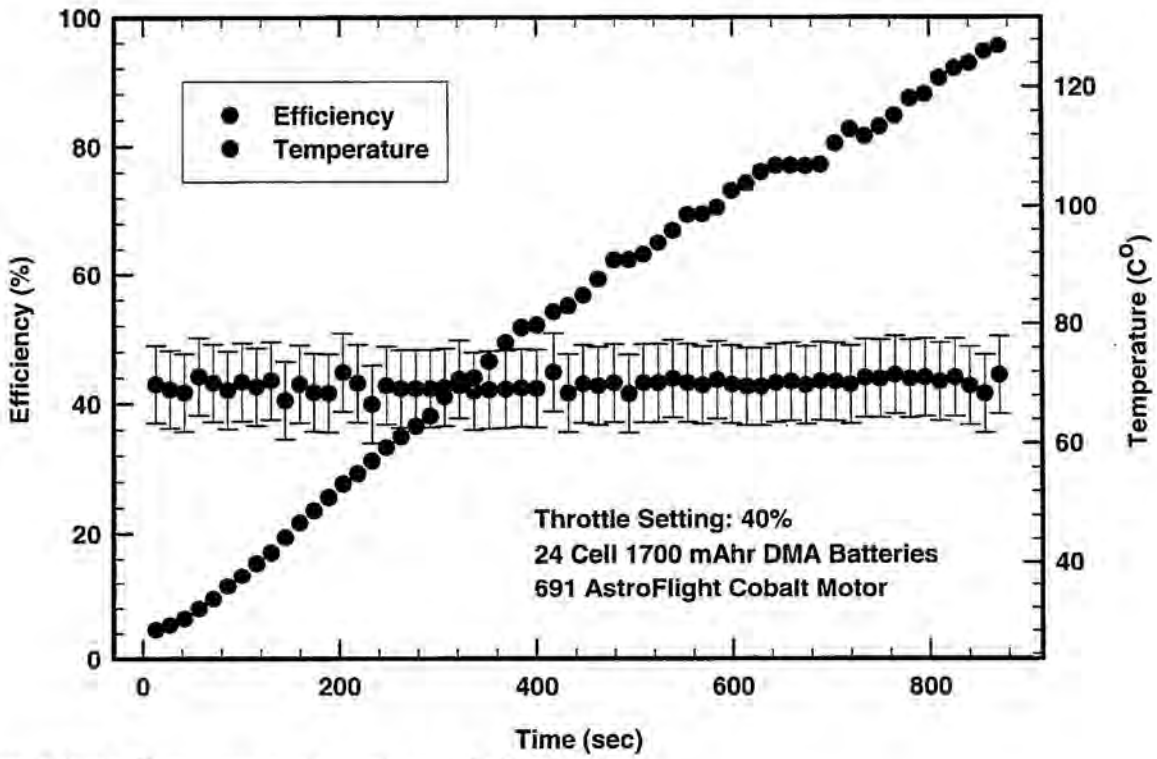

Figure 5.2.10. Temperature dependence of efficiency.

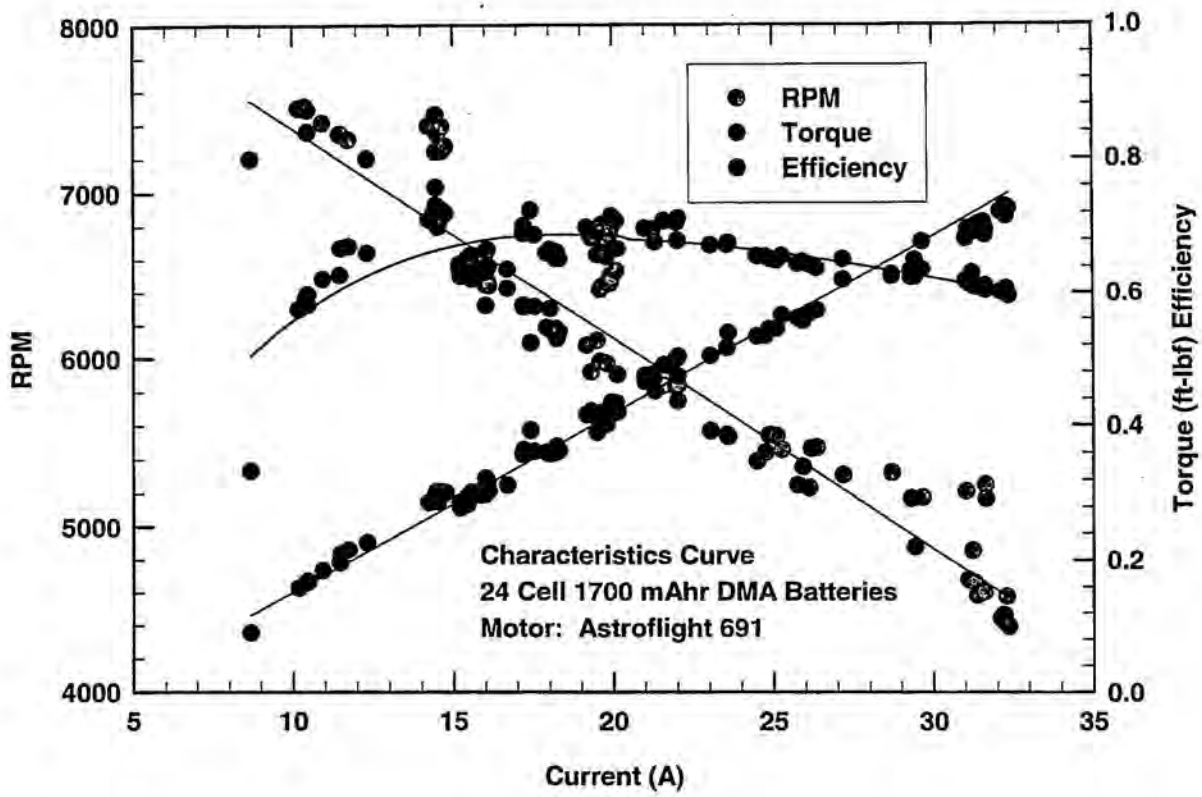

Figure 5.2.11. Characteristic curves of Astroflight 691 motor.

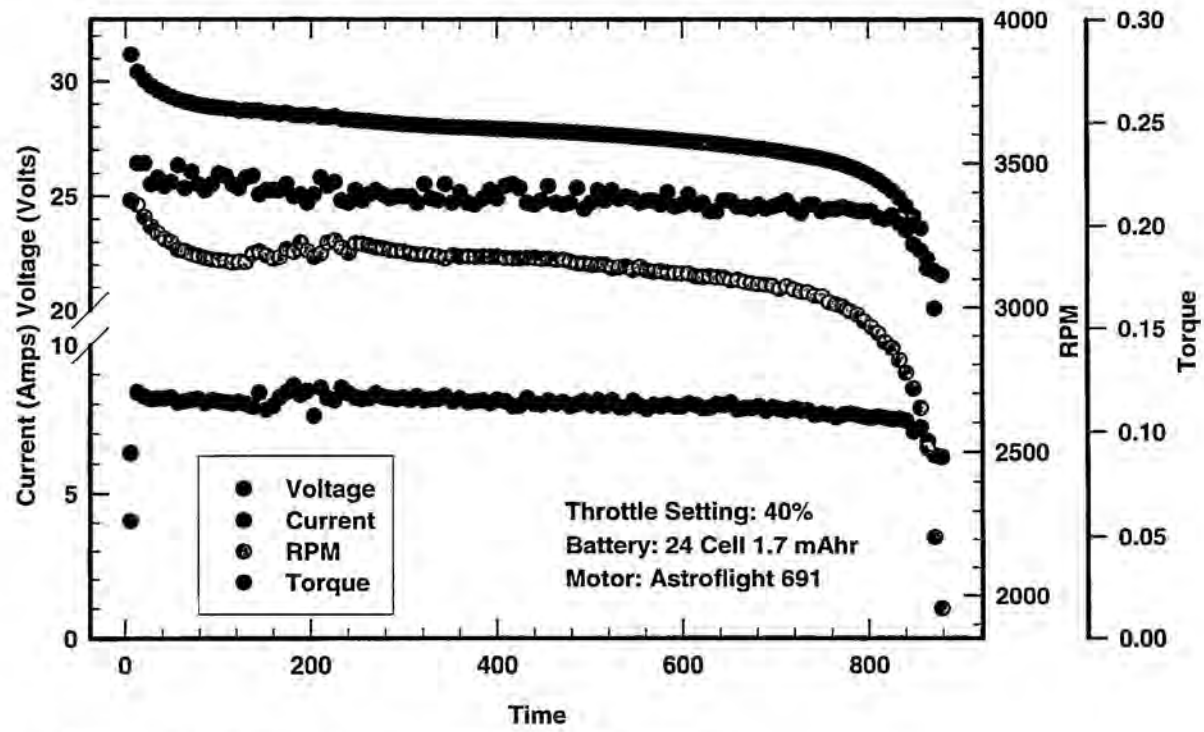

Figure 5.2.12. Motor/Battery performance characteristic curves.

Characteristic Curves. Characteristic curves were generated from these tests showing torque, speed, and efficiency as a function of current draw. Figure 5.2.11 shows samples taken at discrete loads for the same motor/battery combination at full throttle. It can be seen that for this scenario, a peak efficiency of 70% occurs at approximately 20 amps of current. The motor produces 0.4 ft-lbf of torque at this point and is operating at 6000 rpm. It is at this maximum efficiency location that we wish to operate the motor. However, it can also be seen that the efficiency penalty for increasing the current by 10 amps is less than 10%. Based on these curves, a propeller can be selected to give the desired thrust at these conditions.

Batteries. The batteries were selected based on the requirement that a minimum amount of energy, with a reasonable factor of safety, remain in the batteries at the conclusion of each mission. The pack must also provide adequate power to meet mission requirements. Internal battery losses are a major contributing factor in maximum power output. For this reason, a balance was sought between the number of cells and power output of the battery pack. For a given weight of batteries, a tradeoff between capacity and voltage was made. The FOM for battery selection in Table 5.2.1 were based on the flight program and test results. With the 40 amp current limit, a 48-cell, 1700-mAhr battery pack provides more power for a shorter period of time than a 36-cell, 2400-mAhr battery pack, yet still meets the mission requirement for total flight time.

Battery Pack	Power	Weight	Energy*	Resistance	Total
36 cells, 2400 mAhr	0	1	0	0	1
48 cells, 1700 mAhr	1	1	1	-1	2
* Excess energy left over after mission completed.					

Table 5.2.1. Figures of merit for flight battery pack.

In addition to temperature/efficiency profiles and characteristic curves, the motor tests provide information regarding the useful life of the flight batteries. Figure 5.2.12 shows the voltage and current of the flight battery and the torque and speed output of the flight motor. By integrating the area under the current curve for the one battery cycle the total charge in the batteries can be determined. In the same way, total useful output motor energy is obtained by integrating the product of the torque and shaft speed over time. Another useful battery parameter that can be obtained from these tests is the internal battery resistance, which is given by

$$R_b = (E_b - E_m)/(I_m \cdot \#ofcells) \qquad (5.2.1)$$

Figure 5.2.12 shows that the voltage immediately decreases 2 volts from the no-load voltage for a 24 cell battery pack. With the motor drawing 8 amps, equation 5.2.1 yields an internal resistance of 10 mΩ.

Propeller. With the motor and battery pack performance characterized, these values were put into the power plant program used in preliminary design to reiterate on the propellers used for MDM and SDM. Based on best flight score, the optimal propellers dimensions for MDM and SDM are 18X18 and 20X18, respectively.

5.2.4. The Aircraft Structural System. The aircraft's structural design was divided into four major categories for focus during detail design. These are as follows; wing structure, fuselage main support, fuselage secondary support, and aircraft assembly attachments. Each subsystem design involved the input of experts in R/C aircraft, machining, and composites. Along with component testing, this interaction of engineers and manufacturing experts helped minimize costs and redesign.

Wing. Based on the potential for very high accelerations in the turns of every flight, the wing structure needs to support aerodynamic loads in excess of 140 lbf. In order to attain the strength needed for such loads, a very strong, light, and stiff wing was required. The FOM used to select the final wing structure are listed in Table 5.2.2. Based on the selection criteria listed in Table 5.2.2, the best choice for a wing support structure was that of a carbon composite I-beam running through a very light foam core sheeted with balsa. The geometry of the I-beam was engineered to provide the necessary tensile, compressive and shear strength for the flight and wingtip test loads. The I-beam webs were initially sized using a model based on isotropic beam theory. The design was then analyzed using the I-DEAS finite element package to determine the stresses encountered at the transition region between the I-beam and the mounting fixture. The I-beam was modeled with thin shell elements having isotropic properties for the shear web and orthotropic smeared properties of zero degree layers for the flanges. The model was clamped at the attachment point and loaded with a uniform spanwise distributed load of 17.5 lbf/ft. The finite element model results were then verified with component testing. Figure 5.2.13 shows the finite element model, test article setup, and stress plots. The test article withstood an acceptable point load of 80 pounds and failed in the same mode as predicted by the finite element model.

Wing Main Support Structure	Strength to Weight	Total Weight	Manufacturability	Cost	Total	Fuselage Main Support Truss	Strength to Weight	Total Weight	Manufacturability	Cost	Total
Geometry						**Geometry**					
Monocoque Shell	1	0	-1	-1	-1	Monocoque Shell	1	0	-1	-1	-1
Tube	-1	-1	1	0	-1	Tube	-1	-1	1	0	-1
I-Beam	1	1	0	-1	1	I-Beam	1	1	0	-1	1
Box Beam	0	-1	1	0	0	Box Beam	0	-1	1	0	0
Material						**Material**					
Carbon Composite	1	1	0	1	3	Carbon Composite	1	1	0	1	3
Balsa	1	0	-1	-1	-1	Balsa	1	0	-1	-1	-1
Spruce	0	0	-1	0	-1	Spruce	0	0	-1	0	-1
7075-T6 Aluminum	-1	-1	1	-1	-2	7075-T6 Aluminum	-1	-1	1	-1	-2

Table 5.2.2. Design selection matrix for wing and fuselage main support structures.

Fuselage Spar. To meet the desired low wing configuration combined with a vertical drop deployment mechanism a straight spar could not be used. The payload must be located at or slightly aft of the planform center of gravity of the aircraft to maintain stability after deployment. A spar that curves over the payload was designed to meet these requirements. During maximum projected loading the spar will need to support a 190 ft-lbf moment. Aluminum spar designs were discarded because of a small Young's modulus and expensive manufacturing costs. A carbon fiber composite box beam spar was tested using Rhoacel™ foam as the center. This spar failed under relatively light loading because the compressive strength of the foam was exceeded. Carbon fiber I-beam designs were tested with better results. The basic design for the I-beam spar was found using curved beam theory presented in Boresi, et.al. (1993). The web was built using eight layers of 0.010-inch unidirectional carbon fiber laid at 0, 90, 45, and -45 degree angles. The flanges were each made from six layers of the same material laid in the spanwise direction. The figures of merit for the final design of the fuselage spar are listed in Table 5.2.2.

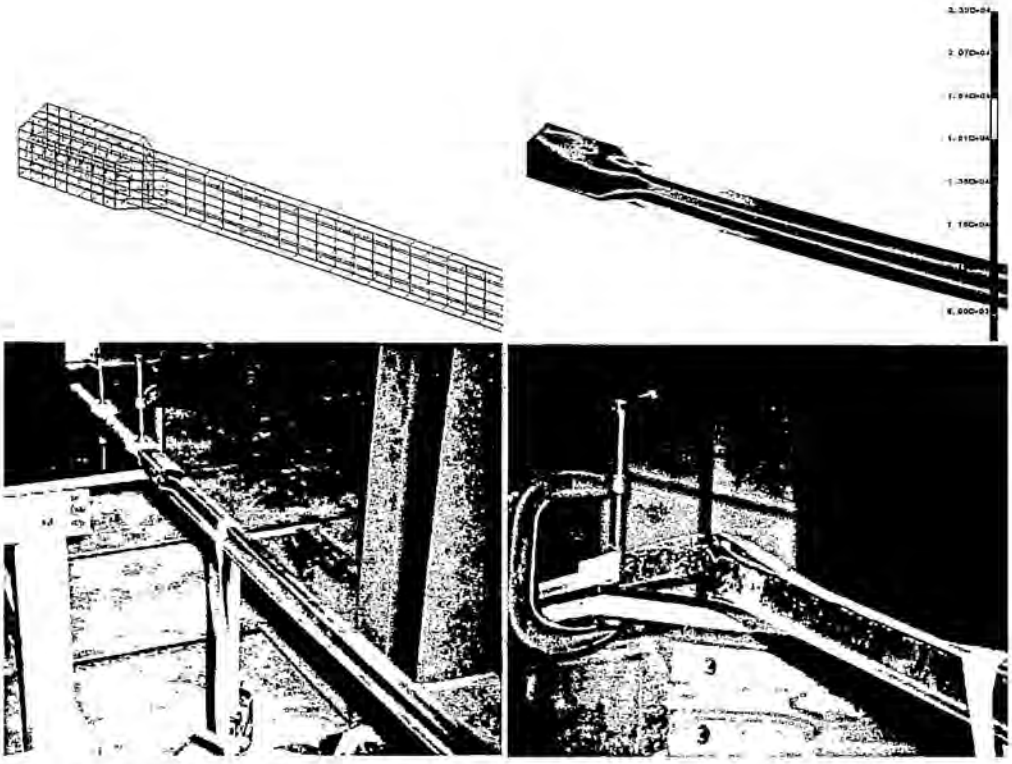

Figure 5.2.13. Clockwise from top left; finite element model, Von Mises stress results, test article failure at 80 lbs, and test article setup.

A finite element analysis of the curved spar was performed using thin shell elements in I-DEAS. The flanges were modeled with orthotropic elements having smeared lamina properties. The web was modeled with isotropic elements, and the model was restrained with plane symmetric boundary conditions. A point load of 80 lbf was placed 26 in out from the plane of symmetry. This point corresponds to the wing center of lift. Stiff beams were used to transfer the applied point load to the end of the spar. The finite model predicted a buckling failure at a 116-lbf load and the test specimen failed at 125 lbf (Fig. 5.2.14). This is less than the required load, so the flanges will be widened in the transition region to provide greater torsional stiffness and increase the buckling factor of safety.

Fuselage Structure. The fuselage structure design is based on the need to provide attachments for the many components required to complete the mission and provide adequate strength to support them throughout the entire flight with a minimum weight penalty. Another important consideration is the access that the structure provides to critical components, such as batteries and servos, for repair or replacement. The fuselage selection matrix in Table 5.2.3 shows the criteria used to determine the general structure of the fuselage. The best choice for the fuselage design is a blended body.

Aircraft Assembly Attachments. The aircraft must fit inside a 4 ft X 2 ft X 1 ft box and be assembled in as little time as possible. This requires that the airframe be modular and easily assembled. Because of the short empennage, the only parts of the aircraft that need to be assembled at the competition are the tips of the tail feathers and the wings.

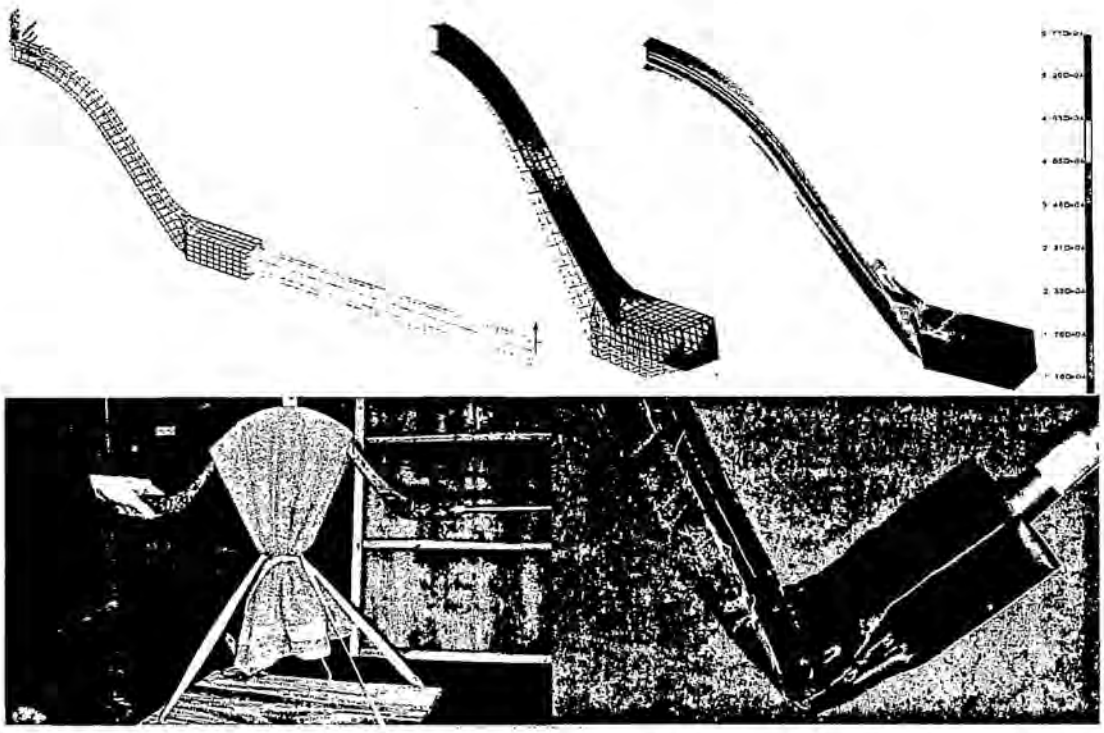

Figure 5.2.14. Clockwise from top left; Finite element model, buckling failure mode, stress plot, buckled truss at transition to mounting block, test setup.

Fuselage Geometry	Drag	Weight	Manufacturability	Cost	Total
Blended Body	1	1	-1	0	1
Lifting Body	0	0	-1	0	-1
Rectangular	-1	-1	1	1	0
Material					
Balsa Builtup	1	1	-1	0	1
Glass Shell	1	0	-1	-1	-1
Foam Core/Balsa	0	-1	0	1	0

Table 5.2.3. Design selection matrix for fuselage structure.

5.2.5. The Payload Support and Deployment System. In order to meet the requirements for MDM and SDM, methods for carrying the missile decoy cylinder and deploying the five pound payload are necessary. To carry the missile decoy cylinder, a small sting attaches the cylinder to the top of the aircraft at the center of gravity. The advantage of this location is that the positive pitching moment it creates reduces the negative lift needed by the horizontal stabilizer to trim the airplane. The possible disadvantage is the turbulent wake that it produces, which shadows a portion of the vertical stabilizer. Because of the unpredictable nature of the wake, test flights will help address the influence of the cylinder on handling characteristics. As for the payload deployment, Figure 5.2.15 shows how the payload is captured by pushrods going thru bearing plates attached at the front and rear of the payload. When released, the payload slides down an attatched rail through a spring-loaded trapdoor.

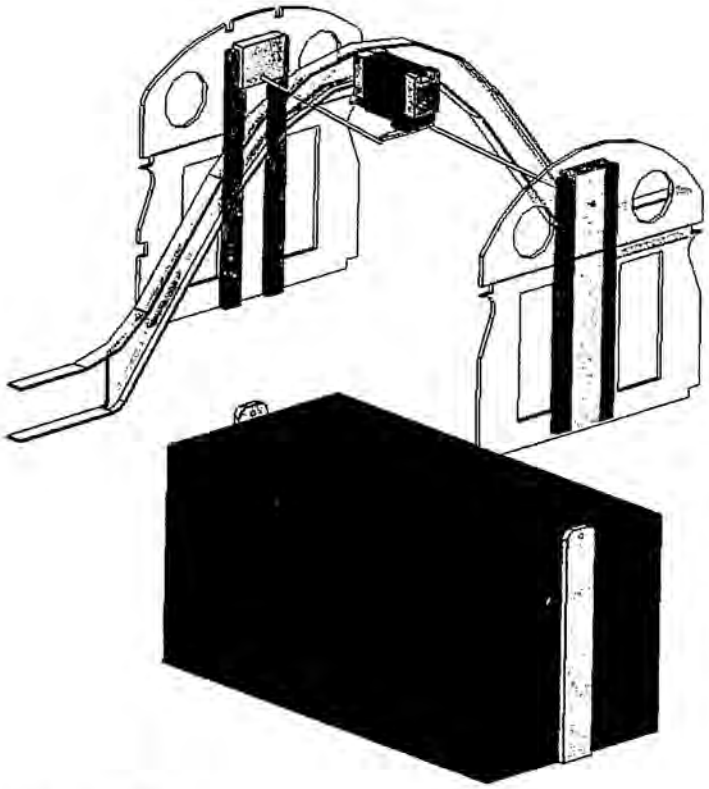

Figure 5.2.15. Deployment mechanism.

5.2.6. Landing Gear. Considerations for the landing gear design were based on drag, ground handling, weight, stopping ability, and compatibility with a rapid payload deployment system. Both stopping ability, and compatibility with a rapid payload deployment system have an effect on mission-effectiveness through the time required to stop and deploy the payload during the SDM. Table 5.2.4 shows the decision matrix used for choosing the landing gear. Based on these results, Robart retracts with BVM Jets proportional brakes were selected.

Landing Gear	Drag	Handling	Weight	Time	Cost	Total
Weighting Factor	3	1	1	2	1	
Fixed Tail Dragger, no brakes	0	-1	0	-1	1	-2
Fixed Tail Dragger, brakes	0	-1	0	0	-1	-2
Retractable Tail Dragger, no brakes	1	-1	-1	-1	0	-1
Retractable Tail Dragger, brakes	1	-1	-1	0	-1	0
Fixed Tricycle, no brakes	-1	0	-1	0	1	-3
Fixed Tricycle, brakes	-1	0	-1	1	-1	-3
Retractable Tricycle, no brakes	1	0	0	0	0	3
Retractable Tricycle, brakes	1	0	0	1	-1	4

Table 5.2.4. Landing gear selection matrix.

5.3. Final Aircraft Specifications

Given the detail design decisions laid out previously, the final design for Utah State University's competition aircraft is given in Table 5.3.1.

Geometry	**Value**
Length, (ft)	4.58
Span, (ft)	9.83
Height, (ft)	1.5
Wing Area, (ft^2)	8.85
Aspect Ratio	10.92
Horizontal Stabilizer Volume, (ft^3)	3.06
Elevator Volume, (ft^3)	1.35
Vertical Stabilizer Volume, (ft^3)	1.01
Rudder Volume, (ft^3)	1.09
Ailerons Volume, (ft^3)	5.4
Main Wing Airfoil, (ft)	Eppler 584
Horizontal/ Vertical Stabilizer	NACA 0009
Weight Statement	**Value**
Airframe, (lbf)	9.6
Propulsion System, (lbf)	7.5
Control System, (lbf)	0.75
Payload, (lbf)	5 & 5.75
Manufactures Empty Weight (MEW), (lbf)	17.85
Gross Weight, (lbf)	22.85 & 24.35
Systems	**Details**
Radio	10 Channel JR 10X
Servos	6 X Hitec NES 517
Speed Controller	1 X Astroflight 204D
Battery Configuration	48X1700-mAhr Diversity Model Aircraft
Motor	1 X Astroflight 691
Gear Ratio	1:1
Propeller(s) (nominal)	Bolly 18X18 or 20X18
Brakes	BVM Jets #5688
Landing Gear	Robart #630, #640

Table 5.3.1. Geometry and weight statement.

5.3.1. Drawing Package. The following assembly drawing package does not include the full set of manufacturing prints that was used to build the aircraft. The assembly drawings include:

5.3.2. Rated Aircraft Cost Calculation. As required by the contest rules, a detailed rated aircraft cost worksheet is included in Table 5.3.2. These values represent the design as presented in this report.

	Value	Computation		Cost (k$)
MEW	17.85 lbf	0.1 k$/lbf(MEW)		1.785
REP			**(lbf)**	
Number Engines (N_e)	1	$[1+.25(N_e-1)]W_b$	5.0	
Battery Weight (W_b)	5.0 lbf	1.5 k$/lbf(REP)		7.500
MFHR			**(hrs)**	
Wingspan (b_w)	9.83 ft	8 hrs/ft(b_w)	78.6	
Max Chord (c_{max})	0.9 ft	8 hrs/ft(c_{max})	7.2	
Wing Control Surfaces (N_{wcs})	2	3 hrs/surface(N_{wcs})	6.0	
Fuselage Length (l_{max})	4.58 ft	10 hrs/ft(l_{max})	45.8	
Vertical Surfaces (N_{vs})	0	5 hrs/surface(N_{vs})	0.0	
Vert. Control Surfaces (N_{vcs})	1	10 hrs/surface(N_{vcs})	10.0	
Horiz. Control Surfaces (N_{hcs})	1	10 hrs/surface(N_{hcs})	10.0	
Servo/Controllers (N_{sc})	7	5 hrs/servo(N_{sc})	35.0	
Number Engines (N_e)	1	5 hrs/engine(N_e)	5.0	
Number Propeller (N_p)	1	5 hrs/engine(N_p)	5.0	
Total MFHR		0.02 k$/hr(MFHR)	**202.7**	4.053
RAC				**13.338**

Table 5.3.2. Rated Aircraft Cost computations for the final aircraft, as designed.

5.4. Final Aircraft Performance Analysis

With a final aircraft geometry and weight determined and the flight speeds and maneuvers known, the method of Phillips and Snyder (2000) was used to determine the flight characteristics of the aircraft.

5.4.1. Aerodynamic Coefficients and Derivatives. Using the method of Phillips and Snyder (2000), all of the aircraft's stability, control, and damping derivatives were calculated for takeoff, cruise, and turning flight. Table 5.4.1 lists the derivates for cruising flight.

5.4.2. Static Stability. The most common measure of an aircraft's flight stability is static margin. For the design presented, the static margin over the lift coefficient range that will be encountered in level flight is shown in Fig. 5.4.1. These values include the influence of the propeller and fuselage.

5.4.3. Dynamic Stability. In order to characterize the flying qualities of the aircraft, a complete dynamic stability analysis was performed. This was done using the method of Phillips and Snyder (2000) to compute the stability and damping derivatives. An original code was used to compute the five dynamic stability modes as shown in Table 5.4.2. All calculations included the contribution of the propeller and fuselage. This analysis revealed a divergent spiral mode with a very short doubling time during takeoff. This is usually attributed to excessive yaw stability. The original vertical stabilizer was sized to have a yaw stiffness in the range of 0.06. With such a short aircraft and a large aspect ratio wing, these values were overly stiff. In order to alleviate this problem, the vertical stabilizer was reduced in size by over 25%. This design change increased the spiral mode doubling time, reduced weight and drag, and simplified the design.

Stability Derivatives		Control Derivatives		Damping Derivatives	
$C_{L,\alpha}$	5.8665	$C_{L,\delta a}$	0.0000	$C_{L,\bar{p}}$	0.0000
$C_{D,\alpha}$	0.0349	$C_{D,\delta a}$	0.0000	$C_{D,\bar{p}}$	0.0000
$C_{L,\alpha}$	0.0000	$C_{Y,\delta a}$	-0.0284	$C_{Y,\bar{p}}$	-0.0613
$C_{\ell,\alpha}$	0.0000	$C_{\ell,\delta a}$	-0.5349	$C_{\ell,\bar{p}}$	-0.6827
$C_{m,\alpha}$	-1.3394	$C_{m,\delta a}$	0.0000	$C_{m,\bar{p}}$	0.0000
$C_{n,\alpha}$	-0.0034	$C_{n,\delta a}$	0.0347	$C_{n,\bar{p}}$	0.0261
$C_{L,\beta}$	0.0000	$C_{L,\delta e}$	0.5608	$C_{L,\bar{q}}$	4.0333
$C_{D,\beta}$	0.0000	$C_{D,\delta e}$	-0.0145	$C_{D,\bar{q}}$	0.1122
$C_{Y,\beta}$	-0.2306	$C_{Y,\delta e}$	0.0000	$C_{Y,\bar{q}}$	0.0000
$C_{\ell,\beta}$	-0.0350	$C_{\ell,\delta e}$	0.0000	$C_{\ell,\bar{q}}$	0.0000
$C_{m,\beta}$	0.0000	$C_{m,\delta e}$	-1.3207	$C_{m,\bar{q}}$	-8.5377
$C_{n,\beta}$	0.0421	$C_{n,\delta e}$	0.0000	$C_{n,\bar{q}}$	0.0000
$C_{m,\dot{\alpha}}$	-2.7262	$C_{L,\delta r}$	0.0000	$C_{L,\bar{r}}$	0.0000
$C_{L,\dot{\alpha}}$	-1.1483	$C_{D,\delta r}$	0.0000	$C_{D,\bar{r}}$	0.0000
		$C_{Y,\delta r}$	0.1471	$C_{Y,\bar{r}}$	0.0931
		$C_{\ell,\delta r}$	0.0086	$C_{\ell,\bar{r}}$	0.0910
		$C_{m,\delta r}$	0.0000	$C_{m,\bar{r}}$	0.0000
		$C_{n,\delta r}$	-0.3500	$C_{n,\bar{r}}$	-0.0312

Table 5.4.1. Aircraft aerodynamic derivatives for cruising flight.

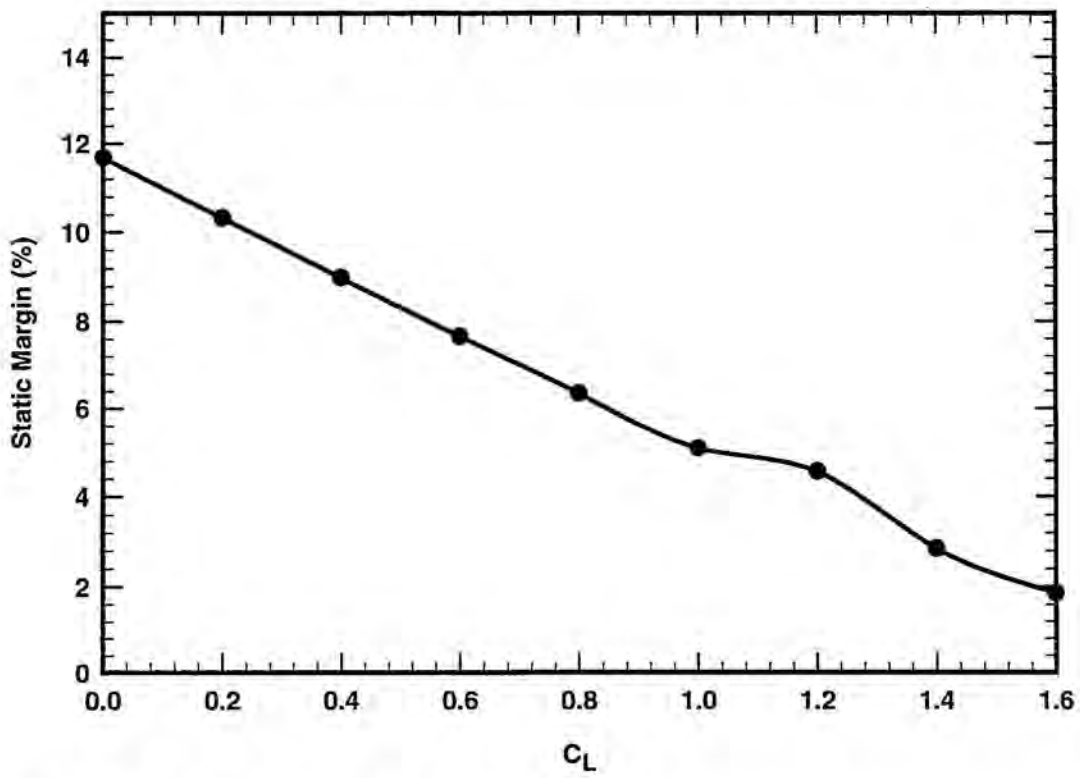

Figure 5.4.1. Aircraft static margin as a function of lift coefficient.

Short	Damping Rate (1/sec)	ωn (1/sec)	ωd (1/sec)	Period (sec)	ζ	99% Damping / Doubling Time (sec)
Takeoff	4.1661	6.3049	4.7324	1.3277	0.6608	1.1054
Cruise	12.7388	20.0834	15.5263	0.4047	0.6343	0.3615
Turn (5g)	12.7422	20.0501	15.4804	0.4059	0.6355	0.3614
Phugoid						
Takeoff	-0.0045					153.2080
Cruise	0.0451	0.3193	0.3161	19.8758	0.1414	102.0050
Turn (5g)	-0.0063					109.8680
Roll						
Takeoff	13.3633	2.232E-08			-4.11E-08	0.3446
Cruise	43.2992	8.212E-06			1.87E-04	0.1064
Turn (5g)	12.7422	20.0501			0.6355	0.3614
Spiral						
Takeoff	-0.2773					2.4992
Cruise	-0.0220					31.5224
Turn (5g)	-0.0063					109.8540
Dutch Roll						
Takeoff	0.8381	2.5219	2.3785	2.6417	0.3324	5.4945
Cruise	0.8322	6.8578	6.8071	0.9230	0.1214	5.5335
Turn (5g)	0.8091	6.8100	6.7618	0.9292	0.1188	5.6916

Table 5.4.2. Dynamic stability modes of final aircraft for critical operating conditions

5.4.4. Predicted Performance. The predicted performance of the aircraft for MDM and SDM are given in Table 5.4.3. Based on the flight model developed, MDM and SDM flight scores have a combined flight score of 0.90. Assuming an assembly time of 30 seconds and a generous report score of 100 the score for Utah State University's entry would be 6.748.

Aircraft Performance		MDM	SDM Loaded	SDM Empty
Takeoff	Distance (ft)	115.8	100.8	68.3
	Time (s)	4.7	4.1	2.9
Landing	Distance (ft)	165.5	161.6	124.0
	Time (s)	5.2	5.2	4.6
Maximum Climb	Rate (ft/min)	726	786	834
Turning	Load Factor (g's)	8.0	8.0	8.0
	Rate (deg/sec)	134.8	111.4	104.2
	Radius (ft)	46.1	67.6	77.3
Flight Speeds	Stall (ft/sec)	36.3	35.4	31.1
	Cruise (ft/sec)	108.5	131.4	140.5
Max Lift Coefficient		1.6	1.6	1.6
L/D	Max	18.1	27.3	27.3
	Cruise	4.4	6.1	5.5
Flight	Time (min)	1.81	1.97	
	Score	0.526	0.377	
Total Flight Score		0.903	**SCORE**	6.748

Table 5.4.3. Predicted aircraft performance for competition.

6. MANUFACTURING PLAN

A primary concern in the design process is the fact that the resulting aircraft must be manufactured in a relatively short period of time, with a limited amount of resources. Manufacturability was considered throughout the design process. To best meet design requirements, the aircraft must be constructed using the best combination of materials and manufacturing processes. To achieve these goals an outline was created to guide manufacturing decisions. This plan defines manufacturing figures of merit, analytical methods for comparison and lead-time prediction, and a schedule.

6.1. Figures of Merit

A list of FOM was prepared for the manufacturing plan. These factors were used to quantitatively compare the manufacturing options and provide a basis for the optimum selection of materials and processes. Decisions were made more objectively using the FOM when choosing the manufacturing processes for various components of the aircraft. The list was designed to aid in the elimination of construction techniques that would be too costly, too time consuming, too difficult to realize or adversely affect the competition score. The figures of merit are as follows:

6.1.1. Availability of Materials (AOM). An obvious limiting factor to the choice of any manufacturing process is the availability of the material or equipment required to carry out that process. If access could not be gained to necessary materials or machinery, the process received a –1. If lead times were long or access was difficult the process received a 0. If everything necessary was readily attainable the process received a 1.

6.1.2. Required Skill Level (RSL). Many manufacturing processes require extensive training and skill to execute effectively. If a process was beyond the expertise available, it received a –1. If the skills required to complete a process were available, but limited, it received a 0. If the expertise to carry out the process was readily available, it received a 1.

6.1.3. Time Required (TMR). A little more than a month is scheduled to build and test the aircraft. If a process required a time period of two weeks or more, it was given a –1. If a process could be completed within a four-day to two-week period, it was given a 0. Any process that could be realized in four days or less was given a 1.

6.1.4. Strength and Reliability (SAR). It was essential that each process reliably produce components that met the aircraft's design and strength requirements. If a process was undependable and thus unable to produce desirable components it was given a score of –1. If a process' reliability was questionable it was issued a 0. If a process could reliably produce quality components it was given a 1.

6.1.5. Actual Component Cost (ACC). A relatively tight budget limited the cost of the final aircraft and individual team members were required to raise the funds necessary for its construction. While the actual cost of manufacturing will not affect the final score, it will affect the team's ability to complete the project. Manufacturing processes that were beyond the financial means available received a –1. Any process considered costly but within the budget received a 0. If a process was inexpensive or donated free of charge it received a 1.

6.1.6. Estimated Component Weight (ECW). The weight that a component adds to the aircraft is detrimental in terms of performance and RAC. For purposes of optimization each process available was compared in terms of the estimate weight of the component built with that process. The processes were scored from lightest to heaviest with 1, 0, -1.

6.2 Manufacturing Processes Investigated

In a process parallel with the design of aircraft components, potential materials and construction methods were researched and analyzed. Though many manufacturing choices were immediately ruled out, some manufacturing options could not be finalized until the very end of detail design. Several of the most important choices were made concerning the wings, empennage, and fuselage.

6.2.1. Wings. The best initial option for the high load factor wing seemed to be the use of a carbon fiber structure and several full-scale wings were built and tested. A full-scale carbon fiber covered Rohacell foam wing and a carbon fiber covered built-up balsa wing were tested. Quality carbon fiber skin structures proved to be difficult to build without very costly tooling. Several designs utilizing a wing spar were also considered. Designs had to incorporate a non-permanent wing joiner mechanism. Mechanisms consisting of one or more plug-in spar pieces of varying cross-sectional shape were investigated. Materials analyzed for each joiner included carbon fiber composites, steels, titanium, and aluminum.

6.2.2. Empennage. Preliminary empennage designs consisted of several boom-mounted and plate-mounted detachable structures. Stability requirements and fuselage geometry made the use of an integral tail boom advantageous. The tail feathers themselves were to be either built-up balsa, balsa skinned foam, or composite skinned foam.

6.2.3. Fuselage. The primary fuselage structure had to be constructed of either built-up balsa, balsa sheeted foam, or glass sheeted foam due to limited resources and experience. Critical secondary structures such as the fuselage spar, the motor and landing gear mounts, and the drop mechanism could be manufactured by different methods. Various aluminum, steel, and carbon-fiber geometries were considered for use in the fuselage spar and landing gear mounts. Metallic designs requiring welding, heat-treating, machining, and/or casting operations were all examined and compared.

6.3 Analytic Methods Used

Materials and processes to be used in building an aircraft must be properly compared using quantifiable ratings. Each FOM was given a weighting value that was indicative of its importance. Scores were given to each process based on the FOM. The RSL scores were based on Table 6.3.1. This table lists the number of team members that have skills in each of the processes considered. Table 6.3.2. illustrates how the FOM chosen were used to determine the methods and materials to be used for the aircraft.

Available or Required Skills	CNC Milling	Lathe Work	Wood Working Skills	Carbon Filament Winding	Carbon Composite Lay-ups	Foam Hot-Wiring	Balsa/Plywood Framing	Balsa Sheeting	Fiberglass Sheeting	Model Painting	Monokote Application	R/C Aircraft Modeling
Number of Personnel	1	1	11	0	2	6	8	2	5	4	3	3
FOM Score	0	0	1	-1	0	1	1	0	1	1	0	0

Table 6.3.1. Skill matrix displaying the number of team members possessing required skills.

		AOM	RSL	TMR	SAR	CST	W 6	Total
	Weighting Factor	2	1	2	2	1	3	
Wings and Empennage	Foam Core w/ Composite Skin	0	-1	-1	1	-1	-1	**-5**
	Foam Wing w/Spar and Balsa Skin	1	0	1	0	1	1	**8**
	Ribbed Balsa Build-up w/ Composite Skin	0	0	0	1	-1	0	**1**
	Ribbed Spar Structure w/ Balsa Skin	1	-1	0	0	1	1	**5**
Wing Spar	Cylindrical Composite Spar	0	-1	0	1	0	0	**1**
	Composite I-beam	0	0	0	1	0	1	**5**
	Aluminum Tube	1	-1	1	1	0	-1	**2**
Fuselage Spar	Aluminum Truss	1	-1	0	1	-1	0	**2**
	Composite I-beam	0	0	0	0	1	1	**4**
	Composite Box Beam w/ Foam Core	0	0	0	-1	1	0	**-1**
Fuselage Frame	Balsa and Plywood Build-up	1	1	0	1	1	0	**6**
	Foam Core w/ Balsa Skin	1	-1	1	0	1	0	**4**
	Foam Core w/ Fiberglass Sheeting	1	-1	0	0	0	0	**1**
Fuselage/WingTransistion Section	Foam w/ Balsa Skin	1	0	-1	1	1	1	**6**
	Foam w/ Fiberglass Sheeting	1	0	-1	1	0	0	**2**
	Balsa Build-up w/ Balsa Strips for Skin	1	-1	-1	1	1	1	**5**
	Balsa Build-up w/ Composite Skin	0	-1	-1	1	1	1	**3**

Table 6.3.2. Manufacturing processes considered for each of the major components of the aircraft

6.3.1. Critical Path. During a production process, dependencies always exist between steps. Recognizing these dependencies is essential to minimizing the production time. The critical path method of Walker (1999) was used to determine these dependencies and estimate the time required to build the aircraft from start to finish. This method determines which processes must be done on time to not delay the end date. It also finds which processes have slack time and how much. It can find processes that can be done in parallel that may not have been obvious. An example of this method is shown in Fig. 6.3.1, which shows a spanning tree that contains all of the necessary processes to build the wings. The process description and dependencies are outlined in Table 6.3.3.

	Process Description	Dependencies	Time Est. (man-hr)
A	Hot-Wire the Foam Core.	-	3
B	Build Joiner Blocks.	-	4
C	Build Composite Spar	B	8
D	Assemble Spar and Wing Core	A, C	3
E	Place Control Linkages	D	3
F	Carve the Leading Edge	-	3
G	Glue Balsa Into Sheets	-	2
H	Carve Wing Tips	-	3
I	Glue Skin in Place	E, G	2
J	Carve openings and Place Servos	I	3
K	Attach Tips	H, I	1
L	Attach the Leading Edge	F, I	1
M	Sand and Apply Monokote to Skin	J, K, L	4

Table 6.3.3. Required processes for wing construction and dependencies for each step.

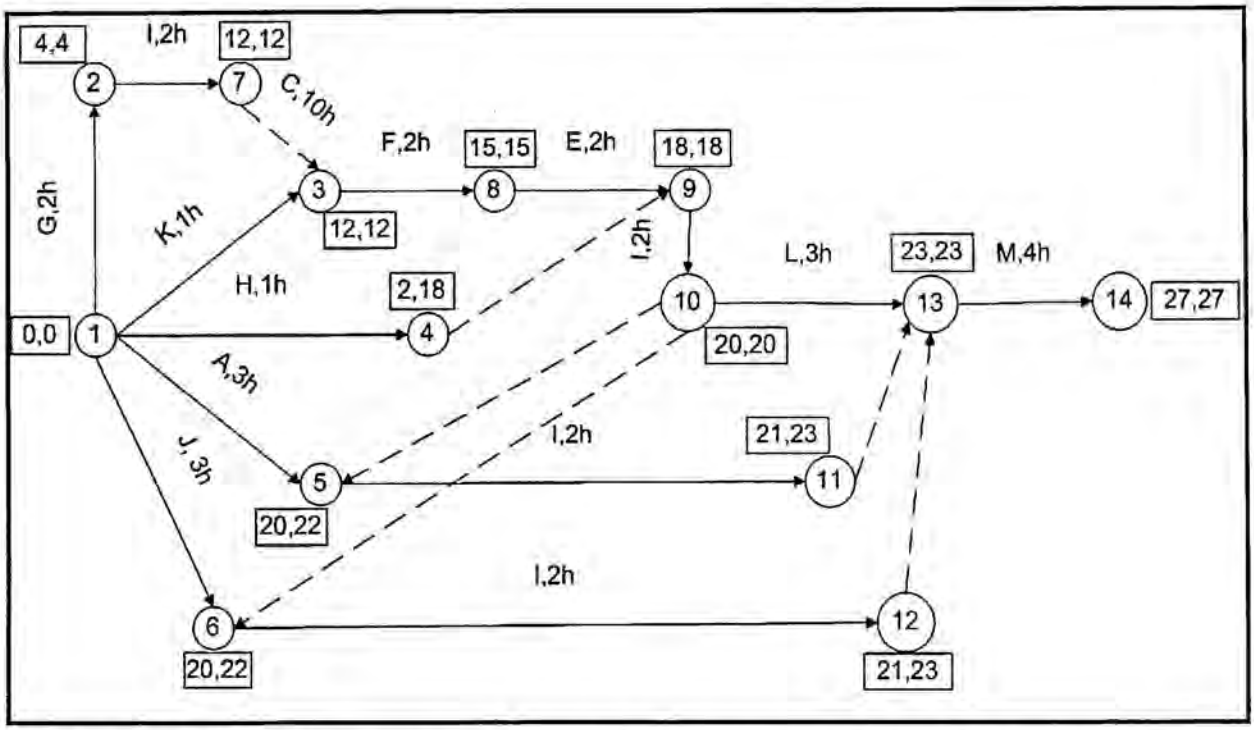

Figure 6.3.1. Critical path spanning tree, depicting necessary steps in the wing construction. Arrows indicate steps and circles mark start and end points. The critical path is marked in red. The values in the boxes indicate when the next step can be started and when the preceding step must be finished to not delay final completion. The dotted arrows indicate multiple dependencies preceding a step.

6.4 Processes Selected for Manufacture of Major Components

After selection of the optimum manufacturing processes, a detailed plan was prepared describing how these processes will be implemented in the construction of the major components of the aircraft.

6.4.1. Wing. The wings will be built of a foam core and a balsa skin. The process that will be used to build the wing was implemented by previous DBF teams. The foam is shaped using a "hot wire". The shape of the airfoil is cut using aluminum templates machined on a CNC mill. Channels in the foam made at this point and the linkages that control the twisterons will be placed. The skin is made from 4x48 in sheets of 1/16-in balsa. The sheets are trimmed to produce a flat edge and then a thin coat of CA glue is used to bond them edge-to-edge. The foam is then coated with a thin coat of slow cure epoxy and the skin is applied. Because the shape of the leading edge and the wingtips are critical to aerodynamic performance they will be carved from balsa and glued to the foam. Openings are then cut for the servos. The balsa is then lightly sanded before a layer of Monokote is applied. The control surfaces will then be cut out of the wing with a straight edge and a razor. They will be hinged on top with a strip of fiberglass tape bonded between the balsa and the foam.

A carbon fiber composite I-beam design was chosen to serve as the wing spar. 4 ft sections of 1 1/4-in square steel tubing will be used as molds. The forms will be wrapped with peel ply material to aid in the removal of the forms from the spar. A sheet will then be constructed consisting of four layers of 0.010-in unidirectional carbon composite (CC) laid at angles of 0, 90, 45 and -45 degrees. Two 1.75x48-in strips will be cut from this sheet. These two strips will then be placed face to face and then clamped between

the forms. The excess material in each sheet will then be folded back onto the top and bottom of the forms making the I-shaped web. The flanges, which are composed of a varying number of uni-directional lamina, will then be laid on the top and bottom of the web and clamped via two more steel molds.

A 1 1/8-in outer diameter 7075-T6 aluminum tube will be used to transfer the wing loads from the wing spar to the fuselage spar. The connection tube will be machined to precisely fit into spar end blocks of machined glass phenolic. The end blocks are 1 1/4 x 1 1/4 inches along the cross-section with a 1 1/8 inch diameter hole bored to a depth of 2.0 in. The blocks are tapered on the opposite end for transition into the web of the spar. The end blocks are sandwiched between the two strips of the web and the flanges. The assembled beam is then wrapped in a layer of shrink-tape and cured.

6.4.2. Empennage. The vertical and horizontal stabilizers will be hot-wired foam cores with balsa skins. The elliptic tips on the horizontal stabilizer will be carved from solid balsa. Both stabilizers will be built to their full span and covered with Monokote. Then the control surface hinges and removable sections will be cut out. Both control surface hinges must allow deflection of 90 degrees for storage. An aluminum piano style hinge will be used for the rudder to allow for equal deflection in both directions. The elevator will be hinged with tape on the bottom side. Here, the bottom surface must be smooth since the elevator deflections will usually be up.

6.4.3. Fuselage. The fuselage will be a classic built-up balsa construction. In a jig, balsa and plywood bulkheads will be glued to four full-length longerons and two full-length balsa sheets. The balsa sheets form the sides of the rectangular structure, which will later be blended into the wing with the fairing. The carbon fiber fuselage spar and other structural components will be joined to the bulkheads and the sheeted sides. Once landing gear, release mechanism, and control hardware are installed, the top and bottom of the fuselage box will be covered with balsa sheets. A portion of both the horizontal and vertical tail is permanently attached to the fuselage. After the fairing is attached the entire structure, except the tail feathers, will be covered with 2 oz. glass cloth, filled, polished, and painted.

A carbon fiber composite I-beam design was also chosen for the curved fuselage spar. This spar will be built in the same way as the wing spar with a few differences. The curved forms will be cut from particle board which will be broken if necessary to remove them from the spar after curing. The two sheets of the shear web will be cut from the four-lamina web sheet to the shape of the forms by laying the forms on the sheet and using a gauging block to keep the knife blade the correct distance from the forms. Relief cuts must be made in the flange attachments before it is folded back to accommodate the curves. The curved spar must be clamped between two molds and the end blocks must be fixed during cure to ensure proper alignment of the wings.

Making a smooth transition from the wing into the fuselage is critical to reducing drag. However the complex curves designed to accommodate this transition are difficult to build. It was this difficulty that necessitated the use of a foam core with a fiberglass skin. Table 6.3.2. shows that for other areas of the aircraft, the balsa skin has usually been chosen because of the ECW. But in this case the geometry is so complex that an easier and quicker method had to be used. The foam will be hand shaped using a hot wire. Then a layer of 2 oz fiberglass cloth will be applied and painted.

6.5 Manufacturing Milestones

An integral part of the manufacturing plan is the schedule. Figure 6.5.1 lists the major components of the aircraft and the time periods over which they are to be built and tested. Milestones and time allotted for the building and testing of the aircraft are outlined with horizontal bars. The blue bars represent the planned schedule while the pink bars show the time periods over which the events actually occurred.

ID	Task Name	Start	Finish
1	**Structural Testing**	**Sep 2**	**Mar 7**
2	Build & Test Composite Wings	Sep 12	Nov 8
3	-Actual-	Oct 23	Dec 3
4	Build & Test Composite Spars	Jan 21	Feb 18
5	-Actual-	Jan 21	Mar 7
6	**Manufacture Preparation**	**Jan 1**	**Feb 27**
7	Order & Receive Materials	Jan 30	Mar 16
8	Order & Receive Factory Components	Jan 20	Mar 16
19	**Build Aircraft**	**Mar 10**	**Apr 1**
20	Wing	Mar 10	Mar 22
9	Hot-Wire Core	Mar 10	Mar 10
10	Composite Spar	Mar 10	Mar 11
11	Empennage	Mar 10	Mar 20
12	Hot-Wire Cores	Mar 10	Mar 10
13	Fuselage	Mar 10	Mar 25
14	Fuselage Spar	Mar 26	Mar 26
15	Cut Bulkheads & Structure	Mar 10	Mar 13
16	Final Assembly	Mar 26	Mar 28
17	**Final Preparation**	**Mar 29**	**Mar 31**
18	Test Mounts and Linkages	Mar 31	Apr 1

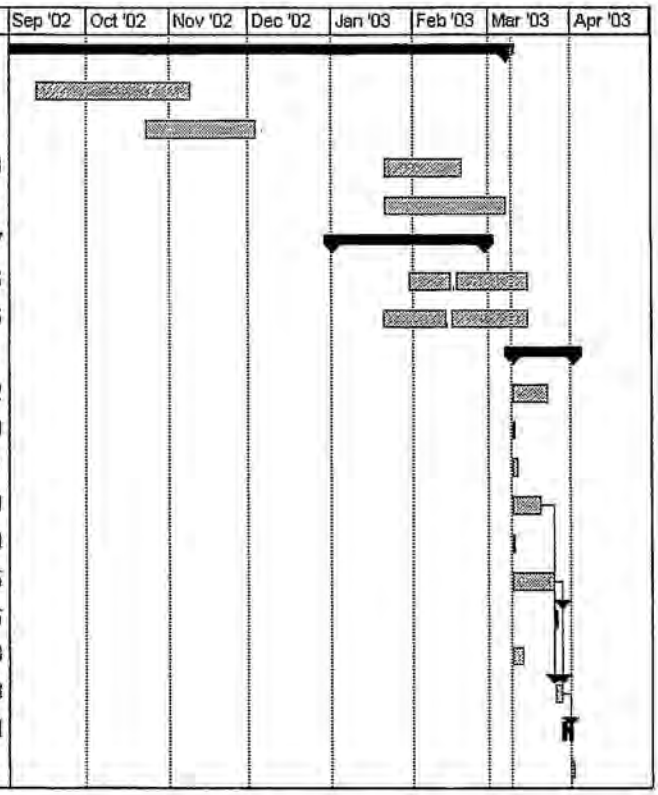

Figure 6.5.1 Manufacturing schedule.

7. TESTING PLAN

Testing is vital to the development of the design of the aircraft and to the formulation of the manufacturing plan. Questionable analytical data is either confirmed or refuted, and new designs are proven, or shown to be deficient. The following testing plan is devised to ensure that the overall analysis was as accurate as possible, to identify possible design flaws or manufacturing oversights, and to tweak the aircraft so as to make its performance as efficient as possible.

7.1 Test Objectives and Schedule

Components of the design requiring testing were identified and a schedule was set forth. Table 7.1.1 lists the various tests and their objectives, as well as the dates during which they occurred or will occur.

Test	Objective	Dates
Antenna Drag Test	Find drag created by the mock antenna used in MDM	9/02-11/02
Motor/Battery Test	Collect motor and battery performance data	9/02-12/02
Wing Structure Test	Investigate strengths and weights of various wing structures	9/02-1/03
Spar Test	Ascertain the strengths and weights of wing and fuselage spars	1/03-2/03
Final Motor/ Battery Test	Determine motor characteristics and optimize the motor and batteries to specific mission requirements	12/02-2/03
Flight Tests	Confirm or disprove the performance and stability predicted for the aircraft and fine-tune its performance	3/03-4/03

Table 7.1.1. Test objectives and schedule

7.2. Flight Testing Checklists

The success of the design depends on the thoroughness and careful execution of the flight tests. A pre-flight checklist (see Table 7.2.1) was developed to accompany the flight-testing checklist. The pre-flight tests are designed to identify structural fatigue or carelessness in assembly of the aircraft and are to be performed before each flight. The flight testing checklist was designed to methodically monitor the performance of the aircraft through a wide range of flight conditions and was divided into six segments; static thrust test, taxi test, first flight, first sortie, second sortie, and third sortie (see Table 7.2.2).

The static thrust test will be performed by attaching a spring scale to the rear of the aircraft while at full-throttle. This test will measure the static thrust generated by the propeller. The thrust data will serve to fine tune the analytical model and allow for more accurate propeller selection.

Low and high-speed taxi tests will demonstrate aircraft controllability on the ground, while the first flight will assess the controllability and stability of the aircraft through gentle maneuvers in the air.

During the first sortie, low to high-speed maneuvers, including stall and tight radius turning, will be used to assess the yaw stability of the aircraft. If the pilot feels that the aircraft has too much yaw-stability, one inch will be removed from the tip of the vertical stabilizer. Completion of the first sortie will occur once the shortest possible vertical tail span is found without compromising stability of the aircraft.

The second sortie will be used to test the total performance of the aircraft. A radar gun will be used to measure maximum and minimum flight velocities. Take-off distances and turning radii will be measured for both mission configurations and compared to predicted values. Wingspan, propeller selection, and battery packs might all be modified due to the results of these tests. This series of tests has been designed to improve the aerodynamic qualities and test the integrity of the aircraft.

The third sortie will consist of competition simulation. Competition tasks will be reproduced to provide practice and experience for the pilot and team. Areas of improvement will be identified and competition skills will be polished. The payload deployment mechanism will be tested extensively as well.

Weight and Balance-C.G. location (≤2" behind ¼ chord of main wing)				
Control Surfaces/Linkage	Flaperons	Elevator	Rudder	Nose Gear
-Linkages/Clevises properly attached?				
-Hinge integrity? (Tug firmly at control surface.)				
-Proper deflection direction and trim location?				
Motor Mount-18 lb longitudinal load?				
Landing Gear/Brake				
-Air Pressure at 60 psi?				
-Proper retract/deploy of gear and use of brakes?				
-Leak check?				
Wing Tip Test-Aircraft loaded +35 lb and lifted from wing tips w/o structural damage?				
Payload Security Test- Payload loaded to 30 lbs. w/o failure of mechanism?				
Range Test- W/ collapsed antennae, no chatter/interference at 50', w/ motor on and off?				
Fail-Safe- Tx off, elevator full up, flaperons/rudder full right, throttle off, payload in place?				
Miscellaneous-Verify all components secured to aircraft and fasteners tight w/ locktite.				

Table 7.2.1. Pre-flight checklist. All tests must be completed successfully before each flight.

(3/31) Static Thrust Test-Readings from spring scale at full throttle (lbf): _____, _____. *Concerns:*
(3/31) Taxi Tests-Sufficient control of aircraft while taxiing at low velocities? -Sufficient control of aircraft at speeds nearing the rotation velocity? *Concerns:*
(3/31) First Flight- Sufficient control of aircraft through majority of operating conditions? *Concerns:*
(4/1) First Sortie-Sufficient yaw stability throughout flight realm (including stall and high-g turns)? -If yes, remove 1" from vertical stabilizer. (Continue shortening vertical stabilizer until min. tail height is found without sacrificing yaw stability.) *Concerns:*
(4/2-4/4) Second Sortie-Test performance of aircraft: Take off distance: _____ Maximum Flight Velocity: _____ Stall Speed: _____. Take off velocity: _____ Turn Radius: _____ Landing Distance:_____. *Suggested Aerodynamic Improvements:*
(4/5-4/19) Third Sortie-Competition Simulation: MDM Flight Times:_____ SDM Flight Times:_____. *Setbacks and Suggested Improvements:*

Table 7.2.2. Flight testing checklist and schedule. Tests must be successfully completed sequentially.

7.3. Summary of Test Results and Lessons Learned

As each individual test was completed its results were analyzed and used to improve the design. The lessons learned through the testing plan thus far have been invaluable. Published values for cylinder drag and motor and battery performance were found to be highly idealized. Structural testing of mock wings and spars greatly influenced the evolution of the design of the wings and parts of the fuselage. Table 7.3.1 outlines the testing results and the knowledge gained through those tests.

Test	Test Results and Lessons Learned
Antennae Drag	Drag coefficient found to be 67% higher than published values (White 1999)
Motor/Battery Test	Battery resistance 300% higher than the manufacturer's listing. Battery capacity was 110% of the manufacturer's listing. Motor torque 85% of the manufacturer's listing. Peak motor efficiency was 70%, 9% below manufacturer's listing.
Wing Structure Test	All wings tested were strong enough to withstand flight loads. Composite skin wings were heavy and difficult to manufacture. Built-up balsa wings with composite spars were light but difficult to manufacture. Balsa/foam core wings with composite spars were light and easy to manufacture.
Spar Test	Fuselage and wing spars failed near loads predicted by F.E. analysis.
Final Motor/ Battery Test	Motor efficiency was independent of temperature, even after significant heating. Motor torque at max efficiency was found, and propellers were matched accordingly. 18x18 and 20x18 propellers were selected for use in MDM and SDM respectively. The 48 cell 1700 mAhr battery pack provided the best overall performance.

Table 7.3.1. Summary of test results and lessons learned.

REFERENCES

Abbot, I. H., and Von Doenhoff, A. E., (1959), *Theory of Wing Sections*, Dover, New York.

Boresi, A. P., Schmidt R. J., and Sidebottom O. M., (1993), *Advance Mechanics of Materials*, 5th ed., Wiley, New York.

Eppler, R., (1990), *Airfoil Design and Data*. Springer-Verlag, Berlin.

Greenberg, M.D. (1998), *Advanced Engineering Mathematics*, 2nd ed., Prentice Hall, Upper Saddle River.

Hepperle, M., *JavaFoil*, http://www.mh-aerotools.de/airfoils/javafoil.htm, Oct. 24, 2002.

Hoerner, S. F., (1965), *Fluid-Dynamic Drag*, Published by the Author, New York.

Phillips, W. F., and Snyder, D. O., (2000), Journal of Aircraft **37**, 4, pp. 662-670.

Phillips, W. F., (2003), *Lifting-Line Analysis for the Effects of Washout on Performance and Stability, AIAA-2003-0393.*

Phillips, W. F., Alley, N. R., and Goodrich, W. D., (2003), *Lifting-Line Analysis for Roll Control and the use of Twisterons, AIAA-2003-4061.*

Phillips, W. F., (2003), *Mechanics of Flight*, Wiley, New York.

Walker, R. C., (1999), *Introduction to Mathematical Programming*, Prentice-Hall, Upper Saddle River.

White, F. M., (1999), *Fluid Mechanics*, McGraw-Hill, Boston.

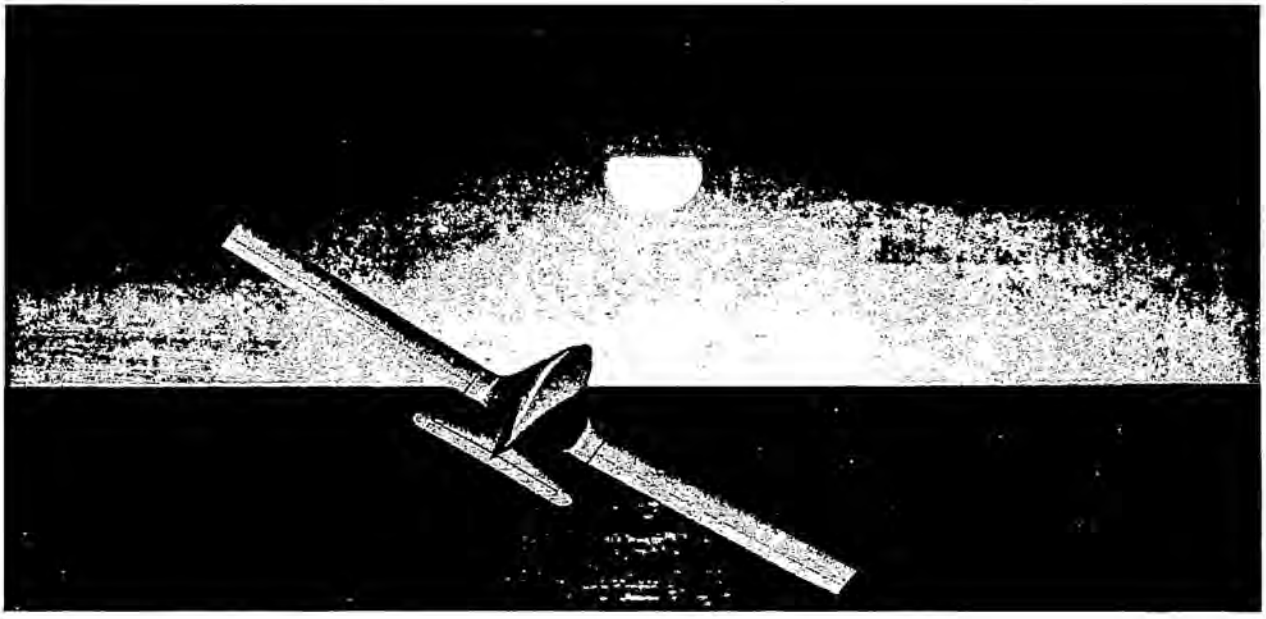

2002/2003 AIAA

Cessna/ONR Student

Design/Build/Fly Competition

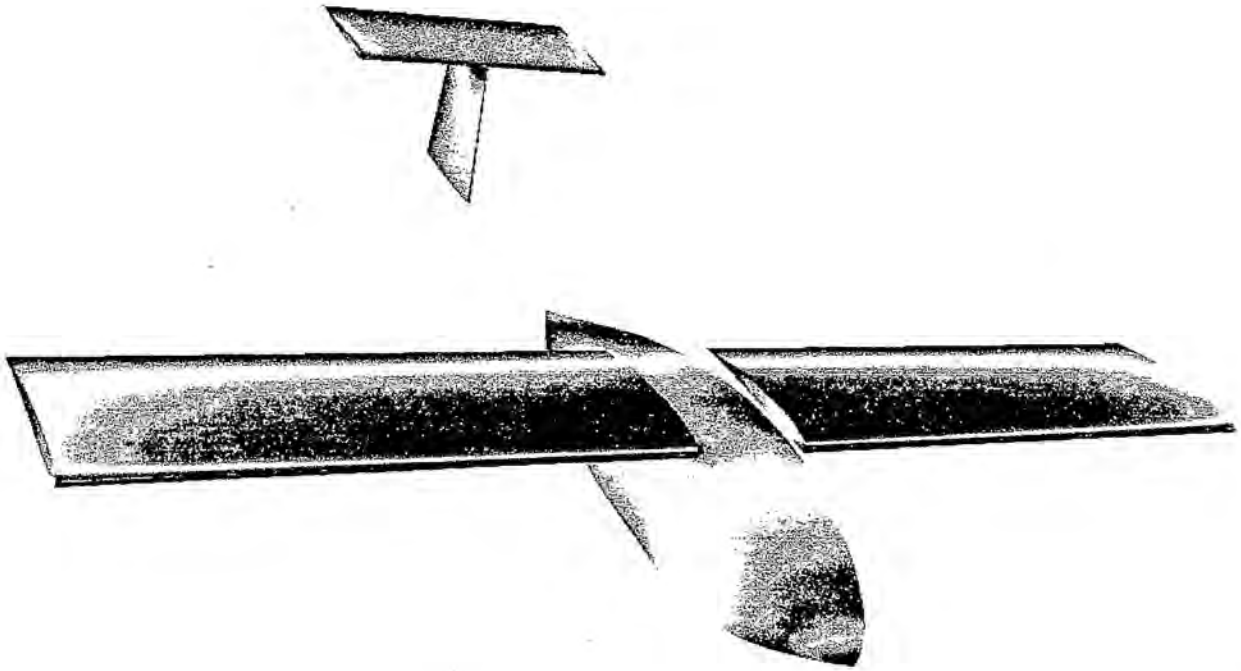

San Diego State University

Spirit of Monty

Table of Contents

1. Executive Summary

The following summarizes the development of "Spirit of Monty", an entry from San Diego State University into the Cessna/ONR Student Design/Build/Fly Competition at St. Inigos, Maryland, on 25-27 April 2003. The competition requires that the students design, fabricate, and demonstrate the airplane that best satisfies the required missions. Three different missions are specified, but only two of the three need to be performed. Depending on the mission there are different types of payloads and flight requirements. The goal is to maximize the Total Score, which is accomplished by scoring the best in three areas. One area is to maximize the flight performance of the aircraft and thereby maximizing the Total Flight Score. Another is to achieve the lowest virtual cost of the airplane called the Rated Aircraft Cost (RAC). Finally, the Report Score must be maximized by well documenting the design, fabrication, and testing process. To accomplish this mission, the team "Spirit of Monty" began its exploration from the conceptual design.

1.1. Conceptual Design

First, the problem statement of the competition was made so that the following assessments would be well targeted. Before investigating alternative designs, some assumptions were made according to calculations as well as to the results from last year's competition entry. These assumptions were necessary to determine the core characteristics of the aircraft such as the minimum planform area and the estimated weight. Next, competition requirements, including a choice of three different missions, were assessed in order to create design parameters for each conceptual design consideration. Evaluating alternative designs of the aircraft with the parameters, conceptual design phase led to one configuration for each of five design considerations, with maximum scoring potentials.

1.1.1. Conceptual Design Considerations

Design considerations included the basic aircraft configuration, payload system, wing configuration, type of the landing gear, and assembly systems. Basic aircraft configurations were discussed such as the conventional with T-tail, conventional with V-tail, conventional with twin-boom, canard, flying-wing, and bi-plane. Concepts for the payload system consisted of a vertical-drop, roll-aft, and roll-front. High-, mid-, and low-wing configurations were evaluated for structural and stability aspects. Type of landing gear resulted in one version without competing concepts. Lastly, effective assembly of the aircraft was examined. Alternative designs for each of these five considerations were evaluated by using the design tools.

1.1.2. Conceptual Design Tools

Design tools included visualization tools, calculation tools, and design parameters that worked in the process of calculations. To visualize alternative designs, Pro-Engineer (CAD) was used to create 3-dimensional images. Excel spreadsheets were one of the main calculation tools, providing a qualitative analysis with embedded programs that were constructed by the team. Design parameters were called

Figures of Merit (FOM). FOM are the factors that would either directly or indirectly affect the scoring potential of the aircraft. Effects of the direct factors, such as RAC, were calculated by the spreadsheet, while effects of the indirect factors were interpreted qualitatively to give the numerical value of the scoring potentials of each alternative design.

1.1.3. Results of the Conceptual Design Phase

The first two of the three specified missions, Mission A and B, were selected for further design because of their scoring potential. Spirit of Monty would be a conventional T-tail (or V-tail) plane with high-wings and a tractor-propeller. Payload would be vertically dropped during Mission B, while the cylinder for Mission A would hang below the fuselage. Wings would be split into two parts in order to fit in the assembly box and the landing gears would be a tricycle configuration: one nose and one on either side of the fuselage. An assembly process was also conceived to allow for a rapid assembly time.

1.2. Preliminary Design

To begin with, schematic drawings of the assembly components of the aircraft were made and were placed in a drawing of the storage box to find a suitable position. This was the foundation to designing the assembly mechanisms. The next step was the determination of the wing design, since it would define the upper surface of the fuselage. Airfoil, planform area, wingspan, and chord length optimization was performed. Using the upper surface of the chosen airfoil (SD7043), the outer mold line of the fuselage came next, followed by the analyses on the tail configurations. Drag and stability of the chosen configuration were evaluated. Power plant and structural analyses were also was performed.

1.2.1. Preliminary Design Considerations

Several assembly methods were considered for each component, from which a concept with the quickest connections was selected. Design considerations for the wing consisted of three different airfoils, including the one from Monty's Revenge, last year's airplane. The fuselage design had two competing concepts concentrating on the trailing edge style. Tail considerations focused on the comparison between T-tail and V-tail. Power plant was designed from different combinations of motors and propellers.

1.2.2. Preliminary Design Tools

Airfoil choice began by researching various airfoils and utilizing the 2-D viscous solver X-FOIL for airfoil optimization. Graphs of C_l vs. α and C_d vs. C_l of different airfoils were used to determine which was best for the mission. Planform area, wingspan, and chord length were determined by designing an Excel spreadsheet, which allowed comparison of RAC values for different combinations. For the fuselage design, X-FOIL was used to create the lowest drag-configuration, and Pro-Engineer (CAD) was used to model it into a 3-D shape. VSAERO, an inviscid 3-D solver, was used to integrate the fuselage, wing, and tail configurations to predict the performance. Lift and drag were numerically calculated and

compared with the computer data. MotoCalc and P-calc, two electric power plant optimization programs, were used to design the power plant configuration.

1.2.3. Results of the Preliminary Design Phase

Final decisions were made on the assembly methods and the configurations of the wings, fuselage, and tail. Component optimization was now complete and estimation of the performance gave satisfactory results to proceed into the detail design.

1.3. Detail Design

The final design was created which included detailed drawings of the major and minor components. Component selection and system layout was also completed. Final Rated Aircraft Cost was determined, which was lower than originally predicted during the early design phase. Performance evaluation, including dynamic stability, was performed to determine if any modifications would be necessary.

1.3.1. Detailed Design Considerations

Since the sizing had been performed and all other specifications of the design are known, the stability and detailed weight tracking were now the focus. Battery placement and the actual weight of the composite materials were only estimated during the previous design phases. To ensure a balanced aircraft a team member was assigned the Mass Properties position to keep track of weights and locations.

1.3.2. Detailed Design Tools

Dynamic stability performance was evaluated by utilizing many sources. Advanced Aircraft Analysis (AAA), a computer aircraft design tool was used to evaluate the stability. Used in conjunction with AAA much of the stability calculations were performed by hand. For that to be accomplished, Pro-Engineer was used to obtain the moments of inertia and other needed measurements. Other performance was recalculated such as take-off distance and maximum rate of climb to compare with the earlier estimations.

Pro-Engineer was the most used tool during the final design phase. Codes were obtained to operate the CNC mill in order to machine the fuselage foam cores. Pro-Engineer was also used to create drawings from the models in order for the Manufacturing Team to build the major components.

1.3.3. Results of the Detailed Design Phase

The final design showed that the extensive work during the Conceptual and Preliminary Design phases benefited the project. The airplane was evaluated to be stable using two separate methods. Take-off distances and other performance characteristics were very close to design parameters

Machining of the foam cores saved the Manufacturing team many hours of shaping it by hand. The team was handed the drawings to begin the fabrication process.

2. Management Summary

Design work started with only five members, who participated in last year's competition. The five gathered in August, after the release of a draft of the 2002/2003 Competition Rules. Greg Marien, the Project Manager, would continue to lead the team, and assigned an Assistant Project Manager and some of the team leaders. As the AIAA Student Chapter at San Diego State University grew dramatically in Fall 2002, the team was able to add members to each design group. Assignment areas for each member depended on both skills and wishes. Ultimately, the team was composed of 1 faculty advisor, 1 graduate student, 12 seniors, 10 juniors, and 5 freshmen.

2.1. Architecture and Responsibilities of the Team

As Figure 2-1 below illustrates the architecture of the team followed by the description of the positions.

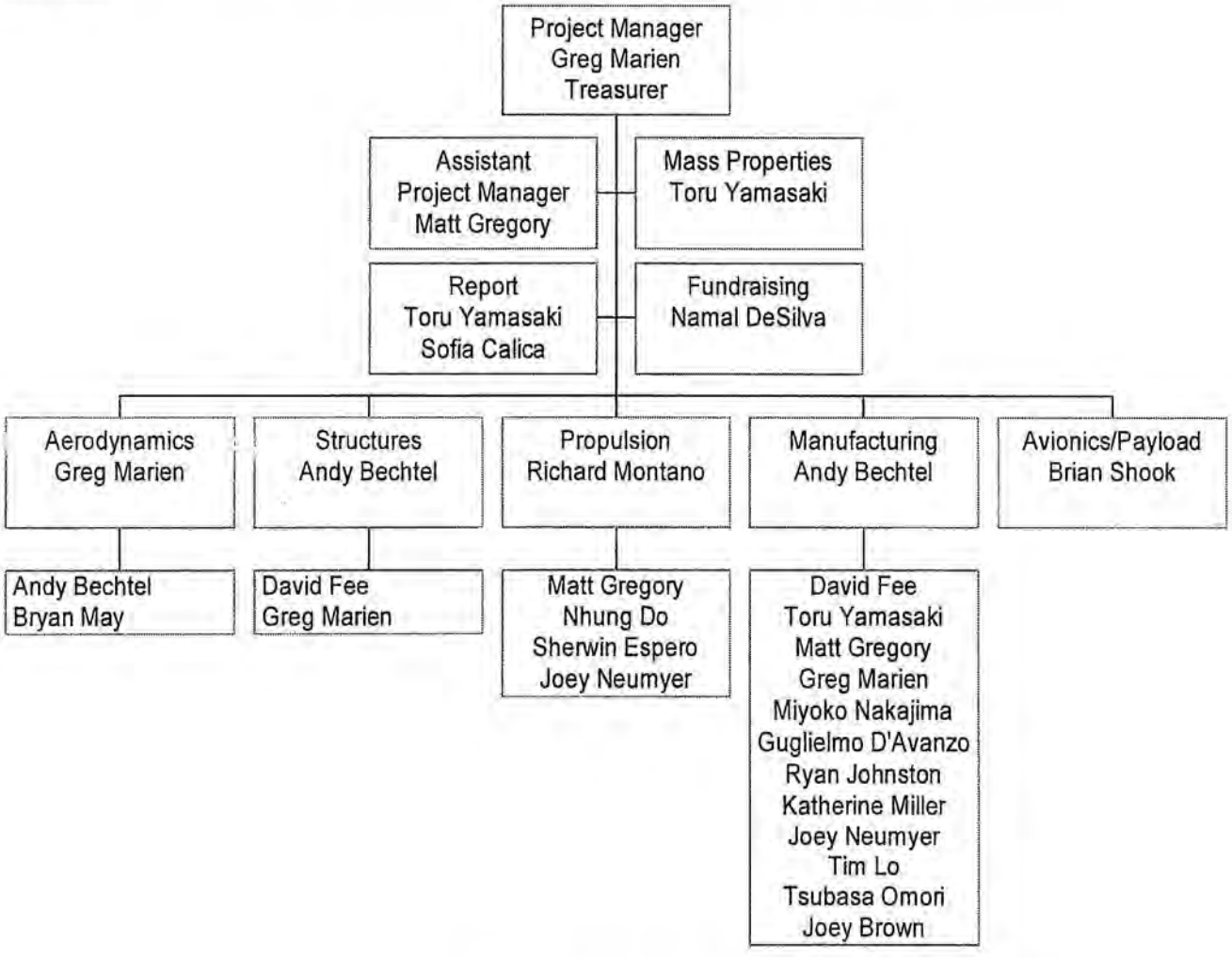

Figure 2-1 Team Architecture

2.1.1. Project Manager

The Project Manager calls the meetings and is responsible for schedule management. Leading the fundraising presentations and approving the budget are also the Project Manager's responsibilities. Important decisions made by the design teams need to obtain recognition from the manager.

2.1.2. Assistant Project Manager

This position was created to train a new Project Manager for the following year. Appointed to the position was a junior member on his second year of Design/Build/Fly participation. The assistant is to be involved with all the aspects of the Project Manager's duties to ensure the transfer of knowledge.

2.1.3. Treasurer

The Project Manager also serves as the AIAA Student Branch Treasurer, so the positions were combined. The treasurer is responsible for the registration of all donors and donations given to the team. The Team Leaders should obtain permission for necessary purchases from the treasurer for reimbursement.

2.1.4. Team Leaders

Responsibilities include organizing each team by assigning duties to individual members, and to report to the Project Manager the status of the group's tasks.

2.1.5. Fundraising

This team organizes fundraising events and presentations. The events include several BBQ's and lunch meetings with permission from the school, and an exposition featuring Monty's Revenge from last year. Also, letters have been sent to alumni, asking for monetary and/or equipment donations. Corporate funding was also received from Northrop-Grumman.

2.1.6. Aerodynamics

This team is responsible for analyzing and aerodynamically optimizing the fuselage, wing, and tail configurations. They are also responsible for stability evaluation.

2.1.7. Power Plant

This team is responsible for wind-tunnel tests on several motor-propeller combinations. Research on the other equipment including batteries is also the responsibility of the group.

2.1.8. Avionics/Payload

This team is responsible for the electrical wiring within the aircraft. The focus is on the security and effectiveness of the connections between assembled parts of the aircraft, as well as the payload interface system.

2.1.9. Structure and Fabrication

This team is responsible for submitting a feasible fabrication plan that met both the budget and skills of the team. Then, the group fabricates the aircraft based on the drawings from the drawing team. Structural analysis and logistics are also assigned to this group.

2.1.10. Drawing

This team is responsible for converting the alternative designs and the final configuration into CAD parts and drawings. This job was a group effort between the Aerodynamics, Structures, and Manufacturing teams.

2.1.11. Report

The Report Team collects the data from the research and development, and compiles it into the final report. The group also provides some design parameters to the other teams, in accordance with the design report requirements from the competition rules.

2.2. Schedule Control

An original milestone plan was made at the first meeting of the team. Table 2-1 on the following page illustrates the comparison between the original plan and actual design processes. Weekly meetings of the Team Leaders along with the Project Manager helped manage the schedule of the design phases. Any changes to the schedule had to be addressed at the weekly meetings and approved by the Project Manager.

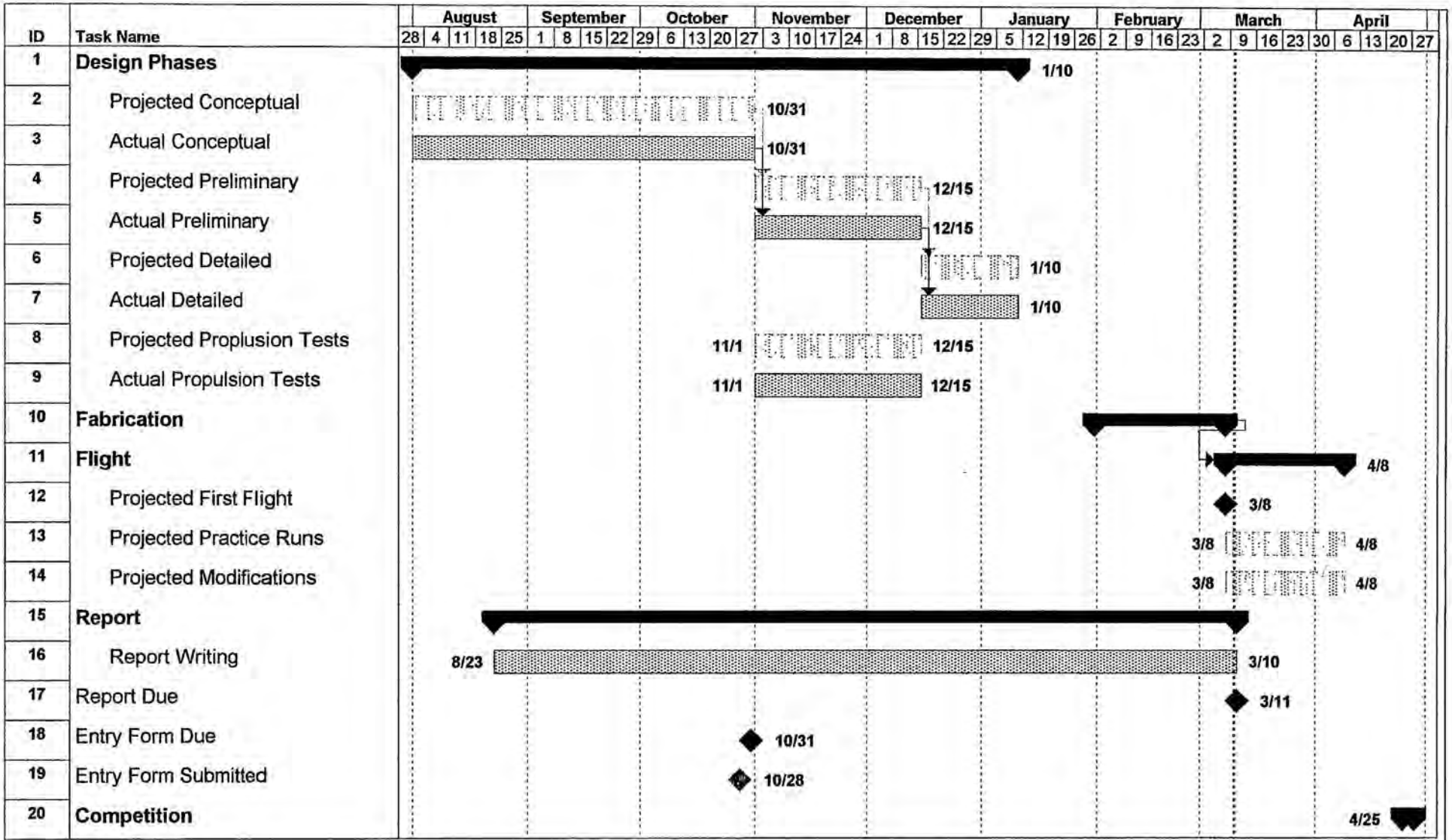

Figure 2-1 Milestones and Schedule

3. Conceptual Design

The conceptual design phase was an investigation of the mission requirements and design considerations, which created the best path to the most competitive design. Alternative designs in each concept competed towards a maximum scoring potential. Design considerations included basic aircraft configuration, payload system, wing configuration, landing gear type, and assembly of the aircraft. For each of the considerations, the best concept was chosen. The remaining structure, shape, sizing, and power plant were evaluated in the preliminary and detail design phases.

3.1. Problem Statement

Total Score of the competition incorporates **Total Flight Score**, **Rated Aircraft Cost (RAC)**, and **Report Score** such that:

$$\text{Total Score} = \frac{\text{Total Flight Score x Report Score}}{\text{Rated Aircraft Cost}}$$

Equation 3-1 Total Score

Report Score was held at 90 (average competition report score) throughout the report for simplicity. Therefore, the conceptual design phase would focus on how **Total Flight Score** and **RAC** affect **Total Score** as they change with respect to alternative design configurations. Following the design analyses, alternatives that offer maximum scoring possibility against the specified missions were selected.

As illustrated in Figure 3-1, the missions would be flown on a specified course to compete toward **Total Flight Score**.

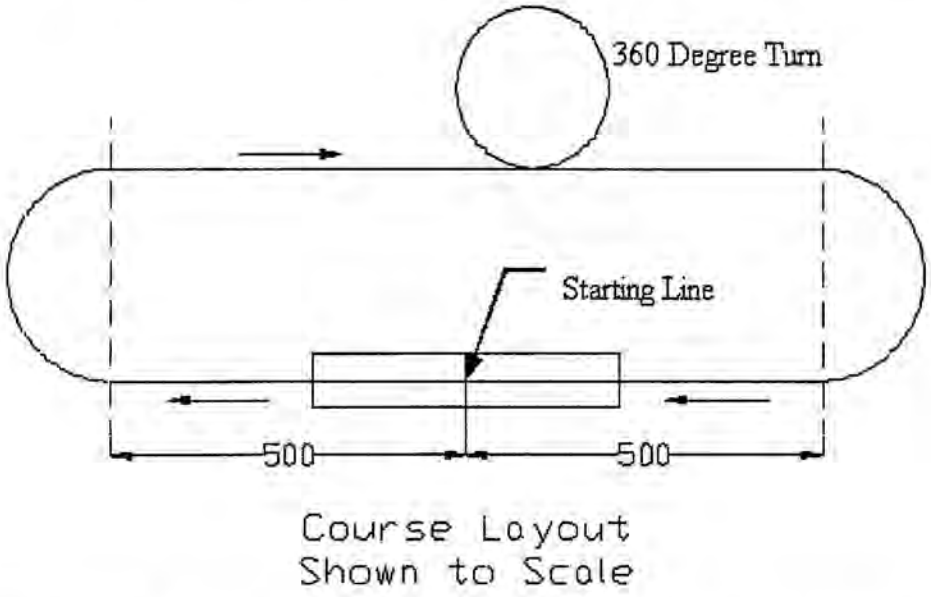

Figure 3-1 Course Description; distances are in feet (reproduced from competition rules)

Total Flight Score is calculated by summing the best **Single Flight Score** (see Equation 3-2) from two of the three missions, A, B, or C. Each of the missions has a numerical difficulty factor of 2.0, 1.5, and 1.0, respectively. Table 3-1 below briefly summarizes the profiles of these missions broken down into its component parts.

$$\text{Single Flight Score} = \frac{\text{Difficulty Factor}}{\text{Mission Flight Time} + \text{Aircraft Assembly Time}}$$

Equation 3-2 Single Flight Score

Mission	A	B	C
Difficulty Factor	2.0	1.5	1.0
Total Laps	4	4	4
# of 180° turns/lap	2	2	2
Total # of 180° turns	8	8	8
# of 360° turns/lap	1	1	3
Total # of 360° turns	4	4	12
Payload	5lb 6"x6"x12" box	5lb 6"x6"x12" box	5lb 6"x6"x12" box
Particular Task	A simulated cylindrical antenna, a section of unmodified 6" PVC pipe 3" tall	Landing and remote deployment of payload after 2 laps	

Table 3-1 Mission Summary

Mission Flight Time is the total time between a "go" signal from the official and the aircraft's complete stop past the starting line after finishing a mission. Included in the **Single Flight Score** is a timed assembly task, which must be performed at least once before the first attempted mission. Prior to the assembly task, the disassembled aircraft must fit in to a 2' X 1' X 4' (inner dimension) box. Three team members are timed on the assembly of the aircraft to make it flight-ready. The wing tip lift test and control system function/orientation test are then performed with a 3-minute penalty added to **Aircraft Assembly Time** for each incorrect operation. This makes the quickness and reliability of assembly an important design parameter.

3.2. Assumptions

Assumptions depended both on calculations and on the data from Monty's Revenge, last year's competition entry. The estimated parameters included the empty/loaded weight, cruising speed, weather conditions, Assembly Time, and RAC. These assumptions were necessary to obtain an estimate of the Total Score on which the design would be based.

3.2.1. Estimated Take-off Weight

Empty weight of the aircraft was set to 12 pounds. This estimation was based upon previous years of fabrication experience. Last year's entry had a 20 pound empty weight and since there is a 4 pound reduction in payload the weight was set to 16 pounds. Furthermore, a reduction in 4 more pounds is achieved from the improved experience in a lighter weight structure and a lighter weight power plant. Therefore, the empty weight was set to 12 pounds and a maximum take-off weight of 18 pounds (5 pounds for box and 1 pound for cylinder).

	lb
Empty weight from last year	20
Payload reduction	4
Structure reduction	4
Estimated empty weight	**12**
Box payload	5
Cylinder payload	1
Maximum take-off weight	**18**

Table 3-2 Estimated Take-off Weight Summary

3.2.2. Estimated Cruising speed

Baseline speed of 100ft/s was used, which was the same speed as last year's competition entry. This speed is only used for initial sizing calculations and estimating flight scores. Further evaluation of the speed is performed in the preliminary design phase. Because this year's design is lighter and more research was to be performed on the power plant, speed was raised to 120 ft/s with the payload box, while the cylinder payload remained at 100 ft/s. The reduction in speed is based on a calculated 2 pounds of cylinder drag from empirical data (Reference 5).

3.2.3. Weather conditions

Historical weather conditions from www.weatherbase.com were used for design considerations. A worst-case scenario of a low atmospheric pressure and a high temperature was used to ensure adequate performance in extreme conditions, shown in Table 3-3 below.

3.2.4. Initial Wing Sizing

Initial wing sizing was based on weather conditions, estimated take-off weight, cruising speed, turn performance and take-off distance (<120 ft). Evaluating different families of possible airfoils (low drag/high lift), a C_{lmax} of 1.6 was used for estimations.

Temperature (T)	100	F			
Pressure (P)	28.75	in Hg	Loaded weight (W)	18.00	lb
Density (ρ)	0.00212	slugs/ft^3	Average velocity (V)	100	ft/s
Viscosity (μ)	3.97E-07	lb-s/ft^2	Takeoff velocity (V)	50	ft/s
Kinematic viscosity (ν)	0.00019	ft^2/s	Dynamic pressure (q)	10.59	lb/ft^2

Table 3-3 Sizing parameter assumptions

Table 3-4 below shows the results of the initial sizing of the wing using the assumptions from Table 3-3 above. The limiting factor was the 4.5-g turn performance; therefore the planform area was set to 5.5 ft^2

Turns	g-loading	4.5	
	ϕ (bank angle)	77.16	degrees
	Turn radius	71.23	ft
	Required planform area	5.50	ft^2
Cruise	Required planform area	3.40	ft^2
Take off	Required planform area	4.86	ft^2

Table 3-4 Planform area requirement to meet the mission

3.2.5. Rated Aircraft Cost (RAC)

The initial working concept must be designed to reduce the RAC as much as possible for the maximum Total Score. There is a limit to the amount of reduction since the concept must still be a stable and flyable design. The following RAC equation is used to simplify the theoretical cost of each team's airplane.

$$RAC = \frac{100 \times MEW + 1500 \times REP + 20 \times MFHR}{1000}$$

Equation 3-3 Rated Aircraft Cost Calculation

Where:

MEW = Manufacturers Empty Weight

REP = Rated Engine Power

MFHR = Manufacturing Man Hours

Table 3-5 below shows a breakdown of the RAC for one conceptual concept.

	RAC	8.71	
	MEW	12.00	
	REP	2.84	
	MFHR	163	
# of cells	24		Sanyo 1700 SCR
weight per cell	1.89	oz	weight includes extra hardware
total battery weight	2.84	lb	

WBS[1]	**Value**	**Hours**	**Multiplier**
1.0 Wings			
wing span (ft)	5.50	44	8 hr/ft Wing Span
chord (ft)	1.00	8	8 hr/ft Max chord
# of control surf	2	6	3 hr/control surface
2.0 Fuselage			
Max length (ft)	5	50	10 hr/ft max length
3.0 Empennage			
# of vertical-nc	0	0	5hr/vertical-no control
# of vertical-ac	0	0	10 hr/vertical-active control
# of horizontal	0	0	10 hr/horizontal-see wing rule
V-tail only		15	v-tail-15 hr
4.0 Flight Systems			
# of servos/control	6	30	5 hr/servo (Note 1)
5.0 Propulsion			
#of engines	1	5	5 hr/engine
#of propellers	1	5	5 hr/propeller

Note 1: 2 ailerons, 2 stabilizer, 1 nose wheel, 1 payload release

Table 3-5 RAC Calculation

3.2.6. Propulsion Configuration

Early in the conceptual phase, use of an Excel spreadsheet shown in Table 3-5 above allowed the removal of a two-motor concept. Using only one motor reduced the RAC by almost 15%, which is significant enough to affect the Total Score.

Using a tractor configuration instead of a pusher was decided early on due to the interference of the pusher propeller and the released payload during Mission B.

[1] WBS is the Work Breakdown Structure. The summation of the WBS is equivalent to the Manufacturing Man Hours

3.2.7. Landing Gear Configuration

Landing gear configuration had two options, tricycle or a tail wheel. First, the released payload would interfere with the tail wheel during the take-off. Second, if the payload release concept was to drop from the fuselage then the payload should be parallel to the ground for ease of deployment. Therefore, the tricycle landing gear was chosen.

3.2.8. Assembly Time

Another assumption was that for the assembly task each step would take 10 seconds; for example, it took roughly 10 seconds to assemble the wings of last year's competition entry, which had a plug-in type design. Three personnel are allowed on the assembly team and therefore up to three steps could be done simultaneously. For example, the time of assembly would be 10 seconds for three parallel tasks. The tasks considered were, assembly of the landing gear, connection of the wing parts, connection of the tail, and connection of the wing to the fuselage. The first three steps would be done in parallel while one person would perform the final step. Total Assembly Time by this estimation is 20 seconds, but 10 more seconds were added for the unforeseen circumstances factor. The final estimated Assembly Time was set to 30 seconds. Further sizing and configuration will reduce this time to a minimum.

3.2.9. Estimated Total Score

Total Score predications were made based on the three types of missions using the assumed flight speeds and estimated RAC. Results are in Tables 3-6 through 3-9 below.

Mission A	**4 laps/ 8-180° turns/ 4-360° turns**		
1 lap	**distance (ft)**	**velocity (ft/s)**	**time of flight (s)**
Straight cruise	2000	100	20.00
2-180° turns	157	80	1.96
1-360° turn	157	80	1.96
Total distance (4 laps)	9256		95.70
	Flight Time (min)	1.60	
	Single Flight Score	0.95	

Table 3-6 Mission A Estimated Flight Performance

Mission B	**4 laps/ 8-180° turns/ 4-360° turns /one landing**		
1 lap	**distance (ft)**	**velocity (ft/s)**	**time of flight (s)**
Straight cruise	2000	120	16.67
2-180° turns	157	100	1.57
1-360° turn	157	100	1.57
Landing			30.00
Total distance (4 laps)	9256		109.23
	Flight Time (min)	1.82	
	Single Flight Score	0.65	

Table 3-7 Mission B Estimated Flight Performance

Mission C	4 laps/4 turns/4-360's		
1 lap	distance (ft)	velocity (ft/s)	time of flight (s)
Straight	2000	120	16.67
2-180° turns	157	100	1.57
3-360° turn	471	100	4.71
Total distance (4 laps)	10512		91.79
	Flight Time (min)	1.53	
	Single Flight Score	0.49	

Table 3-8 Mission C Estimated Flight Performance

Aircraft assembly time	30 seconds	0.50 minutes	
Mission	**A&B**	**A&C**	**B&C**
Report Score	90	90	90
Total Flight Score	1.60	1.45	1.14
RAC	8.71	8.71	8.71
Total Score	16.54	14.95	11.77

Table 3-9 Estimated Total Flight Score

Initial observation shows the best strategy for obtaining the highest Total Score is to design around Mission A and B. But, changing the design to fit only specific missions may improve RAC enough to justify a reduced difficulty flight routine. The next section deals with this exact concern.

3.3. Trade-offs Between Mission Flights

A trade study was performed on whether neglecting Mission B can result in a higher Total Score. Exclusion of Mission B meant an improved RAC due to one less servo, since there would be no payload deployment, and subsequently less weight for the release mechanism. Assembly Time was assumed to not improve, since it is not related with deploying of the payload. Cruising speed may increase by a small amount due to weight reduction.

Figure 3-2 shows how the combination of Mission A & C compares to that of Mission A & B. Even if the aircraft acquires 10ft/s more cruising speed in the first combination, it is apparent that for Missions A & C to beat the Total Score of A & B, a 0.3 decrease in RAC is needed. However, one less servo contributes to only a 0.1 decrease, and negligible weight decrease, which is only 1/3 of what is needed. Hence it is concluded that Mission B is to be accomplished. Mission B & C scoring would be so low that the design would no longer be competitive. The conclusion is to design around Mission A and B; Mission C will still be able to be flown if needed by designing around Missions A & B.

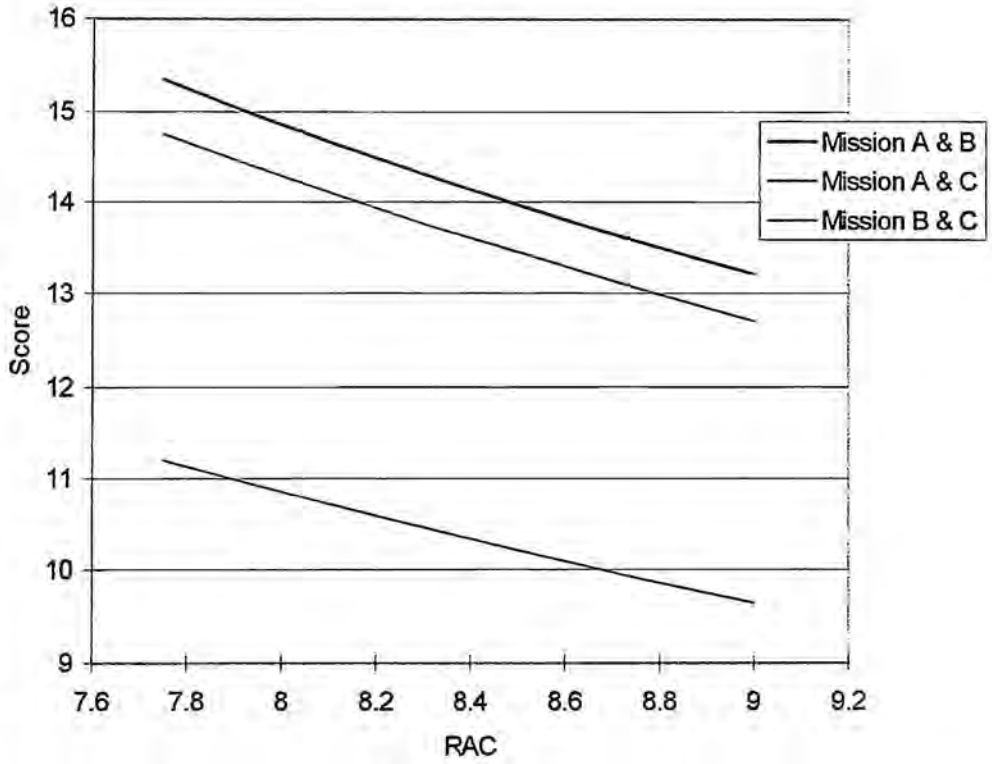

Figure 3-2 Comparison of Total Points for Different Missions

3.4. Design Considerations

Five different areas were considered in the conceptual design phase. The following is a list of the design areas along with the reasons why it was felt necessary to discuss them.

1. **Basic Aircraft Configuration:** The most fundamental characteristics of the aircraft were decided at the beginning. This decision induced restrictions on the other aspects of the design.
2. **Payload System:** Method of deployment affects both internal and external structure of the aircraft, especially that of the fuselage. For instance, if the payload would roll aft for deployment, structure would be required at and around the opening of the fuselage. Landing gear interference was another concern. Along with the payload deployment system is the simulated antenna, which must be mounted externally at least 3" away from the airplane's structure. The location of the antenna must also be in the air stream with no obstructions (not including the tail and the landing gear).
3. **Wing Configuration:** High-, mid-, and low-wing configurations were discussed. While the natural tendency was to choose a high-wing for a cargo plane, the discussion justified the choice. This concept led to detailed assembly methods and fuselage structure, as well as restrictions on landing gear locations.
4. **Type of Landing Gear:** Since the payload deployment system had to be finalized before choosing the landing gear configuration, there were few considerations. A tricycle configuration

was already decided upon, nevertheless, the landing gear configuration led to further exploration in the conceptual design phase for rapid assembly.

5. **Assembly Systems:** Several assembly methods were evaluated for the wings, tail, and landing gear. Reducing the number of parts needed to be assembled and simplifying the way the parts are assembled shortens the time of assembly.

For each design consideration, design parameters are defined as Figures of Merit (FOM), which include Rated Aircraft Cost (RAC). FOM, which vary from one design consideration to another, are the parameters that affect scoring potential. One example of FOM is stability, because poor stability can prevent a design from being competitive. A definition and calculation of RAC is summarized in Section 3.2.5 above.

FOM, which cannot affect Total Score numerically, are rated individually. The ratings range from -0.2 to +0.2 with an increment of 0.1; 0 represents normal. The reason for the small values of the ratings is that the ratio of change to the Total Score has to be small in order to emphasize the significance of its effect. An Effective Score is then calculated by summing Total Score with the sum of the FOM. Effective Score is a numerical equivalent to the potential scoring capability of the design.

$$\text{Effective Score} = \text{Total Score} + \text{Sum of FOM}$$

Equation 3-4 Effective Score Calculation

3.4.1. Basic Aircraft Configuration

Basic designs of the fuselage, wing, and tail were determined during this step. Each configuration with the highest Effective Score was carried through to the next design consideration. Basic aircraft configuration was evaluated using the following Figures of Merit:

I. **RAC:** a numerical value was calculated accordingly.
II. **Ease of Assembly:** each advantage or disadvantage was accounted for by a difference in Assembly Time.
III. **Drag Performance:** increasing or decreasing the cruising speed by 10 ft/s accounted for each predicted increase or decrease in drag.
IV. **Take-Off and Landing Performance:** 3 seconds were either added or subtracted for an advantage or disadvantage in the performance.
V. **Flight Performance:** Flight performance including stability and control is a significant factor since it affects the ability to complete the missions.
VI. **Experience:** The team's ability to design a competitive aircraft affects all design configurations. If the experience does not exist, this could affect the overall competition outcome.

One (I) through four (IV) above were first numerically evaluated for Total Score. FOM V and VI were then used to evaluate six alternative configurations. An Effective Score was calculated to allow a decision to be made of not only the best design, but to help the team decide which one could be more

easily fabricated. Summary of the evaluations are in Table 3-10 below. Pictures of the conceptual configurations are in Figure 3-3.

1. **Conventional with T-tail:** A Total Score of 14.26 set the standard for other configurations. Rating for both FOM V and VI was 0.2 because this was the configuration in which the team had the most experience. Effective Score is 14.46.
2. **Conventional with V-tail:** RAC decreased by 0.1 for the V-tail compared to the T-tail. This change made Total Score 14.75. FOM V dropped to –0.1 because the V-tail has effective area losses and therefore requires a bigger tail to attain the same stability and control. This results in a possible increase in RAC due to the 25% contest rule with the tail versus the wingspan. FOM VI dropped to –0.2 because of the lack of v-tail design experience. Resultant Effective Score is 14.45.
3. **Conventional with twin boom/H-tail:** H-tail increases RAC by 0.1 and an additional boom weighs roughly 0.25 lb more increasing RAC by 0.02. Alignment of two tail booms during assembly is more complicated than one boom; therefore, Assembly Time is increased by 3 seconds to accommodate this resulting in a Total Score of 14.12. Two-boom support gave an improved stability due to the more rigid tail structure resulting in a FOM V of 0.1. Less experience with this design results in a -0.1 rating. The result is an Effective Score of 14.12.
4. **Canard:** First three Figures of Merit were evaluated as the same as conventional because the only fundamental difference between a canard and conventional is the location of the wings and horizontal stabilizers. The result is a Total Score of 13.96. Better stall performance of the canard made the rating of stability 0.1, and since the team has no experience with canard, FOM VI is set to –0.2. Effective Score is 13.86.
5. **Flying wing:** RAC decreased by 0.3 due to removed tail weight and control surfaces. Assembly Time also improved by 3 seconds for not having to assemble the tail. Worse take-off and landing performance added 3 seconds per event. Calculated Total Score is 14.72. Marginal stability of the flying wing resulted in a stability rating of -0.2. Experience was moderately lacking resulting in a rating of -0.1. Effective Score is 14.42.
6. **Bi-wing:** Since layering the wings would require a 6-inch longer combined wingspan due to lower aspect ratios, RAC increased by 0.08. It might be possible to shorten Assembly Time by 3 seconds, assuming that two wings would be attached and fit in the box (1-foot box height), but the wings would also be too close together for proper airflow, which reduces lift. Calculated Total Score is 14.82. Parasitic drag is also a common problem with a bi-wing design. Lack of experience is also a factor, thus ratings for the last two FOM are both -0.2. Effective Score is 14.42.

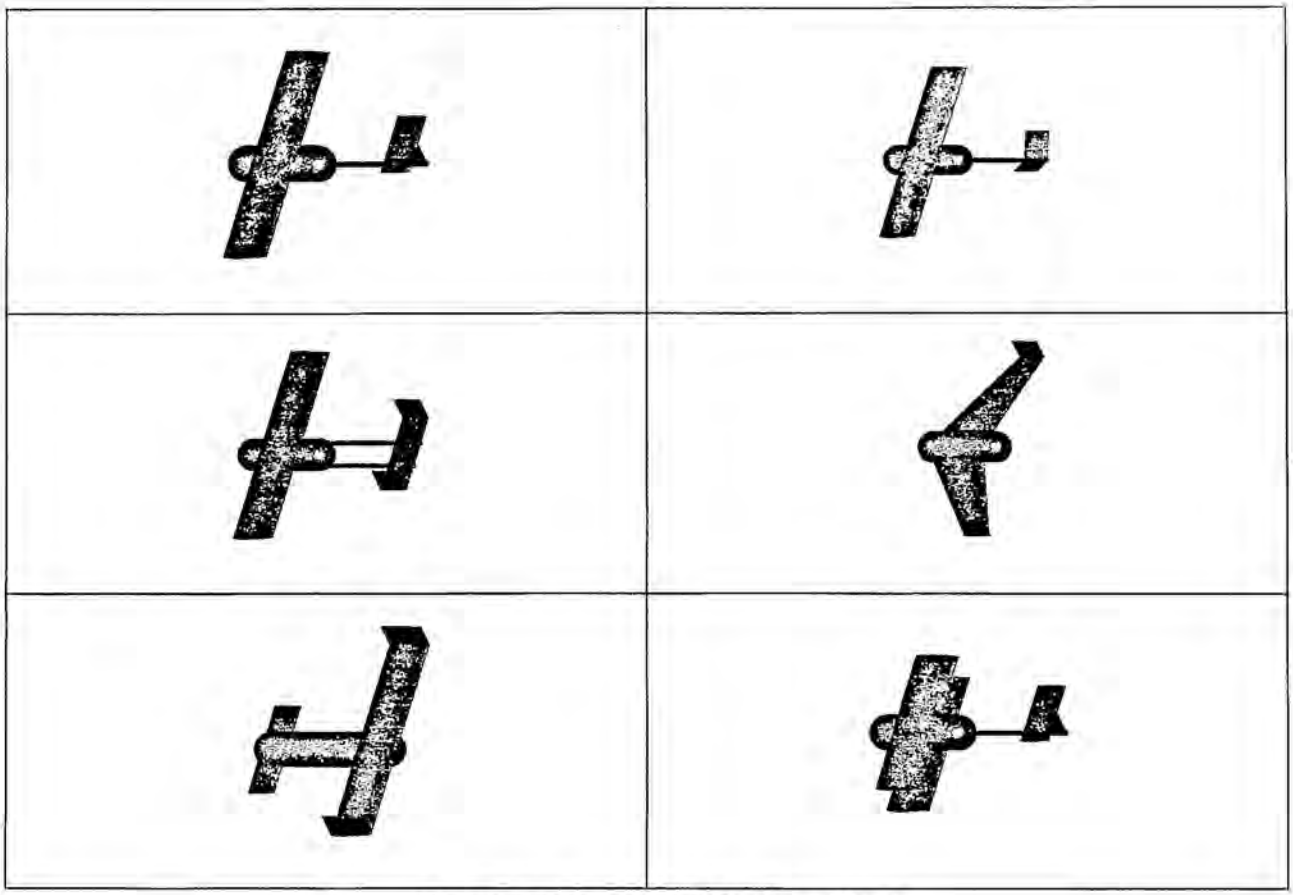

Figure 3-3 Conceptual Configurations

		FOM Ratings		
Configurations	**Total Score FOM I-IV**	**V**	**VI**	**Effective Score**
Conventional w/T-tail	14.26	0.2	0.2	14.46
Conventional w/V-tail	14.75	-0.1	-0.2	14.45
Conventional w/H-tail	14.12	0.1	-0.1	14.39
Canard	13.96	0.1	-0.2	13.86
Flying Wing	14.72	-0.2	-0.1	14.42
Bi-plane	14.82	-0.2	-0.2	14.42

Table 3-10 Configuration Summary

Conventional configuration with T-tail was chosen over the other configurations. The choice was reasonable in the sense that this configuration was balanced in potential Total Score, stability & control, and experience. Because the V-tail configuration also scored high, both designs would be further evaluated in the preliminary design.

3.4.2. Payload System

Remote deployment of the payload is critical to Mission B. The concepts that were presented and discussed include vertical drop, roll-front, and roll-aft. Figures of Merit (FOM) for the system are the following:

I. **Total Score:** This contains estimated flight time, RAC, time of assembly, and drag performance of the components. Values were calculated in the same manner as Table 3-5.

II. **Landing Gear Interference:** Deployed payload should not interfere with the landing gear to ensure the second take-off during Mission B.

III. **Complication:** Complication of the mechanism results in an increase in weight and/or payload deployment reliability problems.

Summary of the evaluation is in Table 3-11 below.

1. **Vertical Drop:** To set a standard, FOM III has rating of 0. The landing gear interference is not anticipated for this concept because the payload would be on the ground between the main gears; therefore, FOM II rating is set at +0.2. Total Score is 14.43, and Effective Score is 14.63.
2. **Roll-front:** Rolling would increase deployment time by at least 3 seconds because a mechanism would be needed to help the deployment instead of using gravity. Necessary space in the fuselage for the rolling would make the body longer by about 3", which increases the weight and therefore increasing the RAC by an estimated 0.05. Total Score is now 14.22. Landing gear might be an interference problem since the deployed payload would be in front of them. A complicated mechanism would also be required to roll the payload while keeping the surface of the fuselage in the same shape after deployment (faired payload doors). Therefore, each FOM was assigned a –0.1 rating. Effective Score became 14.02.
3. **Roll-aft:** In this concept, a longer fuselage was unnecessary because the edge of the payload might be exposed at the back end of the body. However, this increases drag during flights, which would decrease cruising speed by 10ft/s. Total Score calculated is 13.98. Rolling-aft would not interfere with the landing gear, so the rating was 0.2. Mechanism may be as simple as the vertical drop; therefore, the FOM III is set to 0. Effective Score becomes 14.18.

		Ratings of FOM		
Alternatives	**Total Score FOM I**	**II**	**III**	Effective Score
Vertical Drop	14.43	0.2	0.0	14.63
Roll-front	14.22	-0.1	-0.1	14.02
Roll-aft	13.98	0.2	0.0	14.18

Table 3-11 Summary of Payload Release Configuration

The decision process showed that the vertical drop has significant advantage in the Total Score; therefore, vertical drop is the winning concept.

There are two locations to mount the antenna, above the airplane or below the airplane. Above the airplane may cause instability due to an upward shift of the CG. Also, the concern of the wake interfering with tail surfaces prompted the decision for mounting the cylinder under the fuselage.

3.4.3. Wing Configuration

Before a landing gear design or assembly method could be created, wing location had to be determined. Keeping assembly times constant, high-, mid-, and low-wing configurations were evaluated for the following considerations:

I. **Weight:** This FOM was considered since it affects Total Score due to the structural weight. Increased weight of the vehicle results in a higher RAC and slower flight speeds, which reduce Total Score.

II. **Landing Gear Interface:** Mounting location of the landing gear will be affected by wing location. Normal mounting location beneath the fuselage has been removed from consideration because of the payload deployment method.

III. **Stability:** This quantifies the ability of the aircraft to complete the mission flights.

Evaluation of the alternatives is as follows; a summary is in Table 3-12 below:

1. **High-wing:** For high-wing, it is possible to mount the wing on top of the fuselage in which a through-type structure could be attached to the fuselage. Because of the reduced weight, Total Score result is 14.75. Disadvantage of the high-wing is that a retractable landing gear system would not be able to be deployed from it; therefore, a FOM II rating of –0.2 was assigned. On the other hand, a high-wing allows for good roll stability resulting in an assigned FOM III rating of 0.2. Effective Score becomes 14.75.
2. **Mid-wing:** Total Score is 14.43. It is lower than the high-wing because a through-type spar structure cannot be designed due to the payload; therefore, increasing structural weight. Both landing gear interface and stability are average, so their ratings are 0 each. Effective Score stays 14.43.
3. **Low-wing:** Total Score is 14.43. It is low for the same reason as the mid-wing. Low-wing provides an excellent landing gear interface, which makes FOM II rating 0.2. Roll stability is lower, so FOM III rating is –0.1. Effective Score is 14.53.

		Rating of FOM		
Alternatives	**Total Score FOM I**	**II**	**III**	**Effective Score**
High-wing	14.75	-0.2	0.2	14.75
Mid-wing	14.43	0.0	0.0	14.43
Low-wing	14.43	0.2	-0.1	14.53

Table 3-12 Summary of Wing Location

3.4.4. Landing Gear Type

Tri-cycle landing gear configuration was chosen as stated previously in Section 3.2.7. Since the high-wing was chosen the main landing gear could not be reliably deployed from wing hard points. A simple one-piece type gearing mounted to the centerline was also discounted because of the payload deployment method. The only alternative for the main landing gear is to separate the two and integrate them as part of the fuselage structure.

3.4.5. Assembly System

With the conceptual design mostly complete, an assembly method was needed to place the airplane in a flight-ready condition in the least amount of time. Restriction in the size of the 4' X 1' X 2' assembly box forced a partition of the wing into two pieces, which has been conceptually sized to a 5-½ -foot span. For the same reason, the tail boom needs to be disassembled from the fuselage. Fuselage shall remain untouched to avoid a complicated assembly task. Both nose gear and main landing gear also need to be either detached from or tucked into the body. Mechanically retractable gears are yet another consideration, but desired to be avoided due to their unreliability. The goal is to assemble the entire airplane in the least amount of time, thus improving the Total Score. The following is a summary of decisions made during the conceptual design meetings and why.

- **Wing interface:** Last year's wing interface was a rod and socket assembly which worked very well. In addition to this method, it must include a provision for quick disconnect wiring for the aileron servos.
- **Main gear:** Since the main gear had to be split due to the payload deployment, two concepts were discussed. One was a hinged gear that would fold back. The disadvantage of this concept is that there would be a complicated interface with the fuselage structure. The other concept was a plug-in type. The landing gear would have a flat upper portion, which would lock in place. This was the simplest of the concepts.
- **Nose gear:** This was the most difficult part to devise a concept for since the steering mechanism must be a single unit. The complex interface with the servo and the nose gear shaft required it to be permanently installed in the aircraft. Since the landing gear would be too tall for the assembly box, the shaft would have to be cut and have an interface that would allow for quick assembly. The two choices were a threaded assembly or a hinged assembly. The threaded assembly concept was thrown out since there would be possible alignment problems. Although requiring more parts, the hinged method was chosen for it reliability. The hinge would also allow for a rapid deployment of the nose wheel.

3.5. Conclusion of Conceptual Design Phase

In summary, Spirit of Monty shall have:

- Conventional configuration with a T-tail or a V-tail
- Complete Missions A and B
- Vertical-drop payload deployment system
- Simulated antenna mounted below the fuselage
- Plug and socket main gear
- Single tractor power plant configuration
- High-wing with a plug and socket interface
- Tri-cycle gear with separate main landing gear on either side of the fuselage
- Hinged nose wheel

4. Preliminary Design

Preliminary design phase began with using the conclusions from the conceptual design phase to develop the most competitive aircraft to meet the mission requirements. Choosing the best airfoil, designing the best wing planform, and optimizing the fuselage shape are the major factors. Along with these factors the airplane must still be able to fit in the assembly box and be able to be made flight ready in a very short period of time, the goal is 20 seconds. Every design decision was made with these factors in mind.

4.1. Configuration Basics

To create the baseline fuselage shape known components had to be used to ensure proper sizing. Design began by working around a Graupner and an Astro Flight motor. Both types of motors were used to ensure the airplane could be easily modified to accept either motor once the motor and propeller configuration testing was complete. Other components included batteries (main and control), receiver, empennage, landing gear, payloads and wing. A right-handed global coordinate system was first set up as follows: X-axis named Fuselage Station (FS), Y-axis named Butt Line (BL), and the Z-axis named Water Line (WL). Numbers after the WL, BL, or FS abbreviation described the distance in inches from the origin. For example, anything in the YZ plane would be at FS0.

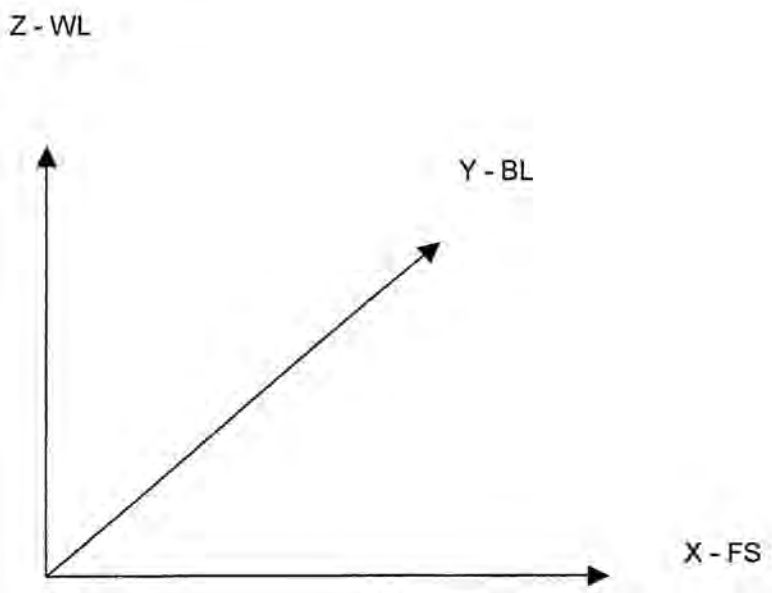

Figure 4-1 Global Coordinate System Used for Design

Two-dimensional components were sketched on a drawing board using the X-Z plane of the above coordinate system and manipulated to determine the best location. The payload's center of gravity (CG) was set at FS15/WL15, which was also the defined CG for the entire airplane; this was to ensure there would be no CG travel concerns after deploying the payload. The high wing was set above the payload with the ¼ chord directly above the CG. Motor placement put the thrust line directly through the CG. Battery packs were placed in the space between the payload and the motor. A tail boom was added passing through the fuselage aft of the payload. An aerodynamic shape was then sketched around the internal components, resulting in a glider-type cockpit area shape. Landing gear locations were added to ensure structure would be included to support them. Some preliminary bulkheads were added for structure including the motor mount bulkhead. A provision for longerons and stiffeners in strategic areas were also included. A horizontal and vertical stabilizer was then drawn to approximate size. The sketch was set as the baseline for the preliminary design and was instrumental in creating the best possible airplane. In addition to the drawing, a weight balance was performed using each of the components approximate weight to ensure there was no extreme nose-heavy or tail-heavy situation.

4.2. Assembly System

With the configuration laid out on the drawing, a method of assembly could be designed. First, a full-scale side-view and top-view drawing was made for the fuselage, wings, and empennage (including the tail boom). Another full-scale drawing was made for the assembly box. The separate parts were then set in the box outline to examine how they would fit. Example side and top views are shown in Figure 4-2 below (not to scale).

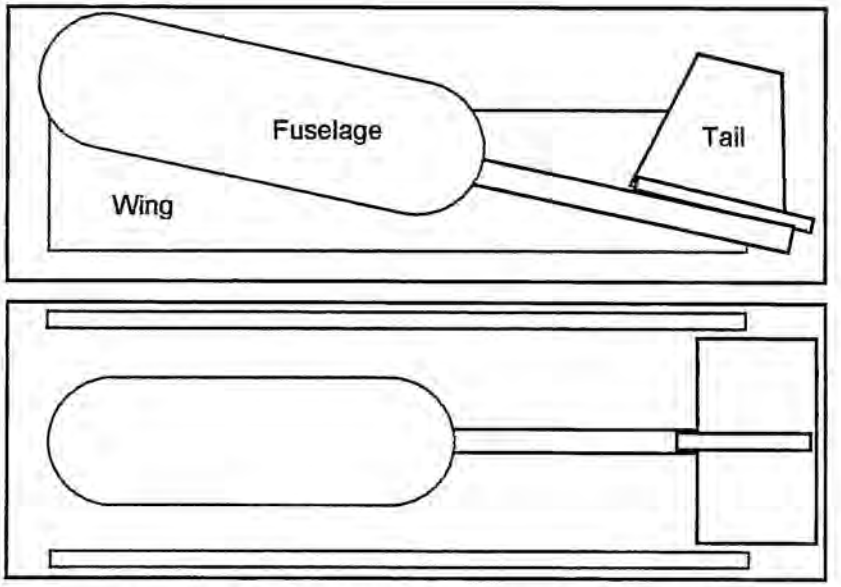

Figure 4-2 Side and Top Views of Assembly Box

1. **Wings:** During the conceptual design, the wings were projected to be too long for the box; therefore, they would consist of a two-piece assembly. The assembly of the wings would be a plug-in type, which would include connectors for the wiring for rapid assembly. This was the method used last year, which was reliable.
2. **Fuselage:** Fuselage had been originally sized to fit in the box in one piece, so no special assembly system was needed.
3. **Empennage:** This was the most difficult part because the tail would have to extend past the box to be effective as stability and control surfaces. A possibility was to size the tail to fit in the box and attach it to the tail boom. Upon the timed assembly, the tail boom could be slid into the fuselage and secured. The problem with this configuration is that the wire connection for the tail servos becomes difficult, a lesson learned from last year's airplane. Another option was to have a retractable tail boom. Since the payload will not be in the fuselage at the time of the assembly task, the boom can be shifted forward into the fuselage. It could then be retracted and secured, with the servo wiring already connected. This would enable a compact design and rapid assembly.
4. **Landing gear:** For adequate propeller, payload drop, and antenna clearances, the main landing gears must be long and have a wide stance. The wide stance is to maintain the 3" distance from the simulated antenna. Since the retractable landing gear had been observed to be unreliable in previous year's designs (demonstrated by the failure cases at the competitions) a method of quick assembly still needed to be devised. The answer was to make a plug-in, screw-in, or hinged type gearing, which would tie into the structure.

4.3. Wings

With the high-wing configuration the goal was to blend the wing into the upper outer mold line of the fuselage. Before fuselage design could continue, an airfoil had to be chosen to accomplish this.

4.3.1. Airfoil determination

Many airfoils were evaluated to determine suitability for the mission. Since this competition requires high-speed turns and fast level flight, the evaluation concentrated on high lift and low drag airfoils. This would also allow for a smaller planform area, which would improve the RAC. NACA 65 and 66 series, RG, Selig-Donovan (SD), and last year's G8-AR high-lift airfoil were compared.

NACA 65 and 66 series were dropped from further consideration because of their higher drag with no advantage of lift. RG airfoils were too low in lift and were also dropped from consideration. The search was narrowed down to 3 airfoils, the SD7037, SD7043, and the G8-AR. Comparison of the Selig-Donovan (SD) airfoils to the G8-AR showed a lower C_{lmax} for the SD airfoils, but a higher α_{stall} (see Figures 4-3 and 4-4). The stall was also not as abrupt as the G8-AR. At this point the choice of the airfoil was heading more toward the Selig-Donovan type.

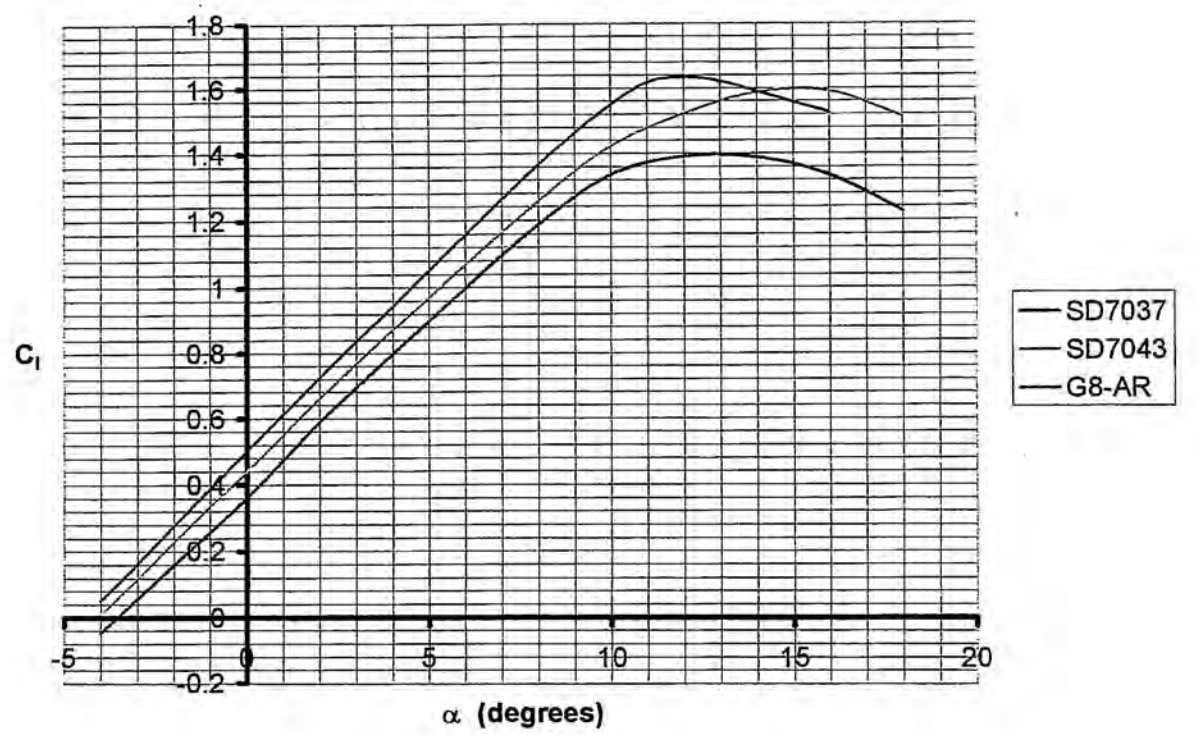

Figure 4-3 Lift versus Angle of Attack for Various Airfoils

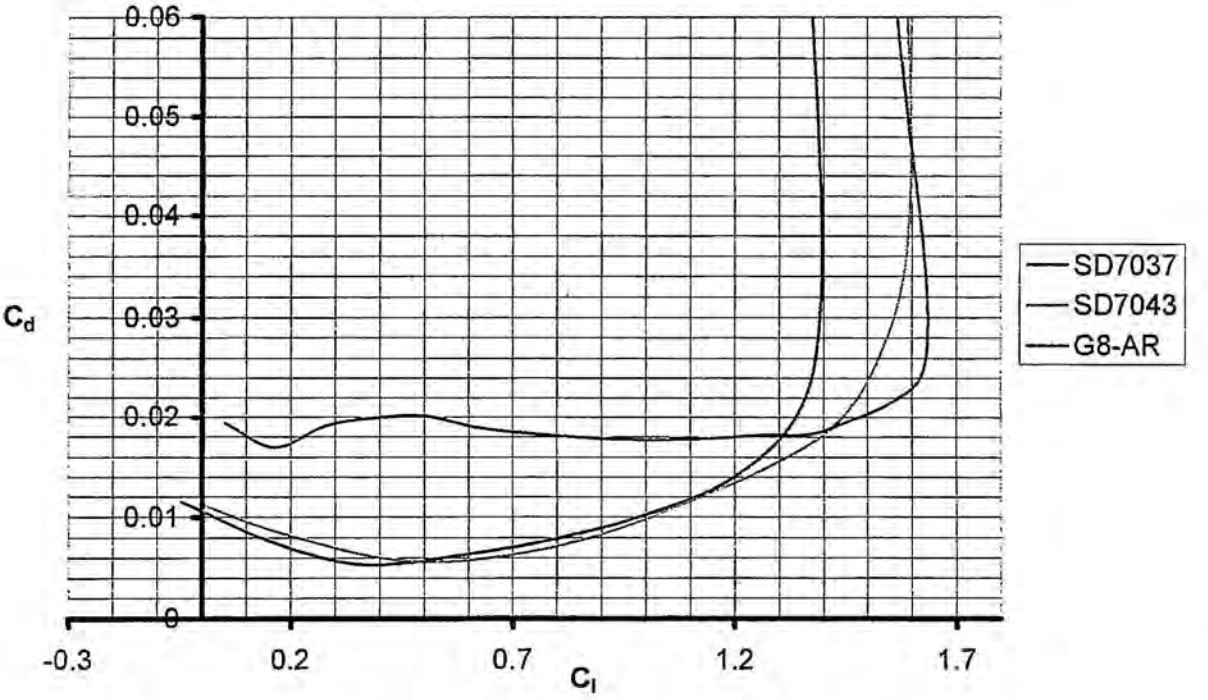

Figure 4-4 Drag versus Lift for Various Airfoils

Since a low drag airfoil was also a goal, the C_d vs. C_l curve for all three airfoils were evaluated. Both SD airfoils were relatively equal in drag, but the G8-AR had twice as much drag (see Figure 4-4). Although the G8-AR had more lift, high-speed demand of the competition led to the decision that this airfoil would not be used.

The choice was now between the SD7037 and the SD7043. To ensure the best turn and take-off performance, the airfoil with the highest C_{lmax} was chosen, SD7043. XFOIL was used to try to improve upon the airfoil, but this airfoil type was already at its peak performance, therefore it was maintained as the original.

Reading from Figure 4-3 and 4-4, minimum drag for the SD7043 is 0.055 at a C_l of 0.525. The respective angle of attack is approximately 1 degree. Design of the wing would ensure a provision for a 1-degree cruise angle of attack.

4.3.2. Planform Shape

Based on turn performance (4.5-g turn) and take-off distance (120 ft), required planform area was calculated to be 5.52 ft^2, turn performance being the limiting factor.

The RAC dictated the decisions on the planform shape. Every foot of wing span increases the RAC; therefore, the wingspan should be minimized. Minimizing the wing span increases chord size, which also increases the RAC, but not as much for a given area; Figure 4-5 illustrates this effect. Span can only be minimized to the point where the chord increases to 1 foot since anything larger would have trouble fitting in the required assembly box. A maximum root chord of 11 inches was chosen to reserve the ability to have some growth if necessary. Changing the taper ratio toward a more efficient (elliptical) planform shape would cause a significant increase in the RAC, as shown by the dashed curves in Figure 4-5. To minimize RAC, taper ratio was fixed at 1, resulting in a rectangular planform.

Increasing the Aspect Ratio (AR) to increase the lift slope of the wing was limited by the increased structural requirements and the increased RAC. Increasing AR would also decrease the drag of the wing, summarized in Table 4-1. Decreasing the AR would not only decrease the lift slope, but would result in the increasing of the chord size, causing a storage issue with the assembly box, as illustrated in Figure 4-6. Applying the range of appropriate aspect ratios from Figure 4-6 to the allowable chord sizes in Figure 4-5, the wing span becomes 6 ft, chord 0.92 ft, and AR 6.5. This allows for the minimum RAC while still accomplishing the mission.

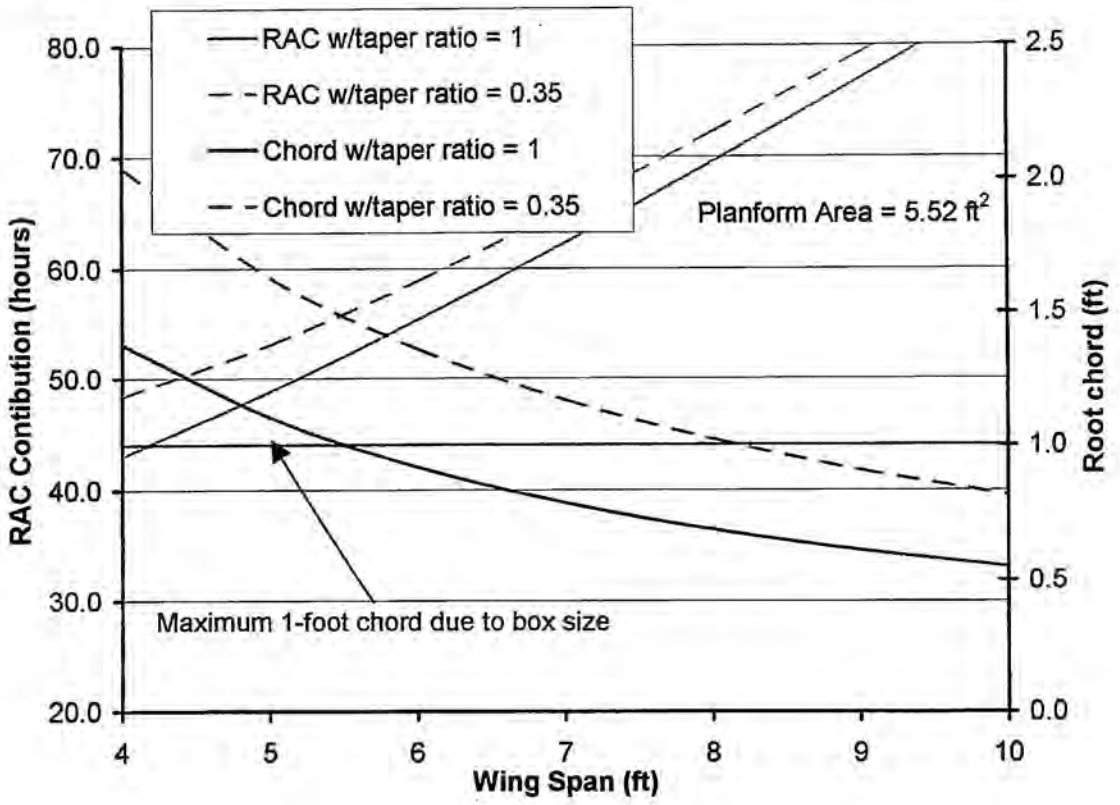

Figure 4-5 Rated Aircraft Cost Contribution from Wing Span

S	AR	b	c	c	b/2	C_D	Drag	RAC
ft^2		ft	ft	in	ft		lb	
5.5	5.5	5.50	1.00	12.00	2.75	0.01252	0.729	52.00
5.5	6.0	5.74	0.96	11.49	2.87	0.01236	0.720	53.62
5.5	6.5	5.98	0.92	11.04	2.99	0.01215	0.708	55.19
5.5	7.0	6.20	0.89	10.64	3.10	0.01203	0.701	56.73
5.5	7.5	6.42	0.86	10.28	3.21	0.01186	0.690	58.23
5.5	8.0	6.63	0.83	9.95	3.32	0.01167	0.679	59.70

Table 4-1 Summary of AR Versus Drag and RAC

With an aspect ratio of 6.5, C_L will be lower than the C_l due to finite wing effects. Calculated C_L due to finite wing effects for various aspect ratios at 1° angle of attack are shown in Figure 4-7 below.

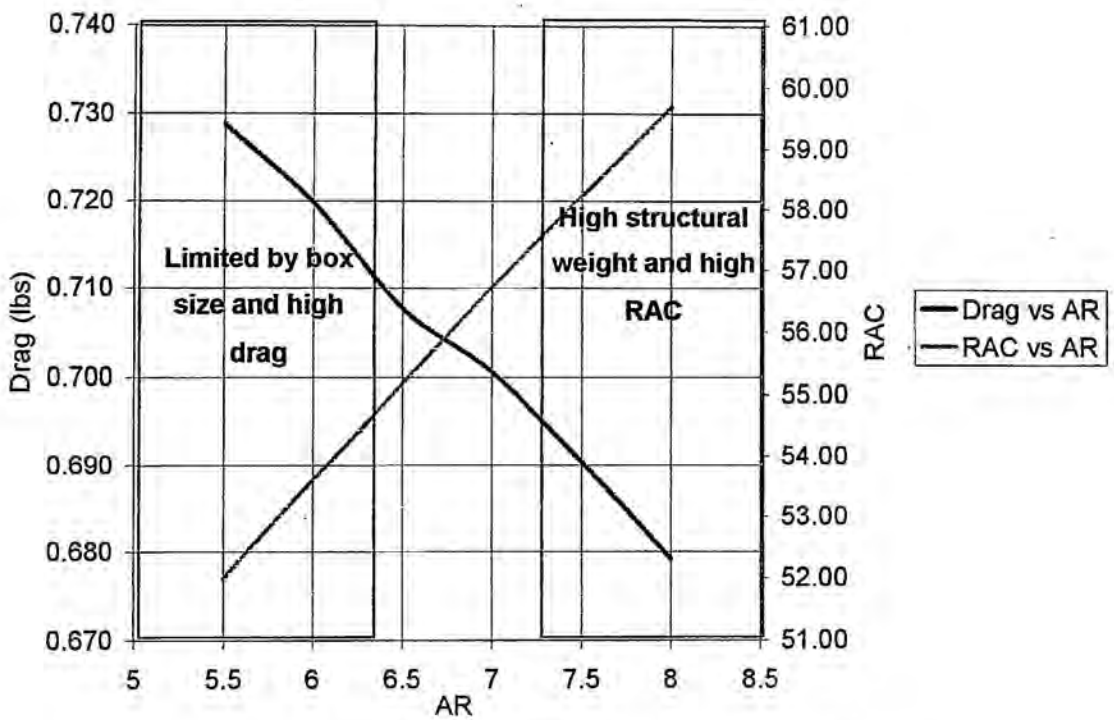

Figure 4-6 Drag and RAC Comparison with Aspect Ratio

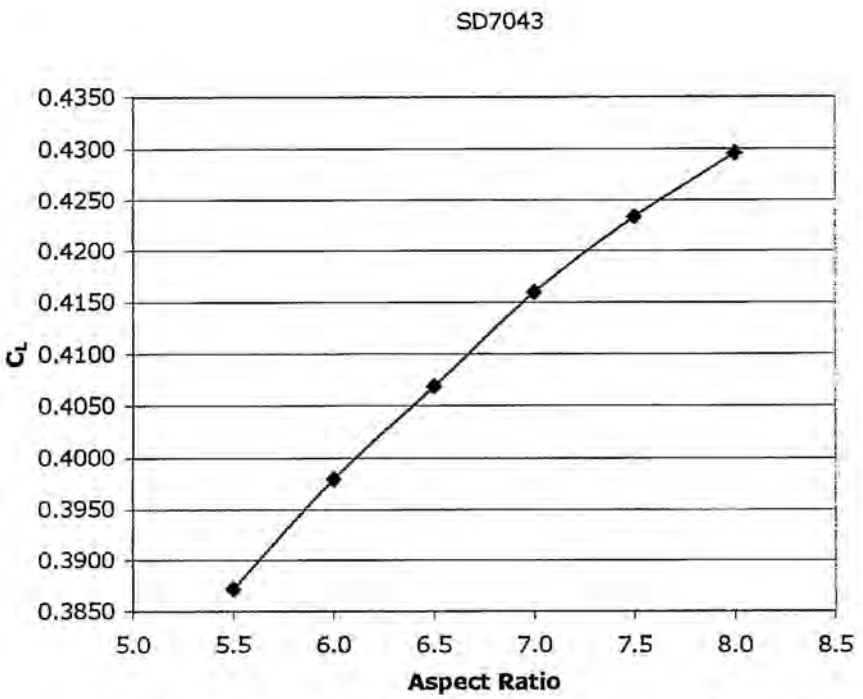

Figure 4-7 Lift Coefficients for Various Aspect Ratios at 1° alpha

Applying the same calculation for the entire lift curve results in Figure 4-8. C_{Lmax} and stall angle were calculated by methods in Reference 7.

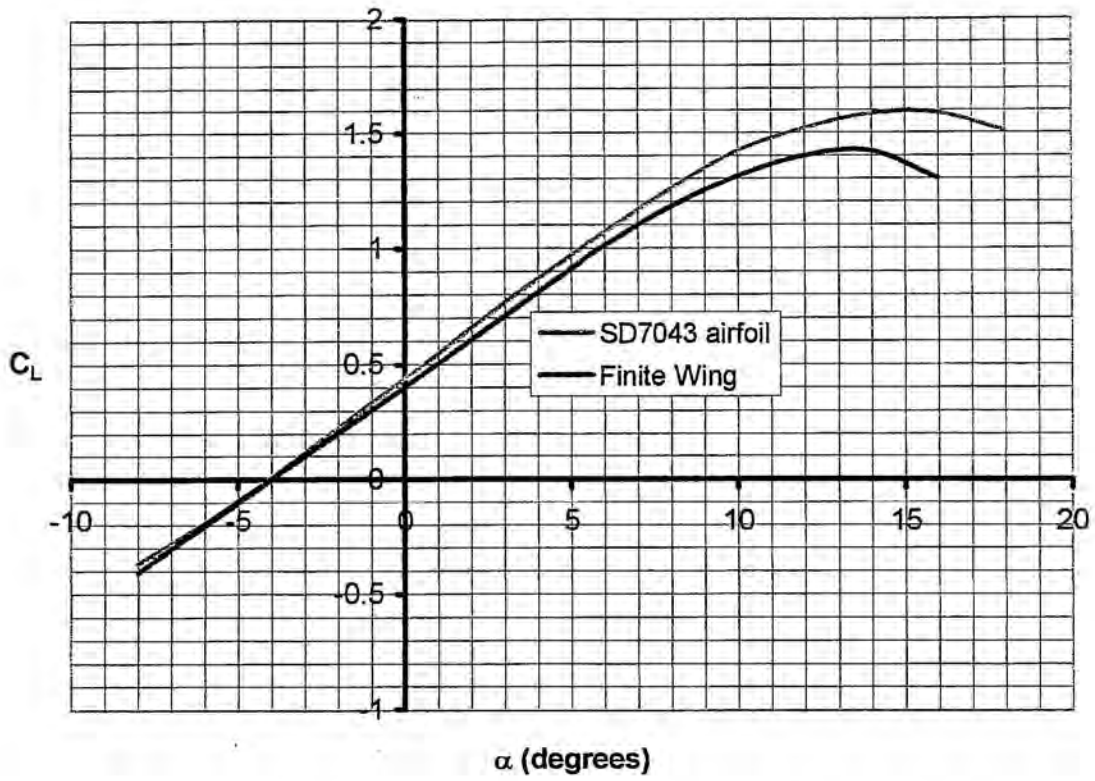

Figure 4-8 SD7043 Airfoil Compared to Finite Wing with an AR of 6.5

4.3.3. Wing Sizing Summary

- Rectangular planform
- Planform area 5.52 ft^2
- Span 6 feet
- Chord 0.92 feet (constant)
- Aspect Ratio of 6.5

4.4. Fuselage

Weight savings had to be considered when evaluating the aerodynamic shape of the fuselage. The first step was to design an aerodynamic type shape around the payload box. A 2-D shape was drawn around the box payload. The points were then used as an input file for XFOIL. Using XFOIL, the shape of the pressure coefficient curve was modified to reduce drag to a minimum. The final shape is shown in Figure 4-9 below. By varying the angles of attack, drag was found to be minimum at 0 degrees.

The final points were then used to reproduce the shape in PRO-Engineer as a 3-D form. Two concepts were designed; one with a pointed trailing edge, and the other with a flat trailing edge (see Figure 4-10). The cross-sections were modified to minimize the size of the body and therefore reducing overall weight, but still able to carry the required payload.

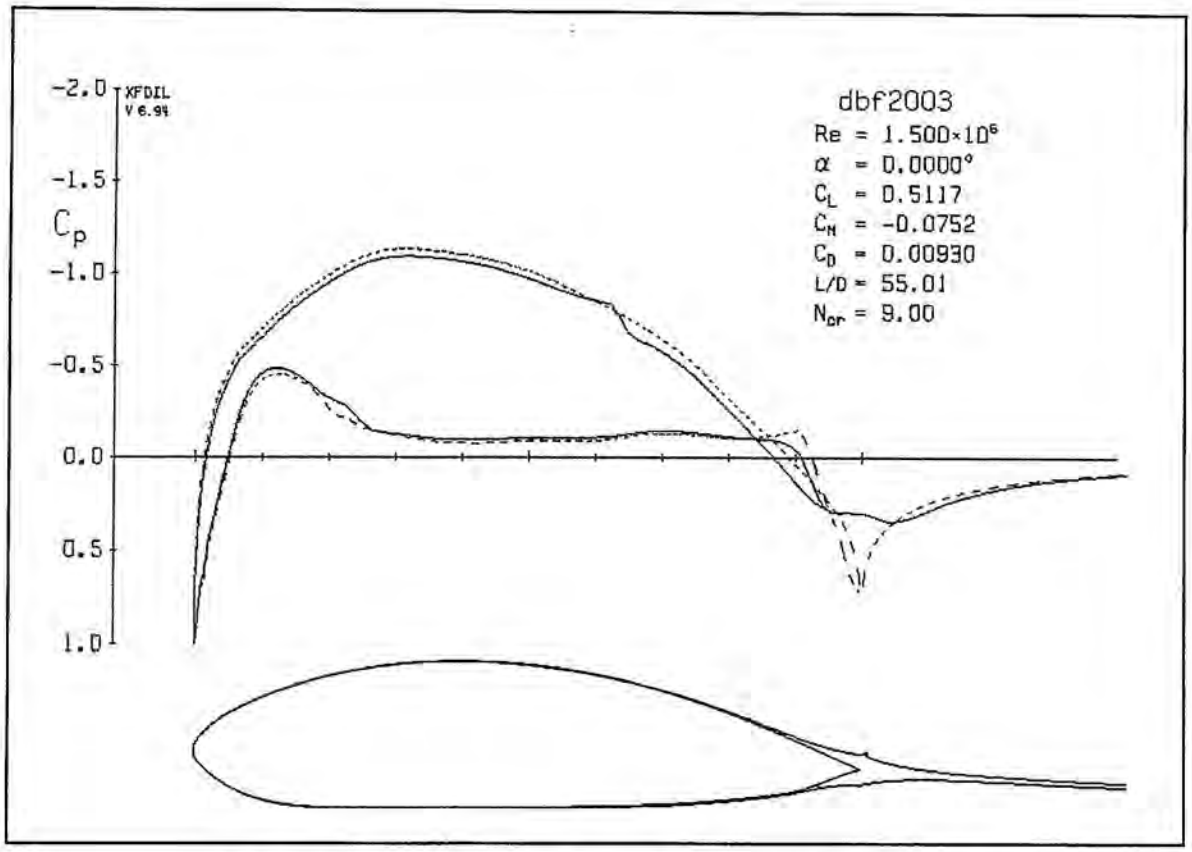

Figure 4-9 XFOIL Pressure Coefficient Diagram of Fuselage

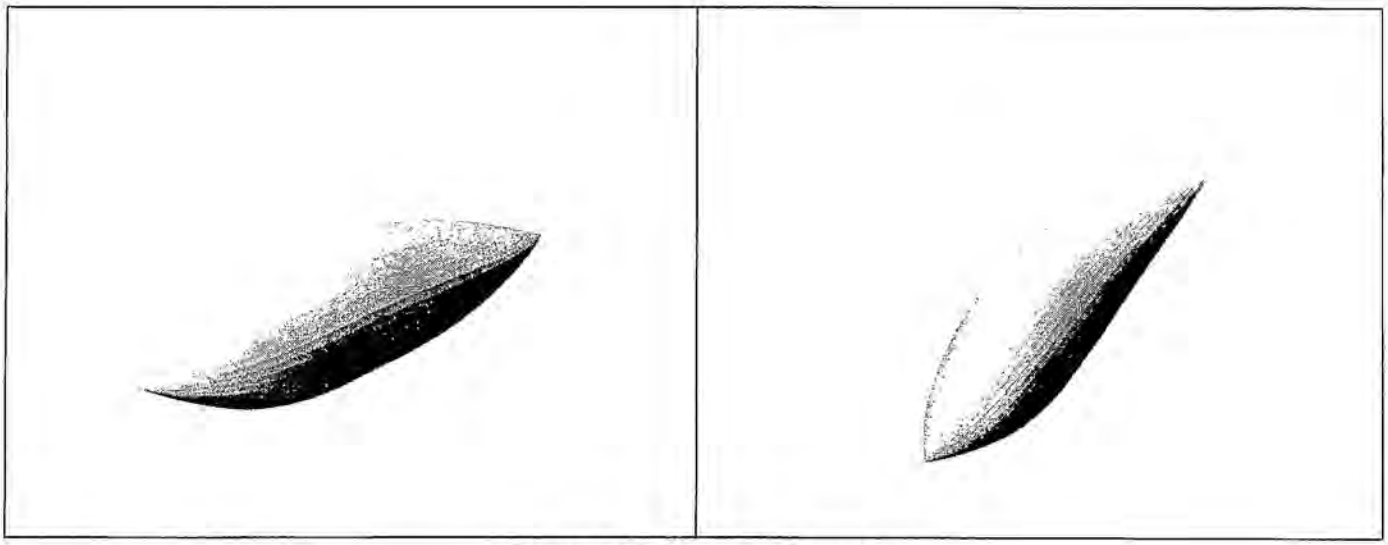

Figure 4-10 Fuselage Concepts

Comparison of the weights, as shown in Table 4-2 below, illustrates a significant difference between the flat trailing edge and the pointed trailing edge; there is a 10% weight savings with the pointed trailing edge. This result shows that the pointed trailing edge version has a significant advantage. Aerodynamic performance (lift, moments, and drag) was then evaluated to screen any advantage for the flat trailing edge. Weight was based on the assumption that the fuselage skin was the same carbon composite as last year's competition entry.

	Surface Area	Weight/Area	Weight
Concept	in^2	lb/in^2	lb
Flat	830.8	0.00168	1.40
Point	750.5	0.00168	1.26

Table 4-2 Weight Comparison of Fuselage Concepts

4.5. Tail Options and Sizing

Tail design had to be evaluated through multiple considerations. First, the concept had to be evaluated by the RAC to determine its pre-sizing competitiveness. It also had to be evaluated for its simplicity to allow for a more rapid assembly time and a higher Total Flight Score. Lastly, it must provide for static and dynamic stability. RAC scoring does not directly penalize for the tail surface area unless its span is larger than ¼ span of the main wing. However, it does penalize for the overall length of the airplane; therefore, the length should be shortened while increasing the tail surface area. A further evaluation in the next section is aimed for sizing the tail to fit in the storage box, shortening the longitudinal length of the tail to minimize the RAC, but still maintaining stability.

4.5.1. T-tail

Using a T-tail is the most conventional approach. As discussed in the conceptual design, it has a lower RAC, but the highest Effective Score. The problem is that the vertical stabilizer may need to be assembled, reducing the Total Flight Score. If a quick assembly could be devised, or if the tail sizing shows that the tail will fit in the box without disassembly, then this type of tail will work. An advantage of this tail is that the pilot has experience flying T-tail aircrafts; also, the fabrication team preferred to have a T-tail. If there is no notable advantage found from the stability evaluation then the T-tail would be the best choice.

Horizontal tail span was set at 18 inches to keep it within ¼ of the main-wing span in order to take advantage of the lower RAC. By assuming a large tail volume ratio of 0.6, the resulting chord is 8 inches. The reason for the higher-than-normal tail volume was to overcome the moment of the cylinder payload. A tail this size would still fit in the assembly box (based on initial packing concepts).

Vertical tail sizing began with the 1-foot maximum dimension of the assembly box, resulting in a vertical ratio of 0.034. This is a reasonable ratio for this type of aircraft. Final vertical tail size has a root chord of 8 inches, tip chord of 6 inches, and a span of 9 inches.

4.5.2. V-tail

A V-tail configuration results in a lower RAC. It also simplifies the assembly phase, if sized correctly. The disadvantage is the loss of effective surface area, resulting in a larger tail. If the tail is too large it may cause the RAC to rise significantly and thereby negating the advantage of the V-tail. More evaluation had to be performed to determine the effectiveness of the concept.

Sizing of the V-tail used the combined planform areas of the T-tail. Angle of the V-tail was set at 110°. The size would allow it to fit in the assembly box without being disassembled.

4.6. VSAERO Configurations Tested

Both of the tail concepts, T-tail and V-tail, along with each of the fuselage concepts were evaluated in VSAERO to determine their effectiveness for static stability. Figure 4-11 shows each of the concepts evaluated, including an inverted T-tail. The inverted T-tail had been removed from consideration due to the concerns of wing and cylinder wakes.

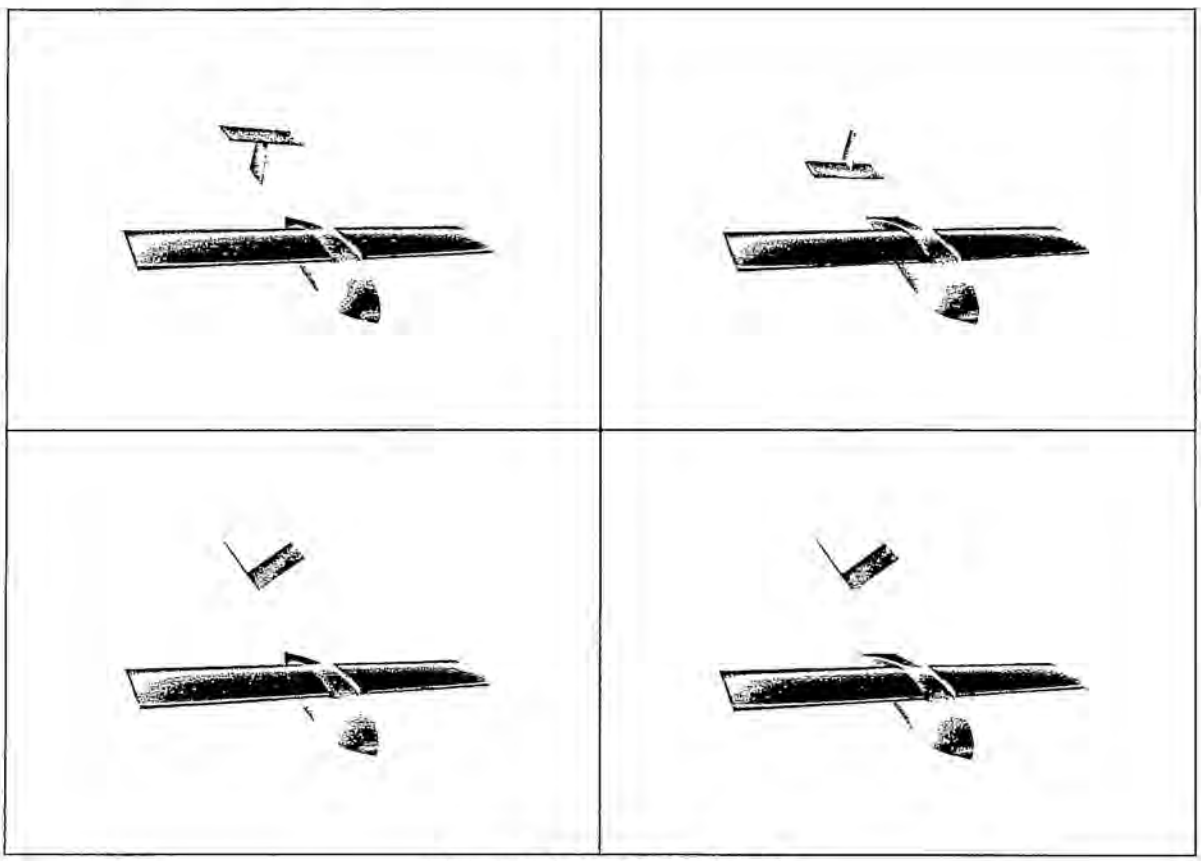

Figure 4-11 VSAERO models

4.6.1. Tail incidence angle optimization

To optimize the tail placement, its incidence angle first had to be found at various distances (as measured by l_t). Placing the body at its cruise angle, 0 degrees, and adjusting the tail incidence angle to achieve a C_M of zero, optimum tail incidence angles were found. This was done to minimize the trim drag during level flight, because last year's airplane suffered from an extreme amount of trim drag. Figure 4-12 was produced using data from VSAERO; it is a summary of tail incidence angles. Once dynamic stability is complete as a function of l_t, the length of the airplane can be reduced to a minimum, then the tail incidence angle (i_t) can be set to the minimum trim drag angle.

4.6.2. Fuselage Static Stability Comparison

Placing the tail at the minimum trim drag incidence angle, static stability was evaluated for each of the concepts. First, the fuselage concepts were compared to see if any static stability advantage is gained from the different trailing edges. The comparison presented a negligible advantage as shown in Figure 4-13. Each concept demonstrated a positive C_{M_o} with a negative C_{M_α} slope, requirements for static stability.

Each tail and fuselage concept was then evaluated to obtain the static margin (K_n); static margin ranged from 0.20 to 0.50. The data shows the expected trend, as l_t increases so does static margin. Slightly higher static margins were achieved by the lifting-tail fuselage concepts.

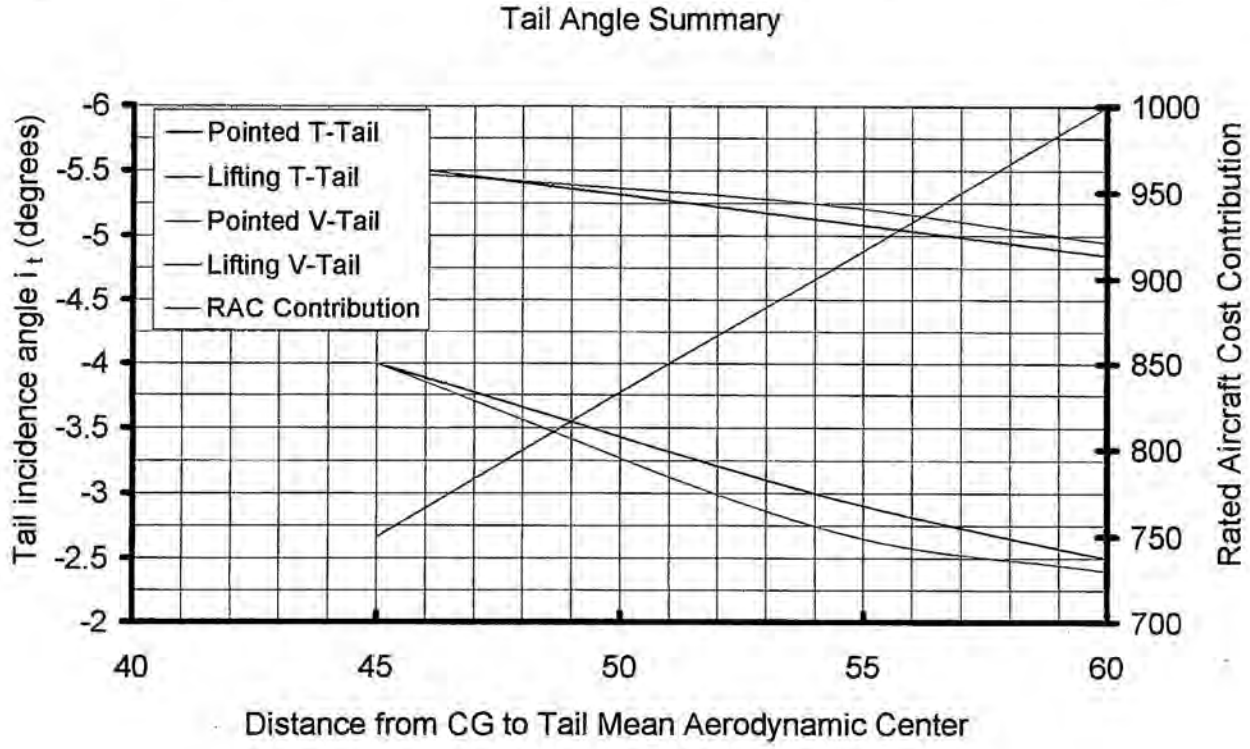

Figure 4-12 Tail Angle Summary

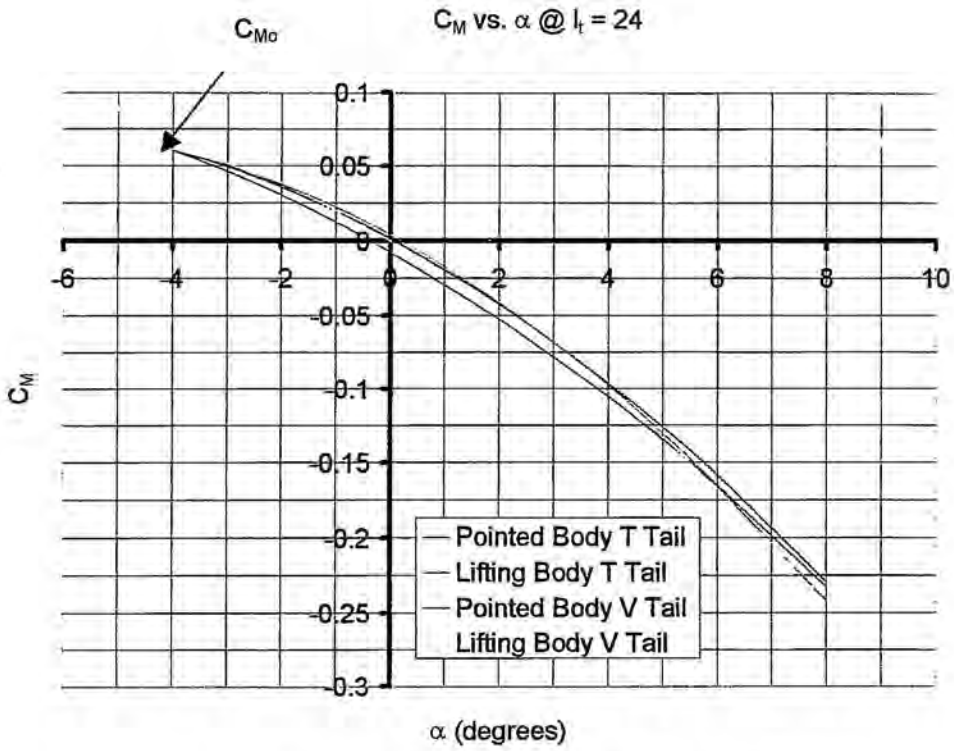

Figure 4-13 Static Stability of Fuselage Concepts

4.6.3. Tail and Fuselage Conclusion

There was little advantage in stability or lift of the flat trailing edge fuselage over the pointed fuselage. Choosing the pointed fuselage as the final design was due to the fact there was a significant weight savings. The V-tail provided no significant advantage and therefore was dismissed.

4.7. Wing-Body Lift Curve

VSAERO was used to find the wing-body lift curve for the final configuration. C_{Lmax} and α_{stall} was determined by the methods of reference 7. The curve did not change significantly from the finite wing curve in Figure 4-8 and therefore is not reproduced here.

4.8. Drag Estimation

Breaking the final configuration down into four component parts, namely the wing, fuselage, empennage, and landing gear, C_{Do} was calculated by the methods in Reference 8. The results are as follows:

C_{Do} =	$C_{Do\ (wing)}$	$+C_{Do\ (fuselage)}$	$+C_{Do\ (empennage)}$	$+C_{Do\ (gear)}$
0.0253849	0.01578482	0.006471667	0.003092458	3.5952E-05

Table 4-3 C_{Do} results

Applying the C_{Do} to the 3-term drag polar equation results in Figure 4-14 below.

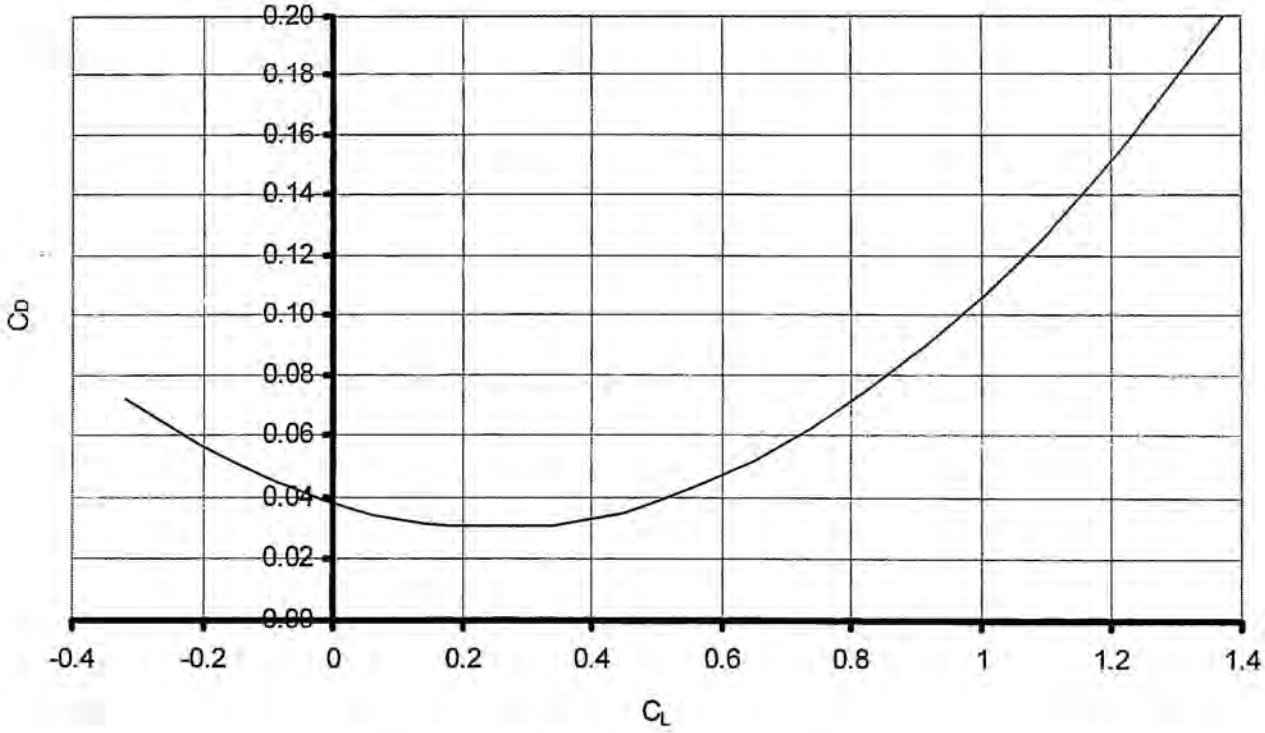

Figure 4-14 Three-Term Drag Polar

4.9. Power Plant Design

Initial investigations suggested that the Graupner Ultra 3300-10 motor would give better performance than the Astro 60, which had been used for last year's design. The Graupner motor was purchased and tested against the Astro, and the Graupner showed a higher efficiency.

Computer simulation using P-Calc and MotoCalc suggested that maximum performance with the 10-turn Ultra 3300 would be obtained from high voltage battery packs with more than 28 cells. In order to investigate lower voltage (lighter weight) systems, the 3300-7 motor was selected. The results from calculations suggested that maximum performance would be obtained from approximately 22 cells. Further calculations predicted that the 3300-5 motor would yield even higher thrust and pitch speed than the 3300-7 on as few as 18 cells. In order to allow for some flexibility in the power system, both the 7-turn and 5-turn Graupner Ultra 3300 motors were purchased.

MotoCalc and P-Calc were used to model the power systems using a number of propeller sizes. The resulting parameters of major interest were a predicted thrust and pitch speed. While the 18x16 propeller was near optimum for the 3300-7, a smaller propeller of 15x16 yielded even more encouraging results for the 3300-5. The 3300-7/18x16 combination yielded 102.7 oz of in-flight thrust, with a pitch speed of 74.6 MPH. The 3300-5/15x16 gave only 68.2 oz of in-flight thrust, but at a pitch speed of 87.6 MPH.

Total battery weight is a very significant factor in the payload carrying ability of any aircraft; therefore, the decision was to keep battery weight to the minimum required to complete the flight missions. Minimizing the battery weight also reduces the RAC considerably. Because the 24% higher in-flight thrust of the 22-cell 3300-7 power system required a 50% increase in battery weight, the 18-cell 3300-5 system was chosen for initial flight testing. For enough duration to finish one mission the Sanyo CP-2400 was chosen.

In conclusion the initial power system is as follows: Graupner Ultra 3300-5 motor, Kruse 2:1 gearing, RFM 15x16 propeller, 18 Sanyo CP-2400 cells, SWN Super 120 speed controller.

4.10. Structural Considerations

Conceptual Design defined a requirement such that the aircraft must be able to sustain a 4.5-g turn. Landing may also cause high loading due to rough conditions. To ensure structural integrity, a skeletal structure was designed with proper load paths between the wings, motor, tail boom, and landing gear. A model was created in Pro-Engineer and evaluated with Pro-Mechanica. Any high stress areas, which were marginal, were redesigned to reduce these stresses.

Although there was a major concern for the wing base, results showed no significant structural problems in this area. Since the fuselage skin is a carbon fiber composite, it will provide enough extra strength to accommodate the high stress areas shown in Figure 4-15 below.

The split-wing interface loading was calculated to have a bending moment of 600 in-lbs at a 4.5-g turn. This translates to a bending stress of about 50,000 psi using a ½ in. solid-carbon rod, which can take four times that amount (safety margin of 4).

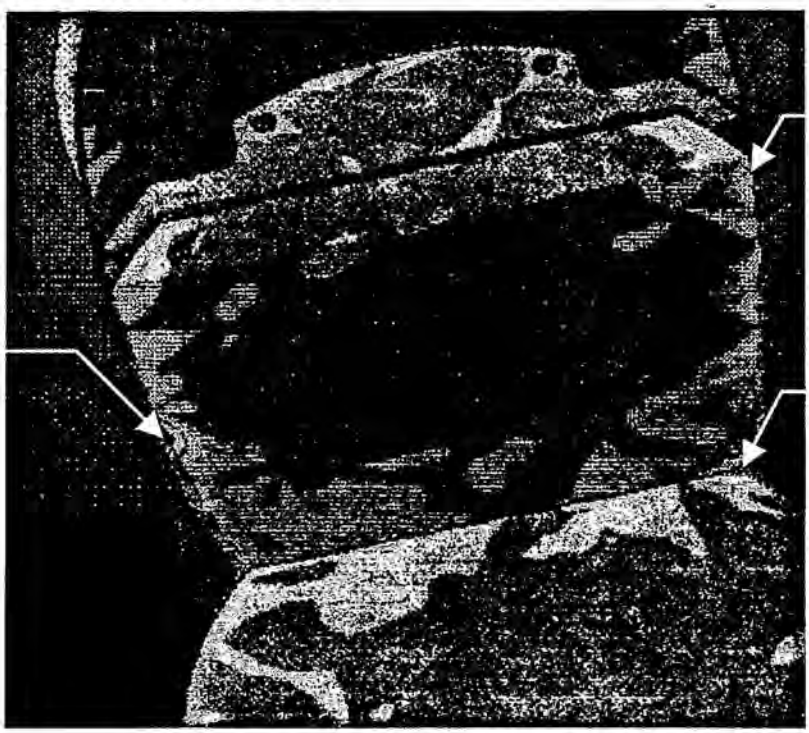

Figure 4-15 Pro-Mechanica Structural Analysis

5. Detailed Design

The detail design was the final step before fabrication could begin. Drawings were created and performance was estimated.

5.1. Configuration Summary

The following table contains all the configuration data as required by the report. Performance was calculated using the methods in Reference 7.

Geometry		Performance	
Length	4.5 ft	C_{Lmax}	1.41
Wing span	6 ft	L/D_{max}	11.0
Height	1.7 ft	Maximum rate of climb	15 ft/s
Wing: root chord	0.92 ft	Stall speed	44.2 ft/s
Wing: tip chord	0.92 ft	Maximum Speed	118 ft/s
Wing area	5.52 ft^2	Take off field length (empty)	50.6 ft
Aspect Ratio	6.5	Take off field length (gross)	119 ft
Horizontal area	1 ft^2	**Systems**	
Horizontal volume ratio	0.58	Radio	Hitec Prizm 7X
Vertical area	0.44 ft^2	Servos	Hitec HS-225BB
Vertical volume ratio	0.034	Battery	18 Sanyo CP-2400
Weight Statement (lb)		Motor	Graupner 3300-5
Airframe	7	Propeller	15x16 RFM
Propulsion	4	Gear Ratio	2 to 1
Control System	0.5		
Payload System	0.2		
Payload	6		
Empty Weight	11.7		
Gross weight	17.7		

Table 5-1 Final Component Selection, Geometry, Performance, Weight Statement, and Systems

5.2. Rated Aircraft Cost

Final RAC is 7.81, based on the following table.

	RAC	7.81	
	MEW	11.7	
	REP	2.34	
	MFHR	156.36	
# of cells	18		Sanyo 2400
weight per cell	2.08	oz	weight includes extra hardware
total battery weight	2.34	lb	
WBS	**Value**	**Hours**	**Multiplier**
1.0 Wings			
wing span (ft)	6.00	48	8 hr/ft Wing Span
chord (ft)	0.92	7.36	8 hr/ft Max chord
# of control surf	2	6	3 hr/control surface
2.0 Fuselage			
Max length (ft)	4.5	45	10 hr/ft max length
3.0 Empennage			
# of vertical-nc	1	5	5hr/vertical-no control
# of vertical-ac	0	0	10 hr/vertical-active control
# of horizontal	1	10	10 hr/horizontal-see wing rule
V-tail only		0	v-tail-15 hr
4.0 Flight Systems			
# of servos/control	5	25	5 hr/servo (Note 1)
5.0 Propulsion			
#of engines	1	5	5 hr/engine
#of propellers	1	5	5 hr/propeller

Note 1: 2 ailerons, 1 elevator, 1 nose wheel, 1 payload release (no rudder)

Table 5-2 Rated Aircraft Cost of Final Configuration

5.3. Dynamic Stability Estimation

Section 4.6 showed that the airplane would be statically stable, but dynamic stability still had to be confirmed. A combination of sources was used to accomplish this task. Pro-Engineer provided the moments of inertia, Advanced Aircraft Analysis (AAA) supplied some information, and the rest was hand calculated using References 4, 7, and 8. The derivatives had to be performed for the vehicle's stabilities in the longitudinal and lateral directions.

Based on an average speed of 100 ft/s the phugoid period is 13.8 seconds, which is enough time for the pilot to make corrections.

Longitudinal and lateral stability derivatives are as follows:

Conditions			Longitudinal		Lateral	
θ_o	0	(degrees)	C_{Xu}	-0.1	$C_{y\beta}$	-0.3826
g	32.2	(ft./sec.^{2})	C_{Zu}	-0.1	C_{yp}	0.0015
M	0.09	(Mach #)	C_{Mu}	0.0015	C_{yr}	0.0846
W	18	(lbs.)	$C_{X\alpha}$	0.2	$C_{l\beta}$	0.0800
I_y	771	(slug*ft.^{2})	$C_{Z\alpha}$	-5.76	C_{lp}	-0.4680
alt	100	(ft.)	$C_{M\alpha}$	-0.7953	C_{lr}	0.3886
a(h)	1117	(ft./sec.)	C_{Xq}	0	$C_{n\beta}$	-0.1059
ρ	0.00237	(lbs.*sec.^{2}/ft.^{4})	C_{Zq}	-6.63	C_{np}	-0.1451
S_w	5.52	(ft.^{2})	C_{Mq}	-10.76	C_{nr}	-0.0863
$c_{bar\ w}$	0.92	(ft.)	$C_{X\alpha}^{dot}$	0		
			$C_{Z\alpha}^{dot}$	-2.056		
			$C_{M\alpha}^{dot}$	-3.27		

Table 5-3 Stability Derivatives

Using the characteristic equation coefficients and Routh's criteria for stability, the aircraft has no unstable modes for this flight condition. An evaluation was performed for takeoff, landing, and different load conditions and no stability problems were found.

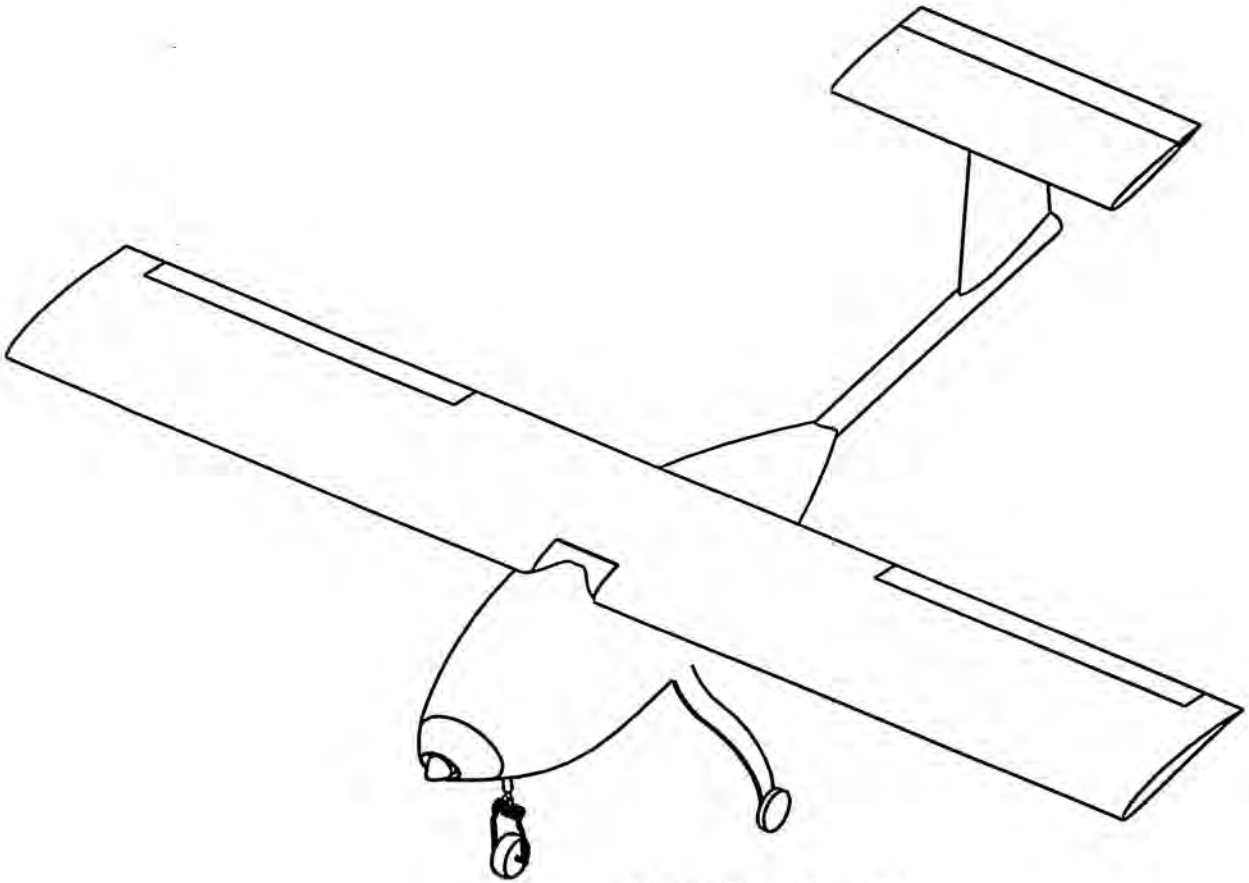

SCALE 0.100

SDSU AEROSPACE ENGINEERING	
DRAWN BY	DATE
SIZE A	DWG NO DBF2003
SCALE	SHEET OF 5

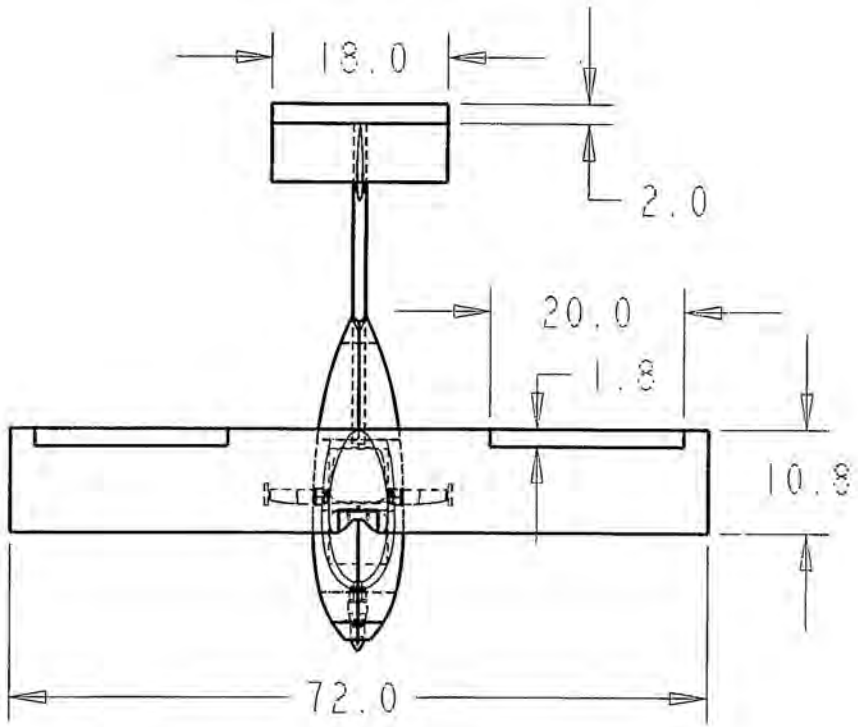

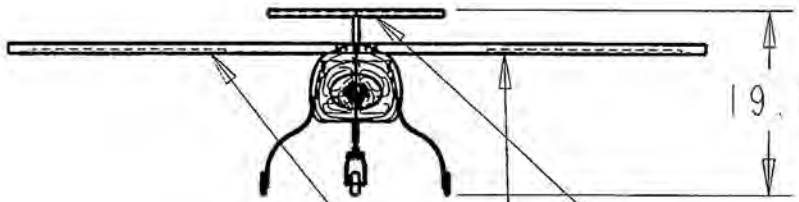

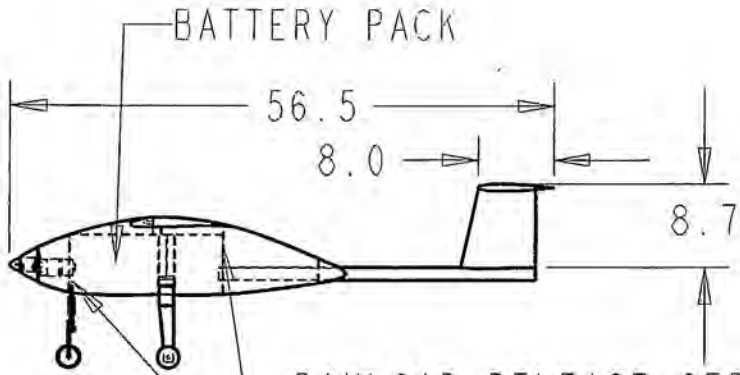

ELEVATOR SERVO

NOSE WHEEL SERVO

PAYLOAD RELEASE SERVO

AILERON SERVOS

SIZE	DWG NO	REV
A	3-VIEW	
SCALE		SHEET 2

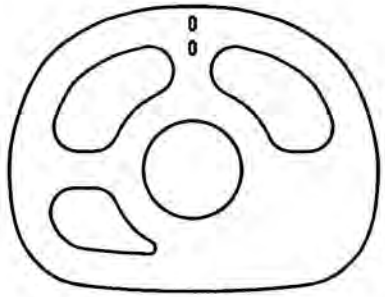

FS 6 BULKHEAD

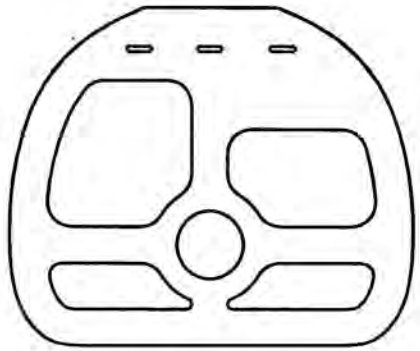

FS 22 BULKHEAD

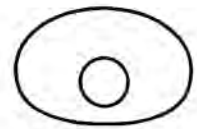

FS 32 BULKHEAD

ALL PARTS SCALE .250

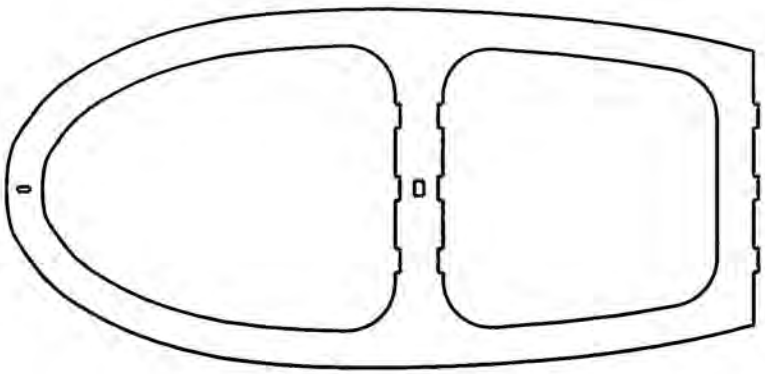

UPPER FRAME

ALL PARTS ON THE SHEET ARE
CARBON/FOAM SANDWICH PLATES

SIZE	DWG NO	REV
A	FOAM CORE CARBON PARTS	
SCALE		SHEET 3

ALL PARTS ON THE SHEET ARE MADE WITH A 7-PLY CARBON/ KEVLAR COMPOSITE

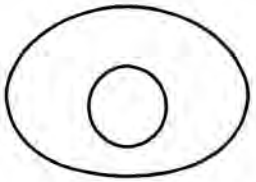

MOTOR MOUNT BULKHEAD

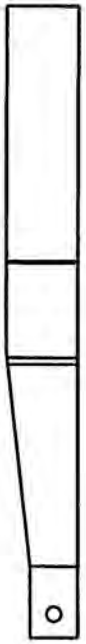

LEFT LANDING GEAR
RIGHT LANDING GEAR
IS A MIRROR IMAGE

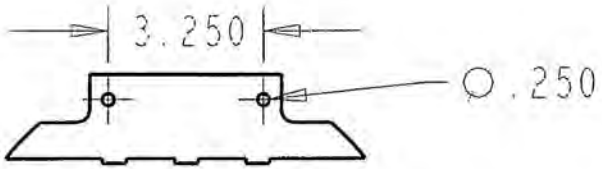

WING MOUNTING BRACKET

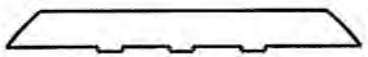

STIFFENER

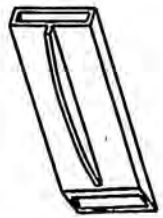

LEFT LANDING GEAR SOCKET

ALL PARTS SCALE 0.250

SIZE	DWG NO	REV
A	CARBON/KEVLAR PARTS	
SCALE		SHEET 4

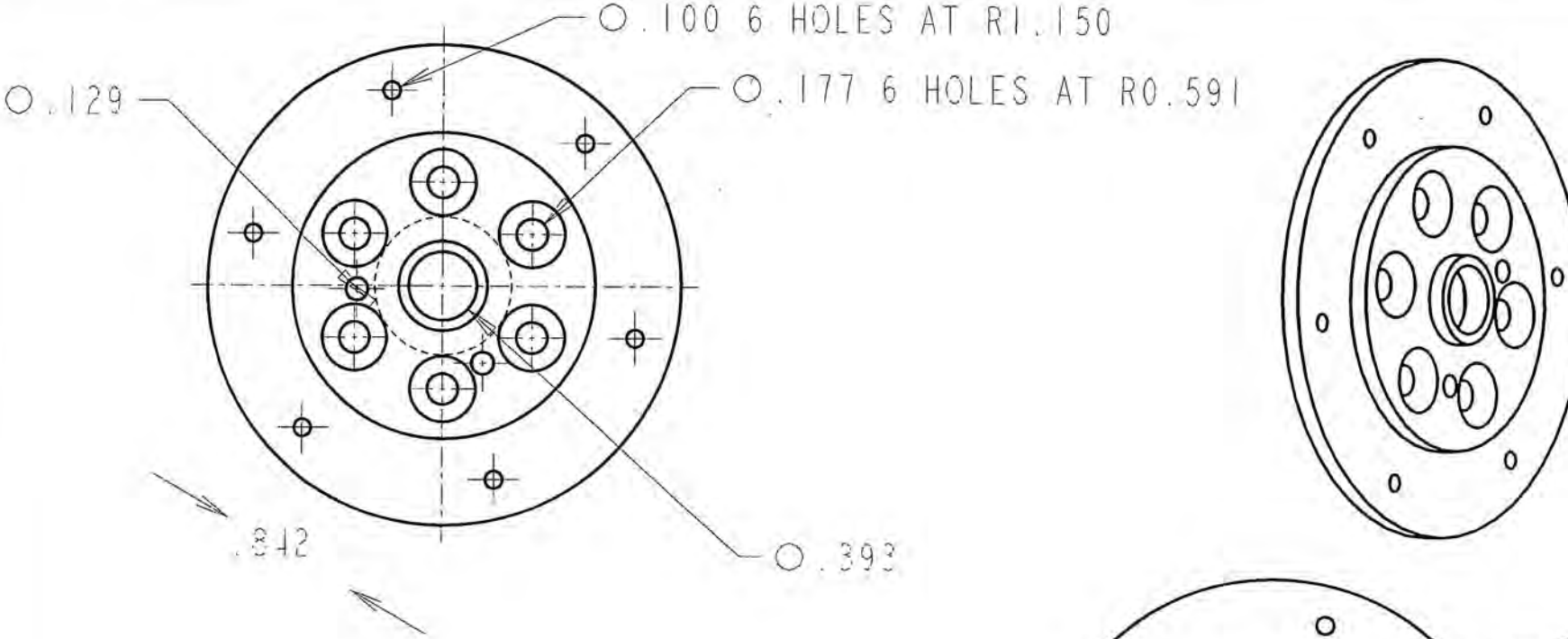

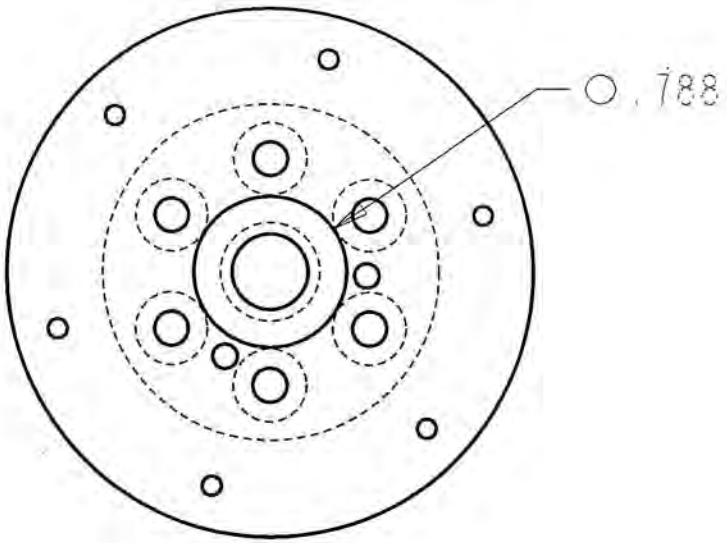

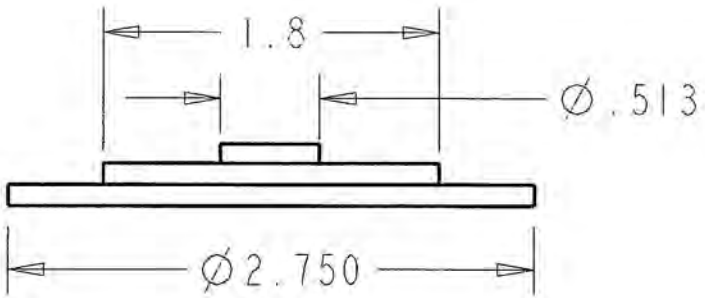

SCALE 1.000

SIZE	DWG NO	REV
A	MOTOR MOUNT PLATE	
SCALE		SHEET 5

6. Manufacturing Plan

Evaluating all the major components with respect to the choices of the materials resulted in choices of fabrication methods. Each process was rated on a number scale in which high numbers were desirable characteristics and low numbers were undesirable characteristics. After the evaluation a manufacturing schedule was created.

6.1. Major Components

Major components were defined as the parts of the aircraft that needed to be fabricated before the propulsion system, assembly systems, and electronic components were installed. The major components were the fuselage, wings, tail, bulkheads, tail boom, motor mount, nose/ main landing gear, and wheels. They also included the interfacing mechanisms with each other. Other parts such as assembly systems were produced in parallel with the major components.

6.2. Materials

Materials that were considered for the major components included carbon fiber, fiberglass, plywood, aluminum, and plastic, and one other commercially available material (steel) in a pre-manufactured form for the nose gear. The materials were rated for each component by using Figures of Merit (FOM). Minor components were made either of the above materials or of brass, Kevlar composite, or balsawood. Because minor components required less lead-time, they were fabricated in various ways and allowed choices to be made based on the component performance.

6.3. Figures of Merit

Figures of Merit (FOM) were used to evaluate the materials for the availability, required skill levels, cost, time to manufacture, and strength to weight ratio.

6.3.1. Availability

Scaling ranged from 0 to 2. If the materials or the components were on hand, it received a 2. If they had to be purchased or they required machining, it received a 1. If the material was not available due to reasons beyond the team's control, it received a 0.

6.3.2. Required Skill Levels

Easy to fabricate materials, which required no previous or limited experience, were issued 5 points. A prohibitively difficult process or an unavailability of the manufacturing equipment received a 1. Skills of the team members were also used in order to make an informed decision about the manufacturing process within each of the categories. Table 6-1 is a summary of number of personnel with the appropriate skills.

	Skills						
	Model plane building	Wood working	CNC	lathe	composites	hotwiring	electric motor power plants
Number of personnel	4	4	2	2	5	5	3

Table 6-1 Skills Matrix

6.3.3. Cost

A value of 1 was assigned if the cost of the material was beyond the means of the project's budget. Inexpensive material received a 5. If the material was already on hand or if it was to be donated in sufficient amount, it was given a rating of 5; carbon fiber and fiberglass were in that category.

6.3.4. Time to Manufacture

This parameter was added as a FOM because the team needed to fabricate the major components in time for flight-testing. Composite materials received the low rating of 1 because the team had to fabricate bulkheads and cut them to size. Material or components available in their final form received the high rating of 3.

6.3.5. Strength to Weight Ratio

A qualitative approach was taken to determine the strength to weight ratio for each material since many of the materials such as some of the carbon fiber fabrication techniques are not readily calculated. Experience and experimental techniques were used to determine the capability of the material properties.

6.4. Summary of Material Choices

Table 6-2 shows the evaluation of the materials for different components of the aircraft. Highlighted numbers are the highest scoring material and therefore chosen for the fabrication method for the specified component. Most components would be fabricated using a carbon fiber composite with only a few exceptions. The motor mount plate is to be made of aluminum and both the wheels and nose gear were obtained commercially; modifications were made to optimize the commercial products to fit the design.

		Availability	Required Skill Levels	Cost	Time to Manufacture	Stregth to Weight Ratio	Average
Fuselage	carbon-fiber	2	3	5	1	5	**3.20**
	fiberglass	2	3	5	1	3	2.80
	balsawood frame	1	5	3	2	2	2.60
Wing	carbon-fiber (foam core)	2	3	5	1	5	**3.20**
	fiberglass (foam core)	2	3	5	1	4	3.00
	balsawood frame	1	5	3	2	2	2.60
Tail	carbon-fiber (foam core)	2	3	5	1	5	**3.20**
	fiberglass (foam core)	2	3	5	1	4	3.00
	balsawood frame	1	5	3	2	2	2.60
Bulkheads	carbon-fiber (foam core)	2	3	5	1	5	**3.20**
	fiberglass (foam core)	2	3	5	1	4	3.00
	plywood	1	5	3	2	3	2.80
Tail Boom (commercial)	carbon-fiber	2	2	5	1	5	**3.00**
	fiberglass	0	2	1	1	5	1.80
	wood	2	3	5	1	2	2.60
	aluminum	1	4	3	2	3	2.60
Motor Mount	aluminum	1	3	3	1	4	**2.40**
	plastic	2	1	0	2	2	1.40
Nose Gear	commercial						
Main Gear	carbon-fiber	1	3	5	1	5	**3.00**
	aluminum	1	4	4	2	3	2.80
Wheels	commercial	2	5	2	3	4	**3.20**
	aluminum	1	5	4	1	4	3.00
	plastic	0	3	2	2	1	1.60

Table 6-2 Figures of Merit Summary for the Manufacturing Process

6.5. Manufacturing Schedule

The manufacturing team leader created the schedule to complete fabrication and test fly a prototype before the report was due. Both projected and actual schedules are shown in Figure 6-1 below.

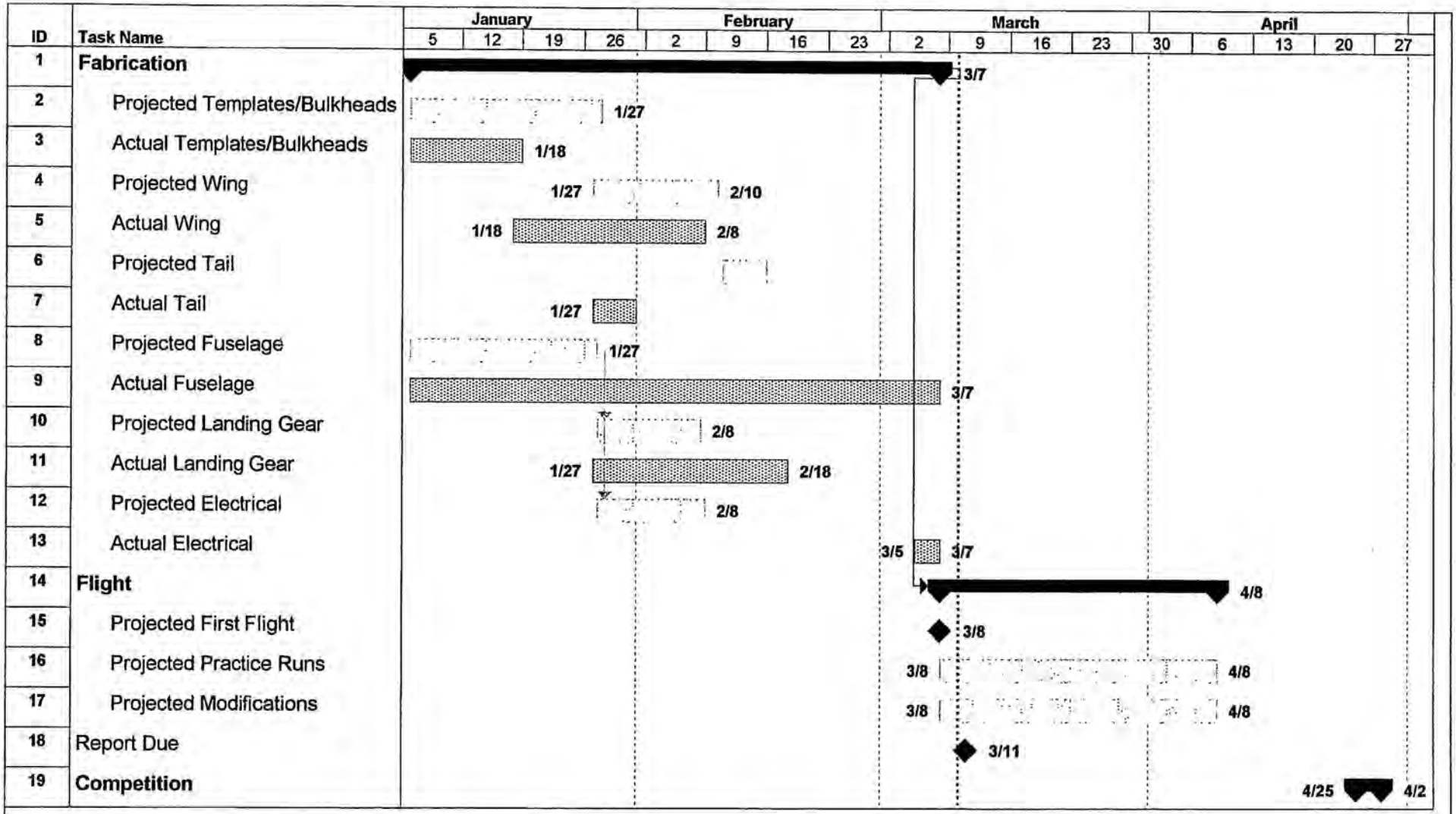

Figure 6-3 Manufacturing Schedule

6.6. Manufacturing Processes

Fabrication sites were at the Aerospace Lab at San Diego State University and at the shop of the Manufacturing Team Leader. Safety during the manufacturing processes was maintained by following the team leader's instructions.

Choices of the materials led to a definitive process of fabrication for each component. Alternative processes investigated were to use a foam core or a female mold for the fuselage fabrication. These two processes were evaluated with respect to the following FOM:

I. Time to Manufacture: With the projected date of the flight-testing approaching, this was the most significant of any other factors; the foam core required less time to manufacture.
II. Expected Product Performance: The foam core would create a rougher finish on the outer surface of the composite skin. Female molds could be smoothened out to reproduce a close shape to the drawings.
III. Required Skill Level: Team lacked the experience in manufacturing the molds.
IV. Cost: The foam was considerably less expensive than the materials required for making the molds.
V. Repeatability: A high repeatability would ensure easy reproduction in case of failure in fabrication or damaged to the finished product. The use of foam core is an irreversible process, whereas the female molds could be used repeatedly.

The alternative with an advantage in each FOM was awarded a 1. Summation of the points led the decision to use the foam core. This evaluation is summarized in Table 6.3 below.

	Time to Manufacture	Expected Product Performance	Required Skill Level	Cost	Repeatability	Sum
Foam Core	1	-	1	1	-	3
Female Molds	-	1	-	-	1	2

Table 6-3 FOM Summation for Fuselage Manufacturing Technique

The following describes the processes of the major component fabrication. Pictures of some of the manufacturing processes are shown in Figure 6-1 below. The processes for each component are chronologically ordered.

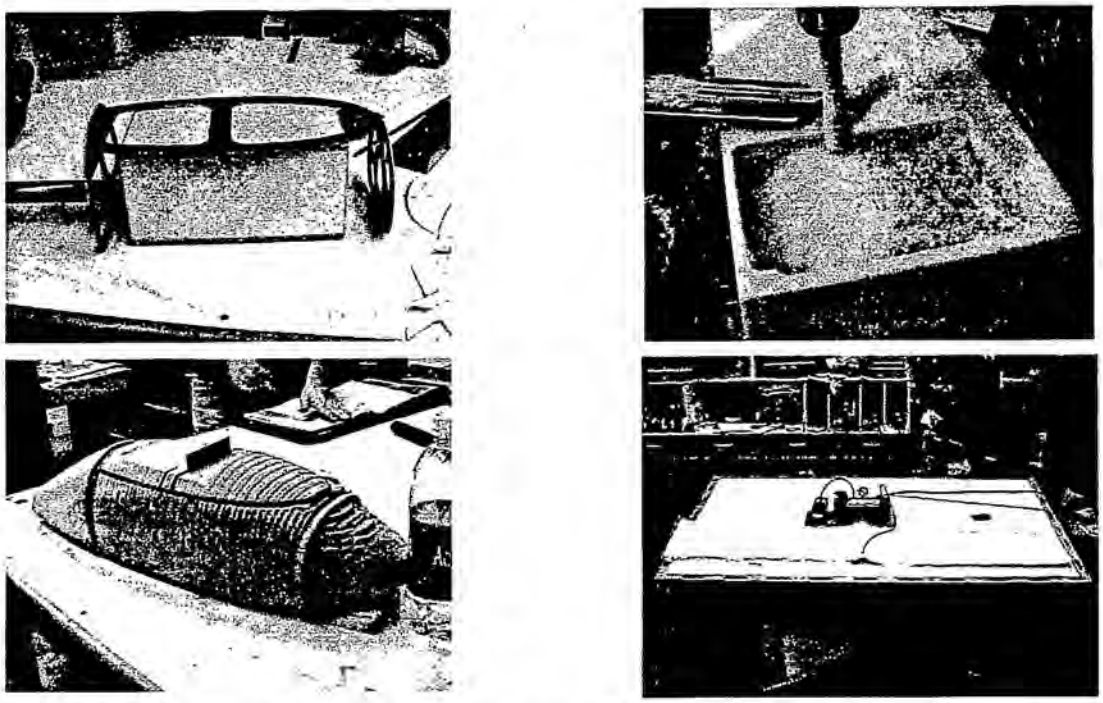

Figure 6-1 Manufacturing processes used (clockwise from upper left: basic internal structure with payload, CNC milling, vacuum bagged wings, foam core prior to sanding)

6.6.1. Structural Framework

Structure framework was first created using carbon fiber/foam sandwich composite sheets. Other parts such as the motor mount bulkhead used a multiple layer of carbon composite including Kevlar. Templates were used to cut the bulkheads to size.

6.6.2. Fuselage

Codes (m-code) were obtained from Pro-Engineer (CAD) of the fuselage outer-mold-line (OML) and then transferred to the CNC for an autonomous milling of the foam core. The foam core was combined with the bulkheads and finished sanded to a smooth surface. Lay-up consisted of carbon fiber and epoxy, using a flexible vacuum bag. Upon curing, the foam was removed and interface areas prepped for the final assembly.

6.6.3. Wings and Tail

The first step was to hotwire the foam cores by using a fabricated endplate template. To obtain a smooth finish and accurate sizing carbon fiber and epoxy lay-up was used along with a vacuum bag and Mylar sheets.

6.6.4. Main Landing Gear

Landing gear shape was designed using Pro-Engineer. The drawing was used as a template to create a wood mold. Landing gear was then fabricated in the same multi-layered method as the motor mount bulkhead.

6.6.5. Nose Gear

A commercially obtained nose wheel had to be modified for the assembly system. The upper shaft was cut and threaded to accept the hinged adapter. The hinged adapter was designed and then machined in the school's lab by the manufacturing team.

6.6.6. Motor Mount

An adapter plate between the reduction gear and the motor was substituted for a motor mount plate designed and machined by the manufacturing team. It was needed to interface the motor to the motor mount bulkhead.

6.6.7. Tail Boom

A wrapped carbon fiber tube was obtained for the tail boom. Because of the expense of the tail boom, a lightweight aluminum was purchased as a standby.

6.7. Electronic Components and Payload Deployment System

The final steps of the fabrication were the installation of electronic components and the payload deployment system. Electronic components, namely wires and servos, were installed in such a way that they would require the shortest length of the connections while reducing the possibility of failure. The payload release system was then placed into the structure. Finally, the fuse was mounted on a relatively flat surface on the side of the fuselage.

6.8. Structural Integrity

Dropping the body with a 15 lb load from one-foot high tested the landing gear interface. The load simulated a rough landing during the actual missions; the test was conducted more than 10 times. Although a large amount of flex occurred on the main gear, the structure did sustain the load.

Based on wing loading during a 4.5-g turn, the wings were tested to ensure they could handle the load. Wings were assembled to the body and an extra 45 lb box payload was hung from the CG. The wings were then lifted from 1/4 span to test the wing body interface; the test was successful.

6.9. Conclusion of Fabrication Phase

Installation of the electronic components and payload deployment system marked the end of the fabrication phase. The propulsion system, namely the motor and the batteries, would be placed into the reserved spaces without affecting the structure. Now the Spirit of Monty was ready for the flight-testing.

7. Testing Plan

Completion of the fabrication phase was in time for flight-testing on March 9, 2003 at Lakeside, California.

7.1. Flight Testing Objectives and Checklist

The objectives were set to simulate the competition, to evaluate the general performance of the prototype, and to obtain information for optimization. Simulation of the competition would be achieved by conducting a safety inspection and by attempting the three mission flights. A completed checklist for first-flight is shown in Table 7-1 below. Results of the testing and lessons learned are described in Section 7.2.

Security Inspection checklist

Check	Order to be followed
x	1. Secure connection of the aircraft components
x	2. Propeller structural and attachment integrity
x	3. Adequate electronic connections and confirmation of the maximum current draw
x	check
x	4. Structural verification to include: lifting with one point at each wing tip, cg location
x	5. Radio range check with motor off and on. Radio fail-safe check
x	6. Control surfaces operations
x	7. Integrity of the payload system
x	8. Static propulsion test

Flight performance checklist

rating	checklist
C	1. Take-off performance.
A	2. Near-stall performance after the take-off.
A	3. High-g turn performance.
A	4. Altitude.
N/A	5. Endurance.
F	6. Landing performance.

rate as follows:
A --- No major/minor problems
B --- Minor problem(s)
C --- Major problem(s)
F --- Failing

	misison A	mission B	mission C
AH used			
Flight time			

AH = Amp-Hour

Table 7-1 Testing Worksheet

7.2. Lessons Learned

Testing began in the late afternoon. As Table 7-1 indicates, the security inspection was completed without problems. However, the flight was limited for one lap without payload, due to the sunset; the aircraft made its first flight with glow-lights attached. The measured take-off distance was approximately 110ft. Time of flight, including the times of take-off and landing, was 44 seconds. The aircraft stumbled and flipped up side down at the end of the landing. The payload box was not installed. Power usage was not measured.

Although the flight was brief, the post-testing conference addressed some key issues in power plant, control surfaces, and landing gear performances. According to these results, recommendations were made for modifications and further optimizations.

7.2.1. Power Plant

A considerably longer take-off distance, compared to the estimated distance in the detail design, indicated that the aircraft was underpowered. The analyses of the combination of the propeller and battery, or the pitch of the propeller, should be reviewed. In the analyses, effects on static performance may need to be emphasized against dynamic performance, so that the take-off thrust is sufficient. Power plant was expected to be a limiting factor since the configuration was the minimum required, which saved on RAC. Steps will be done to try to improve this power plant while marinating a low RAC.

7.2.2. Control Surfaces

The landing-run required more than 200ft, at the end of which the aircraft lost control. This was due to a lack of yaw control, as the pilot alluded to in the conference. The aileron-only-landing provided less than necessary control than expected. A provision was already included into the vertical stabilizer to add a rudder if needed. Although the extra servo will increase the RAC, the team wanted to first attempt flight without it. In addition, the sensitivity or the effect of the elevator was observed to be too profound. Adjustment on the transmitter can be done to accommodate this for the next flight.

7.2.3. Landing Gear

The aircraft was observed to tend sideways during the take-off and landing. Insufficient rigidity of the nose gear and/or main gear could cause this issue. The aluminum socket for the nose gear was spotted as one of the possible causes; a modification will be made on the joint. Also, the placement of the nose gear with respect to the servo structure may need to be assessed whether it was aligned to the direction of take-off with the controller deactivated.

References

1. Abbott and A.E. Von Doenhoff. Theory of Wing Sections. New York: Dover, 1959
2. Anderson, John. Fundamentals of Aerodynamics. New York: McGraw-Hill, 1991
3. Drela, Mark. XFOIL 6.94 User Guide. Boston: MIT, 1986
4. Etkin, Bernard. Dynamics of Flight. New York: John Wiley & Sons, 1996.
5. Katz, Joseph, and Allen Plotkin. Low Speed Aerodynamics. New York: Cambridge, 2001
6. Nathman, James. VSAERO User's Manual Version 6.2. Redmond: Analytics Methods Inc., 1982
7. Nicolai, Leland. Fundamentals of Aircraft Design. San Jose: Mets, 1984.
8. Roskam, Jan. Airplane Design: Part VI. Lawrence: DARcorporation, 2000.

2002/2003 AIAA

Cessna/ONR Design/Build/Fly Competition

Design Report

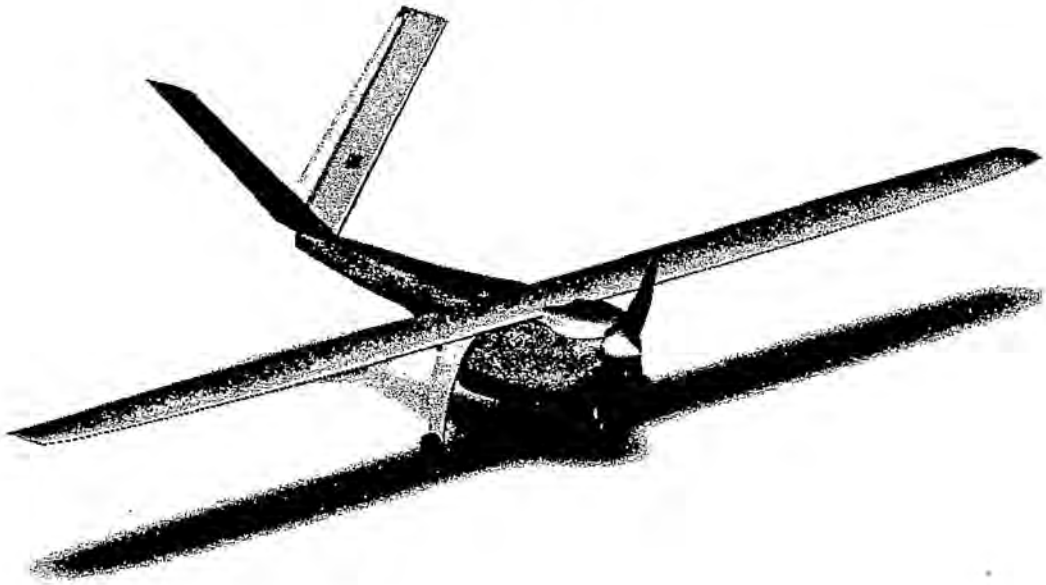

California Polytechnic State University

"Bareback"

Table of Contents

Table of Figures

Table of Tables

1.0 Executive Summary

In response to the AIAA's Design Build Fly 2002/2003 challenge, California Polytechnic State University at San Luis Obispo (Cal Poly SLO) assembled a small group of aerospace students consisting of both upper and lower classmen to design, build, and fly a radio-controlled aircraft in the Cessna Office of Naval Research Student competition. The goal was to create an aircraft designed for optimum performance within the contest rules and requirements. The competition total score was comprised of a written report score multiplied by the flight score, divided by the rated aircraft cost. The flight score was a result of two chosen flight missions and a timed assembly task. The design process of this aircraft consisted of a conceptual design stage, a preliminary design stage, and a detailed design stage.

1.1 Conceptual Design

Cal Poly's DBF team began this year's design by evaluating the three possible missions and picking the two that had the highest potential total scoring potential. Manufacturing methods and basic aircraft configurations which satisfied the mission profiles were discussed and selected, based on data obtained through research, spreadsheet applications, and previous student experience with the DBF competition. Basic configuration components and the payload deployment mechanisms were all researched and selected. In addition, the team continued the development of the design tools that were used for determining the optimum configuration and approximate dimensions.

1.1.1 Conceptual Design Alternatives

The mission profiles were selected by defining figures of merit, and analyzing how each profile met these requirements. The effect that the difficulty factors had on flight score as well as the feasibility of the aircraft was considered. The team also calculated the outputs of a simplified performance estimation program that predicted the score of an aircraft operating in a set of two missions. Having made the mission selection, possible aircraft configurations could then be tailored to meet the requirements. Basic aircraft configurations were chosen. In order to design a fuselage to best house and deploy the payload while having the smallest cost possible, the tradeoffs between a four foot fuselage, which required no assembly, and one with a plug-in tail boom were discussed.

For the wing configuration, the aerodynamics group studied the conventional wing, biplane, canard, flying wing, and blended wing/body. The aerodynamic group analyzed different shapes of fuselage and tail configurations. The conventional tail, cruciform tail, T-tail, V-Tail, and inverted V-tail were all analyzed. The propulsion group discussed and analyzed the number and type of engines to be used. The structures group studied landing gear and keel placement along with assembly choices.

1.1.2 Conceptual Design Results

Mission profiles A and B were selected. Simulation of mission profiles on DBF2003, a program written in Visual Basic consistently showed higher scores for this set of missions. A large portion of the design would be spent on the payload compartment and deployment system. The deployment system chosen was a gravity drop system due to its perceived mechanical simplicity and low weight. Because of the high-keel design of the aircraft, a conventional high wing was chosen to attach to the keel and avoid interference with the payload deployment. For easy ground handling, takeoff characteristics and strength, a tricycle non-retractable landing gear was chosen.

1.2 Preliminary Design

After the mission profiles were chosen and the basic configuration of the aircraft was finalized, the approximate aircraft size, component placement, landing gear, motors, and control surfaces were decided upon. The aircraft was to have 33 ounces per square foot wing loading, and be powered by a Graupner 930-6 motor operating from the power provided by a 12-cell Sanyo CP-1700SCR battery pack.

1.2.1 Preliminary Design Alternatives

Many of the options that were ruled out were based on the assembly time of the aircraft. Wing planform alternatives investigated were swept, elliptical, rectangular, tapered, and a modified Schuemann. The optimum aspect ratio was determined from the outputs of the DBF2003 performance simulation program and practical considerations. Tails such as the T-tail, the cruciform tail, and the canard configuration were discarded early since their disadvantages in complexity outweighed any benefits. Propulsion system components were selected to allow the optimum performance in the missions chosen. Motors from Graupner and AstroFlight product lines, different types of NiCd batteries and propellers of various diameter and pitch were compared in order to come up with the final configuration. One of the important topics for preliminary design was the payload deployment. The gravity deployment system discussed in conceptual design was also expanded upon.

1.2.2 Preliminary Design Results

The modified Schuemann wing planform was used in this design because it posed the best compromise between all of the concepts reviewed. After weighing the benefits of the 3 possible tails, the V-Tail empennage was chosen to decrease the aircraft rated cost, provide for maximum control authority and to simplify construction and operation. The size of the selected tail was calculated using tail volume coefficients equations from Raymer (Ref.1). The optimal landing gear for the mission was finalized as a non-retractable tricycle configuration for reasons of stability and simplicity. The landing gear was designed to have a steering front wheel with brakes. A one-piece conventional fuselage with the V-tail positioned at the end of an upswept tail boom was designed to enable easy payload deployment.

1.3 Detailed Design

After the basic configuration of the aircraft was laid out, the group developed more detail to the design and was able to perform more analysis of the chosen aircraft components. At this point the materials and manufacture processes were finalized. Finally, solid carbon joiner tubes for plug-ins, Velcro, and nylon bolts were chosen for the assembly.

1.3.1 Detailed Design Alternatives

Locations of all secondary components were investigated for aircraft balance requirements. The geometry of the payload deployment system was analyzed and improvements on the design were studied.

1.3.2 Detailed Design Results

At the conclusion of the detail design phase all aircraft dimensions, system components, and materials were decided on, aircraft performance and control characteristics determined and manufacturing processes selected. The estimations conducted by the design team predicted an RAC of 6.29, and an ideal final competition score of 18.75, with a flight time of 3.2 minutes for mission A and 3.1 minutes for mission B. Assembly time was estimated at 30 seconds.

1.3.3 Detailed Design Tools

The tools used in the detailed design process were X-foil and the DBF 2003 performance simulation program. A solid model of the aircraft used for visualization and balancing was created in Solid Works 2001 Plus. Many of the other estimates and design methods used by the team originated from the experience gained in Cal Poly's previous DBF entries.

2.0 Management Summary

Cal Poly's DBF team was organized to maximize productivity. Team members were assigned to areas based on experience and interest. Each person assigned to a specific topic worked continuously in concert with team members who were working in other areas of the design, facilitating immediate integration of parts and compatibility checks. In addition, a timeline was constructed to keep the project on task and on time.

2.1 Design Team Architecture.

Cal Poly's DBF team started its organization by choosing a team leader who had the responsibility for overall team direction as well as completion of each task in the allotted timeframe. After the demands of the project were ascertained, the team broke up the project assignments into four main groups: configuration, aerodynamics, propulsion, and structure. Team members were assigned to one or more groups depending on experience and demand.

The configuration group was responsible for the overall design of the aircraft, for using the simulation program to establish component requirements and calculating the initial dimensions of the aircraft. The simulation program itself was also developed further to be more accurate. This group was also responsible for the design of the deployment mechanism. At all times, this group was responsible for keeping the overall design optimized for maximum score.

The aerodynamics group was responsible for wing planform and airfoil selection and worked together with the structures group to design the fuselage and wing components of the aircraft to best fit the performance requirements. This group was also responsible for the stability and control of the aircraft, and had to integrate with the other groups with regards to location, size and type of empennage chosen, and the means of driving its control surfaces. Similarly, the flaperons had to be integrated into the wing and actuated.

The propulsion group had the responsibility of selecting the motor and batteries requirements to be used along all other radio gear that would be required for mission demands. Research on an optimum gearbox and propeller combination was conducted in parallel with motor and battery selection, and an integrated propulsion system was designed.

Finally, those in the structure group examined the aerodynamic and point loads to be taken, examined the load paths, sized the structural members and chose the best materials and manufacturing methods for the proposed design. The structure group was also responsible for the purchase of the materials chosen, and the construction of the aircraft and all systems involved. In order to carry out the construction of the aircraft, agreements were made with the Aerospace and Manufacturing departments at Cal Poly concerning use of their facilities, and established the 'Cal Poly DBF Shack.'

Few of the problems encountered were completely independent to a specific group, developing an awareness of the overall state of the project necessary for all team members. Having a small team kept the lines of communications shorter and more direct, therefore, there were less opportunities for misunderstandings. While each group member was responsible for a separate part, the group was integrated

into all parts of the project and constant communication between the members was maintained. Modifications to the design were reported to the team leader and the solid model of the airplane was modified accordingly and checked for possible integration problems with other areas of the design.

All team members contributed to the writing of the report in their specific expertise areas. Responsibility for public relationships and funding was equally split. These areas were crucial to securing the funds necessary to complete the project.

Table 2.1 – Team Members and Assignment Areas

Design Personnel	Assignment Areas
Yevgeniy Gisin/AE/SR	Team Leader, Configuration, Aerodynamics, Propulsion, Structure
Francesco Giannini/AE/SR	Configuration, Aerodynamics, Propulsion, Structure
Erin Clare/AE/SR	Aerodynamics, Propulsion, Structure
Matt McCue/AE/SR	Configuration, Aerodynamics, Propulsion, Structure
Nick Christiansen/AE/SR	Configuration
Torrey Smith/AE/JR	Configuration, Structure
Mike Radin/AE/SR	Structure
Renee Pasman/AE/JR	Aerodynamics, Propulsion, Structure
Eric Naess/AE/JR	Structure

2.1.1 Schedule Control

Once the competition rules had been published, the team members evaluated them and a schedule was set up immediately. The timely completion of the various tasks that comprise the construction of an airplane is key to producing a winning DBF aircraft. In order to assure this, a tight schedule had to be adhered to. The team produced a calendar with all the projected deadlines for the different phases of the competition including conceptual, preliminary, and detailed design as well as the manufacturing process, testing and the report write-up. As the project progressed, the actual time of completion was recorded and entered into the milestone chart versus the projected time (Table 2.2). In case of one of the tasks lagging, extra resources could be re-directed to keep the team on track.

Table 2.2 - Milestone Chart: May 2002 – April 200

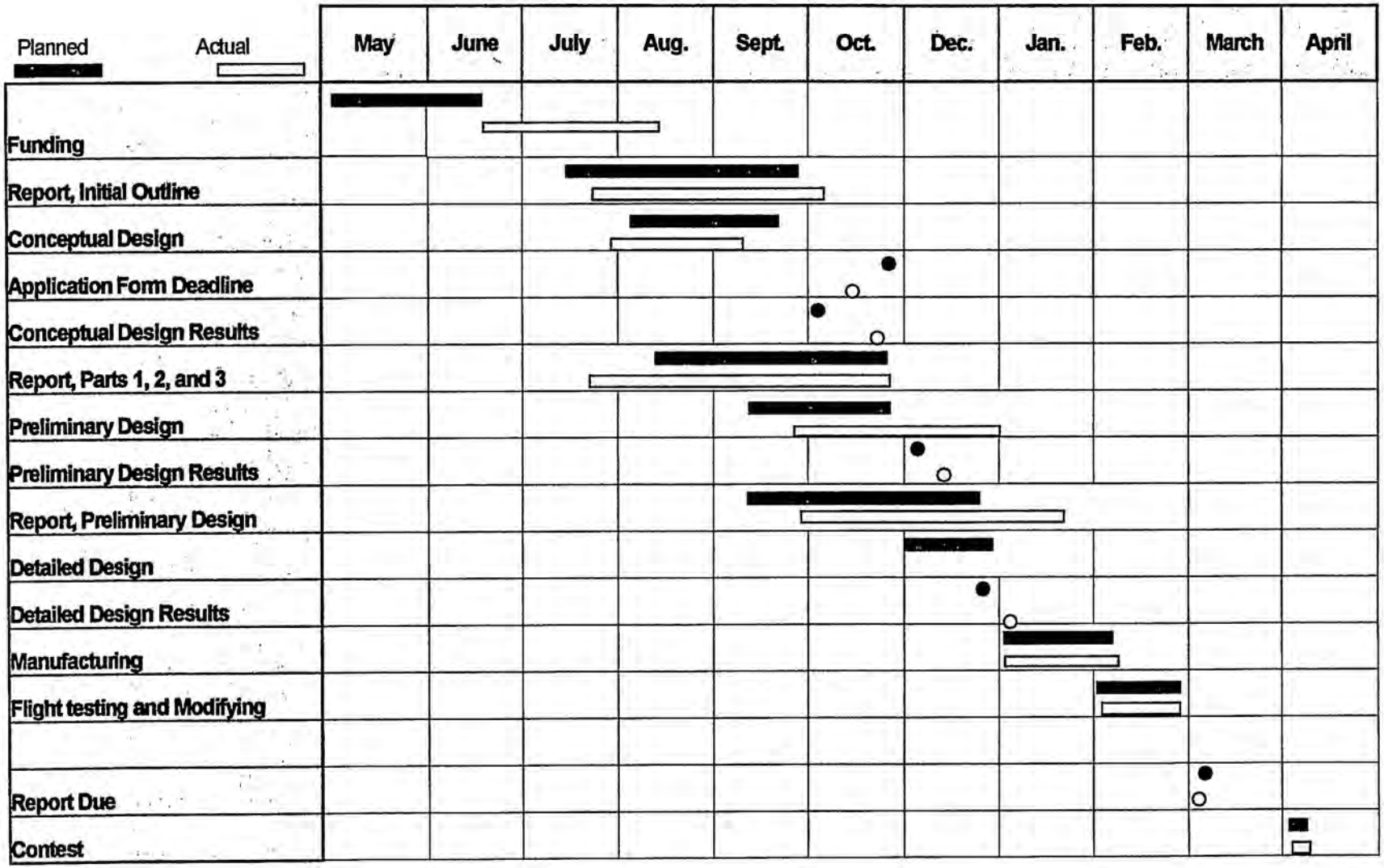

3.0 Conceptual Design

The conceptual design process of CalPoly's2003 DBF aircraft was a difficult task due to the selection of two of the three possible mission tasks specified in the RFP. In the previous years of DBF competition, the aircraft design had to be focused on optimizing a configuration for a specific mission. This year, the first choice that had to be made was the selection of two missions with the highest scoring potential.

The deployment mechanism was identified as the primary concern. This heavily influenced landing gear design, fuselage design, and wing placement. In order to accurately predict mission performance in mission A, the additional drag of the antenna had to be found. This was accomplished through independent methods whose results were matched closely enough for a reasonable confidence level in the predictions.

The final configuration chosen was best suited for the contest rules and mission, providing the greatest scoring potential.

3.1 Mission Selection

In order to initiate the conceptual design, the team first had to determine the two missions that the aircraft would be optimized for. Both the aircraft weight and drag would change from mission to mission, affecting aircraft performance and controllability. It was easy to estimate weight changes that the "electronics payload" container would cause; however, the team did not have any estimation of how the "antenna" would increase the drag of the aircraft. Knowing this amount of drag increase would be crucial in calculating aircraft performance in mission A enabling the down selection to two missions. The antenna model was placed in the Cal Poly open-circuit low speed wind tunnel and drag measurements at a number of airspeeds were taken (Figure 3.1 and 3.2).

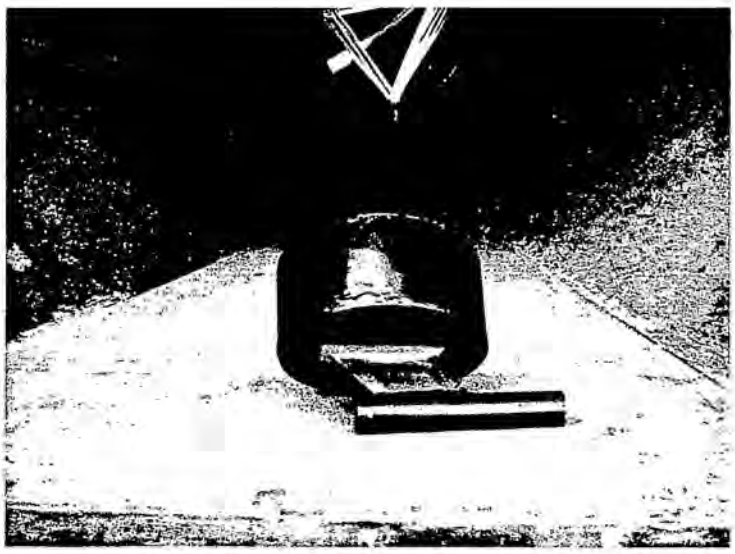

Figure 3.1- Antenna and sting balance strut in CalPoly's 3'x4' wind tunnel

The antenna, because of its shape and size, would constitute a considerable addition to the overall drag of the aircraft. The coefficient of drag of the antenna that was calculated from the test data was later used to predict the total drag of the aircraft during the "missile decoy" mission task. This number was compared to

results of a Floworks simulation of a solid model of the antenna at the predicted cruise speed (Fig. 3.2). The numbers obtained were closed enough that the wind tunnel results were confirmed.

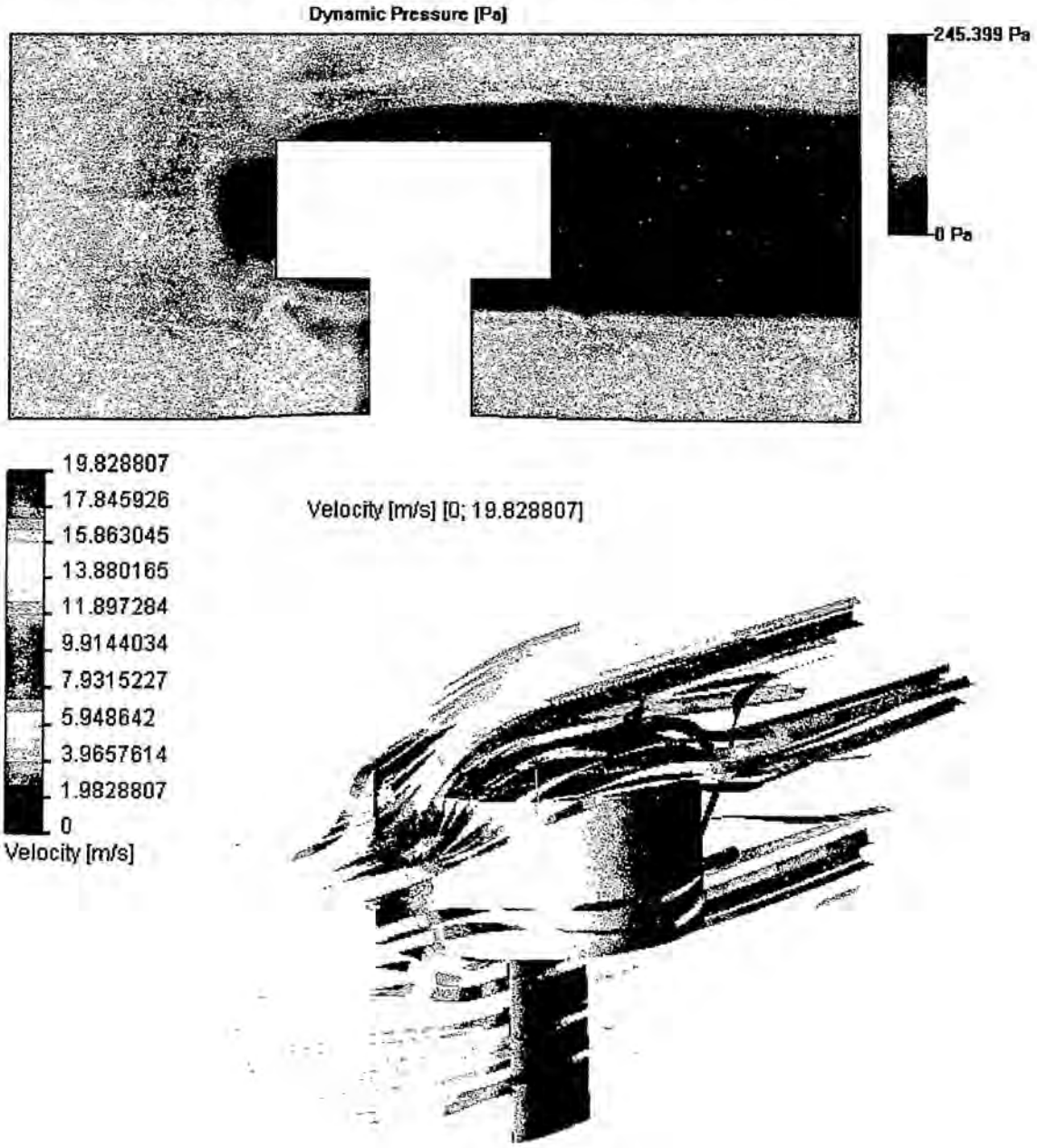

Figure 3.2- Floworks antenna drag estimation (V_∞ = 10m/s)

Having acquired all the necessary data to correctly estimate the effects the different missions would have on the aircraft performance, the selection of the two aircraft mission tasks could begin. The selection process was performed using the DBF2003 program that is described in detail in Section 4.5.1. Using the

program, three different aircraft configurations were optimized, each focusing on a set of two different missions. An important configuration driver was wing loading since it affects every aspect of aircraft performance. Power required on takeoff, C_L required in cruise, most efficient speed and a score of other parameters all depend on wing loading. Because of its importance, it was chosen as the independent variable for the results of the mission merit investigation to be portrayed against. Figure 3.3a&b shows the relative maximum score trend lines that would be attained by the three airplanes, each data point optimized for one of the three possible mission combinations.

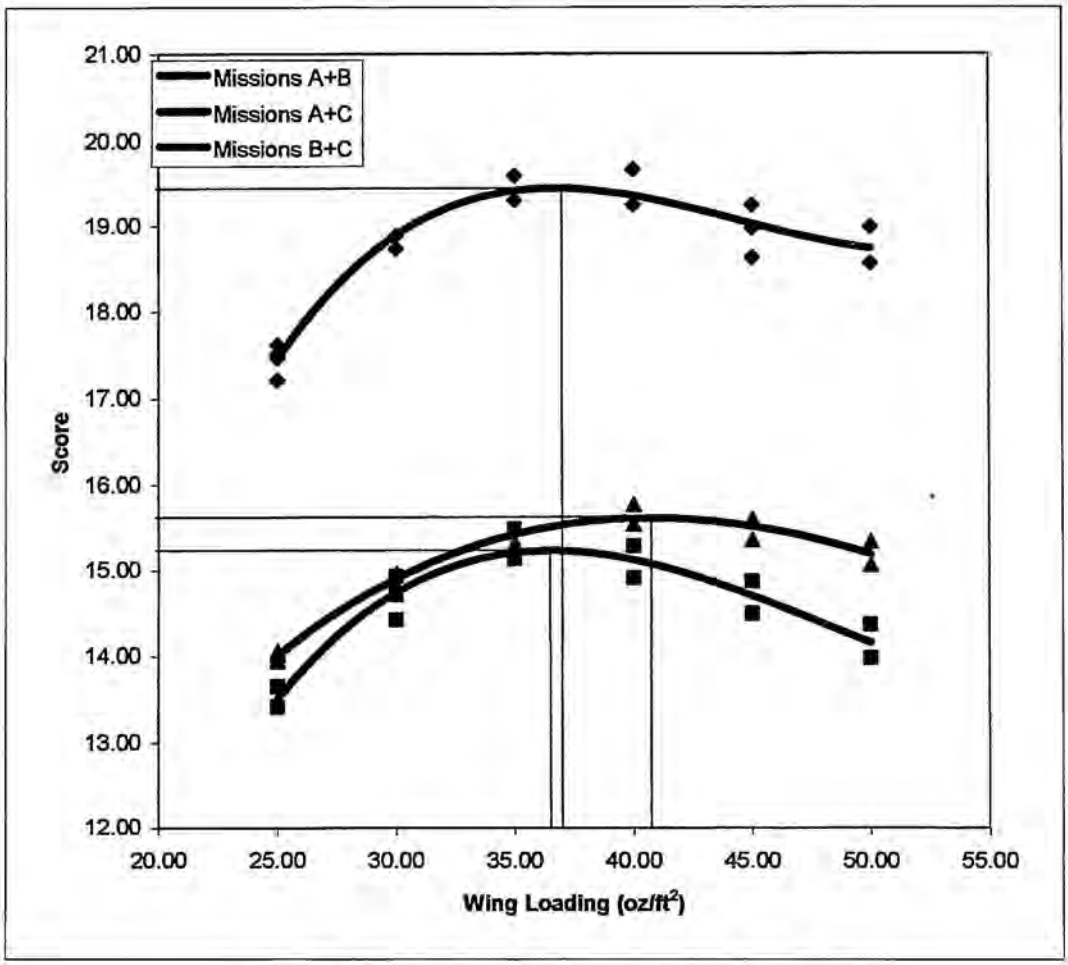

Figure 3.3a – Configuration Score vs. Wing Loading

Due to the definite correlation among score and mission optimization, missions A and B are the two missions that an aircraft should be designed for. For missions A and B, the peak score is significantly higher than the other mission combinations, directly pointing to the optimum mission combination.

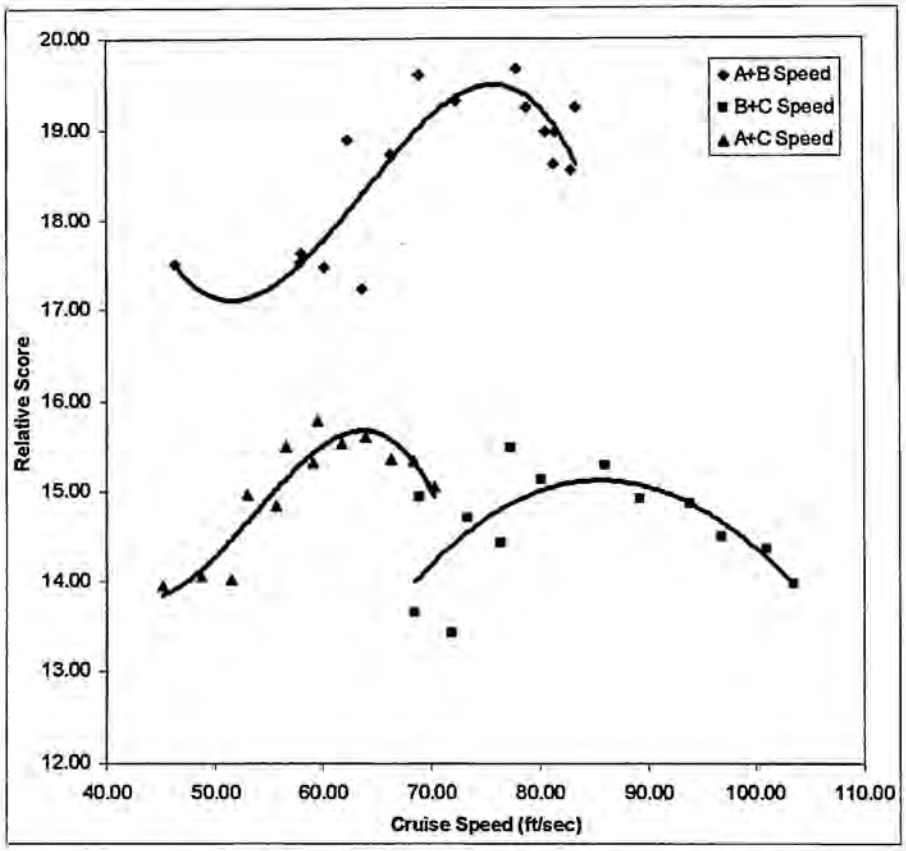

Figure 3.3b – Configuration Score vs. Cruise Speed

Although an aircraft designed for missions A and B would be more complex to construct and also be more challenging to operate due to the inclusion of the weight and complexity of a payload deployment system, and the extra landing-takeoff included in mission B, it was concluded that the demonstrated gain in configuration score would justify the risk taken.

3.2 Payload Configuration

A malfunction of the payload deployment system is an event that is sure to nullify the result of an otherwise successful mission. It was felt that compromising the reliability of the deployment system in order to allow operation from a conventional airframe configuration was the wrong approach to acquire. Selecting an airframe configuration prior to selecting the payload deployment method would automatically rule out many deployment mechanisms. Although the configuration of the airframe certainly has a significant effect on the performance of an aircraft, it was felt that a more conservative approach should be taken.

First, the method by which the payload would be deployed was established, and only then was an aircraft configuration chosen, based on how well it integrated with the deployment method selected. Due to the rigid limitations that the competition rules placed on the antenna mounting, the team could not come up with an innovative way to mount it (a way that would act to increase the performance of the aircraft in a noticeable manner). Therefore it was decided to concentrate on mounting the antenna simply and securely.

3.2.1 Antenna Location

The team was not able to identify an antenna location that would both adhere to the competition rules and have a beneficial effect on the performance of the aircraft as well. Since the rules specify that the antenna must have an unobstructed 360° horizontal field of view, it could not be placed either in front of the aircraft or behind the fuselage in the aircraft wake, a location from which a reduction in parasite drag could be achieved. Therefore it was decided to locate the antenna on top of the fuselage, in a position that would mitigate adverse effects on performance. Two locations were studied: one in front of the CG and one on the same vertical plane as the CG. The former would be calculated so that the moment generated by the drag of the antenna in cruise would cancel out the moment generated about the CG. The latter would not shift the CG location from one mission to the other, when the antenna is not flown. The choice of antenna location was left to later stages of design, when more certitude about the weight and balance would be acquired.

3.2.2 Electronics Box Deployment

Having selected to operate the airplane in mission task A, the issue of payload deployment method was the next to be addressed. Desirable attributes of the deployment mechanism were reliability, serviceability, ease of extraction, weight, and ease of manufacture. After much deliberation, the team decided to investigate the following four deployment methods.

Method 1 – This method involved a single servo rotating an arm in the horizontal plane to which the payload box would be constrained. After sliding on the surface of the cargo hold, the box would be pushed out onto the ground. Such a setup would be heavy, complex and would raise doubts regarding its reliability.

Method 2 – This method involved a simple drop mechanism, similar in action to those used on modern-day bombers. The downside of this method would be that it would theoretically require at least 6 inches of clearance between the bottom of the aircraft and the ground. An aircraft with such a high landing gear would not be able to fit into the storage container without being disassembled. Furthermore, the shackle mechanism must be strong enough to constrain the payload under all conditions, including potentially hard landings.

Method 3 – This method was a modification of the "drop" mechanism described earlier, differing in having a split bottom payload bay door that would split through the upsweep on the rear portion of the aircraft, therefore allowing the dropped payload container to pass through the back of the aircraft. This modification would allow an aircraft with a shorter gear stance to be built, one that could fit into the storage container without being disassembled. One potential disadvantage is that the payload might get stuck in the clamshell doors, preventing the departure of the aircraft.

Method 4 In this case, the payload would be pushed out the back of the fuselage, in a fashion similar to cargo transports. A servo would wind a wire loop constrained by pulleys, causing a plate to push the payload towards the back of the fuselage. This system would be complex and slow, but the payload would cause little interference with the departing aircraft once it is dropped.

Table 3.1- Deployment mechanism figure of merit

Description	Reliability	Serviceability	Manufacturability	Weight	Payload Extraction	score
Weighting factor	.3	.1	.1	.2	.3	1.0
Rotative deployment	1	1	0	1	1	.9
Bomb Drop	3	2	3	3	2	2.6
Bomb drop, clamshell	3	2	3	3	3	2.9
Ramp deployment	1	2	1	1	2	1.4

3.3 Airframe Configuration

Decision matrices were used to determine the alternatives that best met the mission requirements for each component. Figures of merit were chosen and a weighting factor was applied to the rating of each component, yielding a final score. For each alternative, the final score was compared and the highest was chosen.

3.3.1 General Configuration

Configurations considered during this early phase of design included flying wing, canard, biplane, conventional, twin fuselage, and blended wing/lifting body. Significant figures of merit in the selection of the configuration were ease of manufacture, rated aircraft cost, performance, payload ease of extraction and weight.

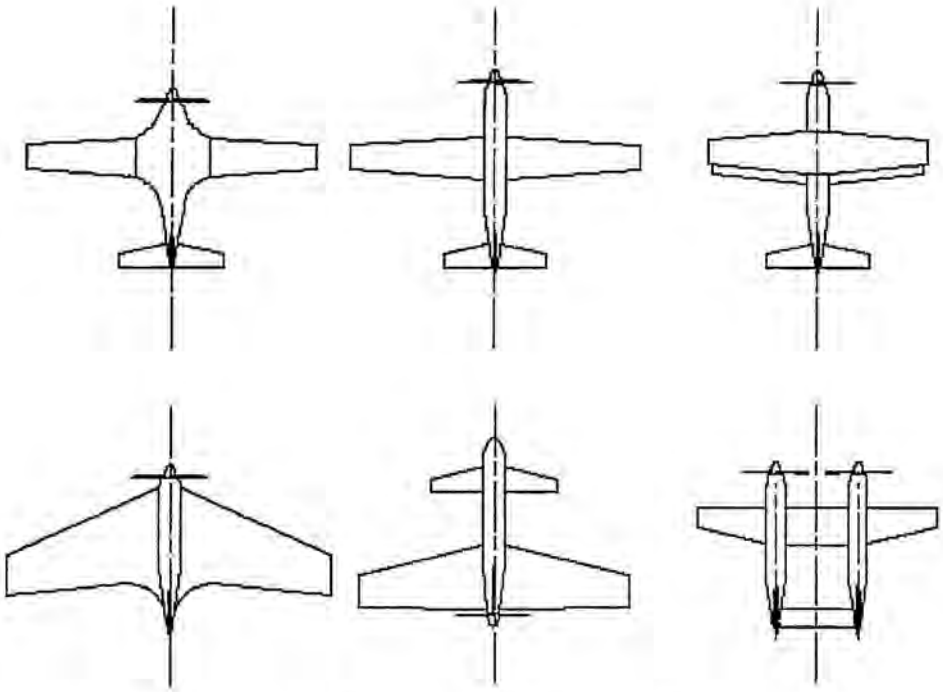

Figure 3.4- Possible Configurations

Flying wings require airfoils with reflexed mean camber lines near the trailing edge. This produces a positive pitching moment that obviates the need for a tail. Unfortunately, the maximum trimmable coefficient of lift for that airfoil is adversely affected, largely negating the benefits of this configuration. Flying wings make the installation of high lift devices problematic; their high pitch-down moment created upon deployment cannot be offset by the limited trim capabilities of a tailless airplane. A quick estimate of development time showed that too much time would be required to fine-tune this configuration.

Biplanes achieve a greater total lift by increasing the wing area and the wing can be made lighter if externally braced, albeit at the expense of drag. The relative closeness of the sets of wings leads to interference drag and a reduction of efficiency. A monoplane with the same reference area but greater aspect ratio achieves greater efficiency. Since this year's rules place no real limit on the wingspan, the biplane configuration was discarded.

The team also investigated the canard configuration. This concept seemed promising because both foreplane and main wing act as lifting surfaces, and a smaller, more compact airframe can be built. On the other hand, the particular lift distribution between the two surfaces requires special consideration. At high angles of attack, the foreplane must stall before the main wing to ensure that an unrecoverable departure does not result. In attempting a dive, however, the main wing must arrive at its angle of zero lift before the foreplanes achieve zero lift. If the foreplanes were to cease to lift while the main wing still lifts, a violent dive

would result. These and other complications involved with fine-tuning this configuration prompted the design group to decide against the canard.

The twin fuselage configuration proves attractive only if a twin-engine solution is chosen. The mass of the fuselages is far from the centerline, which results in high moments of inertia and sluggish lateral handling. The added expense of a second engine makes this arrangement unattractive. Furthermore, the electronics payload would have to be mounted asymmetrically. The blended wing/lifting body configuration was rejected early-on, because of many reasons: at the comparatively low speeds and Reynolds numbers at which the model operates, lifting bodies (basically low-AR wings with a low C_L/C_D) do more harm than good. Given the particular shape of the electronics box, the volume afforded by a blended wing-body configuration could not efficiently be put to use. A blended wing-body would also be much more difficult to manufacture and operate.

A conventional layout presents no technical challenges. It is easy to manufacture, its handling characteristics are well understood, and the design team generally felt that it conformed well to this year's set of rules. Thus a conventional configuration was selected for further study.

Table 3.2- Figures of merit for general configurations

Description	Manufacture	Performance	Rated cost	Weight	Extraction	score
Weight Factor	.1	.2	.3	.2	.2	1.0
Flying Wing	1	1	3	1	2	1.8
Biplane	2	2	2	1	2	1.7
Conventional	3	3	2	2	2	2.3
Canard	3	2	2	2	1	1.9
Blended Wing/Body	1	3	2	2	1	1.9

3.3.2 Wing Placement

In terms of wing/fuselage arrangement, the wing can be classified in three categories: high wing, mid wing, low wing. Figures of merit include: lateral stability, ease of manufacture, interference drag, and serviceability. Cost remains unchanged from one configuration to another. Having selected the deployment, the team proceeded to evaluate the wing placement that hindered operations the least while possessing

adequate performance. A mid-wing is desirable from a drag standpoint; a low wing would keep landing gear height small. However, both interfere with payload positioning, which has to be necessarily close to the center of gravity. The wing placement that allowed for the simplest payload drop was the high-wing design, which was favored throughout the design process.

Table 2.3- Figures of merit for wing placement

	Figures of Merit	Manufacture	Serviceability	Lateral Stability	Payload Deployment	Drag	Score
	Weighting Factor	0.1	0.2	0.1	0.4	0.2	1.0
Low Wing		3	3	2	1	2	1.9
Mid Wing	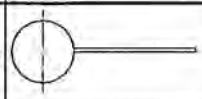	1	1	2	0	3	1.1
High Wing	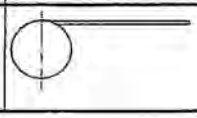	2	3	3	3	2	2.7

3.3.3 Fuselage Configuration

The fuselage had to be sized to carry the payload box, due to the fact that there was not a set of two missions that did not include it. The team also attempted to keep the total length of the airplane below 4 feet, although this would necessitate a large tail in order to obtain the tail volume coefficients required for good control characteristics, it was felt that this would be more preferable then having a plug-in tail arrangement that would both add to weight, complexity and assembly time of the aircraft.

When sizing the fuselage, many variables were considered, namely wetted area, frontal area, total length, and ease of access to internal components.

Because of the mission requirements, the aircraft was essentially molded around the payload. The fuselage was designed as a one-piece structure to minimize assembly time, with the highest possible fineness ratio while encompassing the payload box and fitting in a four-foot long container.

During the mission, aircraft weight will change as a result of the payload being deployed. To keep the payload from destabilitizing the aircraft by shifting the center of gravity location relative to the mean aerodynamic quarter-chord, the center of gravity of the payload was made to coincide with the center of gravity of the airplane.

The size of the tail is influenced as well; the length of the tail moment arm is determined in large part by the distance from the center of gravity of the aircraft to the aerodynamic center of the tail surface.

An important factor that severely affected the preliminary design of the fuselage was the length of the container box that the airplane had to fit in. Length of the fuselage is an important factor, it increases the

moment that the empennage can exert, thereby aiding to the controllability of the aircraft. However a fuselage length of more than four feet would require a plug-in tail arrangement, be more expensive and add to the timed assembly score of the aircraft. Because the control surfaces do not have cost assigned to their areas, it was decided that it would be cheaper and simpler to build an aircraft with a short fuselage and a large empennage to compensate for the short moment arm that would result. Although this configuration decision did not necessarily minimize the drag of the aircraft, it was thought that considering the relative poor aerodynamic characteristics of the fuselage designed to carry the 5lb payload, the extra drag added by the tail surfaces would not add up to a big performance penalty. The larger tail surfaces also increase control authority when functioning in the disturbed air behind the "dirty" fuselage and the antenna.

Table 3.3 – Fuselage Length Figures of Merit

FOM	Construction	Weight	Drag	Complexity	Control	score
Weighting factor	.1	.2	.15	.3	.2	1.0
4ft long body	3	3	2	3	1	2.3
Plug-In Tail Boom	1	1	3	1	3	1.65

The results of the analysis performed on fuselage configuration indicated that overall, the benefits of a one-piece construction would outweigh the disadvantages, and would be preferable to a longer, plug-in fuselage.

3.3.4 Engine Configuration

During the conceptual design of the aircraft it was calculated that a single engine operating with the expected battery pack voltage would be able to provide the takeoff power required while not exceeding the 40 ampere limitation dictated by the rules on the engine current. Since large engines are generally more efficient than smaller ones and the stringent takeoff constraint did not drive the design towards the use of multiple engines, a single large engine would be used instead.

Both single motor and twin motor configurations were considered. It was determined universally that for a given power requirement, the single motor solutions outperformed the twins in final score. This was caused by the additional cost of having more than one motor and speed controller, because for a given power level, two smaller motors, gearboxes and propellers weigh more than a single (increasing empty weight), and because larger motors generally have higher efficiency. It was decided that unless no single motor of sufficient size was available, the aircraft would not have two motors.

Table 3.4- Number of engines selection

Description	Weight	Efficiency	Rated cost	score
Weighting Factor	.3	.4	.3	1.0
Single Engine	3	3	3	3.0
Twin Engine	2	2	2	2.0

3.3.5 Landing Gear Configuration

The landing gear of a propeller driven airplane serves two major functions. The first is to provide adequate clearance between propeller tips and the ground. The second is to permit the plane to rotate on both takeoff and landing so that the wing's angle of attack comes close to the stall angle of its airfoil. At this angle of attack, the wing is near the airfoil's maximum C_L. This permits the aircraft to achieve the lowest allowable landing and takeoff speeds. The configurations considered where realistically limited to taildragger and fixed or retractable tricycle.

A taildragger configuration affords more propeller clearance and low drag. Unfortunately, it would also make the implementation of the deployment method used in mission task A extremely difficult if not impossible. The tail-dragger gear configuration also exhibits inferior ground handling characteristics compared to those of a tricycle gear setup.

For the reasons above it was decided to build the aircraft with a tricycle landing gear system. While exhibiting higher drag than a taildragger configuration, the tricycle gear permits a flat fuselage bottom and wide separation for optimum payload deployment. It also makes landings possible at sideslip angles and is generally more forgiving of rough ground handling.

A retractable landing gear eliminates a major source of parasite drag, but adds considerably to the complexity of the aircraft. An additional set of servos would be required, and it is doubtful that typically delicate retractable systems could cope with hard landings.

Table 3.6 Landing gear configuration figures of merit

	Description	Ground handling	Propeller clearance	Manufacturability	Weight	Payload Extraction	Score
	Weighting Factor	.3	.2	.1	.1	.3	1.0
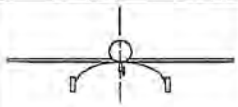	Taildragger	1	3	3	3	1	1.8
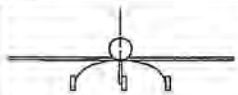	Tricycle	3	2	3	2	3	2.7
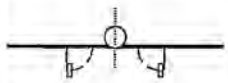	Retractable	3	2	0	1	1	1.7

3.3.6 Empennage Configuration

For an airplane in level flight at its selected cruise speed, the sum of the positive and negative pitching moments must be zero. Four major moment sources must be compensated. The main source is center of gravity location. A CG that is ahead of the mean aerodynamic chord's quarter chord causes a nose down moment and results in a longitudinally stable airplane. Locating the CG further back decreases static pitch stability. The other sources of pitching moments are the wing's drag moment, the thrust moment and the airfoil pitching moment. The balancing is achieved in a conventional and canard design by the use of a horizontal tail or foreplane. The horizontal tail's angle of attack, relative to the wing's downwash, should be sufficient to provide lift or most often, down force required to provide equilibrium.

The H-tail configuration was considered as having a set of benefits for the particular mission that this airplane would be designed for. An inverted H-tail has the benefits of not requiring assembly after removal from the storage box and at the same time not being blanketed with turbulent air from the payload or the fuselage. However, the H-tail might cause ground clearance issues and is also more expensive, requiring two servos for control and being counted as two vertical surfaces with control. On other hand, the aircraft rated cost formula showed a small cost break for a V-tail compared to all other tail plane configurations. As a result of conceptual design, conventional, V, and H-tails were both considered to have enough merit to be deliberated upon further in the design process.

3.4 Material selection

Three material and construction methods were considered: conventional buildup of lightweight wood skeleton and Monocote skin, conventional buildup of carbon fiber skeleton and skin, and composite skin with foam core. The figures of merit that were selected for the conceptual material selection were: ease of manufacturing, repairability, and durability

Table 3.7- Material Selection

Description	Manufacture	Reparability	Durability	Score
Weighting Factor	.3	.3	.4	1.0
Mixed Carbon/glass with foam core	3	3	2	
Wood with Monocote	2	2	2	
Molded composite	2	2	2	

3.5 Conceptual Design Results

As a result of the conceptual design stage, a gravity retraction (clamshell) system in a one-piece conventional fuselage was selected. This configuration, together with a high-set wing and tricycle landing gear, promises trouble free payload deployment operations, which was a key concern in this design phase.

4.0 Preliminary Design

During the preliminary design stage, the team studied and made a variety of design choices that shaped the configuration of all of the aircraft components. One of the overall goals that the team had for the preliminary design of the airplane was to ensure a quick and simple assembly of the aircraft. This would both simplify the operation of the aircraft and increase the final score. The team believed that a quickly assembling aircraft could be created without detrimental effects to either weight or complexity.

4.1 Aerodynamics Preliminary Design

Building on the analysis performed during the conceptual design phase, further analysis of the aircraft was performed to refine the design. The areas examined included: wing aspect ratio, airfoil and high lift devices, tail type and sizing. The concepts for each aspect were evaluated in a decision matrix and a down selection was performed on the basis of the highest scoring concept.

4.1.1 Wing Planform Design

Planform is the shape of the wing as viewed from above. The wing planform is important in defining the performance of the aircraft. It may be swept, elliptical, straight, tapered, or a combination of both. Swept wings were ruled out immediately because they only offer disadvantages at the expected flight conditions.

- Elliptical wings: This is the ideal wing planform. It has the lowest induced angle of attack and induced drag, and stalls evenly across its span. These factors increase for rectangular and tapered wings. Structurally, the elliptical wing is difficult to manufacture, especially using some of the methods likely to be used on this type of an airplane.
- Rectangular wings: Rectangular wings are the easiest to design and build. All chord sections are the same, and wing skins have a single chordwise curvature. While it suffers in comparison with an elliptical wing, for small models, it maintains a constant Reynolds number across its span. A tapered wing of the same area could have tip Reynolds numbers in the high drag/ lower lift and stalling-angle range of low Reynolds numbers, leading to premature tip-stalls at low speeds. Structurally, the wing roots need reinforcing, owing both to narrower root chords and higher bending moments that are generated as a result of the center of lift of each wing being farther from the centerline than an elliptical or tapered wing.
- Tapered wings: A tapered wing with a tip chord of 40 percent of the root chord closely approximates the ideal elliptical planform both in induced angle of attack and induced drag. For wings of model aircraft, this taper ratio results in narrow tip chords and undesirably low Reynolds numbers at low speeds. Increasing the taper ratio produces larger tip chords. Lift is lost at the tips; the wider the tip chord, the greater the loss. The resulting loss in efficiency isn't great and is the lesser of the two evils. Structurally, the tapered wing has lower root bending moments, and the wider, deeper root chord provides the greatest strength where it's needed most- at the root. A tapered wing can be lighter yet stronger than a rectangular wing of the same area.

- Modified Schuemann wings: This planform has an elliptical leading and trailing edge for 70% percent of the semispan and a sheared wingtip. It comes close to the elliptical wing in efficiency and is more easily produced than an elliptical wing. The rectangular inner portion is wider in chord, which provides a strong root, and bending moments are lower than for a rectangular wing.

The design team chose the Modified Schuemann wing because it represents the best compromise in terms of performance.

Table 8- Wing Planform Design

	Figures of Merit	Ease of Manufacture	Efficiency	Strength to Weight	Stall	Score
	Weighting Factor	0.3	0.4	0.1	0.2	1
Elliptical		1	3	3	2	2.2
Rectangular		3	1	1	3	2
Simply Tapered		2.5	2	2	2.5	2.25
Modified Schuemann		2	2.5	2.5	2.5	2.35

4.1.2 Wing Aspect Ratio Design

The aspect ratio of the aircraft's wing was determined by using the DBF03 performance simulation program to produce data points based on aircraft configurations of maximum performance at a range of aspect ratios. The conclusion of this trade study can be seen in Figure 4.1, which shows a light peak in score at the aspect ratio of 9. The graph also shows that relative to the score difference that is provided by picking Missions A+B, the effects of aspect ratio on the aircraft final score are close to linear. Before making the final selection, some of other advantages that high-aspect ratio wings possess were considered. It was realized that the efficiency of a high aspect ratio wing also has benefits that could not be simulated by the Oswald's efficiency approximation in DBF03 program. First benefit of the high-aspect ratio wing is to increase the rolling moment of the aircraft, making it more "stable" in the roll axis. A high aspect ratio wing also allowed the designers to have a higher span horizontal tail surface (span of which is constrained by the rules to 25% of the wing span). A shorter-chord empennage can be mounted further back on the fuselage, effectively increasing the tail moment arm. Both from the team's experience with the composites construction technologies used by the previous years' DBF teams, it was concluded that wings of aspect ratios up to 12 could be easily built without incurring a weight or strength penalty. Thus a wing with an aspect ratio of 12 was picked for this year's aircraft.

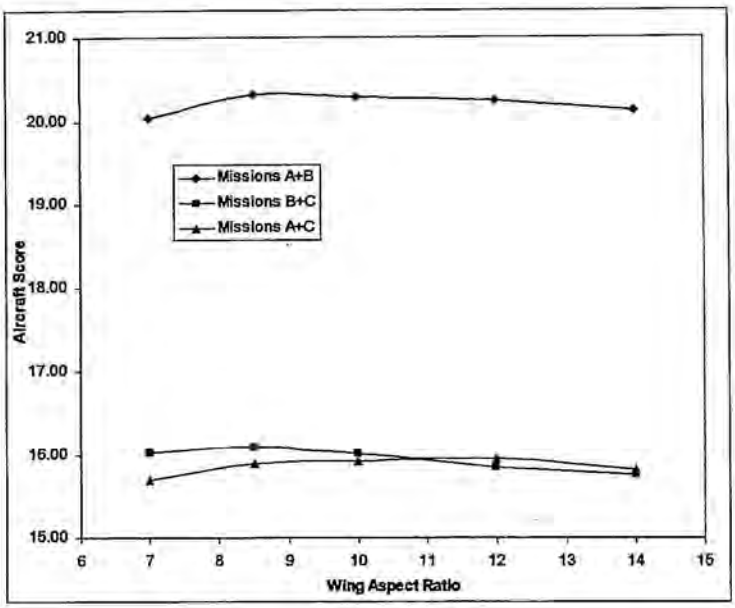

Figure 4. 1 – Effects of Aspect Ratio on Score

Table 4.1- Wing Planform Design

	Figures of Merit	Efficiency	Horizontal Tail Span	Strength	Roll Rate	Score
	Weighting Factor	0.4	0.3	0.2	0.1	1.0
High		1	1	-1	1	0.6
Medium		0	0	0	0	0
Low		-1	-1	1	-1	-0.6

4.1.3 Final Wing Configuration

When determining the final configuration of the wing, the team was trying to achieve a very difficult goal. The wing needed to produce high levels of lift when operating during the high-lift laps, but had to produce as little drag as possible when generating low levels of lift (when flying the empty laps).

The planform finally adopted was a modified Schuemann wing as seen in Figure 4.2. The wing has elliptical leading and trailing edges for the inner 70% of the span and a sheared wingtip design. This closely approximates the ideal span wise lift distribution (Figures 4.3, 4.4), without incurring the low Reynolds numbers at the tips that can lead to the stall occurring at the tips earlier than at the roots. More specifically, the wing was designed so that at a given angle of attack, the outer section of the wing would be operating at a CL

that is .1 lower than that of the root section. All the span wise sections of the wing can thus fly near peak efficiency while still preventing the tip-stall characteristic.

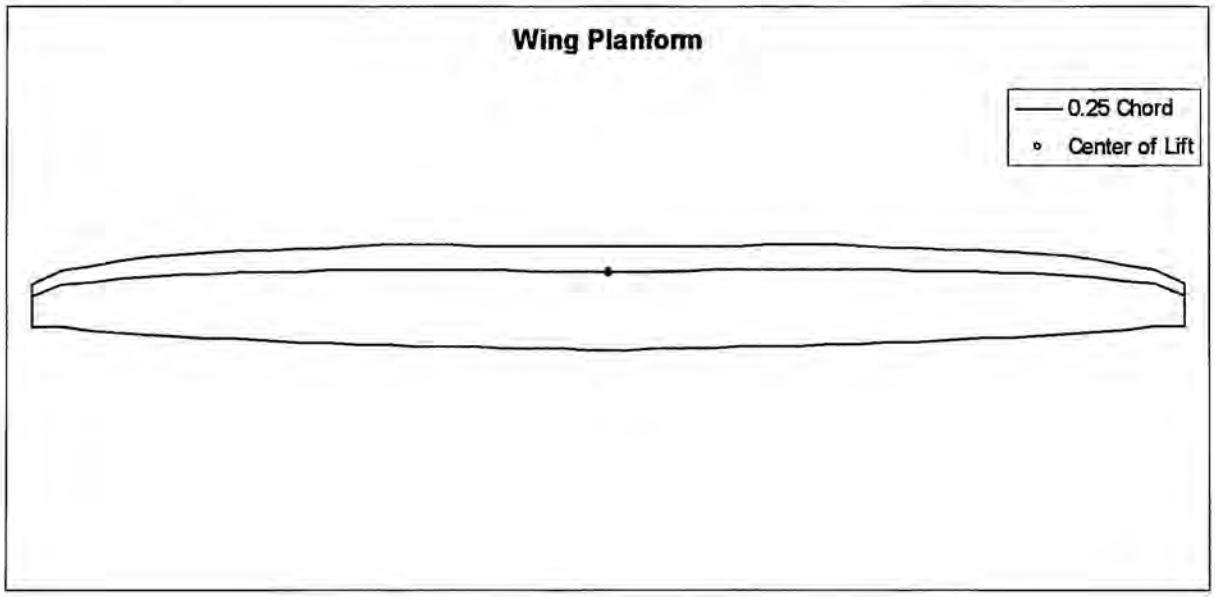

Figure 4. 2 – Wing Planform

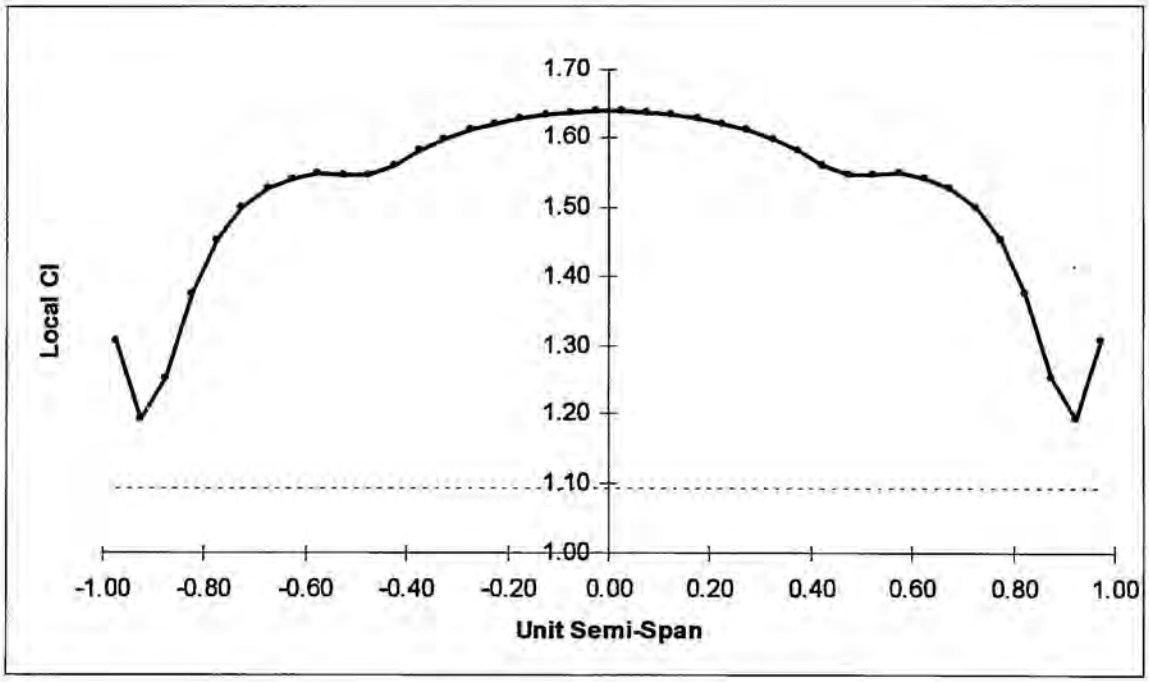

Figure 4. 3 – Local Lift Distribution

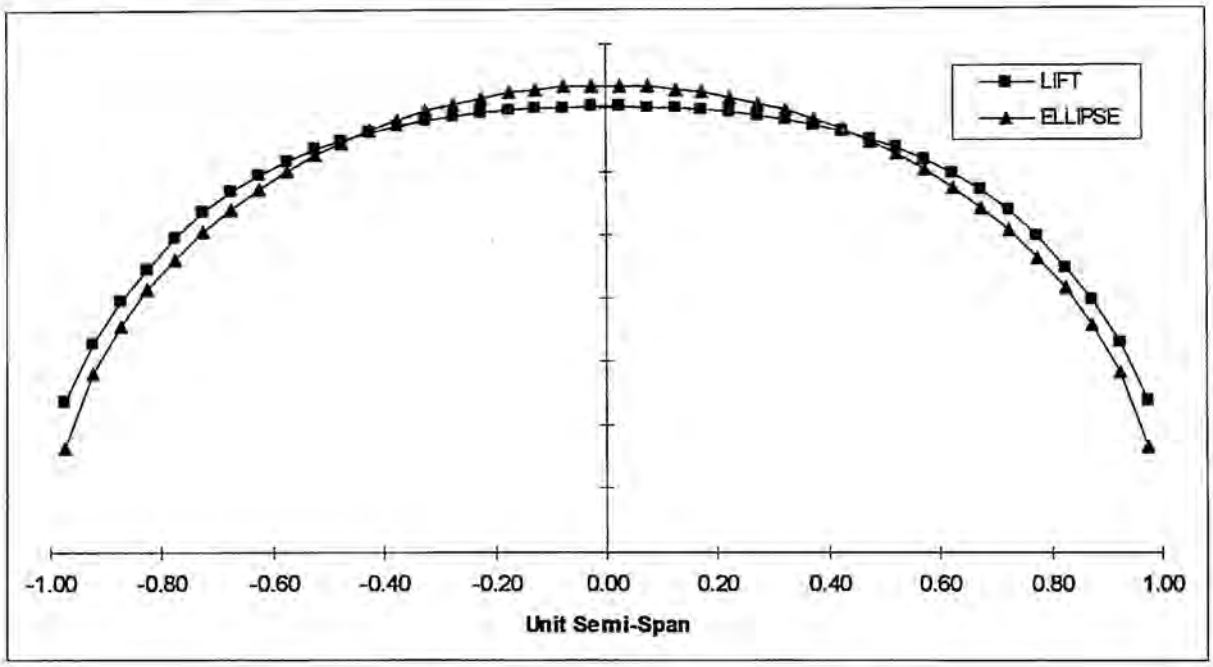

Figure 4. 4 – Lift Distribution and Elliptical Approximation

4.1.4 High-Lift devices

In order to meet the takeoff constraint, and to attain efficient climb, the team investigated different ways to increase the maximum wing C_L. Simple leading and trailing edge devices were the most obvious choice in this situation, with wing tilting, area increase devices (fowler flaps), and thrust vectoring deemed too complicated and not overly efficient on this type of an airplane. Keeping in mind the penalty that the competition rules assign for extra servos (which would be required to power separate control surfaces), flaperons seemed to be the most obvious choice.

The flaperons extend for the inboard 80% of the wingspan and 20% of the chord, and are used for roll control. Model airplanes with moderate-chord flaps fully extended, and reduced throttle tend to porpoise upward. In order to prevent this behavior, elevator down trim must be applied. The sharp increase in angle of downwash from the flaps forces the tail-plane down and creates a greater force than the increase in nose-down pitch. Increasing the flap size to 20% of the chord produces a balance between nose-down and nose-up forces, producing little change in pitch trim.

4.1.5 Airfoil Selection

Early in the design phase, it was recognized that the cost of the wing represented 20-40% of the total cost of the airplane. Wing cost was largely dependent on wing area, so in order to reduce cost as much as possible, the wing was designed capable of operating efficiently at high lift coefficients. This was a function mainly of the airfoil selected for the design. The wing planform was also considered in the design because of its impact on handling, aerodynamic efficiency, and the maximum lift achievable given a constant wing area.

In sizing the aircraft, many different airfoils were compared to find the airfoil and wing configuration that would maximize score and performance. It was recognized early on that the majority of flight time in the missions picked was spent in low-speed high-CL cruising flight. Likewise, the sizing software results favored thick, highly cambered high lift airfoils for the payload carrying laps. Out of the 8 laps flown in the course of the two missions, only two were flown with the airplane unloaded. With the lightly loaded airplane, a high lift airfoil is not desirable because of the lighter wing loading and the relatively low efficiency at low CL (0.3-0.4). During these two laps, a thinner, lower camber airfoil is optimal. These different lift requirements were very difficult to meet with any single, commonly used model aircraft wing section. In attempt to achieve both, an adjustable trailing edge camber changing airfoil was investigated.

JA-161, the airfoil chosen for the 02-03 Cal Poly DBF airplane is an excellent example of such an airfoil. JA-161 is a high-lift airfoil especially when coupled with a 10° flap deflection used to achieve a maximum CL of 1.9. With the flap set to an angle of 0° the airfoil operates efficiently during the relatively high-CL cruise.

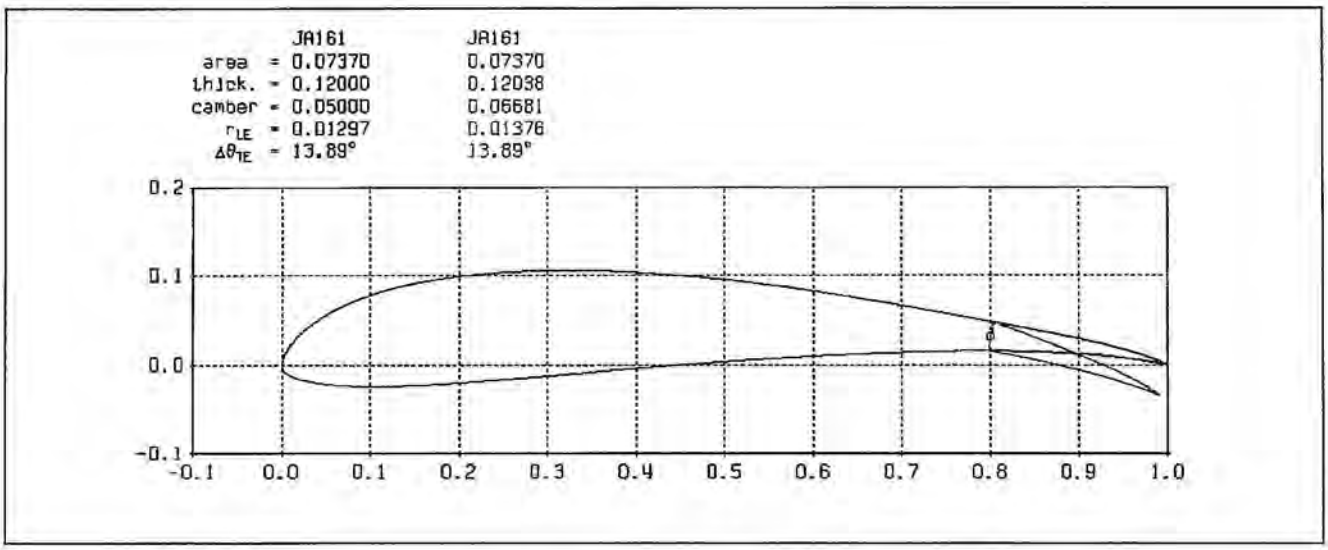

Figure 4. 5 – JA161 Airfoil Profile (Clean and 10° Flap Deflection)

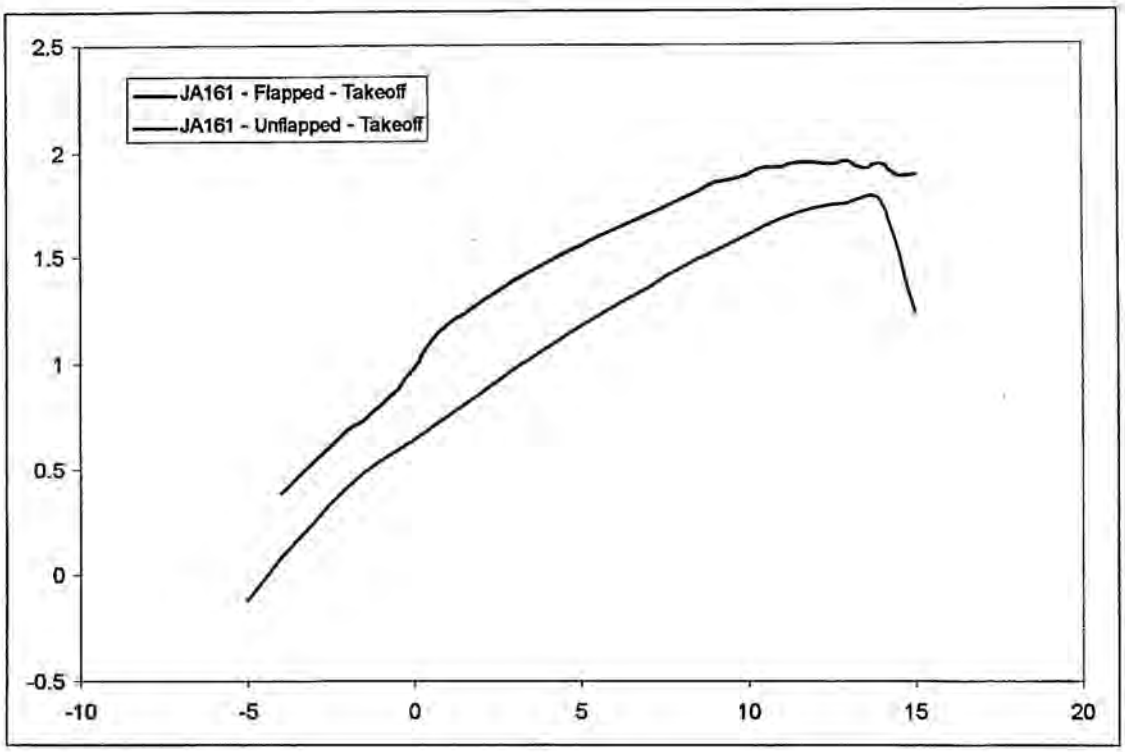

Figure 4. 6– Cl versus CD at Different Cambers

The design team investigated the camber changing airfoil concept using the same tool used to evaluate the commonly available model aircraft sections, X-foil. The design goal was to create an airfoil able to reach a CL of approximately 1.9 at the takeoff Reynolds number (~100,000) and to provide higher efficiency than the other candidate airfoils during both the payload and ferry missions. Maximum lift coefficient, drag at loaded cruise (CL 0.5-1.0), usable CL range, unloaded fast cruise (CL 0.3-0.4), and behaviors near stall were all considered. The design Reynolds number range for the final configuration was Re(CL)^0.5 = 180,000. After much iteration, JA161, the final design of the airfoil was far more capable and well suited for the aircraft than any of the other considered airfoils. Figure 4.7 shows the other candidate low Reynolds number airfoils considered for the design compared to the composite polar of the camber changing section. The Ja-40 is the airfoil used on the 01/02 DBF aircraft, the LA202 is an airfoil used in the past by the University of Southern California DBF team, the RAV is the AeroVironment Raven airfoil, and the SD7032 is a Selig-Donovan low Reynolds number airfoil. From Figure 4.7 it can be seen that the JA161 airfoil used on the 02/03 DBF aircraft outperforms all of the competitor airfoils in the loaded cruise CL range.

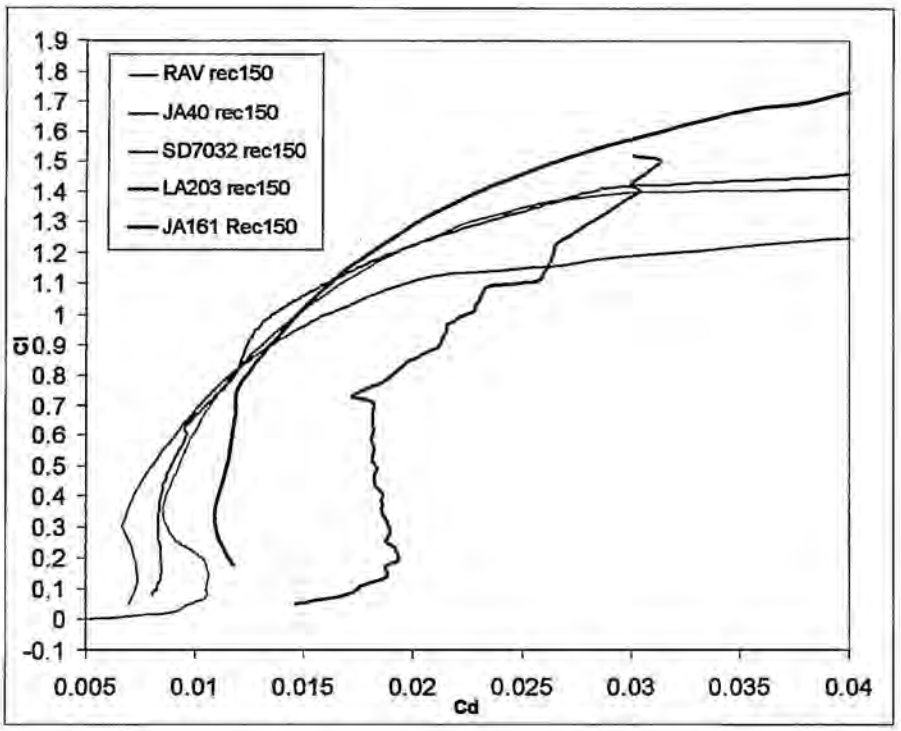

Figure 4. 7 – Airfoil Comparison (No Flaps)

The airfoil thickness is a moderate 12%, which is not optimum for drag reduction, but since most mission time is spent in comparatively low-speed flight this is acceptable. In addition to increasing the stiffness for a given weight of wing structure, the high thickness also tends to keep the efficient CL level quite broad.

4.1.6 Tail Type Selection

Although technically there are many different tail configurations that could have been used, only three ended up being a point of serious deliberation. Configurations such as the T-tail, the cruciform tail, the canard configuration, and other unorthodox configurations were quickly discarded. The team weighted the moderate performance advantages offered by some of these configurations versus the increases in systems complexity and the amount of time required to build, test and fine-tune these advanced configurations and decided against using any of them.

The three configurations that the team deliberated between were the H-Tail, the conventional tail and the V-tail. In order to not increase the assembly task time, the team hoped to spend as little time as necessary on tail assembly. If the horizontal tail were to be permanently mounted to the fuselage, it would have to be less than two feet in span in order to fit into the payload box, therefore not using up the entire span allowed by the rules. If the vertical and the horizontal tail were to be made as a "single piece", it could be made of a higher span, but then would be difficult to store in the box when removed. Since the team did not want to include the assembly of the horizontal surface in the timed assembly task, and it would be quite difficult to "package" an appropriately-sized tail in the box it was decided to investigate other options.

Both the V-tail and the H-tail have the advantage of being affected less by the air disturbed by the antenna payload, however, the two tails greatly differ in cost. With the servos, the V-tail has a RAC cost of only 35 hours, while the H-tail would drive the cost up to 60 hours. The H-tail's high cost was unlikely to have been recouped by its virtue of having a zero assembly time, but "the final nail in the coffin" for the configuration was the minimum upsweep (for "rotation" clearance) requirement that made the vertical tail volume coefficient too low for stable flight.

Table 4.3 – Empennage configuration

	Figures of Merit	Manufacture	Assembly	Rated Aircraft Cost	Handling Qualities	Score
	Weighting Factor	0.1	0.3	0.4	0.2	1
Conventional/ Cruciform		3	2	2	3	2.3
H-Tail		1	3	1	2	1.8
T-Tail		2	2	2	3	2.2
V-Tail		2	2	3	2	2.4

After considering the above arguments and comparing their numerical figures of merit, it was decided to build an aircraft with a V-tail empennage.

4.1.7 Tail Size Selection

Vertical and horizontal tail sizes were calculated using tail volume coefficient formulas on page 124 of Aircraft Design[1]. The conversion of the appropriate horizontal and vertical tail areas to V-tail areas was done using the following equations:

$$S_{VT} = c_{VT} b_W S_W / L_{VT}$$

$$S_{HT} = c_{HT} \check{C}_W S_W / L_{HT}$$

where L is the moment arm taken to be the length from the tail's quarter chord to the wing's quarter chord. S_W is the wing area, b_W is the wing span, and $\check{C}_W$ is the wing mean chord. The vertical and horizontal tail volume coefficients are c_{VT} and c_{HT}, respectively. The tail volume coefficients were chosen based on experience gained from the past three Cal Poly DBF aircraft. The handling qualities of these airplanes were very good and the tail volumes were chosen using them as a model.

The Charles River Radio Controllers' website provided a conversion equation to convert the horizontal and vertical tail area components into the V-tail area.

$$S_{V\text{-}tail} = S_{VT} + S_{HT}$$

$$\theta = \arctan[\sqrt{(S_{VT} / S_{HT})}]$$

$$S_{HT} = S_{V\text{-}tail} \cdot [\cos(\theta)]^2$$

$$S_{VT} = S_{V\text{-}tail} \cdot [\sin(\theta)]^2$$

"$S_{V\text{-}tail}$" is the area of both halves together, rotated flat. "θ" is the V-tail's dihedral angle from the horizontal. The formulas taken from the Charles River Radio Controllers' website are only to be used for large tail aspect ratios. These formulas do not account for the local interference and lift cancellation at the V-tail roots during yaw or "rudder" application. Using the equations above, the V-tail panel sizes were calculated to be 20 in. in length with an average chord of 8 inches, set at an included angle of 80°.

4.2 Fuselage Components Preliminary Design

Building on the analysis performed during the conceptual design phase, further analysis of the aircraft was performed to refine the design. The areas examined included: antenna payload and retraction mechanism. The concepts for each aspect were evaluated a down selection was performed on the basis of the highest scoring concept.

4.2.1 Antenna Payload

The mounting of the antenna on the aircraft is going to be accomplished by a simple airfoil-shaped 3-in. long strut positioned on the center of gravity of the aircraft. Mounted to the rules' minimum of 3 inches, the antenna is not in a position to minimize drag – in order to decrease interference drag, pods are usually placed at least a diameter away from the surface of the aircraft. This aspect of antenna mounting was investigated in some detail – the decrease in interference drag was compared to the increase of trim drag to cancel out the higher moment generated by the drag. As a result of this comparison, it was concluded that the increase in trim drag produced was higher than the decrease in interference drag.

4.2.2 Retraction Mechanism

The implementation of the general concept picked for the payload retraction mechanism deserved a lot of discussion. Because of the payload retraction concept chosen, the fuselage needed to have a large amount of upsweep immediately following the cargo compartment. This was necessary in order to minimize the length of the payload hatch, which negatively affects the torsional stiffness of the fuselage. A step-by-step diagram of the operation of the payload retraction mechanism is presented in Figure 4.8. Having been released, the payload box falls to the ground, forcing the spring-loaded aerodynamic fairing doors of the compartment to split open. As the plane powers away, the five pound box forces the doors to swing out further, letting the plane pass the box through the cutout in the back. As soon as the box is no longer pushing

on the doors of the compartment, they spring back closed. The exact method for restraining the electronics payload container in the fuselage of the aircraft was left to be determined during detailed design.

Figure 4. 8 – Retraction Mechanism Operation Schematic

4.3 Propulsion Preliminary Design

Fabricating on the analysis performed during the conceptual design phase, further analysis of the aircraft was performed to refine the design. The areas examined included: battery selection and motor selection. The concepts for each aspect were evaluated in a comparison matrix and a down selection was performed on the basis of the highest scoring concept.

4.3.1 Battery Selection

The contest rules specify that the propulsion system must be powered by a nickel cadmium battery pack no more than 80 oz in weight. Numerous types and sizes of NiCd batteries were available. Approximately 30% of the rated aircraft cost of most configurations was due to the battery cost, which is directly related to battery weight. Because of this, battery selection heavily drove the design. Choosing a battery that just met the energy and power requirements was vital in fielding a competitive aircraft. Depending on the characteristics and type of NiCd cell used, there are limits to the maximum power and efficiency to the rate of discharge. Research on the characteristics of NiCd cells was conducted to choose the best battery to fulfill both the aircraft's energy and maximum power requirements. The 40amp fuse restriction and the voltage requirements/maximum current capabilities of the available motors were all considered during the search.

Two styles of NiCd cells were investigated in detail, the high capacity Sanyo KR series, and the NiCd cells typically used for electric powered R/C models, the fast charge Sanyo R series. Table 4.1 shows the characteristics of each cell type.

Table 4.4- Battery Cell Comparison

Nicad Cell	mAh	Weight (oz)	Package	mOhm/cell	Amps @ 1.0V	Watts/oz	Watt-hr/oz
KR-1100AAU	1100	0.85	AA	20	10	11.8	1.55
KR-1500AUL	1500	1.09	4/5A	16	13	11.5	1.65
KR-1700AU	1700	1.25	A	14	14	11.4	1.63
N-1250SCR	1250	1.50	4/5sub C	4.5	44	29.6	1.00
RC-2000	2000	2.00	sub C	3.8	53	26.3	1.20
RC-2400	2400	2.15	sub C	3.6	56	25.8	1.34
CP-2400SCR	2400	2.1	sub C	3.6	56	26.5	1.37
CP-1700SCR	1700	1.65	4/5 sub C	4.5	44	26.9	1.24
CP-1300SCR	1300	1.25	½ sub C	6.5	31	24.6	1.25

The fast charge cells are designed to handle high maximum current and therefore are well suited for typical electric aircraft motors. The specific power density of these cells is on the order of 25 Watts/oz. These cells have a specific energy density of approximately 1.2 Watt-Hours/oz. The new Sanyo "CP" series cells have the highest energy density and excellent power density compared to all of the fast charge cells. Table 4.4 shows the different NiCds considered for the design.

The high capacity KR cells were considered because of their higher energy density (1.6 Watt-hours/oz). The compromises in the cell design that give them the high capacity also hurt the cells' internal resistance – affecting their maximum discharge rate. Therefore, the power density is only half that of the fast charge cells, approximately 11 Watts/oz. Unfortunately, most of the design concepts required nearly 600 Watts of peak power to meet the take off constraint and minimum climb requirement, making the high capacity cells unsuitable. NiCd cells delivering power at their maximum rate are not operating efficiently which significantly reduces their delivered energy.

Charge or discharge comparison of batteries is done using the term "C" or "C rate". The term "C" is numerically equivalent to the rated capacity of a cell discharged at the "C" rate will expend its minimum capacity in one hour, while taking only 15 minutes if discharged at a rate of 4Cs. The resistance of the cells is extremely important when one considers that the energy lost to the resistance is mainly converted into heat. With the C discharge rate for the 2003 aircraft approaching the value of 15, the team was extremely

concerned with the cooling of the battery pack – both construction of the pack and its location had to be optimal in order to allow for the best possible air circulation.

Every nickel-cadmium cell or battery has a specific rated capacity, discharge voltage, and effective resistance. Individual cells are rated at 1.2 volts and voltage for batteries are multiples of the individual cell nominal voltage of 1.2 volts. Twelve cells connected in series would result in a 14.4-volt battery. As can be seen, however, the discharge voltage will exceed 1.2 volts for some portion of the discharge period (during the takeoff and climb segments). Most manufacturers rate cell capacity by stating a conservative estimate of the amount of capacity that can be discharged from a relatively new, fully charged cell.

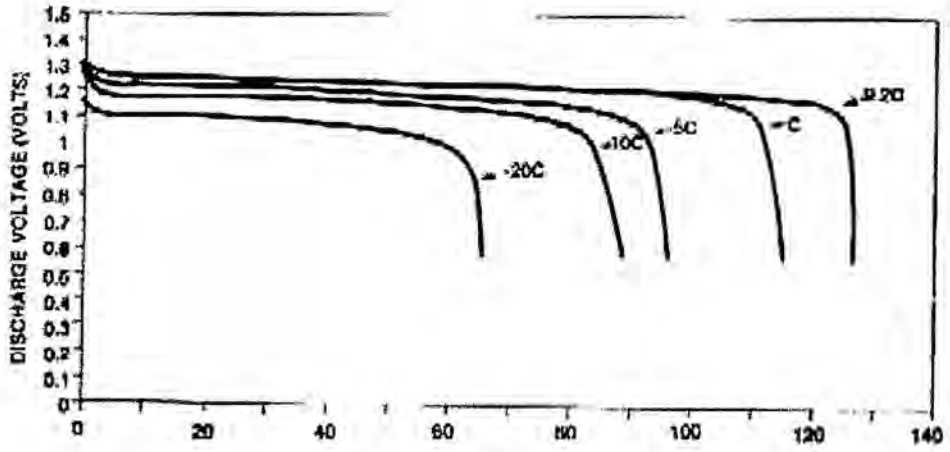

Figure 4.9 – Typical NiCd Discharge Rates

This graph shows that when rates of discharge are increased the available capacity becomes more dependent on the discharge rate. Therefore, at a discharge rate of approximately 15C, the battery efficiency will drop below 80%. When rates of discharge increase, the available capacity decreases as the discharge rate increases. The above trends were also very important for the application in this year's aircraft – working to decrease the C rating would result in higher battery energy available.

Most electric motors available for powering a 12 lb aircraft require 10-15 Volts input instead of the near 100 Volts that a series pack of high capacity cells would be. A combination parallel-series pack was considered to reduce the voltage and increase the current capabilities, but the difficulties in charging and maintaining balance between the cells eliminated this idea.

The energy requirement for the battery was approximately 15 Watt-hours. The aircraft was sized to use 12 CP-1700SCR cells because they provided the highest energy density, allowing the lightest, least costly battery pack. This pack potential is approximately 13.8 volts under load. Factoring the 40amp maximum current allows 600Watts for takeoff and climb. The Sanyo CP-1700SCR cells were chosen because of their high performance, availability, and suitability for the design.

4.3.2. Motor Selection

After initial sizing, it was determined that the aircraft needed a propulsion system able to run on approximately 11-12 NiCd cells, and be capable of handling 550-650 watts to attain the necessary takeoff and climb performance.

To evaluate the performance of the motors available for the aircraft, a Visual Basic subroutine modeling electric motors was written. This model uses motor parameters including Kv (RPM/V), idle current, armature resistance, RPM and thermal limits to calculate output power and efficiency for DC motors. This program was used in conjunction with a propeller model and the mission simulation to compare the various motors offered by Astro Flight and Graupner.

Although during the 2002 DBF year the team intended to use Astro Flight motors, after testing of sample motors from both AstroFlight and Graupner, it was discovered that the Graupner motor (290-8) tested was more efficient than a comparable size AstroFlight motor (Astro 40). Even though the 2003 aircraft carries about half the payload of the 2002 aircraft, it has a much shorter takeoff constraint, which drives up the peak power required. Using the output from the performance calculation program, the peak power requirement for this year's aircraft was determined to be about 90% of that required last year. Learning from the conclusions reached the year before, the team decided to select motors from the Graupner product line.

The power requirements of the design limited our selection to two motors in the Graupner line: the Graupner 290-30 and the Graupner 290-20. Table 4.2 shows the available winding configurations of the two Graupner motors that were considered in the propulsion configuration of the 2003 aircraft. With the battery pack picked from the endurance requirements of the missions flown, the motors were expected to handle 600Watts of electric power input at a voltage of 11 volts that would be provided by a 12 cell CP1700SCR battery pack under load. Generally the motors with lower turn armatures were more efficient at full takeoff power while suffering in efficiency during the relatively low powered cruise. The higher turn motors showed lower efficiency at full power while being much more efficient during cruise. Most of the propulsive energy during the mission is used during cruise so the decision was made to optimize cruise efficiency. Another constraint to consider, however was the fact that a high-winding motor would not be able to function at the current it has to operate at during the takeoff segment.

Table 4.5 – Candidate Motors

Motor	Weight (oz)	Max Watts	RPM/V	Ohms	Idle Current	Gear
Graupner Ultra 920-4 7V	11.3	420	3298	0.016	3.480	5.1:1
Graupner Ultra 920-5 7V	11.3	450	3422	0.02	3.91	5.1:1
Graupner Ultra 930-6 8V	13	500	1975	0.04	2.0	3.7:1
Graupner Ultra 930-7 10V	13	630	1667	0.0463	2.0	3.7:1
Graupner Ultra 1300-6 12V	12	1200	1511	0.052	5.6	1:1

All of the motors come available with various gear reductions. Although the gear reduction reduces the mechanical efficiency of the motor, the larger, lower disk-loading propeller usually makes up the difference in efficiency while also providing significantly higher static thrust for takeoff. Another advantage of the high-diameter propeller is that, with the fuselage being at least 6x6 inches in frontal area, a large propeller is needed to avoid thrust loss due to the effects of fuselage interference. The Graupner motors are capable of producing more power using a gear reduction because they can be run at higher voltages. Because of the above reasons and using numerical output of the motor efficiency program (Figure 4.10, in the end of chapter), the decision was made to use a motor with gear reduction.

The Graupner (Ultra 1300) is capable of running at 1200 watts of input power, but is oversized for this mission. This motor was nonetheless considered in the preliminary motor selection stage as a possible direct-drive solution. The Graupner 920 and 930 motors can operate at power levels up to 800 watts, which is higher than the takeoff power level projected for the aircraft in takeoff. The mission profile calls for short periods at full power for takeoff and climb followed by extended cruise periods well within the normal power limits of both of the Graupner motors. The Graupner 930 motor possesses a comfortable "safety margin" that would allow extra power to be input to the power system in case of the built aircraft having takeoff performance inferior to that of the predictions. The 930 motor is also projected to be very efficient at the cruise level of operation. The 920 motor, although lighter in weight is also smaller, which negatively affects the torque it can output – this torque limitation is something that is quite important during the stringent heavy takeoff segment of the mission. Since the 920 is lighter, it has a smaller magnet, causing the 920 to not have as much peak torque as the larger 930. The 920 motor also has a low "safety margin" when compared to the 930 motor. During the takeoff segment, the 920 motor would be operating at very high power levels. The disadvantage of running the motor at such high power levels is premature erosion of the brushes and

commutator, and loss of efficiency due to increased resistance and demagnetizing of the permanent magnets.

After considering all the alternatives, the team decided to use the 930-6 motor because of the safety margin provided and the high efficiency during cruise. This motor choice provides the aircraft with a good power to weight ratio, high cruise efficiency and improved scoring potential, along with its larger armature spinning causes the 930 produce more torque which is needed to use a large diameter propeller.

The propeller performance model indicated propellers 14 to 17 inches in diameter with 10 to 13 inches of pitch would load the selected motor to the required 550-650 watts. The relatively high pitch of the propeller was chosen because of the aircraft's high cruise speed (60ft/sec). This pitch was a compromise between the advance ratio required for efficient cruise, and for good full throttle takeoff and climb performance. Because of variation in efficiency and power absorption between different propeller manufacturers, the propeller model was calibrated using data gathered from the motor manufacturer and with testing performed with the Graupner 930-6.

The finalized drive system combinations were also evaluated using the MotoCalc software, with the propulsion systems evaluated presented in Table 4.6.

Table 4.6 – Propulsion Systems Evaluated in MotoCalc

Motor	Reduction	Propeller	Max. Efficiency	Weight (g)
1300-6	3.71:1	16x13	40	420
1300-6	1:1	11x6	28	340
1300-6	1:1	12x7	29	340
930-6	3.71:1	16x12	55	370
930-6	3.71:1	17x13	55	370
920-5	5.1:1	14x13	50	320
920-6	5.1:1	16x12	50	320

4.4 Analytical Tools

Several analytical methods were used in design analysis, including tools used by previous Cal Poly DBF teams, and additions in both Visual Basic and Microsoft Excel.

4.4.1 Spreadsheet Application

Throughout the past years of the DBF competition, the performance design of the DBF airplane was analyzed using an interactive spreadsheet program in Microsoft Excel. Although extremely simple, this program provided good indication of the parameters driving the design.

During the summer of 2002, a new performance design program (DBF03) was created from the ground up using the Microsoft Visual Basic programming language. This program used a Microsoft Excel front end similar to that used by the previous version of the design software, but was more powerful and provided a much higher ease of expansion than the previous version. This software simulated the

performance of the aircraft through all the stages of the mission, iteratively calculating thrust, drag and other characteristics of the aircraft performance. For example, DBF02 used a simple approximation formula to calculate takeoff distance. DBF03 iterated through increments of 0.1 second, calculating thrust, drag, lift, power input to the engine and other parameters in order to output an answer with a higher degree of precision.

The program estimated the overall performance of the airplane by combining many specific performance calculations and estimation methods.

- Weight – This estimate was created from weight/area constants that were obtained from weighing model parts created via different traditional RC-model construction methods. Multiplying these weight/area constants by their respective areas created the weight estimate of the airplane.
- Drag – A flat-plate drag estimate was created based on CD estimates and experience compiled by the previous year's DBF teams.
- Thrust –The curve predicting thrust was derived using a combination of two methodologies – using momentum methodology to predict the decline of thrust with increase in forward speed and using static thrust equations from Chuck Gadd's Electric Electric Motor Calculator.(Ref 7).
- Energy accounting – A propulsion system efficiency constant (efficiency in converting electric energy into volts – motor + propeller + drive efficiencies) was used to estimate the amounts of current/energy that will be drawn out of the batteries during the duration of the contest.
- Mission time – This parameter was created by adding together the following separate mission segments: Takeoff, Climb, Turns, Cruising, Landing, Payload Drop. Constant acceleration on takeoff and constant-G turns were assumed to simplify the calculation.
- Cost – A cost estimate was easy to create by simply applying the given rules to the airframe parts, the dimensions of which were estimated by the simulation components described above.
- Mission score – This result was obtained by using the preceding estimates in the context of the competition rules.

The 4 main variables that were systematically modified in order to achieve the highest possible flight score were Airplane Weight, Wing Loading, Aspect Ratio, number of batteries. A load of other assumptions and initial values were used, but those did not vary when trying to select an optimum airplane configuration.

The program DBF03 was the main software package used in the design of the aircraft. This performance estimation program could take as input any of the 7 following mission segments: Accelerate, Climb, Land, Brake, Cruise, Turn180, Pause. The user would then proceed to enter a distance or quantity for each mission and the aircraft parameters (Δ drag, Δ weight, speed, turn G) during the mission. A set of required parameters for the general aircraft to be simulated would also be entered – based on those aircraft and mission parameters the simulation would be run. The program would output a variety of relevant data for each segment, examples of which are listed below:

Energy Used	CL	L/D
Peak Power	Distance in segment	Stall Speed
Battery Efficiency	Energy Left	Total time

A comprehensive set of data was output to show the performance of the aircraft in the entire mission, allowing educated design choices to be made and new designs to be evaluated.

Being written in Visual Basic, the program could be made modular, having different functions and subroutines that would execute the same calculation using data inputs from different sources. For example, the drag calculation functions IDragCalc and PDragCalc needed inputs of current speed, current Cl and a set of general airplane characteristics to calculate drag for any of the 5 mission segments simulated: Accelerate, Climb, Land, Brake, Cruise, Turn180. Because of the program's modularity, new functionality could be added with minimum effort, or effects of different methods of calculation could be compared against each other. Presented in Figure 4.10 is a small portion of the input-output interface of the program.

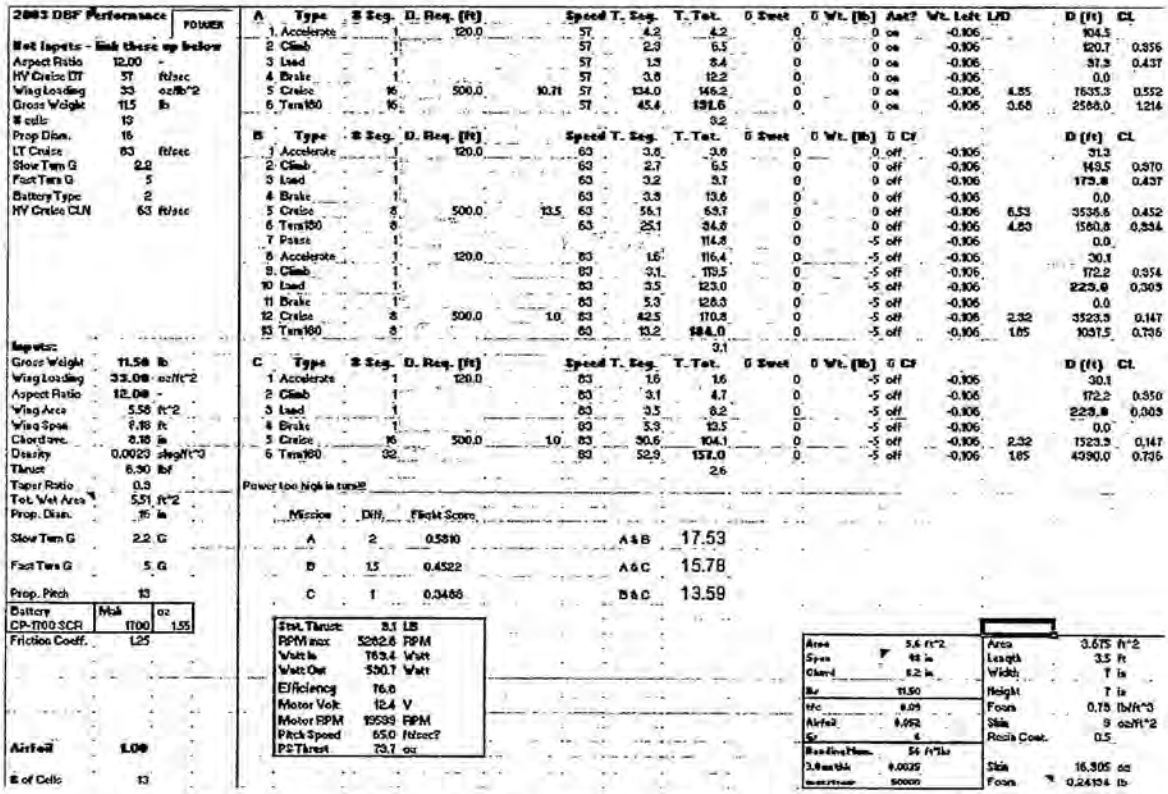

Figure 4.10 – A Small Portion of the Input-Output Interface of DBF03

Besides doing performance estimation for the aircraft, the program evaluated many other variables, all of which affected the preliminary design decisions made.

- Estimation of the effects of aspect ratio on weight (because of the varying strength required from the spar cap) and on wing efficiency (induced drag).
- Estimation of wing root bending moment and output of necessary spar cap thickness.
- Estimation of weight breakdown of the aircraft's components based on configuration.
- Effects of wing planform on efficiency
- Effects of tail area increase vs. fuselage length increase
- Aircraft longitudinal static stability
- Wing lift distribution depending on the planform picked
- Wingtip deflection

The price breakdown output of the spreadsheet enabled the team to visualize which components of the aircraft were of the most impact on the final score, therefore allowing the optimization process to focus on addressing those significant score drivers.

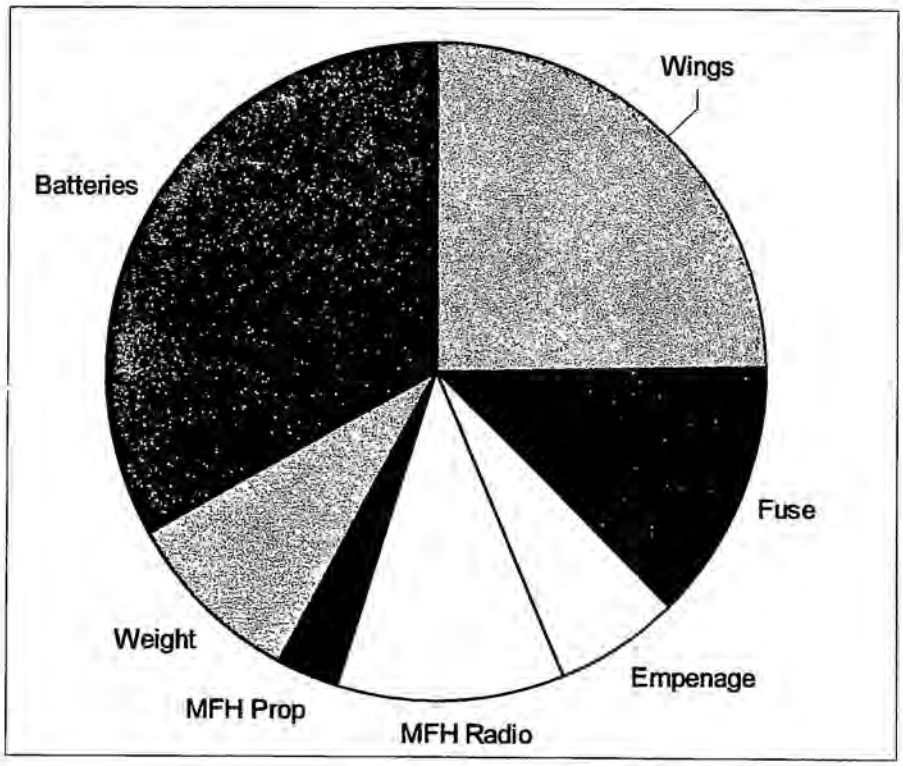

Figure 4.11 – The RAC Component Breakdown

The breakdown of the mission segment time allowed the team to visualize which segments took the longest, and thus allowed us to see the which segment's power needs had most effect on the total mission

energy consumption. This data allowed us to both make a better choice in propeller/motor combination selection (correct pitch speed, power level for the longest task).

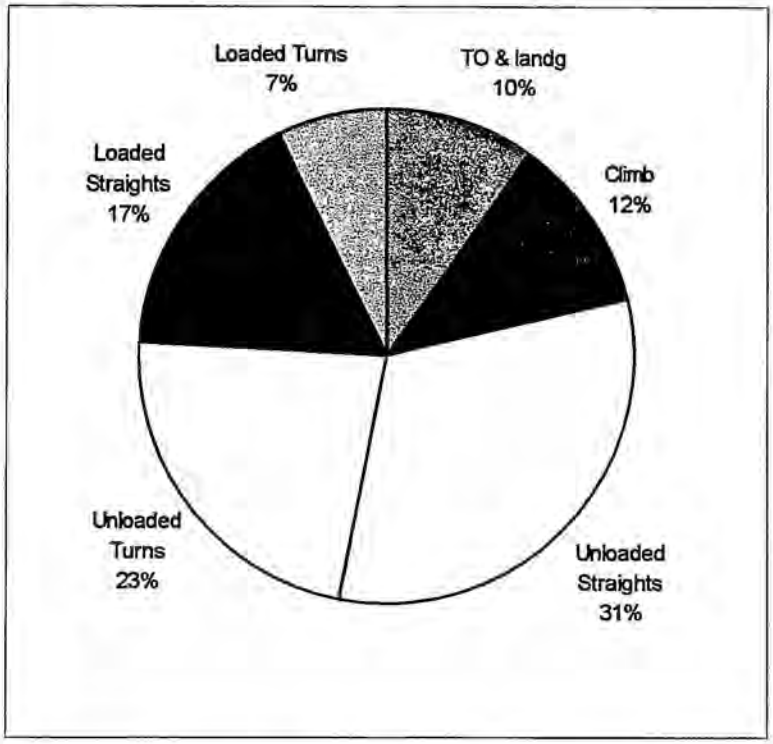

Figure 4.12 – Time Breakdown of Mission A

The simulation program helped to define some of the directions on which the development of the airplane should focus.

4.4.2 Other Simulation Methods

Besides the DBF03 program, the team also created numerical figures of merit in order to choose the design components best suited for this year's mission. After evaluating the combined effects of the characteristics inherent to each design choice with the figures of merit, more educated decisions could be made. Figures of merit were used in the decisions made in/on the following components: Deployment mechanism, general configuration, wing placement, fuselage length, number of engines, landing gear configuration, empennage configuration, materials, wing planform, and aspect ratio.

Many of the tools used in the design process were created by the team members using Visual Basic or in Microsoft Excel. Nearly all the programs were written some time before work on the 02/03 Design/Build/Fly aircraft began and had been already well tested and validated. These programs include an electric motor/ propeller model, an aerodynamic model, a weight estimation spreadsheet, a longitudinal static stability model, takeoff and climb simulation, and a lift distribution spreadsheet. These tools were incorporated

into a 02/03 DBF mission simulation model that included a cost model. To check validity, aircraft with known performance from the 99/02 competition years were also run through the simulation successfully.

One tool not developed by the team members was X-foil, written by Mark Drela of the Massachusetts Institute of Technology. After learning to use X-foil, results from low Reynolds number wind tunnel testing performed at University Illinois Urbana Champaign were compared with data produced by X-foil. At the relatively high Reynolds numbers that this aircraft will fly at, the correlation between test data and predicted performance was excellent. Experience gained with these correlations and the good results obtained with the JA40 airfoil designed using X-foil and flown during the 01/02 DBF contest gave the team confidence in the design tool. The X-foil predictions for the performance of the JA-161 airfoil can be seen in figure 4.9 below.

The MotoCalc electric flight performance prediction program available at www.motocalc.com was also used to evaluate and fine-tune the final propulsions systems configurations output from the VisualBasic software.

4.5 Conclusion

At the end of the preliminary phase, the primary components of the configuration were all sized and placed according to the figures of merit. Based on the scores obtained in the decision matrices, the aerodynamic characteristics of the airplane were defined. The aircraft now sported a high aspect ratio wing with a modified Schuemann planform, and a custom-designed airfoil. The propulsion system was agreed upon and consisted of a Graupner 936, battery pack size of 12 Sanyo CP-1700SCR cells. The fine-tuning of the less general details of the aircraft was left to be performed during the detailed portion of the design process.

5.0 Detailed Design

After all of the preliminary aircraft characteristics had been established, design leading up to the manufacturing of the aircraft could be undertaken. Motor performance characteristics were evaluated and the correct batteries for the propulsion system were selected. With a more definite knowledge of the aircraft configuration and components, the simulation model could be modified to provide a detailed prediction of the mission performance of the completed aircraft. The aircraft center of gravity and control characteristics were calculated, and components were adjusted in order to move the CG to the desired location. The methods by which to secure airframe components together were picked.

5.1 Power System Optimization

The performance of the final selection Graupner 930-6 motor was evaluated in more detail when coupled with the RFM 17x13 propeller. After constructing a detailed solid model of the aircraft, it was discovered that the ground clearance of the 17-inch diameter propeller was not satisfactory – it is possible that during strut compression a ground strike would occur. Because of this, the team investigated lower-diameter propeller solutions, stopping at a 16x13 diameter propeller. Although the efficiency of this propeller is slightly lower, it enables the plane to fly faster and lowers the chance of a ground strike.

The battery pack underwent modification during detailed design. In order to receive maximum power output from the cell bank, a technique termed "cell matching" was used – each cell was selected to have the same exact voltage and resistance before being assembled into a pack. This allowed for better use of every cells' internal capacity and for higher overall energy to be recovered from the battery pack. After being discharge tested, the battery pack performance compared favorably to the spreadsheet predictions.

Some other modifications were made to the standard battery pack design. First off, the battery pack used "end-to-end" soldering as much as possible, thus decreasing unnecessary weight and resistance in the pack – therefore reducing the voltage losses that a high resistance leads to in a high current drain situation. Rather than keeping the standard long battery leads, the connectors were soldered straight onto the battery pack, reducing the pack weight.

5.2 Aircraft Flight Characteristics

A detailed design of the wing was undertaken – relative twist of wing panels was implemented to modify the aircraft's moment coefficient in the pitch axis. The resultant figure below shows that the wing is designed to have a zero-moment coefficient the aircraft's cruise CL of roughly 0.5. This allows for better control authority and trim drag reduction during the longest flight times (cruise section of the mission). The team will avoid induced drag from the fuselage by setting the wing relative to the fuselage such that the fuselage is at a 0° angle of attack during cruise. Figure 5.1 also shows that the moment coefficient at the takeoff lift coefficient is relatively low; this requirement being taken into account during the design of the elevator control surface.

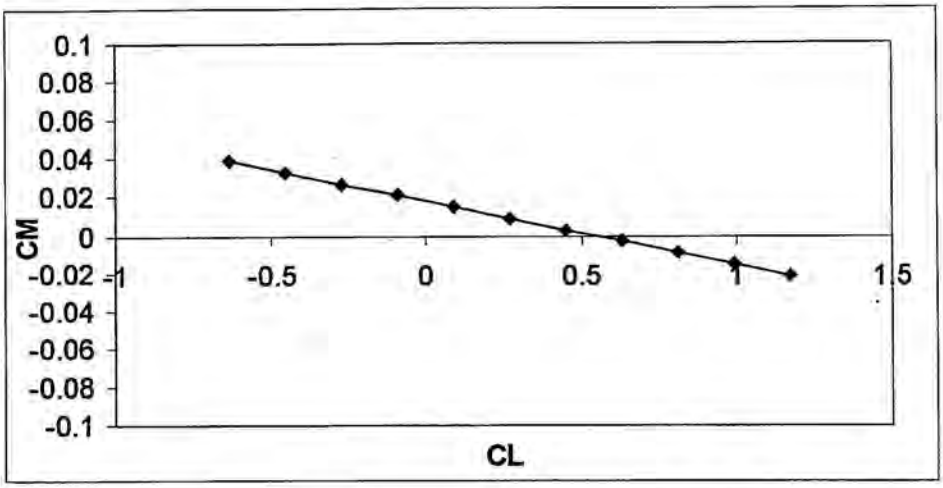

Figure 5.1 – Moment coefficients vs. Cl

5.2 Simulated Aircraft Mission Performance

The performance of the finalized aircraft configuration could be predicted using the DBF03 program, and can be seen in Figure 5.2.

A	Type	# Seg.	D. Req. (ft)	Speed	T. Seg.	T. Tot.	Δ Wt. (lb)	Antenna	D (ft)	CL	kJ used	kJ left	EPower	Vstall.	η Batt.
	Accelerate	1	120.0	57	4.7	4.7	0	On	117.3		3.53	88.28	600.00	38.00	0.8
	Climb	1		57	2.7	7.4	0	On	141.1	0.956	2.03	86.25	600.00		0.8
	Land	1		57	2.0	9.4	0	On	102.5	0.437		86.25			
	Brake	1		57	3.8	13.2	0	On	0.0			86.25			
	Cruise	16	500.0	57	133.3	146.5	0	On	7597.8	0.552	56.33	29.92	375.00		0.8873
	Turn180	16		57	45.4	**191.9**	0	On	2588.0	1.214	25.99	**3.93**	485.00		0.84737
						3.2	minutes				**87.87**	KJ Total Used			
B	**Type**	**# Seg.**	**D. Req. (ft)**	**Speed**	**T. Seg.**	**T. Tot.**	**δ Wt. (lb)**	**Antenna**	**D (ft)**	**CL**	**kJ used**	**kJ left**	**Power**	**Vstall.**	**B. Eff.**
	Accelerate	1	120.0	63	4.2	4.2	0	Off	100.8		3.15	88.65	600.00	37.72	0.8
	Climb	1		63	3.0	7.2	0	Off	164.9	0.970	2.25	86.40	600.00		0.8
	Land	1		63	3.2	10.4	0	Off	**179.8**	0.437		86.40			
	Brake	1		63	3.9	14.3	0	Off	0.0			86.40			
	Cruise	8	500.0	63	55.7	70.0	0	Off	3512.0	0.452	18.67	67.73	305.00		0.91069
	Turn180	8		63	25.1	95.1	0	Off	1580.8	0.994	11.92	55.81	415.00		0.87327
	Pause	1				115.1	-5	Off	0.0			55.81			
	Accelerate	1	120.0	83	1.8	116.9	-5	Off	34.3		1.35	54.46	600.00	29.50	0.8
	Climb	1		83	3.3	120.2	-5	Off	181.1	0.954	2.47	51.98	600.00		0.8
	Land	1		83	3.5	123.7	-5	Off	**229.0**	0.309		51.98			
	Brake	1		83	5.4	129.1	-5	Off	0.0			51.98			
	Cruise	8	500.0	83	42.3	171.4	-5	Off	3509.2	0.147	34.24	17.74	635.00		0.78402
	Turn180	8		83	13.2	**184.6**	-5	Off	1097.5	0.736	15.13	**2.61**	795.00		0.69494
						3.1	minutes				**89.19**	KJ Total Used			

Figure 5.2 - finalized aircraft configuration from DBF03

Aircraft Datasheet

School: California Polytechnic State University

Name: Bareback

Aircraft Parameters	
Maximum Length:	4.08 ft
Wing Span:	8.33 ft
Height, Assembled:	2.17 ft
Wing Area:	5.7 ft^2
Aspect Ratio	12 -
Control Volumes	
Vertical tail	0.9 -
Horizontal tail	0.8 -
CL max	-
No Flaps	1.75
10° Flaps	1.9
L/D max	15 -
Maximum ROC	4 ft/sec
Stall Speed	
Empty Weight	29 ft/sec
Gross Weight	38 ft/sec
V Max	85 ft/sec
Takeoff Field Length	
Empty Weight	80 ft
Gross Weight	105 ft

Component Weights		
Component	Weight (oz)	Weight (lb)
Wing	20.8	1.3
Tail	7.2	0.45
Body	17.6	1.1
Gear	16	1
Motor	7.68	0.48
Batteries	20.8	1.3
Nose Gear	4	0.25
Propeller	2	0.125
Reciever/Servos	9.6	0.6
Hardware	3.2	0.2
Total Empty Weight	**108.88** oz	
	6.8 lb	

Systems	
Radio:	Airtronics 7ch Rx
Servos:	Hitec HS-85M
Battery:	12-cell Sanyo S-P1700SCR
Motor:	Graupner Ultra 930-6
Propeller:	RFM 16x13 Carbon Folder
Gear Ratio:	3.7:1 Planetary

Figure 5.3 – Aircraft Datasheet

5.2.1 Center of Gravity Calculation

Using the detailed solid model and the estimated component weights, a center of gravity calculation could be undertaken, in order to enable the design team to locate the aircraft components with respect to each other. This also allowed the team to make some specific design decisions regarding the components yet to be manufactured. For example, the keel could be reinforced in thickness with extra plys of carbon fiber in the location where the landing gear and the wing attachment points were calculated to be. Likewise, the tail strike angle could be calculated with more precision, the position of the landing gear now accurately determined.

Table 5.1 Center of Gravity Calculation

Component	Weight (oz)	Arm (in)	Moment (oz-in)
Wing	20.8	13	270.4
Tail	7.2	43	309.6
Body	17.6	15	264
Gear	16	15	240
Motor	7.68	4	30.72
Batteries	20.8	6	124.8
Nose Gear	4	6.8	27.2
Propeller	2	3.2	6.4
Total Moment (oz-in)			1273.12
Total Weight (oz)			94.08
CG Location (in)			**13.53**

5.3 Rated Aircraft Cost

The rated aircraft cost was calculated using the contest supplied cost model. The total cost was found to be $6,210 dollars.

Table 5.2 – RAC Calculations

Component	Value		Multiplier	Result	WBS Section
Wing Span	8.3	Ft	8	66.4	WBS 1.0
Max Exposed Chord	0.8	Ft	8	6.4	
Control Surfaces	2	#	3	6	
Max Body Length	4.00	Ft	10	40	WBS 2.0
No Act. Cont. Vert. Surf.	0	#	5	0	WBS 3.0
Act. Cont. Vert. Surf.	1	#	10	10	
Horizontal Surfaces	1	#	10	10	
Servo/Controller	6	#	5	30	WBS 4.0
Propellers	1 #		5	5	WBS 5.0
Engine Number	1 #		5	5	
MFHR TOTAL				**178.8**	

Rated Aircraft Cost, $ (Thousands) = (A*MEW + B*REP + C*MFHR)/1000

MEW = 6.8lb REP = 1.3lb

A=$100 B=$1500 C=$20

RAC = (100*6.8+1500*1.3+20*178.8)/1000 = **6.21**

5.4 Wing Strength Calculation

Using the DBF03 program, the wing strength and weight could be easily calculated. Both the bending moment at the root and the thickness of the carbon-fiber spar cap necessary to resist the loads taken during flight were included in this estimate. The results can be seen in Table 5.3.

Table 5.3 – Wing Weight/Spar Cap Thickness Calculations

Area	$5.7ft^2$	Root Thickness	5.7	in
Span	99Ft	Spar Cap Area	0.0164	in2
Chord	8.3In	Spar Cap Width	4.7	in
		Total Area	373	in2
Aircraft Weight	11.8Lbs			
		Skin	3	oz/ft2
T/c	0.09	Resin Content	0.5	
Airfoil	0.052	Foam	1.6	lb/ft3
G's	6			
		Caps	1.7	Oz
Bending Moment	59Ft*lbs	Skins	8.8	Oz
3.0 oz thickness	0.0035	Foam	6.0	Oz
max stress	50000ksi	Misc	5.5	Oz

Total	**22.0 Oz**
	1.4 Lb

5.5 Aircraft Assembly

Although most of the aircraft components would be secured together using quick plug-in connections, some had to be connected permanently. Since the aircraft could fit into its storage container with these components on, the main landing gear and the wing root were both attached with bolts. In order to lessen the damage that would be taken in a crash, both the wing and the landing gear used nylon bolts that would shear in a crash, reducing the damage taken by the actual airframe components. The V-tail was attached using a quick "pin" connection, utilizing a set of carbon fiber tube plug-ins.

5.6 Payload Extraction Mechanism

Although the preliminary design of the aircraft ended up selecting a method for the retraction of the electronics payload box, the exact method by which the box would be restrained in the fuselage was yet undetermined. The design of this deployment system was one of the most important tasks the team accomplished during detailed design. The goal for the payload deployment system design was simplicity and reliability of operation. The system that resulted from the detailed design stage was a simple one – it consisted of a thin aluminum "plate" in which a Y-shaped pin moved by a servo could slide. This moveable pin would go through tabs on the top of the payload box, and be pulled out for retraction. The schematic of the retraction mechanism can be seen in Figure 5.3.

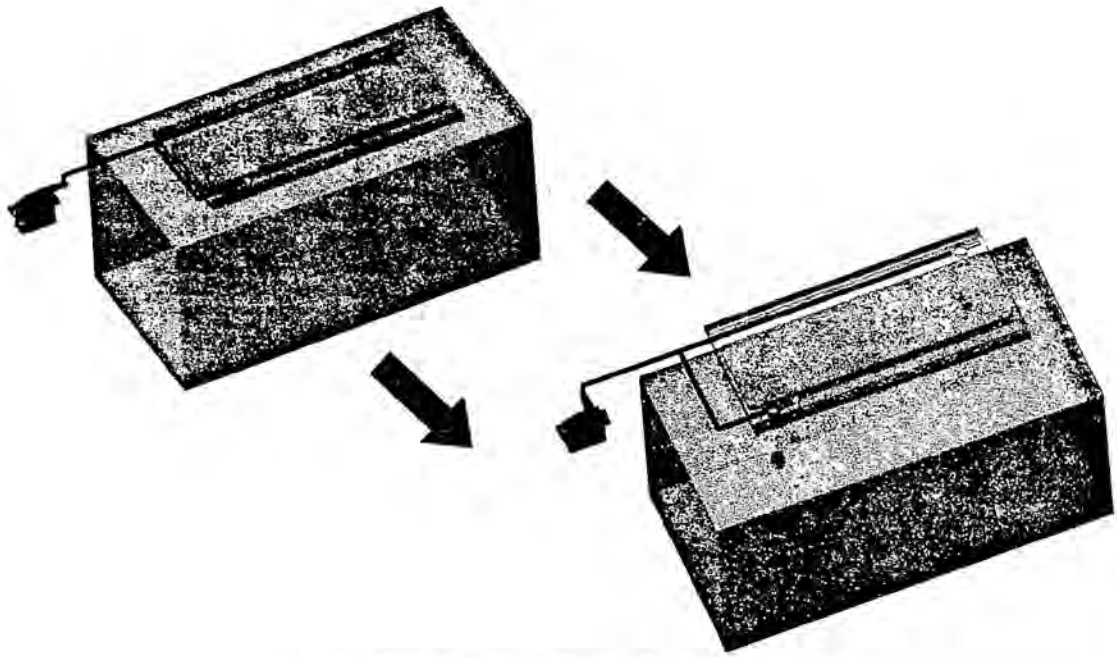

Figure 5.4 – Retraction Mechanism Operation

Once the pin was pulled, the payload box would fall out of the fuselage, pushing the payload doors open as it slid out. The payload doors were designed such that there was a substantial moment arm about the door hinges for the points of contact between the payload box and doors, to insure that the payload doors did not get stuck during deployment. After deployment, the aircraft could be taxied away, with the doors closing via springs upon clearing the payload box.

6.0 Manufacturing Plan and Processes

In constructing the aircraft, different manufacturing techniques were used to manufacture the primary components. While several different concepts were considered, composite construction was used extensively on the aircraft for its relatively high strength and low weight characteristics.

6.1 Manufacturing Concepts

As the team completed the detailed design, the construction method had to be determined. Several construction methods we available at the team's disposal and using figures of merit, the team rated each of the methods. First, the team considered the traditional balsa-hardwood construction with heat shrinking plastic covering such as Monocoat. This method was found to be heavier then other methods and much more rudimentary. Next, the team considered foam core composite construction. This method used a foam core material which was cut or sanded into the desired part geometry and then applied a composite cloth with resin along with heat and pressure. This method was found to have great strength to weight characteristics and moderate durability. The final method considered was a hollow mold composite method in which a negative mold was created, then adding a composite cloth with resin, or using pre-impregnated resin composite (prepreg) material with the application of heat and pressure. This method was found to have the highest strength to weight characteristics, but a much lower durability than the foam core due to lack of a core material providing compression resistance.

6.1.1 Competing Concepts

After thinking about the options, the team found that balsa-hardwood built up construction, has many benefits. It is cheap, requires little skill, and few pieces of equipment. The dilemma is that it would not have the desired strength, especially in shear stress and is heavier than the composite methods therefore eliminated. The hollow-core composite method had many benefits. It is the lightest method, but required a high level of expertise, tirne, and effort. The part required a negative mold which was laid up into using conventional wet layup techniques or prepregnated composites. Using this method the aircraft would be more prone to compression damage due to handling and assembly which would be more difficult to repair.

6.1.2 Downselect

Due to the high strength to weight ratio, along with simpler manufacturing procedures, the foam-core composite process was selected to be used as the primary construction technique. The foam core method permitted the part to be cut or sanded out of foam and then laid up using the desired orientation and thickness of composite material. The foam core allowed a much quicker final part compared to the hollow-core parts while much stronger parts than that of a balsa build up. If the aircraft were to be mass-produced, the long-term benefits of the hollow-core method would out weigh that of the foam core in particular areas of the aircraft, producing an ultimately lighter aircraft.

6.2 Manufacture of Primary Components

After the manufacturing concepts were narrowed down to a mostly foam-core composite construction, the team drew on experience gained in past years to determine the proper manufacturing techniques for the individual components. Different techniques and materials were utilized depending on the part be manufactured. The team selected this comparatively advanced method of construction despite of its higher level of complexity because of the potential it offers to builders experienced enough to utilize it. Although the method of construction is complex to learn; once learned, it delivers results that are superior in most respects to the alternatives.

6.2.1 Fuselage

Fuselage construction began with the general cross section of the fuselage cut out of white foam using templates generated from a solid model. The entire form was then sanded to bring out the detailed shapes, such as the nose and rear of the payload area tapering to the tail. Once the fuselage was sanded, a cutout was made on the top surface, into which the keel was set into. The entire surface was then filled with a light weight spackle to reduce the number of imperfections on the surface. With this step completed, the fuselage was ready for the composite lay up.

The composite lay up began with a layer of fiberglass, which was laid down on the foam surface "on the 90" after being coated with a light layer of spray adhesive. Next, unidirectional carbon fiber strips were applied to parts of the fuselage that were load-carrying. These parts were the underside of the tail boom, the hinge and cutout lines of the payload doors, and the nose of the aircraft. Over this layer of carbon fiber, two more layers of fiberglass were applied. After these layers were adhered with spray adhesive, the entire fuselage was brushed with epoxy. The excess epoxy was then removed by "squeegeeing" in order to reduce weight. The entire assembly was then cured in an oven at 135 ^{o}F for 12 hours. After the curing cycle, the fuselage was further sanded, and the doors were cut out. The fuse was then hollowed out where payload and propulsion items were to be located.

One would think that the keel and shell method of construction compromises strength when compared to a fiberglass fuselage with load-bearing walls. In fact, the choice to not build the fuselage using a construction with load-bearing walls was made because of the big hole that was to be cut out of the fuselage. The doors would have seriously compromised the structural integrity of a fuselage built without a load-bearing keel. Another advantage of the keel-shell configuration is that it is much lighter and easier to modify, making it more aerodynamic therefore giving the airplane higher performance.

6.2.2 Wing

Due to the fact that the wing must be able to fit into the 4'x2'x1' shipping container, the team decided that the wing should be broken into three pieces, a 2 foot center section that will have two 3 foot tip panels. The tip panels are to be adjoined with the center section with a solid joiner tube comprised of a 3/8" OD carbon tube that is to be inserted into the 3/8 ID wrapped carbon tube. The use of ribs and sub-ribs made of ¼" aircraft plywood at the faces of both the adjoining surfaces of the wing panels and center of tip panels will

allow the transfer of flight loads from the wing into the hollow-wrapped carbon tubes and the solid carbon joiner tubes. The joiner tube will not only carry the flight bending load of the wing, but also allow quick and easy assembly of the wing panels onto the aircraft.

Then the wing will be manufactured using standard vacuum bag foam core construction, wrapping a foam core with thin sheets of fiberglass and layers of carbon fiber arranged in the spanwise direction to act as the spar cap along with the carbon joiner tubes. Unidirectional carbon fiber will be placed on the quarter chord to resist bending moment in the wing. The wing core will be constructed out of 2.3 lb density white spyder foam, commonly used for surfboard cores.

A unidirectional carbon fiber spar cap laid up on top of the foam core will take up the bending loads in the tip panels. The direction of the fibers in the spar cap will be placed from the root to the tip of the wing because this is the direction of the bending force and the fibers only have strength lengthwise. The fiberglass has fibers placed ninety degrees to each other and will be placed at a forty-five degree angle with respect to the leading edge of the wing. The fiberglass will provide strength for the wing in torsion.

After the carbon fiber and fiberglass are attached with epoxy, the wing is placed in a vacuum bag. The vacuum bag is very convenient. It provides uniform pressure around the part while curing holding everything together and producing consistent parts.

6.2.3 Tail

The tails were constructed in the same manner as the wing. Again, the tail must be detached from the fuselage to fit inside the shipping container utilizing the the plug-in approach as described with the wing. The tail will plug together with the keel using carbon fiber joiner tubes.

The tail consists of a foam core, with carbon fiber spar caps, a fiberglass skin. The cores were cut out of spyder-foam, using templates created from the solid model program. The skin consists of one layer of two-ounce fiberglass. The spar caps were constructed out of two layers of unidirectional carbon fiber. Mylars were used to achieve a smooth surface finish, and to transfer the paint pattern to the tail. The paint pattern was selected to provide pilot visibility. After the tail is laid-up, it is vacuum bagged and cured in the oven for the prescribed curing cycle.

When the basic construction is completed, the control surface and spars are placed. The control surfaces were controlled by a servo, which was placed in a cavity dug out of the lower surface of the tail. Wires were run through the wing up to the servo. To construct the actual control surface, a cut was made in the fiberglass skin from the underside of the tail, up to the surface of fiberglass. This allowed the fiberglass to serve as the hinge for the control surface, eliminating additional complexity. The servo attachment was located at the heel of the control surface. The wires connected from the receiver to the servo were run through the fuselage.

6.2.4 Keel

Since the keel carries most, if not all, of the bending load in the fuselage, extra care was taken with its construction. Rohacell ® foam was cut into the shape of the keel. It was treated with a wet lay up of several layers of both uni and bi-directional carbon fiber, to provide stiffness and strength. After vacuum bagging and curing in the oven for the prescribed cycle, the keel was ground to the final dimensions. The engine mount was created in the same manner, and then attached using more Rohacell ® foam and carbon fiber. The entire assembly was then placed in the fuselage.

6.2.5 Landing Gear

The landing gear was constructed using a dry composite lay up. The landing gear went through several iterations, and the final gear was created using 30 layers of prepregnated unidirectional carbon fiber, placed at both 90 and 45 degree orientations. The gear was vacuum bagged over the gear form before being cured in the oven. After the cure was complete, the landing gear was ground to its final dimensions, and holes were drilled into the mounting part to attach it to the keel. The tires were attached using collets and 5/16" axles.

6.2.6 Release Mechanism

The release mechanism construction began with the fuselage. The doors were cut out of the fuselage and shaped to properly fit the payload. Additional fiberglass and carbon fiber was applied to strengthen the doors. The interior of the payload area was hollowed out, and further smoothed to provide a proper fit for the payload. The mounting plate was attached to the keel, and the servo was placed in the rear end of the payload area. The servo could be freely moved in the tail and could be used to fine-balance the aircraft.

6.3 Manufacturing Milestone Chart

When building the aircraft, it was not unusual to have several components under construction at the same time. The primary difficulty in scheduling the construction, especially for the composite materials, was the difference in curing cycles for the different materials used. Because of this constraint, it was vital certain parts were constructed in the correct order. Figure 6.1 shows the manufacturing milestone chart illustrating the scheduled event timings.

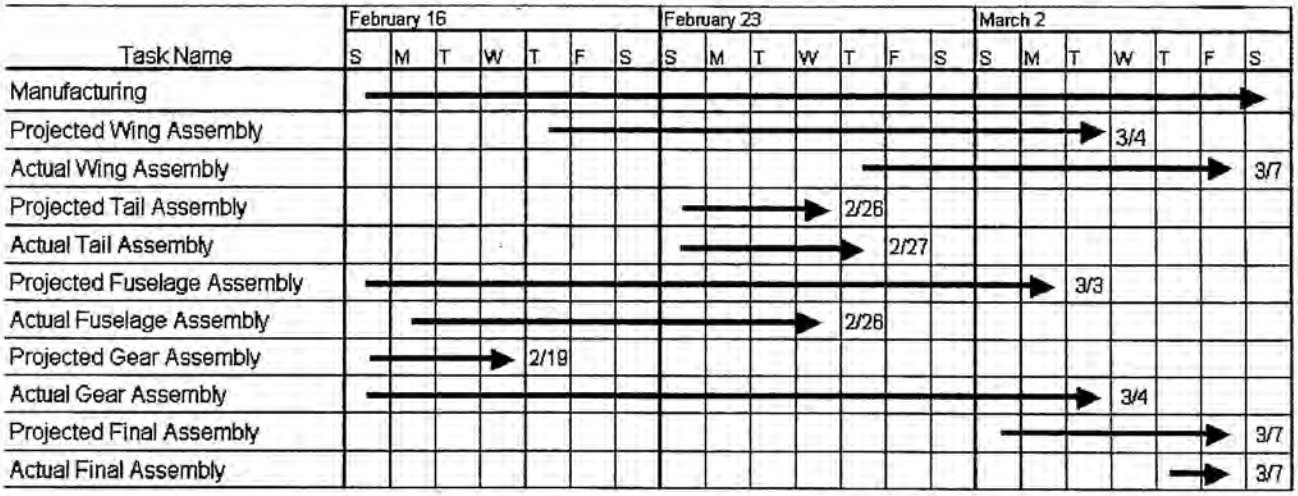

Figure 6.1 – Manufacturing Milestone Chart

7.0 Testing Plan

When designing the aircraft, several factors remained unknown, including structural capabilities and proper manufacturing techniques. By testing components before and after final installation, the aircraft's final configuration was confirmed to be strong enough to withstand the design loads, and controllable enough to fly the selected missions.

7.1 Testing Objectives

The static tests conducted on the components as well as the full aircraft confirmed the structure was capable of handling the design loads. The testing processes also afford the team opportunities to test the ease of assembly for the aircraft, and helped improve the manufacturing techniques used for the components. The dynamic testing will help gain valuable experience relating to the real-life handling qualities of aircraft, as well as gain pilot experience. Overall, the testing allowed the team to ensure the aircraft was fit for competition, and functioned in the way that was expected. It also allowed for validations of the assumptions made in the early stages of the design.

7.2 Testing Schedule

In order to ensure all the required testing was completed before the competition, a testing schedule was created. The schedule allotted time for general testing of components, static testing of the entire configuration, and dynamic, or flight, testing of the final aircraft.

7.2.1. General Testing

The testing schedule was largely dictated by the manufacturing schedule, since components were tested as they were produced. Table 7.1 shows the basic checklist used to ensure uniform testing for each component.

Table 7.1- Testing Check List

Testing Check List		
Component	Pass	Not Pass
Dimensions Surface defects		
Stresses (if applicable)		
Torsion Bending Normal Axial		

The actual testing was conducted by a combination of visual inspection and force application. The surfaces and dimensions were visually inspected for any problems that might cause undesirable effects such

as stress concentrations. The stress testing was done by placing predetermined weights on the components in such a way as to produce torsion, bending, normal or axial stress, depending on the component being tested. The weights used were chosen in such a way to simulate the maximum design load the given component would have to withstand. Yielding was taken as the criteria for failure – even small plastic deformations would cause a part to fail the stress test. Since fiber reinforced composites do not generally allow for a large plastic deformation before yielding, this was a good estimate of the maximum strength of the parts manufactured.

Due to the large amount of composite construction used on the aircraft, surface defects such as de-lamination were important indicators of weak components. In some cases, such as the landing gear, having surface de-lamination caused a part to fail.

Another component of the aircraft that had to be tested extensively was the engine. Its testing cycle was dictated primarily by its arrival date. Before mounting the engine on the aircraft, its static thrust was tested, to ensure our initial assumptions were reasonable.

7.2.2 Static and Dynamic Testing

In order to better organize the time allotted for testing, a schedule was drawn up. Figure 7.2 shows the static testing schedule, which was largely adhered to.

Table 7.2- Static Testing Schedule

First Round 3/01	Horizontal Tail	
	Vertical Tail	
	Fuselage (foam)	
	keel	
	Landing Gear	
Second Round 3/02	Fuselage (full)	
	Cargo Doors	
	Wing	
Third Round 3/03	Connections	
	Release Mechanism	

After all the static testing was completed, the separate components were assembled for a final static test. At the time of writing, the entire model has not been flight tested because of a delay encountered with motor shipment. Once the motors arrive, the entire model will be flight tested – this will allow for "real-life" testing of the deployment system, as well as testing of controllability of the aircraft. This process was also scheduled, as shown in Figure 7.3.

Table 7.3 – Dynamic Testing Schedule

Test Flight #1 TBA	Takeoff Requirement Release Mechanism Release Mechanism (2) Correct Flight Path Landing Visual Inspection	
Test Flight #2 TBA	Takeoff Requirement Release Mechanism Release Mechanism (2) Correct Flight Path Landing Visual Inspection	
Test Flight #3 TBA	Takeoff Requirement Release Mechanism Release Mechanism (2) Correct Flight Path Landing Visual Inspection	

7.2.3 Flight Testing

After each test flight the aircraft will be visually inspected for any surface damage or weak parts. The deployment system will be tested sufficiently to ensure the mechanism works reliably. The flight path used in the test flights will be the same as that used in the competition.

7.3 Testing Results

While the testing the individual components and the full aircraft, several discoveries were made. The component testing showed problems with pre-preg carbon construction, while the full aircraft static testing showed no problems.

7.3.1 Component Static Testing Results

No major problems were encountered during the testing phase. Several lessons were learned, mainly dealing with the composite construction methods employed. Several landing gears failed their initial test due to delamination before the proper pressure and temperature levels for curing were determined. The gear was fairly strong in bending, but the sections that delaminated plastically deformed during the normal stress test. After the correct curing procedure was determined, the component passed all the stress tests, and was ready to be installed on the aircraft.

Test Flight #1 TBA	Takeoff Requirement Release Mechanism Release Mechanism (2) Correct Flight Path Landing Visual Inspection	
Test Flight #2 TBA	Takeoff Requirement Release Mechanism Release Mechanism (2) Correct Flight Path Landing Visual Inspection	
Test Flight #3 TBA	Takeoff Requirement Release Mechanism Release Mechanism (2) Correct Flight Path Landing Visual Inspection	

Figure 7.3 – Dynamic Testing Schedule

7.2.3 Flight Testing

After each test flight the aircraft will be visually inspected for any surface damage or weak parts. The deployment system will be tested sufficiently to ensure the mechanism works reliably. The flight path used in the test flights will be the same as that used in the competition.

7.3 Testing Results

While the testing the individual components and the full aircraft, several discoveries were made. The component testing showed problems with pre-preg carbon construction, while the full aircraft static testing showed no problems.

7.3.1 Component Static Testing Results

No major problems were encountered during the testing phase. Several lessons were learned, mainly dealing with the composite construction methods employed. Several landing gears failed their initial test due to delamination before the proper pressure and temperature levels for curing were determined. The gear was fairly strong in bending, but the sections that delaminated plastically deformed during the normal stress test. After the correct curing procedure was determined, the component passed all the stress tests, and was ready to be installed on the aircraft.

Another part that experienced problems due to construction was the horizontal tail. The tail's fiberglass coating had not properly cured the first time it was put in the oven. This caused its ability to take bending stresses to be compromised to such a degree that it was no longer usable. In order to test the sample structure, the unusable tail was destructively tested for the normal stress case. This test showed that even the weakened tail was able to withstand the design normal load. This test is illustrated in the photo shown in Figure 7.4 below:

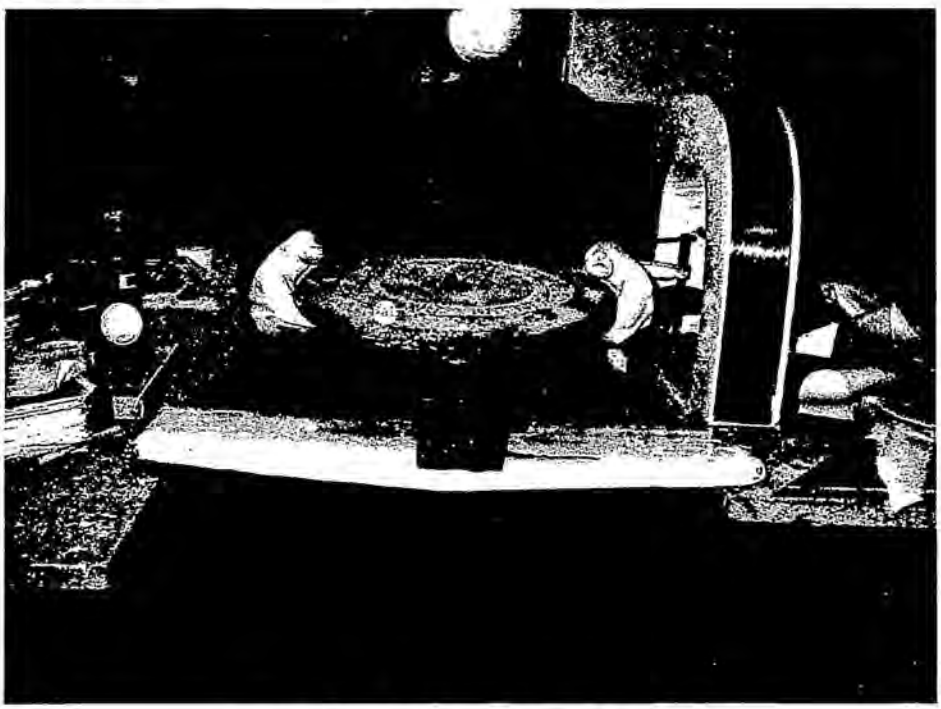

Figure 7.1 – Destructive Testing of the Tail

Other than these two components, no other problems were encountered. Due to the composite construction used, all the components were strong enough to withstand the design loads. The engine testing proved our original assumptions were reasonable. With all the parts statically tested, they were assembled into the final configuration for the full aircraft static and dynamic tests.

7.3.2 Completed Aircraft Static Testing Results

The full aircraft static test was conducted in much the same way as the individual components' static tests. One of the most important tests was the wing-tip test that the aircraft is expected to pass after assembly at the competition. Special attention was paid to any vital connectors, such as wing plugs, tail plugs, and servo connections. The aircraft was loaded to the maximum design load, and inspected for signs of stress or strain. Due to the careful component testing, none were found.

References

1. Raymer, Daniel P., Aircraft Design: A Conceptual Approach, AIAA Education Series, 2001.

2. Lennon, Andy. Basics of R/C Model Aircraft Design: Practical Techniques for Building Better Models, Motorbooks International, September 1996.

3. Abbott, Ira H., and Von Doenhoff, Albert E., *Theory of Wing Sections* Dover editions, 1956.

4. Simons, Martin. *Model Aircraft Aerodynamics,* Motorbooks International, 2000.

5. Randolph, Randy. *R/C Airplane Building Techniques* Motorbooks International, 1997.

6. Roskam, Jan. *Airplane Design Part I : Preliminary Sizing of Airplanes*, DAR Corporation; June 1989.

7. http://www.csd.net/~cgadd/eflight/calcs_motortest.htm

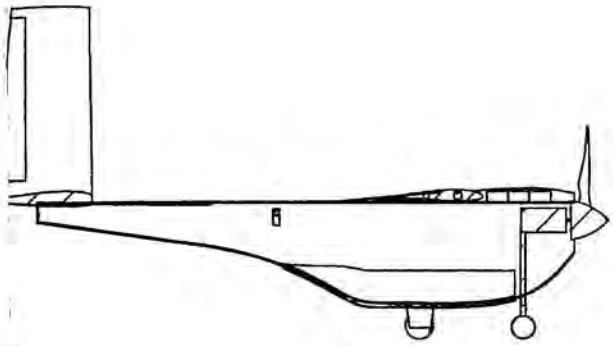

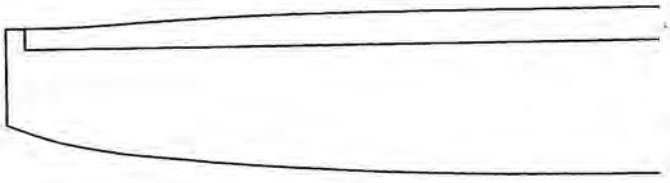

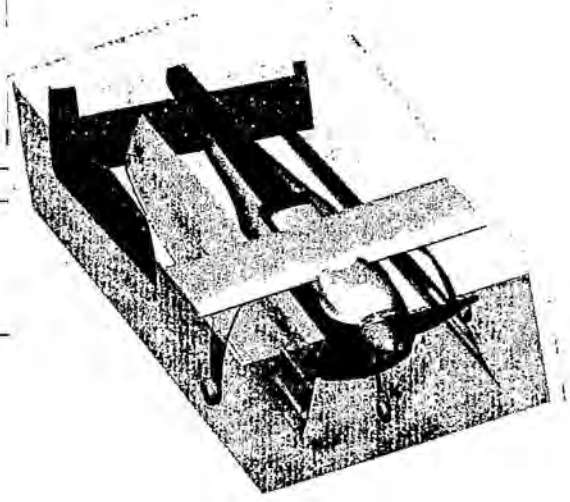

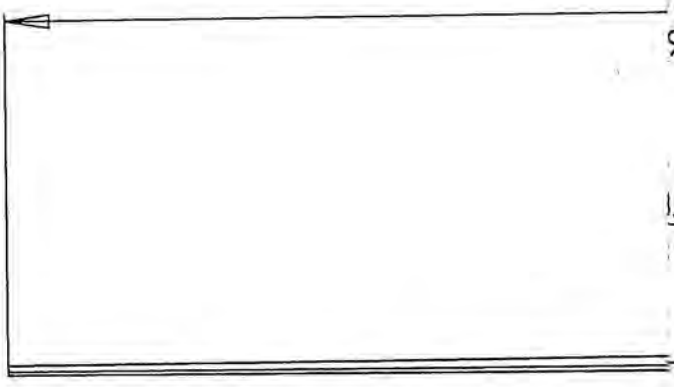

9 in.

.5 in.)

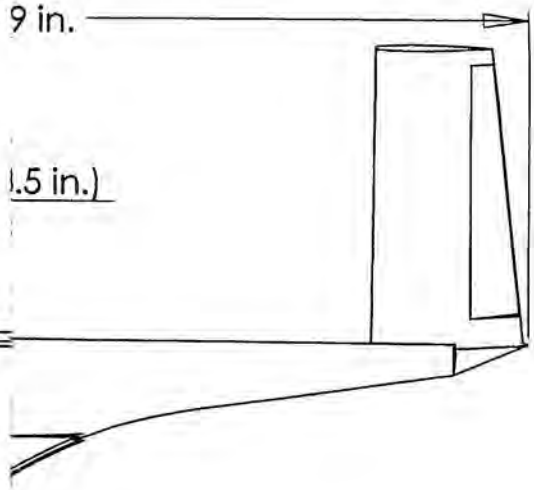

(9 in.)

NAME	Cal Poly DBF Team		
Gisin			
McCue	TITLE: "Bareback"		
	SIZE B	DWG. NO. 1	REV
	SCALE: 1:10	WEIGHT:	SHEET 1 OF 1

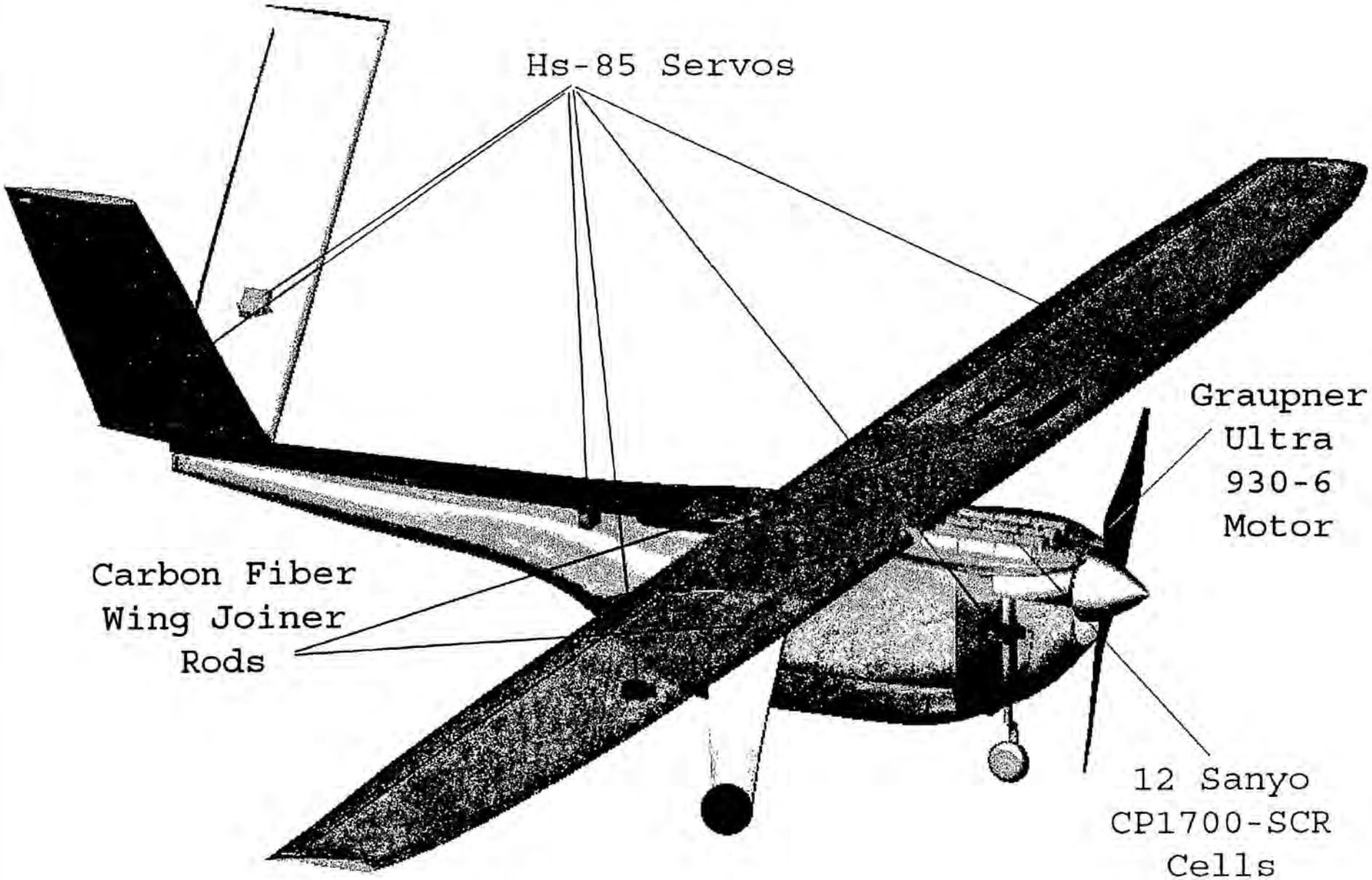
Hs-85 Servos
Graupner
Ultra
930-6
Motor
Carbon Fiber
Wing Joiner
Rods
12 Sanyo
CP1700-SCR
Cells

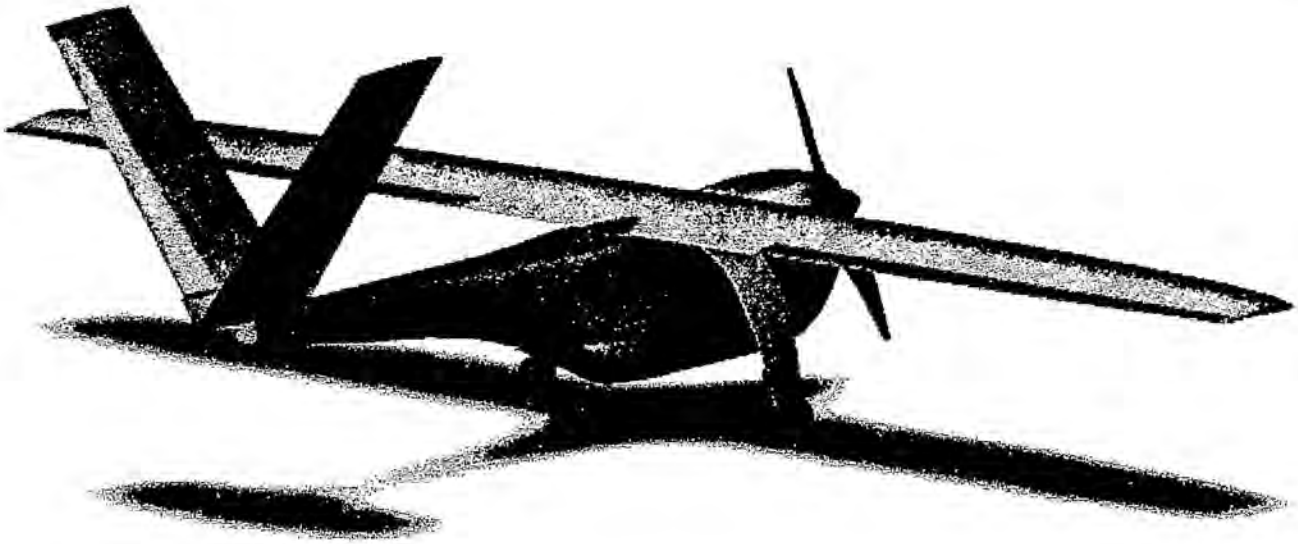

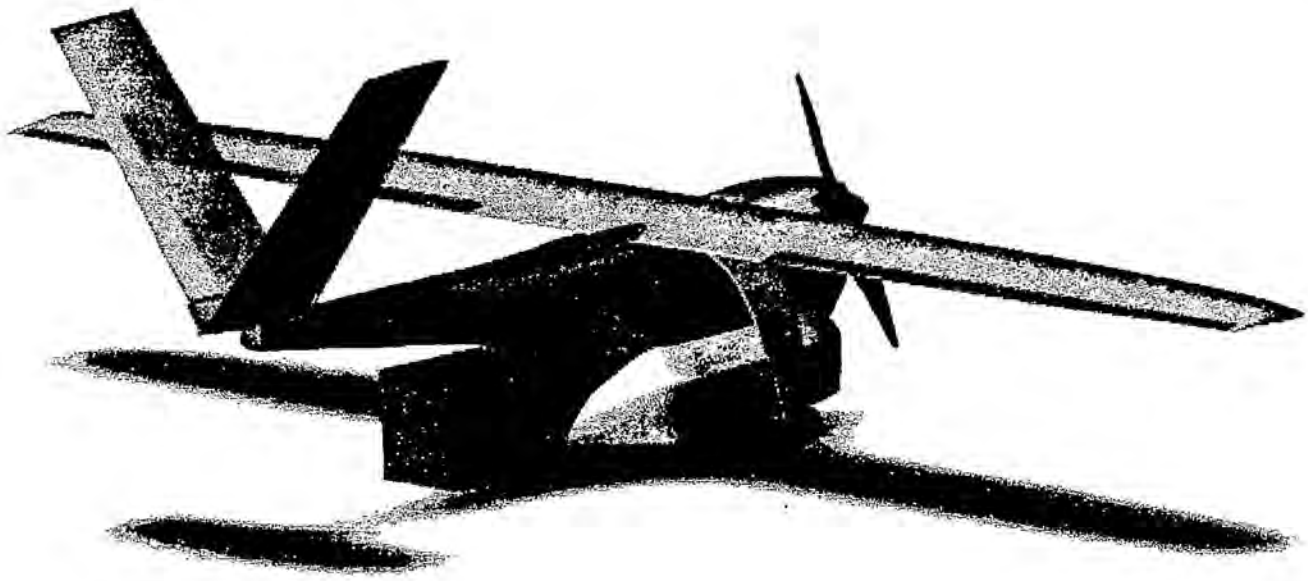

AIAA / CESSNA / ONR Student Design / Build / Fly Competition 2002/03

Università degli studi di Roma "La Sapienza"

Design Report :

The Flying Centurions

... saggi, tranquilli e combattivi

Table of Contents

1 Executive Summary

1.1 Introduction

This report documents the complete study carried out by the Flying Centurions team from University of Rome "La Sapienza", to realize the UAV Galileo IV for attending to the AIAA/Cessna/ONR Student Deign/Build/Flying 2003 Competition. Beginning by accurately analyze the contest rules, we tried to develop a design able to best meet mission requirements and to be competitive in the final phase of the contest, i.e. the fly-off held at Webster Field in April 2003. The rules for this edition keep the same layout of previous year, regarding the scoring and the RAC calculation scheme, but include different kinds of missions. The aim of the team, dealing with this new experience, was to improve the results achieved in the previous editions of the contest. To reach this target, we focused the main attention to improve those aspects of the design process that penalized teams from our University during previous editions. We sought from the beginning to optimise the RAC function and to give our new aircraft the proper aerodynamic, structural and propulsive solutions. Particular attention was paid to the model assembly procedure, because the need of a fast way to mount the plane is the real new for this year.

1.2 Conceptual Design

At the beginning of the design process, four main areas of interest were identified. The team was split into four design groups: each one performed a study aimed to identify the configuration with could gain the highest potential score. A first group (aerodynamic) attended to the aerodynamic branch of the design; a second one (flight mechanics) developed methods to predict aircraft performances, and to find a way to optimize them. A third one (structures) focused its attention to the structural solutions and the problems related to the assembly; the fourth one (propulsion) studied how to give the plane the proper propulsive system. For each choice each group would deal with, figures of merit had been introduced. This is a way to take into account how each option affects the final score and how this option can be implemented. After each group had proposed the solutions it judged the best from its own point of view, brainstorming within the groups' leader allowed us to define the final aircraft configuration, tooling and material to be used for manufacturing, and the kind of propulsive scheme. Aerodynamics and Flight Mechanics considerations had been esteemed the most important for shaping the configuration (monoplane with high wing, axis symmetric fuselage and H tail), while structural and manufacturing requirements drove the selection of self-made composite materials to build nearly all the structural components. The propulsive group selected the motors number (one), gave a rough estimation of the number of cells needed and proposed the location of each component of the propulsive subsystem.

1.3 Preliminary Design

The first objective of this stage of the design process was the implementation of an optimization program which could lead to size the configuration able to reach the maximum total score. The study started by summarizing configuration data previously obtained. Then, we had to take into account each phase of the possible flight missions. A "standard mission" was identified to this purpose. Then we identified the main design parameters we wanted to be determined by running this program, and a broad range of possible

variation for them (wing airfoil, wing area, cruise speed, turn loading factor, cells number, propulsive subsystem). These parameters, input in the program with a large range of values, were linked to the global performances of the virtual plane, and to the global score it could reach performing the standard mission. By running the program, we could narrow the range of variation of design parameters, but we could not identify yet a unique solution for each of them. So, groups had to focus their attention upon the possible choices left, trying to extrapolate the best one. The aerodynamic group studied different airfoil types and found out an approximation of lift and drag for each surface and for the whole aircraft. The flight mechanics group studied the static stability and developed models to predict the flight performances of the aircraft. The structural group used analytical and numerical methods to find the stress field in the main components and sized them, selecting for each the most suiting material. The propulsive group selected the motor model, the most opportune reduction and a set of propellers. At this point the first components were sized, and we could find out the performances of the plane in term of range, speed in the various flight phases and mission time. A 1:2 scale moke-up was carried out to visualize the choices and to take familiarity with the whole project. We could produce the first CAD model.

1.4 Detail design

After the preliminary sizing, we led a detail analysis of each component, each subsystem, and their integration in the global project. So doing we became able to build the first prototype to test the choices we had maiden. The aerodynamics and flight mechanics group studied the dynamic stability, by calculating the stability derivatives. A more precise estimation of the aerodynamic loads allowed sizing the servo controls and their location. The structural group completed the sizing of all the parts; particularly it defined the payload release system and the assembly. Then the locations of receiver and cables were defined. A final solution for the manufacturing process was identified. By using opportune software, the propulsive group tested several propellers and cells with the motor selected. At the end of this study, we could produce final CAD drawings of each component of Galileo IV, and the assembly schemes.

1.5 Manufacturing Process

The production phase was the benchmark to value the goodness of the choices carried out. In some cases building difficulties or non-satisfying results (most of all about the preparation of composite materials) led us to introduce little changes on the earlier design. In other cases we felt the need of further studies on some components or alternative solutions.

1.6 Testing Sessions

To check our choices, and to identify the way to optimize the whole design, experimental analyses were performed in each design area. Mechanical tests on standard specimens allowed us to evaluate the properties of the material to be used. Testing entire half-wings till their failure provided us the confidence about their actual loading capabilities. Wind tunnel tests of a semi-model 1:2 scaled gave the whole aircraft polar drag and important indications on the shape of the aerodynamic fairings of the fuselage. At last, the propulsive group tested the motor-propeller set, obtaining experimental data on thrust at various flight speeds. Finally, flight test have been planned to indicate the way for further optimization.

2 Management Summary

2.1 Team Organization

2.1.1 The first step: organization and "pre-conceptual" design

When our team was born, at the end of July 2002, it was immediately clear it would have to solve two main problems: to organise into an engineering team a big number of students (there were 58 of us at the beginning!) and to supply them with enough funds, tools and items to reach the targets. More over, our main suppliers, the Rector of University of Rome La Sapienza, wanted us to prepare a didactical project, which could engage so many students. Only in this way it could be possible to receive the aid of University to carry on a new experience in DBF competition. The first step of the organization process was to split the team into 5 littler groups. The work they had to do along the summer was mainly didactical: the students with previous DBF experience had to lead the junior ones into the major areas (technical an logistical) the competition affects. The objective of this session was to perform a pre-conceptual design: each group had to take confidence with the rules and to propose one or more possible concepts.

2.1.2 Driving lines in team management

At the end of this first stage, back home from holiday, we reorganized the entire team trying to realize a well-ordered structure. We knew that to design, build and fly an aircraft best fitting the requirements of the competition it is necessary to coordinate the work of many people, in such a manner that any decision affects the work of anyone. In this way, a group of students can produce what no one within them could on his own: this is the aspect of a teamwork we have learned to appreciate most of all. But it is quite evident that this work has to be properly coordinated. So, we organized the architecture of the team on the basis of the following principles of management: 1: to clearly identify people who would have the responsibility of leading the team along the design process; in particular, there should be a person, the team manager, able to make decision, schedule work-packages, assign tasks and check for they are performed. 2: tasks must be shared to specialized groups, each one with its own leader; the latter should play inside his group the same role the team manager plays within the team. 3: the authority should be delegated to the groups' leader who organize their group's work to make specific, "local" decisions, in such a manner that the flow of tasks assignation goes from up to bottom, and problem resolution goes from bottom to up. 4: "global" decisions must be made by the team manager with the help of technical "staff tables", masters in the subject is being discussed.

2.1.3 Team architecture

Driven by such considerations, we organized the team trying to meet the requirements of the competition: designing / building / testing / flying /documenting a little plane. Figure 1 outlines the architectural structure of the team, and displays individual contributions. Note that the direct implication of our official advisor, prof. G. De Matteis, has been very precious: he has furnished to us his suggests in any phase of the design process, and has vested the student leaders with the authority needed to drive the team along the way to Maryland. The team manager was responsible for overall team direction, both technical and logistical. He had to identify the major areas of the work, to assign tasks and check for they were performed, to supply the different groups with the items, tools and information they needed to reach their targets. He had to control the development of the design process by marking deadlines and scheduling timings. In such a charge of coordinating the teamwork, he was supported by a "seniors council", composed by students taking part to previous DBF competitions. He could also count on the help of two graduate students who has played an

important role in precedent contest. At the subsequent level, the team was divided in three main areas, including 6 groups of study, each one with its own leader who drove the work within the group. Another task of each group leader was to observe the didactical aspects of the studies to be conducted. There have been a few studies the various group leaders carried on together with the team manager; that concerned multi-subject studies as the conceptual design stage and the realization of the optimisation algorithm to analyse overall performances of the plane.

2.1.4 Design Area

Aerodynamic Group: tasks of this group, along the entire process of design development, were the shaping and sizing of external surface of the aircraft and the evaluation of aerodynamics loadings. Tools used were analytical, numerical an experimental ones. Flight Mechanics Group: it concentrates on the study of aircraft performances, stability and handling qualities, identifying the solutions to best design the plane answering the mission requirements. Its work based most of all on analytical and experimental tools. Structural Group: this group was responsible for sizing of main structural elements, choice of materials and integration methods. It was also its task to supply the building group with the drawings needed for manufacturing process. During the different phase of the design process, the group used analytical, numerical and experimental tools to reach the goal of design lightweight, reliable structures fast to assembly. Propulsive Group: it was responsible for the selection of the system motor-propeller-batteries. It used analytical and experimental tools to narrow the possible combinations to a few solutions to be tested directly during the prototype flight test session.

2.1.5 Building Area

The leader of the group of buildings had to implement in real things the input he received about the shape and the internal structure of the plane. He had to coordinates building activities and to control the work so to answer the design requirements. Nearly all the students had to partake in the manufacturing process of the moke-up, prototype, or final model since we felt this experience would teach us what academic courses could not.

2.1.6 Testing Area

The activities of this area regarded three main fields: aerodynamic, structural, propulsive and flight test. Since the results of such tests were extremely useful for the design process, their organization and planning was strictly linked with the design process. Leaders of the Design Area's groups were also responsible for test activities regarding the subjects of their studies.

2.1.7 Report Area

Students who took a part in last year team of our University in DBF competition know very well how report preparation is important to reach a high overall score! That is because since the beginning of the work we started to think to report and selected a report group, with each own leader. Along the process of designing, building and testing each group of study, also the ones of the pre-conceptual phase, had to produce papers documenting the work they produced and the results they achieved. Those documents have been collected, organised and revised by the report group so to produce an organic review fitting the requirements of the competition.

2.1.8 Logistic Area

This area collected activities not properly connected to the design or building process, but fundamental for the progress of the work. In fact, to carry on the work the team should be supplied with funds, tools, facilities,

hardware and software instruments, and any item to improve the configuration sizing, realizing, testing. In particular, we felt the need to identify 2 people responsible for the management of funds, one person for looking for and deliver materials and components, 2 persons for dealing with the laboratories; 1 person for external relationships and contact to AIAA organisation.

2.2 Milestone Chart

To meet the requirements of the competition it was also necessary to consider its deadlines. So, we identified early in the design process a series of scheduled timings for the major activities we had to do, and marked some deadlines representing the main milestones we would have to meet along the work. An overall summary of main timings and deadlines is represented in figure 2. Many more detailed monthly plans were produced during the work, so to guarantee not to disagree with the dates imposed AIAA organisation.

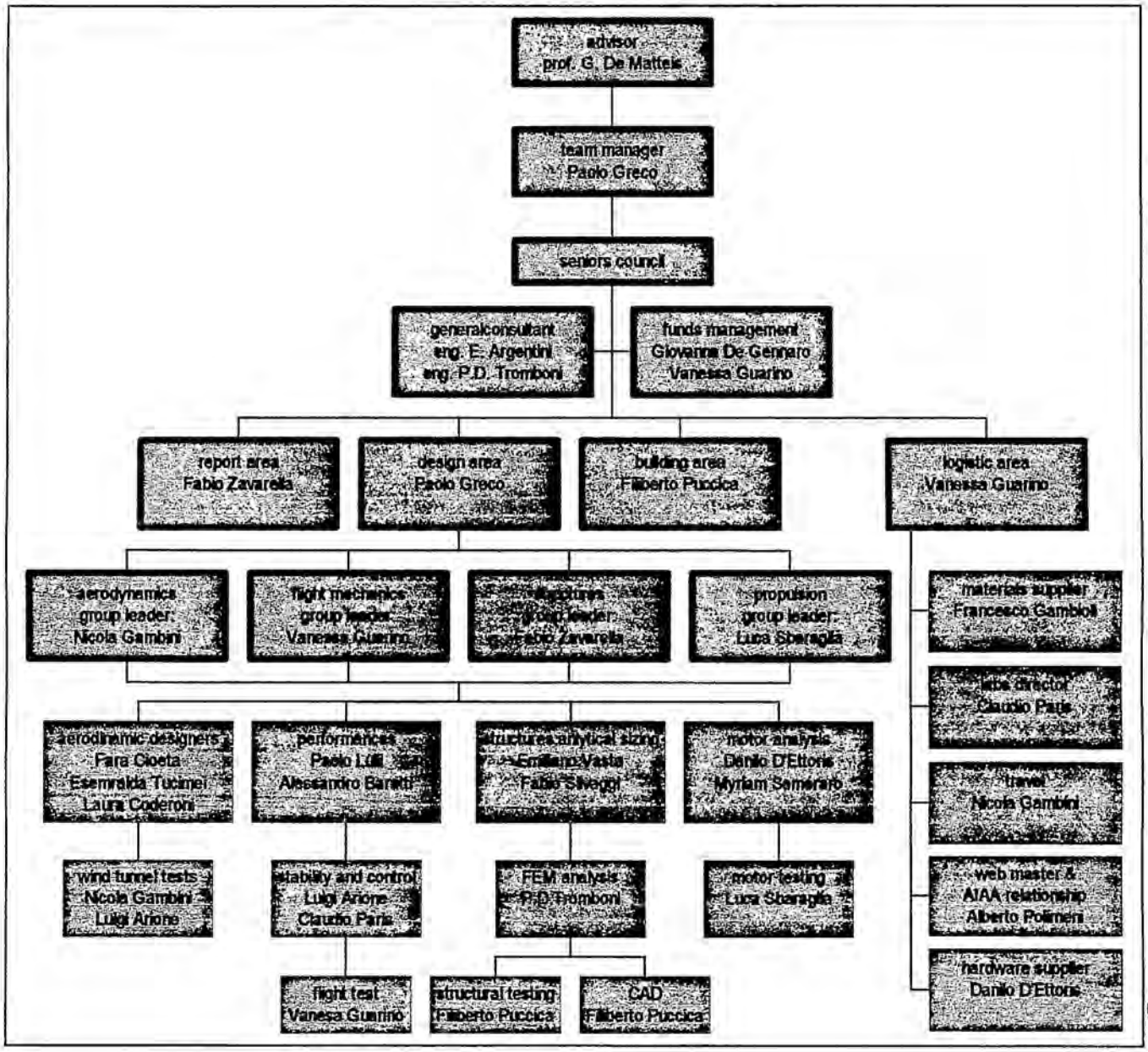

Figure 2.1: team architectural structure

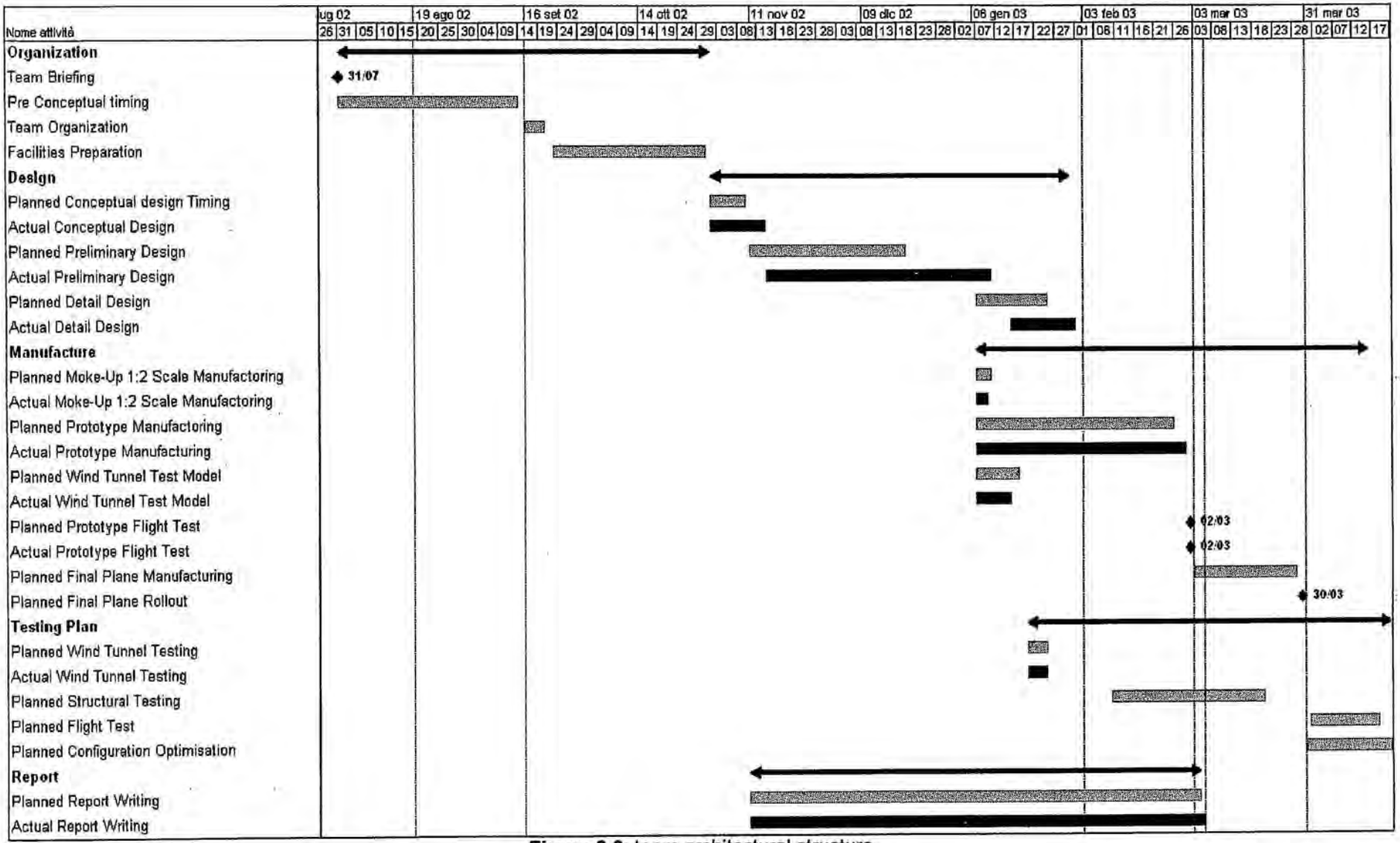

Figure 2.2: team architectural structure

3 Conceptual Design

3.1 Problem Statement

The rules request to design an aircraft able to fit the following major requirements: 1) it must be stowed in a box with defined sized, 2) it must be assembled in the shortest possible time, 3) it must take off in assigned run space, 4) it must be able to perform at least two out of the three missions, 5) it must earn a high total score, then it must have a low RAC and be fast and efficient. So we have defined some primary design parameters whose optimization led us to the final configuration.

3.2 Design Parameters

Constraints on the dimensions of the aircraft have been considered because the aircraft must fit in the box and must be fastly assembled. Next, since the beginning of the design process we have assigned a maximum value for the fuselage length and the wing span. We have investigated different configurations according to the following design parameters: missions to perform, number and location of lifting surfaces, wing planform, tail configuration, propulsive system location and configuration, structural solutions.

3.3 Mission Concepts

The rules allow only 5 flight attempts. In the final score only the best scores achieved in each of two different missions are taken into consideration. For this reason we felt important to select in this early stage the missions we will fly to achieve the highest final score. Indeed, the mission selection affects the final design. For example in mission A a housing for the antenna is needed; in mission B an unloading system for the payload is required. In mission C a greater range is necessary, and an optimisation of the aerodynamic and propulsive performances is important. To select the mission to perform we have introduced the following Figures of Merit (FOMs):

- RAC: this parameter is strongly linked with the final score. It is affected by the mission because it depends from the propulsion system (mission C) and from the number of servos (one more for the mission B).
- Flight distance: this parameter is linked with the flight range. To obtain a larger range, a greater aerodynamic and propulsive efficiency is needed.
- Difficulty factor: it multiplies the single flight score.
- Mission time: the shorter time mission the higher single flight score.

		ALTERNATIVE MISSIONS		
FOMs	***Weighting Factors***	**Mission A**	**Mission B**	**Mission C**
FACTOR	0.50	4	3	2
TIME	0.25	5	3	2
RAC	0.15	5	4	3
DISTANCE	0.10	5	5	3
Tot	1	4.5	3.35	2.25

Table 1: mission selection: weighted decision matrix

The most scoring missions are mission A and mission B. This is good, because it does not prevent us from adapting the design, born for mission A and B, to the mission C (back-fitting the following preliminary

design), simply enhancing the propulsion system (cells #, motor-propeller coupling).

3.4 Alternative Configuration Concepts

Once the design parameters were selected, we evaluated the different possible solutions introducing adequate FOMs. The problem of choosing the configuration consists in selecting, among every possible configuration, the one that best suits the design requirements. We found two ways to solve this problem:

- The first one is to consider at one time all the variables and create a single global decision matrix,
- The second one is to consider a set of "sub problem", each with a reduced number of variables; the configuration selection goes on in a cascade of solutions of these local problems.

We found this second "modus operandi" more efficient because it permits to unveil, by suitable FOMs, the influence of each parameter on a reduced set of design targets,.

3.4.1 Aircraft Configuration

The first and more general sub system concerned the choice of number and location of lifting surfaces. The investigated configurations were:

- The canard solution was considered because it is globally more efficient, due to the absence of trim drag and the higher global Cl_{max} at take-off with respect to a conventional configuration. This allows, at the same thrust level, a reduction of the wing area, compared with the conventional configuration. Considering that in a canard the gravity center is usually backward and the gear is aft, there are no take-off rotation problems. This leads to a smaller landing gear and a simpler stowing of the pieces in the box. Drawback: the longitudinal stability is worst, either for the fore position of the elevator, or for the lack of tolerance in the mass distribution. Yet, in spite of the advantage of a short gear, there is the problem of unloading the payload: selecting this configuration probably would lead to discard mission 2.
- The conventional solution is very well known, allows an accurate prediction of performances and flight characteristics, especially for stability and flight qualities. For these reasons it requires a faster and easier research and development program, suiting the requirements of the contest. It is used as a standard to evaluate the other concepts. Although its drawback is in the absolute performances, a bit worst than the other concept, the reliability is a significant advantage.
- The fling wing has a very low RAC, having no tail, control surfaces and associated servos. Also, it usually has a very low drag. Drawbacks: very poor flight and handling qualities, due to the low number of control surfaces, high airfoil thickness, which gives low Cl_{max} and, therefore, requires a larger wing surface and/or take-off thrust. This leads to a higher RAC. Another drawback is that we have no reference for the design.

To evaluate the configuration which best fitted the requirements of the contest we considered the FOMs in table 1, with adequate weighting factors:

- RAC: rated aircraft cost was considered as the main figure of merit for screening the concept, since it is directly related to the final score and it is a method for quantifying the cost of different solutions. It was therefore heavily weighted.

- Mission: this FOM shows how a configuration is able to perform different missions as stated by the rules. A configuration providing the same level of performance in all the missions would give a wider choice; on the other hand, every configuration investigated seems to be able to perform at least two of the three missions. For this reason the weighting factor is low.
- Drag: a configuration with a low aerodynamic drag needs less power, then allows us to reduce the number of cells and use a lighter motor. This point heavily affects the single flight score, because variations of both the RAC and the flight speed are involved.
- Handling qualities: The evaluation of stability and maneuverability is another considered parameter. An aircraft with good handling qualities allows a more accurate tracking of the flight profile, reducing flight time, and, above all, take-off and landing times. Yet, the weighting factor is low because expected wheatear conditions on the site are rather calm.
- Easy to build: the need to build the aircraft in a short time, with somewhat limited resources led us to consider this important FOM, also if it is non directly linked to the contest score. This FOM has the second higher weighting factor.

The values assigned to the FOMs for the different configurations were evaluated in a qualitative way. Being the RAC the most important parameter among the FOMs, it was calculated for the different configurations using a first quantitative sizing.

Table 2 shows the weighted decision matrix used to chose the configuration considering the previous FOMs. Even if RAC is the parameter with the greater weight, the winning configuration is not the one with the lowest RAC, that is the flying wing. In fact this configuration presents several problems concerning maneuverability, construction and assembly. The canard also has a good RAC, but has the same maneuverability problems as the flying wing. It appears that the conventional solution is the best option, as it suits very well the requests of the FOM.

		ALTERNATIVE CONCEPTS		
FOMs	**Weighting Factors**	**Canard**	**Conventional**	**Flying wing**
RAC	0.40	4	3	5
EASY TO MOUNT	0.20	4	5	3
DRAG	0.15	4	3	5
EASY TO BUILD	0.15	3	5	1
MISSION	0.05	2	5	4
HANDLING QUALITIES	0.05	2	5	1
Tot	1	3.65	3.9	3.75

Table 2: aircraft configuration: weighted decision matrix

3.4.2 Wing Configuration

The second addressed problem was the selection of the shape and location of the wing. The FOMs adopted in this screening are:

- Unloading: it evaluates how the unloading of the payload is simple, fast and reliable. Its fundamental importance for the mission B, explains the high weighting factor assigned.

- Mountability: a solution simple and fast to be mounted allows to obtain a higher score. Therefore, the assigned weighting factor is high.
- RAC: it was considered as a very important FOM, since it is directly related to the final score. The number of surfaces, their extension, and the weight of the required structures all affect this FOM. As a result, RAC was heavily weighted, even though not as high as the two above.
- Structure: it measures the difficulty of the process of sizing and building a tough and reliable fuselage-wing junction. We did not consider this parameter very critical, so it was given a low weighting factor.
- Stability: it quantifies the roll stability contribute; also in this case the weighting factor is low because we can correct the instability with other wing parameter (ie. dihedral, sweep...).
- Aerodynamics: indicates the aerodynamic efficiency of the wing-fuselage system. Once the wing span is fixed, a lower wing is more sensitive to interference between the boundary layers of wing and fuselage, and therefore requires greater attention in designing appropriated aerodynamic fairings. It was given a medium weighting factor because it affects cruise speed and mission time.
- Landing gear interface: provides a measure of the easiness in designing and building the main landing gear in the different cases. Our target was a configuration with the gear already mounted, and then the study of the interface system was quite important.

		WING CONFIGURATIONS		
FOMs	***Weighting Factors***	**High wing**	**Bi-wing**	**Low wing**
UNLOADING	0.25	5	1	2
MOUNTABILITY	0.25	5	2	5
RAC	0.20	5	2	4
AERODYNAMICS	0.10	5	2	3
LANDING GEAR	0.10	2	4	5
STRUCTURES	0.05	4	3	4
STABILITY	0.05	5	4	2
Tot	1	4.65	2.1	3.65

Table 3: wing configuration: weighted decision matrix

For the wing, the following solutions were considered:

- The mid-wing was discarded immediately due to the difficult solutions necessary, in designing and building the aircraft, to avoid interference between the carrying structures and the payload.
- The high-wing is the best solution for the unloading problem. It has good efficiency without fairings if compared to a low-wing. It also provides a positive contribution to the roll-stability. Finally it is easy to connect to the fuselage, but not with the gear system.
- The low-wing needs greater attention in designing the unloading system. Compared to the high-wing, it has a lower aerodynamic efficiency and a negative contribute to the roll-stability. These problems can be solved introducing supplementary devices (fairings, wing twist, ...) that have a negative effect on the RAC. The low wing can be easily coupled with the landing gear.

- The biplane-wing was also considered to celebrate the 100th anniversary of the first flight of the Wright brothers. It allowed obtaining a good aspect ratio with a short wing span, clearing more room (longitudinally) available in the box. Unfortunately, this solution is ruled out by high RAC, low aerodynamic efficiency, mounting and unloading difficulties.

Table 3 shows the decision matrix that led to the select in the high wing. Once a high-wing configuration was adopted, the problem of wing planform was addressed. The proper FOMs for this screening are:

- RAC: considering that the RAC depends from the wing span and the maximum chord, we felt important to find how the planform, keeping unchanged the area, affects this parameter. We gave to this parameter the highest weighting factor because it affects the final score more than the others.
- Drag: measures, at a fixed wing area and flight C_L, the aerodynamic drag produced by the wing. It has a double influence on the flight mission. Also, it affects the flight speed and, consequently, the mission time. Moreover, it affects the RAC through the battery consumption. For these reasons it has an high weighting factor.
- Construction: this parameter measures the difficulties related to the wing construction, from the point of view of the requested tools, the complexity and the time of assembling the parts. This is less important than the previous two.
- Stall behavior: this FOM measure how the different planforms affect the behavior of the aircraft in incipient stall conditions. The considered effects are the Cl spanwise distribution and the Reynolds's number at the wing tip. These considerations, very important from a theoretic point of view, were considered less important with respect to the problems introduced so far.

The considered planforms are:

- Elliptic wing: this is the best shape from the aerodynamic point of view because the induced drag is minimum. The RAC value is between rectangular and tapered wings and the wing has a quite good stall behavior. The main drawback is the higher complexity in realization.
- Rectangular wing: keeping unchanged the area, this solution presents the minimum RAC value. Moreover it can be built very easily leaving aside the building techniques used. However it has a poor efficiency from the aerodynamic point of view.
- Tapered wing: has a quite good aerodynamic efficiency, but lower than the elliptic wing. The building difficulties of this solution is intermediate between those of other two planforms but the RAC is higher. The stall behavior of this configuration is particularly critical. In fact, considering for example a taper ratio 1:3, which minimize the induced drag, the Reynolds number decreases from the root to the tip of the wing. Considering the typical sizes of our model, this would lead to a very low tip Re (about 70'000), with a negative effect on airfoil performances (for an elliptic wing this fact is less important because the part of wing with reduced chord has a far smaller surface). Another problem for the wing tip is due to the spanwise Cl distribution of the tapered wing, where Cl grows from the root to the tip. A negative twist angle would solve these problems realizing a good stall behavior. However, this would significantly increase the building complexity.

Table 4 shows the decision matrix that led us to select the rectangular planform.

		WING PLANFORM		
FOMs	***Weighting Factors***	**Elliptic**	**Rectangular**	**Tapered**
RAC	0.4	4	5	2
DRAG	0.3	5	3	4
CONSTRUCTION	0.2	1	5	3
STALL BEHAVIOR	0.1	4	5	2
Tot	1	3.7	4.4	2.8

Table 4: wing planform: weighted decision matrix

3.4.3 Fuselage configuration

The FOMs for the analysis of the fuselage configuration are:

- RAC: the fuselage configuration affects the RAC through the structural weight
- Aerodynamic efficiency: measure the global aerodynamic efficiency of the configuration.
- Lengthenability: this FOM evaluates the possibility of realizing a fuselage with an overall length greater than the box size, without compromising the assembly time.

		FUSELAGE SHAPE		
FOMs	***Weighting Factors***	**Axial sym.**	**Lifting**	**Pod-like**
EFFICIENCY	0.5	5	3	3
RAC	0.4	4	5	5
LENGTHENING	0.1	1	1	5
Tot	1	4.2	3.6	4

Table 5: fuselage shape: weighted decision matrix

In order to choose the fuselage configuration we required that total length is lower than the maximum box size. In this phase of the project we did not want to freeze the fuselage length yet, but this constraint makes easier the screening process. Once the length and the cross size of the fuselage (equal to the payload size) were grossly specified, there were few possibilities for fuselage shape. So the analyzed solutions were:

- Axial sym: the axial symmetric is the worst solution from the RAC viewpoint, because the larger volume leads to heavier structures. Nevertheless this solution has a good aerodynamic behavior, with a low drag.
- Lifting body: the lifting force produced by this configuration allows a reduced wing span, reducing the total structural weight. This leads to a lower RAC compared to the other configurations. During the cruise, which represents the larger part of the mission, this configuration has a higher drag; this affects both flight time and propulsive sub-system and therefore the RAC.
- Pod-like: this configuration has an axis symmetric section, carrying only payload and propulsive system; tail surfaces are connected to the fuselage by a boom. It has the advantage of using less material than the conventional axial symmetric solution, and then it is lighter, with a lower RAC. The aerodynamic efficiency is not very good, because the limited length of the fuselage does not

allow the realization of fairings in the aft region. On the other hand, this solution permit to build a fuselage the length of which is over the 4' limit. It is possible to build an extendable boom to achieve the required tail-fuselage distance.

Table 5 shows the decision matrix that led to the selection of the axial symmetric configuration.

3.4.4 Tail configuration

The FOMs considered for the analysis of the tail configurations were:

- RAC: the RAC directly affects the overall score, and so the weight of this FOM is high. The tail parameters that influence the RAC are the number of surfaces and the number of controls.
- Control moment: this parameter is strongly dependent on the tail configuration. It affects the take-off and cruise performance of the aircraft. It should ensure a high global value of Cl, a high control power at take-off, and low drag and good longitudinal stability during cruise. Control moment contribution to the final score was estimated less important than that of the RAC.
- Efficiency: an aerodynamically efficient tail produces a low drag, requiring less thrust for take-off and cruise, and making less critical the sizing of the propulsion system.
- Mountability: this FOM evaluates the time necessary to mount the tail once the box is open. In particular we gave the maximum score (5) to the configurations that can have the tail connected to the fuselage in the box. A weight equal to the RAC was assigned to this FOM because a fast and simple assembly was regarded as a key factor to earn a high score.

The considered alternatives are:

- H-tail: after the definition of the wing and fuselage configuration, similar considerations led us to introduce the H-tail like a potentially high-scoring solution. The box dimensions with the requirement of an easy assembly lead to a horizontal surface with no more than 2' span. It is also to be considered that the expected wing span should be less than 8' (twice the length of the box) and that the RAC rules states a limit to the size of the tail. On the other hand the maximum size of the box calls for a very short fuselage, so that the maximum distance of the tail from the center of gravity is somewhat limited. Furthermore, due to fuselage shape and wing position (high wing), the horizontal surface is expected to be in the wake flow, particularly at take-off, when the tail is more important. As a result a highly efficient horizontal surface is necessary. The H-tail solution, with the two fins acting like winglets, was a way to increase the effective aspect ratio of this surface, without a significant penalty on the RAC, particularly when the use of vertical control surfaces is ruled out. Also, this configuration can be stored in the box, already mounted on the fuselage. Note that a single vertical surface (cross-tail), fitting the box dimensions, that would be undersized.
- Conventional tail: this configuration has the advantage of a reduced RAC. However, as explained before, it would give an aircraft with lower performances, due to the low efficiency of the horizontal surface. We felt that a conventional tail already mounted (in the box) was less convenient because the fin would be undersized for the directional stability requirements.

- Cross-tail: compared to the conventional tail, this solution would solve the "accountancy" problem, allowing a double size of the vertical surface. As a disadvantage, with the same number of controls, the RAC would be higher.
- T-tail: the great advantage of this solution is to be immune from the wake effects of wing and fuselage. The efficiency is higher than the conventional tail, but lower than the H-tail. The RAC is similar to that of the conventional tail. However the mountability is penalized: for a really efficient T-tail, the vertical surface should be realized in two sections, to be assembled outside the box.
- V-tail: apart from the great advantage of optimizing the RAC, this solution has lower scores on the other FOMs. It has to be assembled outside the box, has a low aerodynamic efficiency since the equivalent horizontal surface would be undersized, giving insufficient longitudinal stability and control.

Table 6 shows the results of weighted decision matrix. The winning configuration is the H-tail.

		TAIL CONFIGURATIONS				
FOMs	***Weighting Factors***	**T**	**V**	**H**	**Conv.**	**Cross**
RAC	0.35	4	5	3	4	3
MOUNTABILITY	0.35	2	3	5	4	5
CONTROL MOMENT	0.15	5	2	5	2	2
EFFICIENCY	0.15	4	2	5	3	3
Tot	1	3.45	3.4	4.3	3.55	3.55

Table 6: tail configuration: weighted decision matrix

3.4.5 Motor and Propeller position

Excluding configurations with more than two motors because too complicated, we analyzed advantages and drawbacks of three alternatives:

- One motor with one battery pack: it has the advantage of a weight lower than the bi-motor configurations, and of being less penalized by the RAC. With the same number of cells this configuration has an intermediate shaft power, but has the advantage of allowing the mounting of nearby motor and batteries, which results in short supply cables.
- Two motors with one shared battery pack: it is the typical solution for a wing-mounted bi-motor and allows the highest power to be obtained, because the full voltage powers both motors. Yet, it has the great drawback of high energy loss due to the long supply cable connecting the centrally mounted battery pack with the far motors.
- Two motors, each with its own battery pack: this is the perfect solution for push-pull configuration; it has low power loss, but shows its limits in term of RAC and maximum available power.

For this selection we considered the following FOMs:

- RAC: this parameter is directly affected by the number of motors and by the weight of the battery; among the bi-motor configurations the one with two battery packs gives a little advantage.
- Power: measures the maximum available power, strictly connected with the take-off performances.

- Weight: is affected by the configuration; it has a small influence on RAC but it is also a very important parameter for the aircraft performances (take-off, mission time...).

Table 7 shows the results of weighted decision matrix. The winning motor configuration is 1M-1BP.

		MOTOR CONFIGURATIONS		
FOMs	***Weighting Factors***	**1 Motor 1 Battery Pack**	**2 Motors 2 Battery Packs**	**2 Motors 1 Battery Pack**
RAC	0.4	5	3	2
Energy loss	0.3	5	4	2
Power	0.2	4	3	5
Weight	0.1	4	3	3
Tot	1	4.7	3.3	2.7

Table 7: motor configuration: weighted decision matrix

Once the number of motors and battery packs was decided, we examined the relative positions of the three components of the propulsion system: motor, battery pack and propeller.

The related FOMs were:

- Center of gravity: it quantifies the possibility of balancing the aircraft. This is highly affected by the position of the propulsive system, because it has the heaviest components (motor, batteries). Furthermore, it would be better that motor and batteries were as near as possible, to avoid energy loss in too long cables.
- Rotation: this FOM measures the problems in the take-off rotation, critical for the pushing aft propeller.
- Propulsion efficiency: this FOM measures the thrust loss due to the interaction of the propeller flow with the surfaces in the wake. It is strongly affected by the relative position of propeller, fuselage, and wing. The propulsion efficiency has a double effect on the global score. An higher efficiency allows limiting the number of cells for the same range, reducing the RAC, and increasing the thrust of the same propulsion system, so that the flight time is shorter. Therefore, the weighting factor of this parameter is the highest considered.
- Structures: this FOM quantifies the structural difficulties of integrating the propulsion system with the aircraft fuselage. The effect of a weight increase was considered less important with respect to the other parameters.
- Energy loss: this FOM measures the loss of electric energy due to the length of the supply cables. The weight of this FOM is quite important.
- RAC: it is affected by the configuration propulsive efficiency (higher efficiency leads to fewer cells) and by the weight of the structures containing the different propulsive systems (motor housing, transmission shafts).
- The fore position of the motor-propeller system is poorly efficient, because the fuselage is in the propeller wake. Nevertheless, it is the configuration that best fits the design requirements.
- The aft position is the most efficient; but generates the issues of rotation at take-off and aircraft balancing. The latter problem can be solved by putting the batteries in a forward position, but this

would require long cables. The use of a long shaft, leaving motor and batteries in front, would cause greater structural complexity.

Table 8 shows that the wining configuration is the one with fore motor, propeller and batteries.

		PROPULSION CONFIGURATIONS		
FOMs	***Weighting Factors***	**Fore Motor Fore Propeller Fore Batteries**	**Aft Motor Aft Propeller Fore Batteries**	**Fore Motor Aft Propeller Fore Batteries**
EFFICIENCY	0.25	3	5	5
ROTATION	0.20	5	2	2
RAC	0.20	3	4	3
ENERGY LOSS	0.15	5	1	5
CENTER OF GRAVITY	0.10	5	3	4
STRUCTURES	0.10	5	4	1
Tot	1	4.1	3.3	3.5

Table 8: propulsion configuration: weighted decision matrix

3.4.6 Landing gear configuration

The study of the landing gear configuration considered four options, using the following FOMs:

- RAC: it takes into account the effect on the RAC of the structural weight and the number of servos, needed for the considered configuration. The weighting factor is the lowest, for the little effect of the landing gear configuration on the RAC.
- Aerodynamic efficiency: it measures how configuration affects the aircraft aerodynamic performances, in terms of additional drag. This FOM is very important, because it directly affects the aircraft range and speed and, therefore, the weighting factor is high.
- Unloading interference: it measures the difficulty of implementing the unloading system, in terms of volume and limitations of the mechanics of the cargo bay door. To this FOM the highest weighting factor was assigned.
- Reliability: this is an estimation of the landing gear reliability. It penalizes the retractable configurations, because a possible failure of the deploying system during the landing, would be fatal for the whole aircraft. For this reason this FOM has an high weighting factor.

Considered landing gear configurations are:

- The fixed fore tricycle configuration has the drawback of an additional drag during the cruise flight, penalizing the aerodynamic efficiency. It has an excellent reliability and offers several solutions for the unloading system.
- The fixed aft tricycle configuration has an aerodynamic drag and structural weight a little lower than the previous one, but presents great limitations for the unloading system solutions, due to the short distance from the ground. It is hardly possible to produce a ventral payload unloading.
- The retractable fore tricycle configuration, compared to the fixed one, improves the aerodynamic behavior. But it has a negative effect on the RAC, because of an additional servo and of higher weight. It could have reliability problems.

- The retractable aft tricycle configuration has the advantage of producing low additional aerodynamic drag, but is penalized in term of RAC, reliability and unloading interference.

Table 9 shows how the fixed fore tricycle configuration better meets the requests of the selected FOMs.

		LANDING GEAR CONFIGURATION			
FOMS	***Weighting Factor***	**Fixed Fore Tricycle**	**Retractable Fore Tricycle**	**Fixed Aft Tricycle**	**Retractable Aft Tricycle**
EFFICIENCY	0.30	2	5	3	5
CARGO	0.30	5	5	2	2
RELIABILITY	0.25	5	3	5	3
RAC	0.15	4	1	5	2
Tot	1	3.95	3.65	3.5	2.9

Table 9: landing gear configuration: weighted decision matrix

3.4.7 Structural Configuration

At this point the different building technologies to implement the main parts of the aircraft were analyzed: wing, fuselage, tail, and landing gear. The FOM used for each study were:

- RAC: it is affected by the weight of the structures, as a function of the used building technology.
- Cost: it measures the economical resources needed to realize the component with the selected building technology.
- Reparability: it measures how simple is to recover the strength of the damaged structure, in the shortest possible time.
- Know how: it measures the experience and the skill of the team to use the selected technologies.
- Technologies: it measures the availability of the tools required to implement the selected production technology (i.e. machines as lathes for the moulds, pressurized vat, vacuum bags, ...).
- Strength: it is an estimation of the strength to weight ratio.
- Unloading: it is a FOM for the fuselage, and measures the easiness of realize the unloading system (cargo bay door).
- Payload interference: it evaluates the landing gear interference with the payload release system.

The structural configuration technologies are:

- The traditional wooden structure with ribs and spars (frames and spars for the fuselage) is the cheapest and lightest, and requires simple technologies; however, it also requires a long and complicated building process and is very difficult to repair after an accident.
- The shell configuration has important advantages in terms of weight, strength, volume (and then frontal area) and has a maximum assembling easiness; but this configuration requires a good knowledge-base and expensive techniques.
- Skin + core configuration, i.e. a structure with a core of a light material (nomex, polystyrene, aerogel) covered with a composite skin (glass fiber, Kevlar, carbon). Compared with the shell structure, has a lower structural strength and required technologies and skills intermediate between the two preceding solutions.

- The sandwich box configuration, for the fuselage, has the advantages of the assemblability and reparability of the traditional configuration, coupled with the strength of the skin + core structure, from which also inheres the higher technological and building complexities.

		WING STRUCTURE		
FOMs	***Weighting Factors***	**Traditional**	**Shell**	**Composite skin + core**
KNOW HOW	0.25	4	2	5
TECHNOLOGIES	0.20	5	2	4
STRENGTH	0.20	3	4	5
REPARABILITY	0.15	1	2	4
RAC	0.10	5	1	3
COSTS	0.10	5	1	3
Tot	1	3.75	2.2	**4.25**

Table 10: wing structure: weighted decision matrix

		FUSELAGE STRUCTURES			
FOMs	***Weighting Factors***	**Traditional**	**Shell**	**Composite skin + core**	**Sandwich box**
KNOW HOW	0.20	4	2	5	5
TECHNOLOGIES	0.20	5	2	4	5
STRENGTH	0.20	3	5	4	4
RAC	0.15	4	1	3	4
UNLOADING	0.15	1	5	4	5
COST	0.10	5	1	3	4
Tot	1	3.65	2.8	3.95	**4.55**

Table 11: fuselage structure: weighted decision matrix

		LANDING GEAR STRUCTURES			
FOMs	**Weighting Factors**	**Aluminum bow**	**Aluminum single leg**	**Composite bow**	**Composite single leg**
STRENGTH	0.4	4	3	5	4
RAC	0.3	1	2	4	5
REPARABILITY	0.2	3	2	1	2
COST	0.1	5	4	1	2
Tot	1	3	2.6	3.5	**3.7**

Table 12: landing gear configuration: weighted decision matrix

		TAIL STRUCTURES		
FOMs	***Weighting Factors***	**Traditional**	**Shell**	**Composite skin + core**
KNOW HOW	0.25	4	2	5
TECHNOLOGIES	0.20	5	2	4
STRENGTH	0.20	3	4	5
REPARABILITY	0.15	1	2	4
RAC	0.10	5	1	3
COST	0.10	5	1	3
Tot	1	3.75	2.2	**4.25**

Table 13: tail structure: weighted decision matrix

Tables 10-11-12-13 show that a sandwich solution and a composite solution are required, respectively, for wing and fuselage structures, and for tail and landing gear structures.

3.5 FOMs Analysis Results

At the end of the conceptual study we found a high potential score configuration. The axial symmetric fuselage gives a reduced front area, and then a low shape drag. The high wing, gives a good behavior in term of stability with cross wind (the worst condition), and the interaction between wing and fuselage gives advantages during the take off run. The H-tail increases the horizontal surface efficiency; being the vertical surfaces both over and below the horizontal one, it causes a better behavior in spin recovery. The ventral unloading offers high reliability and an easy construction. The selected missions are the ones with the highest score coefficients.

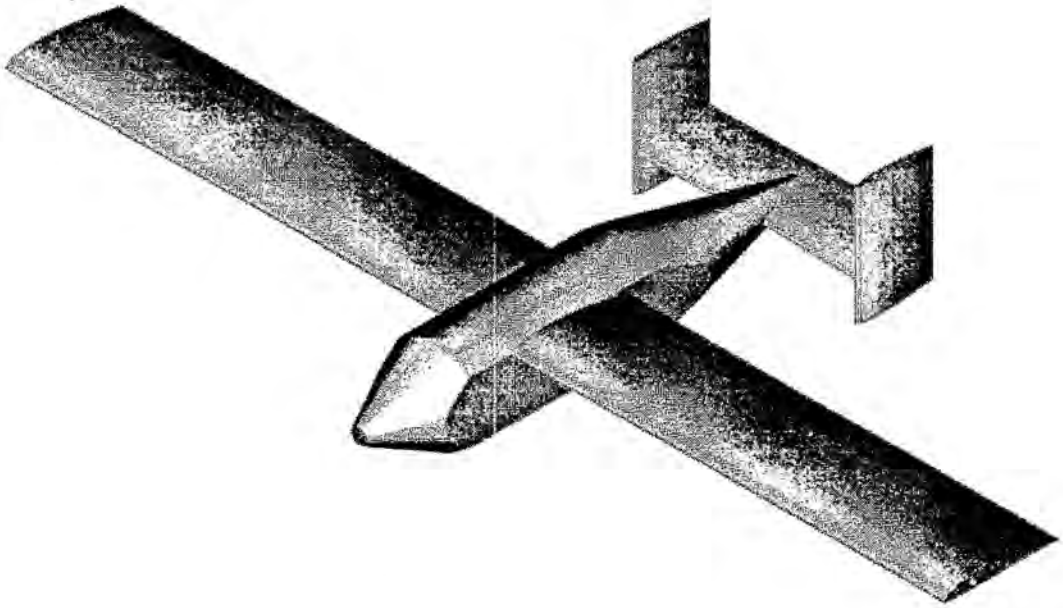

Figure 1: final concept

4 Preliminary Design

4.1 Introduction

At the end of the conceptual design phase, the concept configuration of our aircraft was stated, and the technological solutions necessary to realize the different subsystems were found. The adopted analysis methods had a statistic-qualitative character, and the actual aircraft performance was not accurately determined. The aim of the next study phase was the sizing of the main subsystems, so that their integration would give an aircraft able to gain the highest contest score. To this end, we needed to find out suitable criteria to deal with this problem. We needed to lay out an optimization method able to evaluate the global efficiency of the possible set of design parameters. It required analysis and calculation tools able to faithfully estimate the actual performances of the various subsystems, and how these affect the behavior of the whole aircraft. To reduce the problem complexity, due to the large number of variables, we proceeded with two level of study. The first goal was carry out sizing trade studies able to evaluate the influence of the various parameter sets on the overall score and to reduce the range of the design variables. Then, we executed fine trade studies in major design areas, refining the solutions pointed out by the first study phase. At the end of the preliminary design phase, the sizing of the main aircraft subsystems was done.

4.2 First Sizing Trade Studies

In the first phase of the sizing process, we implemented an optimization algorithm capable to evaluate the effects on the score of the various sets of the design variables investigated, and to give the optimum configuration as output, that is the one with the highest score. Yet, a computation with the design parameters varying in a discrete way gives results suffering from intrinsic limits (the iteration steps of each variable have a finite space, while the relative optimum could fall in one of the gaps). More, an algorithm dealing with a problem with a high number of variables, unavoidably introduces approximations and simplifying hypotheses. As a consequence, we decided not to take into account every factor, leaving the more detailed analyses, regarding the particular aircraft subsystems. For these reasons, the results given as output by the optimization program, were not considered as the unique and definitive solution for the configuration sizing problem. Instead they reduced the range or variation of the considered design parameters. In particular, each set of parameters, gaining a score within 15% of the maximum, was considered for the following fine trade studies.

4.2.1 Main assumptions

To formulate the optimization algorithm some simplifying hypotheses were introduced:

1. In the optimization algorithm we needed to know the aerodynamic parameters of the whole aircraft. For the sake of simplicity, we chose to link these parameters to the adopted airfoil: known the characteristics of an airfoil and the actual dimensions of a finite wing, is possible to find out the lift, the drag, and the pitch moment of the wing. In addition, we need to sum the contribution of the tail, the fuselage, the landing gear, and the antenna. These contributions can be considered as known parameters in agreement with the following assumptions:

- the geometry of the horizontal tail (span, chord, planform, and airfoil) was fixed because the most important effects on the performance of the whole aircraft are the reduction of the maximum take off C_L and the increase of the cruise C_D. These effects can be easily found from the wing geometry (chord and airfoil). In fact, chosen the airfoil, from the pitch balance, the angle of attack of the horizontal tail during take off and cruise can be found, and so we can evaluate which % of C_L and C_D must be added or subtracted to those developed by the wing. A more accurate study on the parameters of the horizontal tail (airfoil, chord, coupling angle, % of elevator, maximum elevator deflection) will be also conducted.
- We considered that the effect of vertical tail, fuselage, and landing gear was to increase the C_D with respect to wing and horizontal tail. During the conceptual design the fuselage shape and dimension were determined, together with maximum dimensions of the tail vertical surfaces and landing gear (mainly for the needs to fit in the box).

As a consequence, the variables for the aerodynamic design were reduced to the coefficients of the selected airfoil: Cl_{MAX}, Cm_{AC}, k e Cd_0. So we identified five families of low Reynolds airfoils (about 10e5). For each one of them, we considered only an airfoil, in order to represent the main characteristics of its family. The optimization process analyzed these airfoils and pointed out which one was the best. That meant to select for further studies the family it belonged to.

2. For the stability and handling qualities, we set the aerodynamic center of the wing (i.e. the 25% of the chord) about half an inch aft the center of gravity (c.g.). The latter, due to the mission with the payload deployment, was located in the middle of the cargo-bay, 0.42 m (16.5") from the aircraft nose. Therefore, the distance among c.g. and tail remained fixed, equal to about 0.63m (24.8").
3. An analytic relation between propulsive configuration and thrust was introduced in the optimization algorithm. We found this relation by extrapolating the data of maximum thrust, as a function of the number of cells and of the system motor/propeller/reduction-gear, obtained from a set of analyses performed with commercial software, MotoCalc. This software uses a database with the characteristics of several electric motors and other components and, for a set motor/cells/reduction/propeller gives useful data on:
    - Available thrust at various airspeeds.
    - Shaft power.
    - Voltages e currents.
    - Temperatures reached by the motor and the cells.

    The latter two data allow to exclude some options of propeller diameters or cells numbers, which lead to excessive temperatures or currents higher than the 40 A limit imposed by the rules. The results were filtered with the following criteria:
    - Current < 40 A
    - Power loss < 100 W
    - Discharge time > 5 min

A preliminary analysis allowed us to limit the possible motor-propeller-reduction configuration to 5 options, which gave the best results in term of shaft power, efficiency, and cell discharge time (table 1). For each configuration the T_{MAX} vs. #cells curve was found. Then, the parameters in the optimization process were the number of cells (8 to 24) and the motor/propeller/reduction set (out of 5 selected).

4. In the conceptual design phase a maximum take-off weight of 8 kg (17.6 lbs) was considered. We found that this value is slightly affected by the change of the design parameters, in particular by the wing surface and the number of cells: increasing the first, for the take-off requisites, the second decreases.

4.2.2 Known parameters:

Hence, as stated before, and by the conceptual design results, the following parameters are known:

- W gross take-off weight: 8 kg (17.6 lb)
- bw wing span 2.4 m (8 ft) (due to maximum box dimension)
- bt horizontal tail span: 60 cm (2 ft) (=25% bw)
- ct horizontal tail chord: 20 cm (8")
- μ friction coefficient: 0.05
- Cd fuselage + vertical tail + landing gear = 0.03 + 0.008 + 0.04 = 0.042
- Tail distance from the center of gravity = 0.63 m (25")
- Wing planform (selected in the conceptual)

4.2.3 Major Design Parameters

The variables considered in the optimization algorithm were reduced to the ones shown in table 4.1. For any of them, the table indicates the lower and upper limits of the considered range of variation.

		Range	
variable	**description**	**minimum**	**Maximum**
Sw	Wing surface	0.5 m^2 (5.4 sq ft)	1 m^2 (10.8 sq ft)
Ncell	Number of cells	8	24
"motor"	Motor-propeller-reduction set	ULTRA 920,930,1800,2000,3300; propeller: 18" to 23"; reduction set: compatibles.	
Vc	Cruise speed	15 m/s (49 ft/s)	30 m/s (98 ft/s)
Nv	Turn loading factor	1	2
"airfoil"	Clmax, Cm, k, Cd0	families: SD, FX, Eppler, NACA 4 digit , CH.	

Table 4.1: First Sizing Trade Studies: Major Design Parameters

4.2.4 Standard mission:

The standard mission introduces, among the possible flight missions, the most critical conditions from the energetic point of view. This standard mission consists in flying the course of mission A, always with the full payload and the antenna, without landing and deploying the payload. Therefore the mission phases are:

- take-off run; starts with the aircraft motionless and ends when the take-off speed, that is 1.1 times the stall speed, is reached;

- climb: from the end of the take-off, till an altitude of 30 m (about 100 ft); the analytic model used to describe this phase is the one for the maximum rate of climb at the maximum excess power;
- cruise: this phase sums up the 7 straight parts (about 7000 ft);
- turn: sums up the 2 turns at the pylons and the 360° turn in the downwind leg for each lap, in a total of 16 180° turns; the analytic model used is the one for the correct turn at the cruise speed; the loading factor is a variable;
- landing: a glide from the cruise altitude to ground and braking: from landing speed to zero.

4.2.5 Cost function:

For each set of design variables, the algorithm calculates the RAC and the time spent to perform the standard mission. The target function to be maximized by the optimization tool is:

Final Score = 100/ (Flight Time*RAC)

4.2.6 Analysis Methods

The "skeleton" of the optimization algorithm is described (figure 4.1) with a block diagram. This was implemented in the Optim program (written in Matlab 6.5), which carries out the computations sketched in the figure, varying input sets and selecting the one that provides the higher overall score. In the **OPTIM 5.4** final version, the program calls the following Matlab subroutines:

- **TAKEOFF**: from the thrust vs. speed law, it integrates the motion equation (from zero to the take-off speed) considering the aircraft aerodynamic characteristics, the weight, and the effect of the wheels-runway friction.
- **CLIMB**: finds analytically the fastest-climb speed, depending on the wing loading and the parameters of the polar curve for the whole aircraft, namely C_{D0} and K. It integrates the aircraft motion equation, from the take-off speed to the climb speed; finds out the time spent to reach this speed, and then the time to reach the cruise altitude of 30m (100 ft). The flight path angle is found analytically; so that it is possible to have in output the horizontal range flown.
- **CRUISE**: finds out the length of the path flown in this condition, subtracting from the sum of straight segments the horizontal length run in take-off and climb. From the cruise speed, it gives the elapsed time.
- **TURN**: uses a bonded turn model with constant speed (equal to the cruise speed). From the turn loading factor, it finds out the required thrust, C_L and the turn radius, and then the length flown, the time and the energetic expenditure.
- **LANDING**: it uses a descent model of glide with turned-off motor and at angle of attack for maximum efficiency. It integrates the motion equations from cruise altitude to ground in these conditions and finds out the residual horizontal speed. Then, the motion equations are integrated from this speed to zero speed, considering the braking action of the wheel friction on the runway and of the aerodynamic drag. It gives as output the distance run and the time for the descent and braking phases.

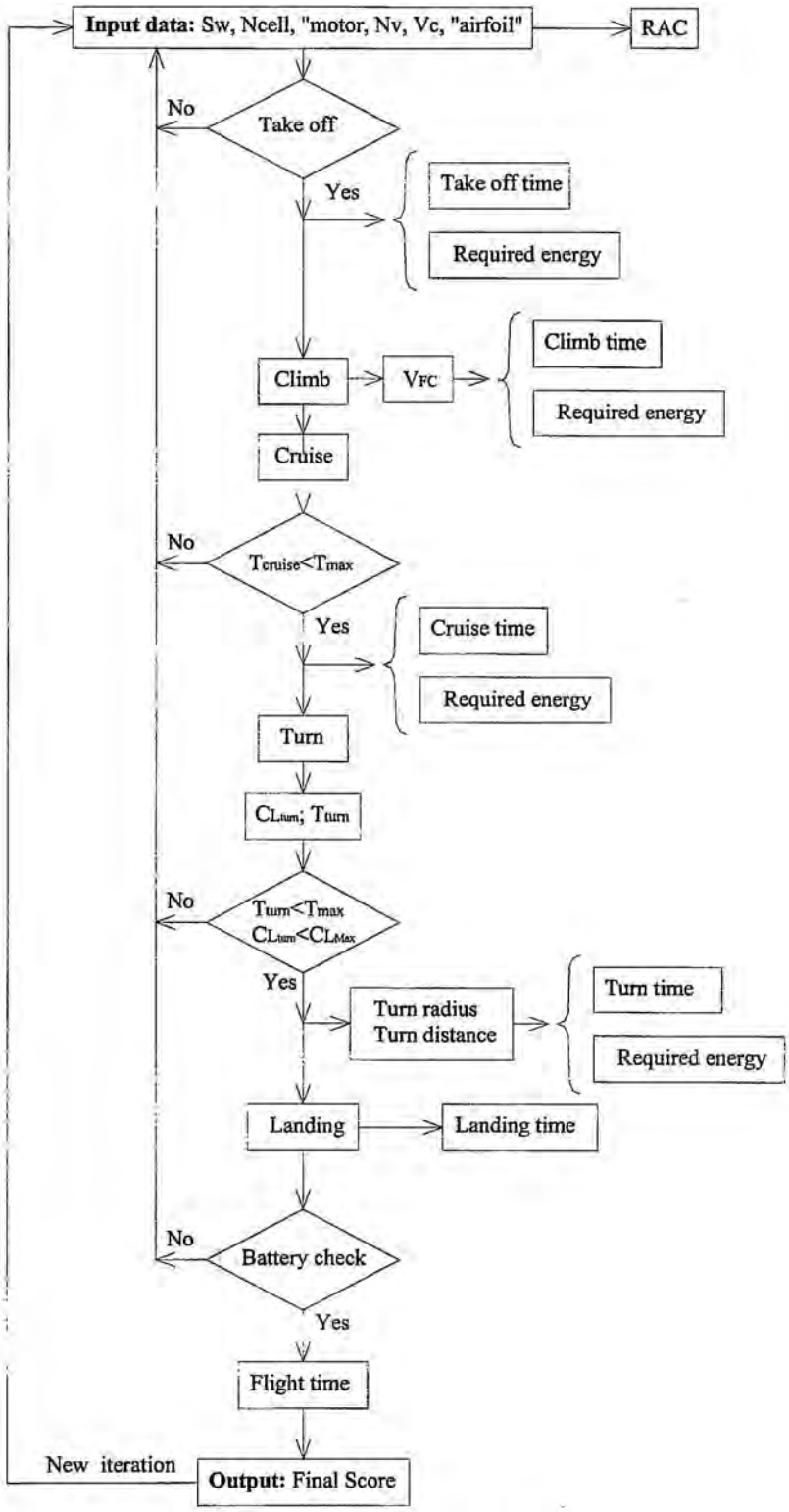

Figure 4.1: optimization algorithm

The OPTIM 5.4 executes as follows: it takes as input a set of design variables, from which the RAC is calculated. Therefore, considering the particular relation Maximum thrust vs. Speed of the selected propulsion system, the TAKEOFF subprogram is run. Then it performs a check on the lifting equation at the end of the runway. If the requirement is not satisfied, the execution stops and a new set of design variables is considered. Now the elapsed time and the energetic expenditure for take-off are calculated. Next, the CLIMB subprogram is executed, and the time and the energetic expenditure for this flight phase are found. From the cruise speed it is possible to find the cruise thrust. At this point the program checks if the cruise thrust is lower than the maximum thrust available for the adopted propulsion system. If the requirement is not satisfied, the execution stops and a new set of design variables is considered. Then the CRUISE subprogram is called. It takes as input the cruise speed and gives as output the time and the energetic expenditure. In the turn analysis a double check is performed: on the turn thrust, lower than the maximum one, and on the C_L, lower than C_{Lmax} (to be sure than the aircraft does not stall during this maneuver). The TURN subprogram works like the preceding ones, computing turn time and energetic expenditure. Next, the LANDING subprogram is executed, giving the same data as output. Now it is possible to perform the "battery check", to verify that the mission energetic demand is lower than the battery configuration supply. Finally, in this case the total flight time and the Final Score are calculated.

4.2.7 Analysis Results

The results of the program, when the final score is within 15% of the maximum overall score, indicate, for each design parameter, the following range:

Sw:	from 0.66 to 0.75 m^2 (7.1 – 8.1 ft^2)
Tmax:	from 26 to 30 N (5.8 – 6.7 lbf);
Cells:	from 11 to 17;
Motor:	Ultra 930-8 12V, Ultra 1800-3 10V, Ultra 3300 -3 10 V.
Propeller:	19" to 21";
Airfoil:	SD family;
Vc:	from 20 to 25 m/s (65 – 82 ft/s);
nv:	from 1,4 to 1,7;
Vto:	from 12 to 15 m/s (39 – 49 ft/s);

4.3 Fine Trade Studies and design Optimisation

4.3.1 Aerodynamic Considerations

The airfoil more advantageous in term of overall score belongs to the "SD" family; now there is the problem of choosing the exact airfoil to be used on the aircraft. Out of the nine airfoils analyzed from this family, we disregarded those with a very low Cm_{ac}, because the double camber on the upper surface makes too hard to build the wing with sufficient accuracy. We also discarded the laminar ones, because the cusp on the trailing edge causes the same building problems. The other six airfoils are very simple to produce (no sharp trailing edge, no high camper or cusp), and don't have moment coefficient too high (no more than –0.1), condition that our OPTIM 5.4 shows to be particularly penalizing. At this point we

compared the polar and C_l curves. Once wing surface and geometry, weight and flight speed (and then the whole aircraft C_L) are defined, the cruise C_l of the airfoil is determined. Comparing the polar for various family SD airfoils, we found out that the difference in the C_d at C_l near the cruise value is quite small, also considering the trim drag. By focusing on the curves with the higher maximum C_l (always taking into account the trim loss), in its two versions, "S" and "D" we concluded that the SD 7032 airfoil has superior characteristics. Among these, we selected the "D" variant, for the higher maximum C_l (but only some %) and for the smoother stall. The wing dimensions, allowing us to take-off safely and with an high cruise efficiency, are 240 cm (8 feet) in span (as previously fixed) by a chord of 30 cm (about 1 foot). A NACA 0012 airfoil was used for the tail, because the high H tail efficiency does not make necessary a cambered airfoil, more difficult to build and with a worse behaviour when the camber is changed by the deflection of a control surface. The most efficient tail, for the requested control moments, has a span of 60 cm (2 feet) (25% of the main wing span) and 20 cm (8") chord. The aerodynamic characteristics were found with software, developed by us in Excel which, from the aircraft geometry, generates the curves of lift, drag, efficiency and the polar for the single components and for the whole aircraft, considering the interference between the parts regarding the wakes and the induced speeds. To deal with the stall, the program finds the spanwise lift distribution using the Shrenk method. It considers only the linear part of the lift curve, and the related polar, using experimental data to update the curves and foresee the behavior of the non-linear parts.

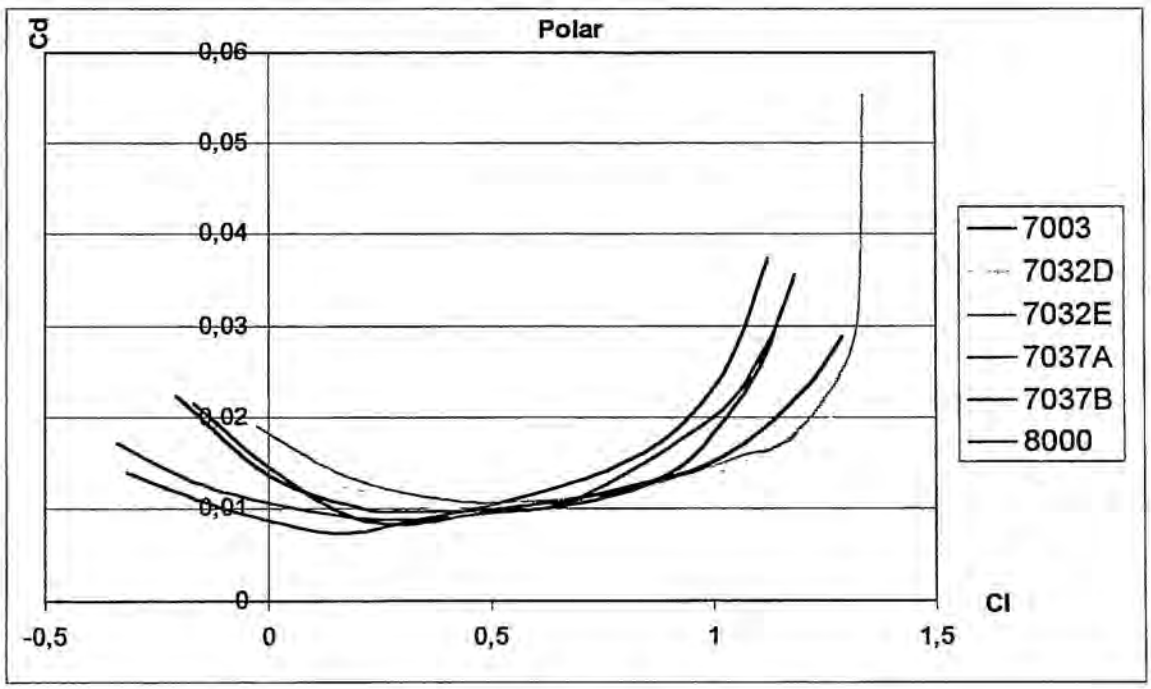

Fig

Figure 4.2: SD family polars

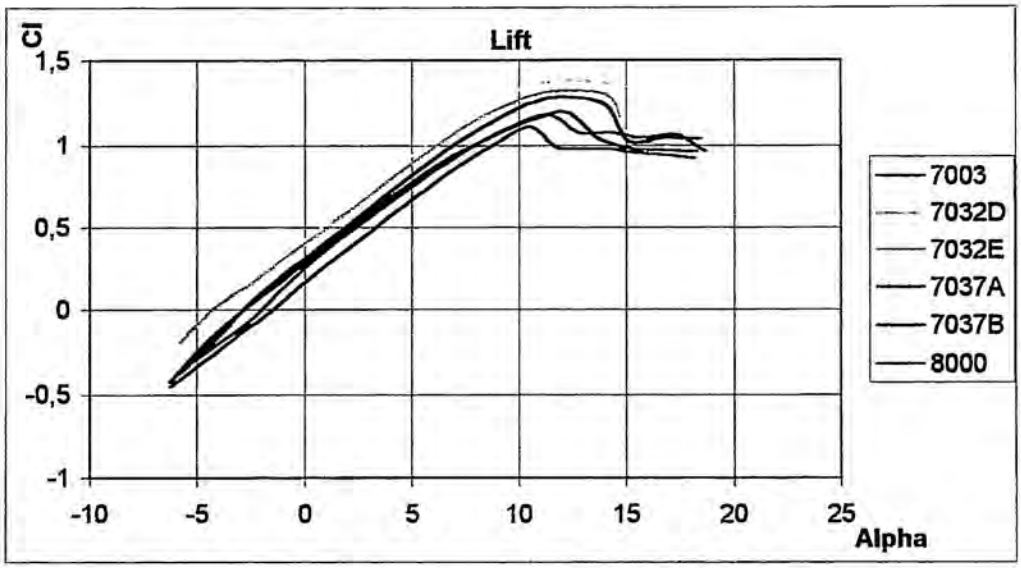

Figure 4.3: SD family lift

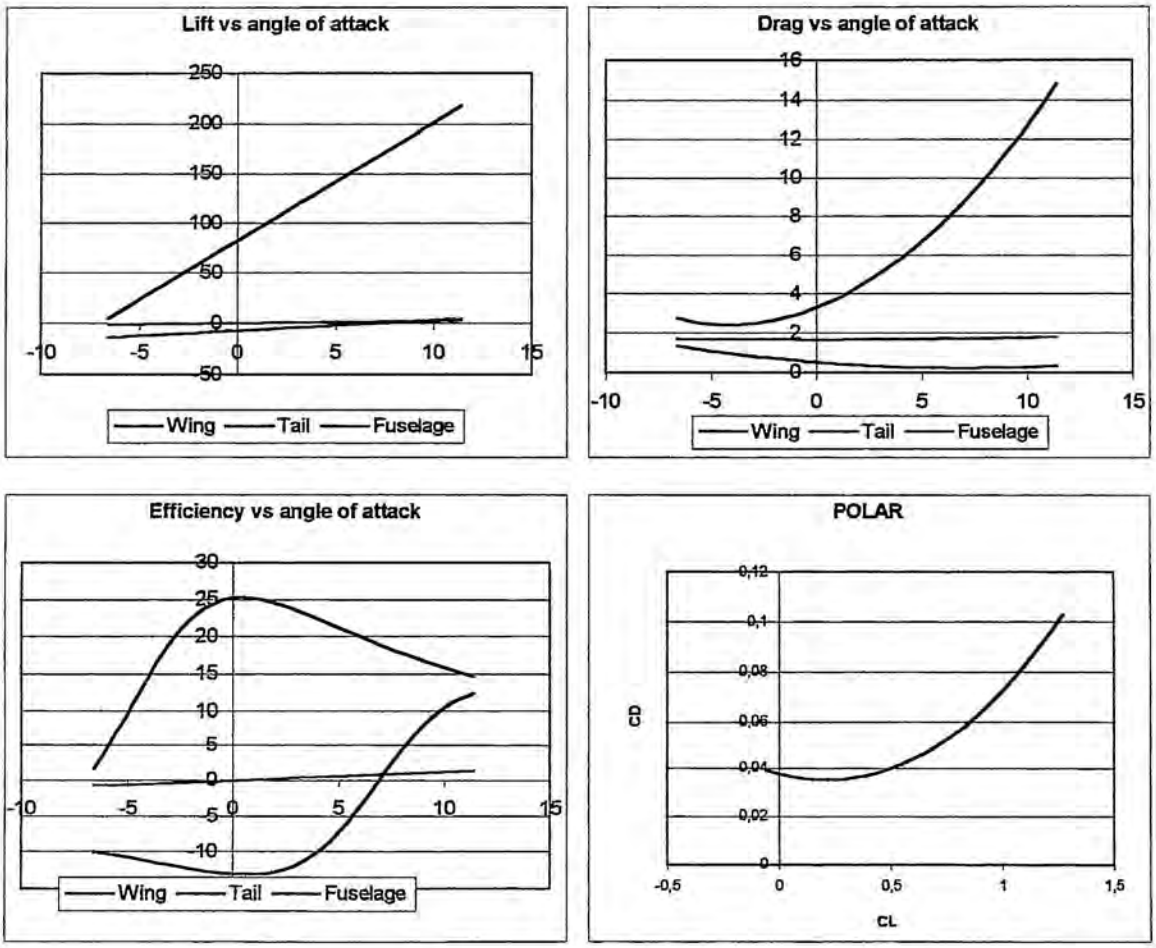

Figure 4.4: Whole aircraft

The angle of attack of the fuselage was used as reference. As a result, the cruise is at 0° angle of attack, with the minimum of the fuselage drag. From the efficiency curves it can be seen that, for the design angle of attack, the efficiency of each aircraft component is very near to the maximum, (minimum for the tail because with negative lift) which is proof of a good design. For the choice of the fuselage shape, stated the axis-symmetric shape, which minimizes the form-drag, we looked for the best trade-off between shape and cross-section, but we did not trust completely in the results, being impossible to model the rotating flow induced by the propeller. Then we postponed to a following phase the final choice.

4.3.2 Propulsion Analysis

The optimisation program OPTIM 5.4 shows that we need a thrust of 26-30 N at zero speed. Suitable motors are the three Graupner models: Ultra 930-8 12V, Ultra 1800-3 10V and Ultra 3300 -3 10 V. These models have low values of both the torque constant, Kt, and the speed constant, Kv. At this point we tried to use these motors without a reduction, (changing only diameter and pitch of the propeller) to limit weight and cost; but the simulations with the program "Motocalc" and the Matlab code "Motor1_testprop", gave us non acceptable results: it is necessary to use a reduction. Among the models fitting the Ultra series, we choose the HP 3.7:1. Each motor was considered working at zero speed and full throttle. We considered number of cells from 11 to 17, and the coupling motor-reduction-propeller, with propellers form 18" to 23" of diameter. For each value of the number of cells we found the performances (thrust, input power, RPM etc) and the propeller diameter giving the highest global efficiency.

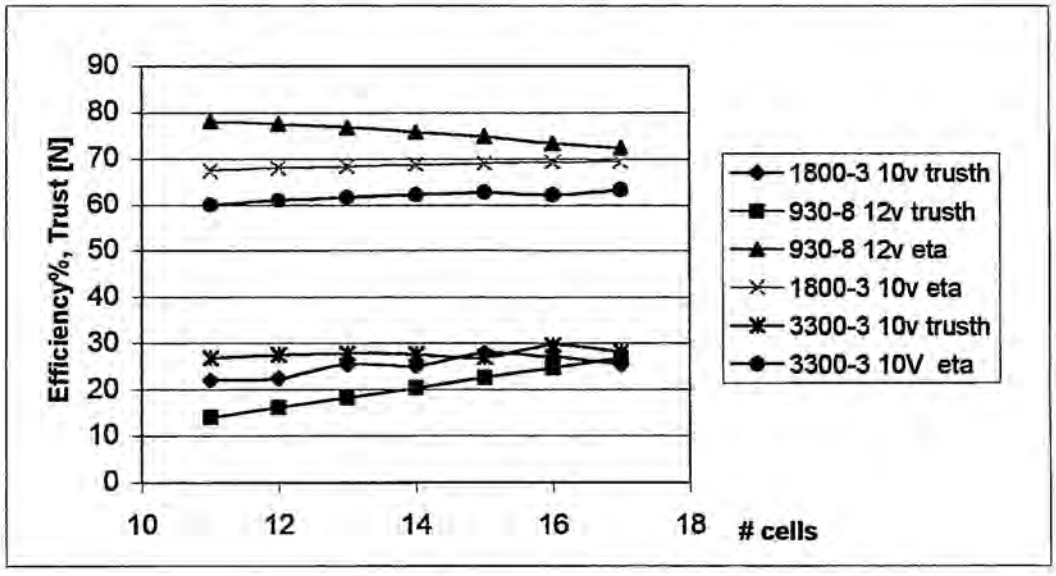

Figure 4.5: motors comparison

It can be seen from figure 5 that the 930-8 has the highest efficiency, but the lowest thrust. On the other side, for some cells numbers, this motor can produce the same thrust, with higher efficiency values. From these studies the best set is Ultra 930-8 12V, HP 3.7:1 reduction, 20" x 10" propeller, 17 cells; this configuration allows the generation of a zero speed thrust equivalent to 28 N (6.3 lbf).

4.3.3 *Performances & Flight mechanics*

Steady level flight: The first considered condition was the steady level flight at an altitude of 30 m (about 100 ft). From the aerodynamic analysis we knew the polar of the complete aircraft, and from the propulsive analysis the thrust as a function of the flight speed. Then, considering the balance of forces and pitch moment, we found out a cruise speed for the full payload case (with a total weight near 8 kg, 17.6 lb) of 20 m/s (65 ft/s). For this condition we studied the fixed command longitudinal static stability. For zero elevator deflection and angle of attack, we found the pitch coefficient of the whole aircraft, given the static margin and the tail distance, and considering the wing, tail and fuselage contributes, and the downwash effect on the tail. With an iterative method we found coupling angles of wing and tail that would make the aircraft stable, i.e. with $Cm_0>0$ and $Cm_\alpha<0$. It results: $i_w = 2.2°$; $i_t = -2.5°$.

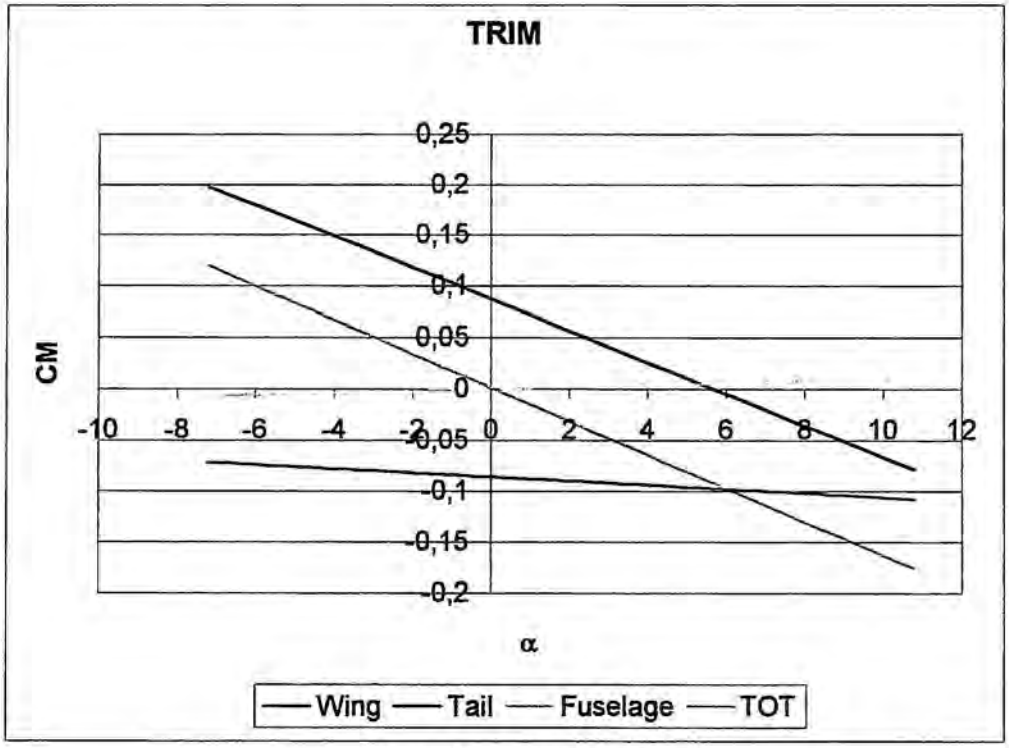

Figure 4.6: trim analysis

Thrust and Power: From the propulsive analysis we obtained the maximum shaft power, the available power and the thrust as functions of the flight speed. The required power and thrust were easily found form the aerodynamic parameters. The graphical analysis of the power shows the excess power at different flight speeds: at the higher speed flown for the largest part of the mission and at the lower ones, which represent the speeds of second regime. The required power curves were determined for the maximum aircraft weight, with payload and antenna, and for the unloaded aircraft, and are put into evidence the stall speed for both the conditions. Indeed, the stall speed deeply affects the take-off and climb phases analysed in the following points. The other characteristic speeds were also calculated too, and they will be utilised further during the mission analysis. The stall speed is $V_S = 11.5$ m/s (38 ft/s) at full

load and 10m/s (33 ft/s) empty. The minimum required power speed coincides with horizontal tangent to the curve and is equal to V_π = 12 m/s (39 ft/s); the maximum efficiency speed, which can be found tracing the tangent curve from the origin of the axes, is V_E = 17 m/s (56 ft/s).

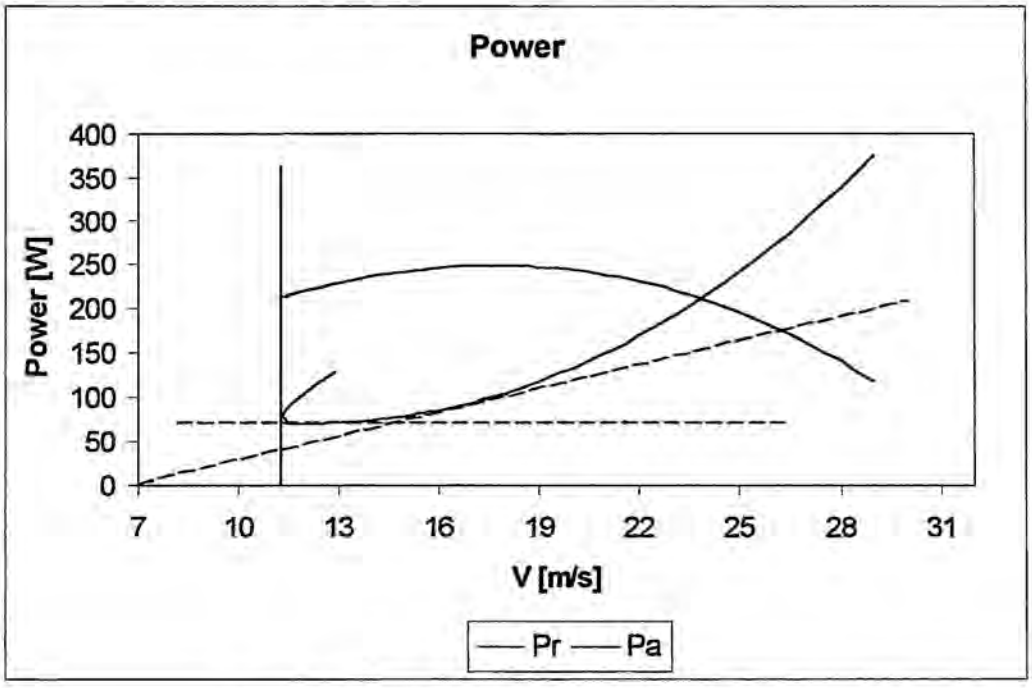

Figure 7: power analysis of loaded configuration

Take-off analysis: the take-off analysis in the optimisation algorithm indicated the take-off speed range: Vto=12-15 m/s (39-49 ft/s). In the previous point we determined the stall speed, setting Vto=1.1 V_S, we had Vto_{load}=12.65 m/s (41 ft/s), Vto_{empty} = 11 m/s (36 ft/s). Then, it was possible to calculate the take-off distance in the two conditions: loaded and empty weight. It is:

- T/W_l = 0.36; T/W_e =0.52; the thrust to weight ratio, with the take-off thrust equal to the maximum;
- W_l/S: =109 N/m^2 (2.28 lbf/ft^2); W_e/S = 69.55 N/m^2(1.45 lbf/ft^2); the wing loading;

from the force balance we calculated the acceleration during the run from zero to take-off speed, which is function of the two above parameters and of the aerodynamic data. Then we calculated the take-off distance integrating from zero to the take-off speed, as shown:

$$S_G = \frac{1}{2g}\int_0^{V_{TP}} \frac{d(V^2)}{K_T + K_A V^2} \quad ; \quad \text{where } K_T = \left(\frac{T}{W}\right) - \mu ; \; K_A = \frac{\rho}{2(W/S)}\left(\mu C_L - C_{D0} - K C_L^{\,2}\right)$$

The aerodynamic coefficients were taken at the ground angle of attack, measured with respect to the zero lift angle. These are the obtained distances:

S_{Gl} = 27.57 m (90 ft) ; S_{Ge}= 12.53 m (41 ft).

Climb: for a constant speed climb, it is possible to follow a graphical approach, considering that the rate of

climb (RC), i.e. the vertical speed, is $RC = V\sin\gamma = \frac{\Pi_a - \Pi_r}{W}$. From the previous analyses, we knew the powers as function of the speed and for the weight in two loading conditions: empty and full load. Then, it is simple to compute the RCs, for both conditions, as function of the flight speed, and the maximum RC, corresponding to the maximum excess power flight speed. Then, we can find the fastest climb speed and the flight path angle. The obtained values are:

$RCmax_{empty}$ = 7.217 m/s (23.7 ft/s); $RCmax_{load}$= 4.456 m/s (14.7 ft/s);

Vfc_{empty} = 13 m/s (42.7 ft/s); Vfc_{load} = 15 m/s (49.2 ft/2);

γ_e = 33.72° γ_l=17.28°.

In both the considered conditions, the fastest climb speed is higher than the stall speed. It is then possible to perform the climb with the maximum excess power. For this condition we easily found out the thrust to weight ratio, from the level flight efficiency and the flight path angle:

$T/W_e=(1/(L/D)e)+\sin\gamma_e$= 0.672; $T/W_l=(1/(L/D)g)+\sin\gamma_l$ = 0.385;

On the other hand, it is impossible to perform the climb at the steepest climb speed, i.e. at the maximum flight path angle, because it is lower than the stall speed.

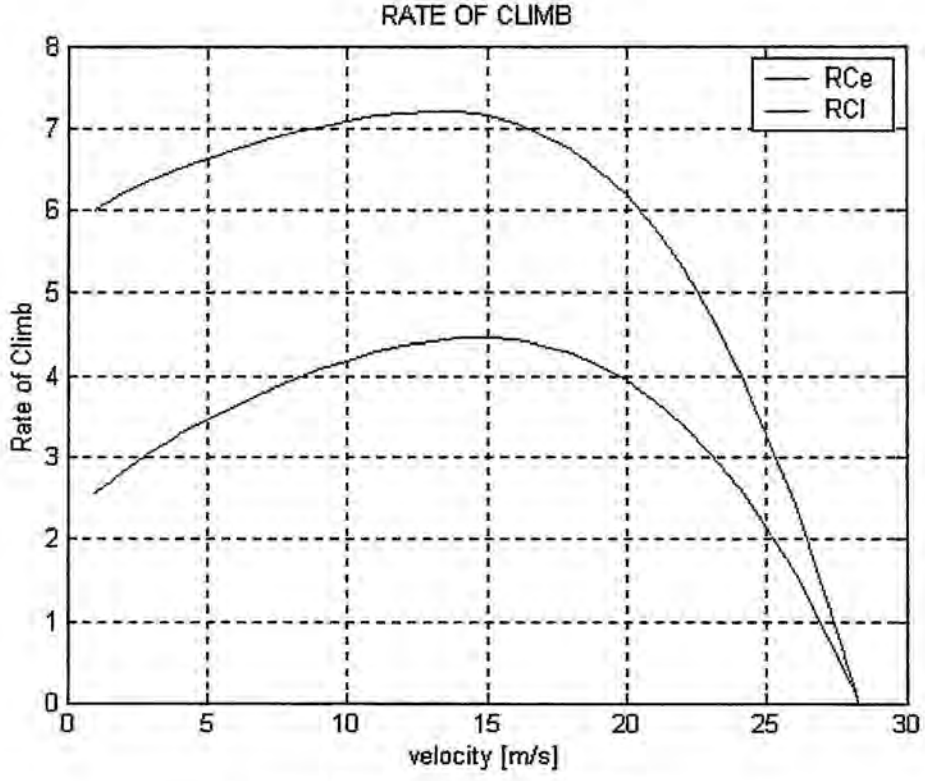

Figure 4.8: rate of Climb vs. flight speed

Level turning flight: we decided to perform the turn at the maximum efficiency speed, which is near to the cruise speed, as shown in the aerodynamic analysis. We calculated the loading factor, and then the bank

angle ϕ and the turn radius rt. These are the results for the two configurations, empty and loaded:

nv_e= 1.53;	nv_l= 1.34;
Rt_e= 19.73m (64.7 ft);	Rt_l= 33m (110 ft);
ϕ_e= 49.32°.	ϕ_g= 41.83°

Gliding flight: this flight condition was considered because the landing is carried out without thrust, to optimise the cell consumption and/or in the case of a propulsion system failure. The basic parameters we need to know are: the (negative) flight path angle γg, which, from the force balance with zero thrust, has the trigonometric tangent equal to the inverse of the efficiency, and the glide speed Vg. These parameters were determined in the case of a glide from the altitude of 10 m (33 ft), when the aircraft exits from the last turn. The results are:

γg_l = 5.05°;	γg_e = 6.6°;
Vg_l= 20.31 m/s (66 ft/s);	Vg_e = 24.83 m/s (82 ft/s);
time=5.6 s	time= 3.52 s

Analysis of the two missions: in this analysis the mission time as function of the energetic consumption is determined for A and B.

- Mission A: the weight remains constant and equal to the maximum (payload + antenna), the aircraft performs four laps, with a 360° turn on each downwind leg, one take-off and one landing.
- Mission B: there are two different phases: in each one the aircraft has a different weight (payload + antenna and only antenna) and performs 2 laps, with a 360° turn on each downwind leg, one take-off and one landing.

In splitting the course into sections, we took into account the short part of cruise the aircraft flies after the climb and before the pylon turn. This section is the *semi-cruise*, in dark green.

	MISSION A		MISSION B			
FLIGHT SEGMENT	# Segments	Time	# Segments		Time	
			Loaded	Empty	Loaded	Empty
Take-off run	1	4.6	1	1	4.6	2.5
Climb	1	7.7	1	1	7.3	5.4
Cruise	7	15.2	3	3	15	14.5
Semi-cruise	1	0.9	1	1	0.9	1
Turn	8	6.3	4	4	5.5	4.1
360°	4	12.5	2	2	11	8.2
Descent	1	5.6	1	1	5.6	3.5
Brake	1	6	1	1	6	8
Mission time	**231.6**		**210.1**			

Table 4.2: mission analysis

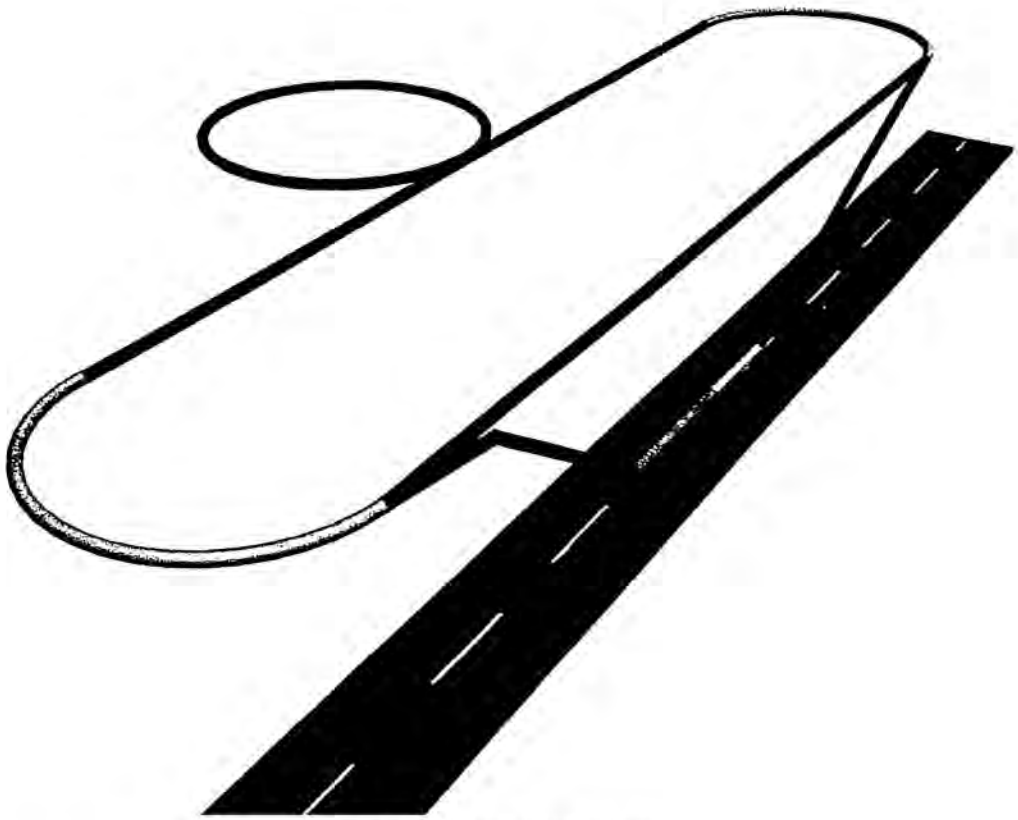

Figure 4.9: flight path segments

4.3.4 Structural Analysis

The structural design group investigated all the main components of the vehicle: wing, fuselage, tail and landing gear. We performed an analytical study followed by a numeric validation of the obtained results. The numerical analysis was developed using the MSC Nastran software and it reached a growing reliability, year by year, thank to accurate tests on mechanical property of the utilized composite materials.

Wing structural analysis

Designing the wing means to identify the critical operating conditions: structural test verification the aircraft will sustain corresponds approximately to a load factor of 2.5. The load diagram of our UAV predicts a maximum load factor equals to 2. The most critical condition for a wing is gust load. Considering such situation we designed the wing to resist a load factor equal to 3.6. We modelled the half wing as a cantilever beam, fixed to the root and loaded with elliptic lift and constant drag and momentum. Thanks to previous years experiences, the lightest and the most suitable choice appeared to integrate a single sandwich spar (polystyrene core + composite caps) in the maximum airfoil thickness. It will sustain the whole bending moment of the wing. Bending stresses versus spar caps thickness along the half wing span led us to laminate the spar caps with

two ply of the carbon ribbon for a total thickness of 0.5 mm (0.02")(figure 4.10). It is sufficient to resist to the maximum stresses (230 MPa) on the root section. Twist analysis verified that a single ply of glass fiber 0.25 mm thick (0.01"), weighting 80 g/m^2, is generously resistant. The half wing critic element is the cylindrical tube joining the fuselage. We were not able to find or built carbon tubes with the correct diameter and thickness, so we looked for commercial glass fiber tube with a diameter of 25 mm and a thickness of 3 mm. They suited our strength request but they were too much heavy. A lime wood pole with a diameter of 25 mm provided the necessary strength with a lesser weight, so that we decided to use it unless we will find a correct composite tube. The pole runs into the core of the half wing for 39 cm, from the root balsa rib to the inner balsa rib, both 10 mm thick. It extends itself out of the root rib for 85 mm to join with the fuselage. A finite element (FE) analysis confirmed our analytical results; figure 13 shows the half wing deformation under structural test load conditions.

Fuselage structural analysis loaded

The fuselage is basically made up of 5 composites plates (nomex honeycomb + carbon skins); it must bear the load sent by the half-wings, the tail planes and the landing gear, coupled to it with cylindrical connectors (wing and tail) or directly laminated on it (gear). The sandwich thickness was analytically determined for the most loaded plates, i.e. the lateral ones where are connected the half-wing. Were available nomex core of two different thicknesses, 6 mm and 8 mm (0.24" and 0.32"), while for the skins we used one layer of carbon fabric weighting 100g/m^2. Then a whole fuselage FE model was developed to check the analytic study and, above all, the shear strength of the glued zones of the landing gear legs.The primary structure has been modeled with different properties laminate elements, dividing it in the following three parts: a front portion, putting up the motor-battery group; a middle portion, putting up the payload; a tail-cone rear portion, connecting to tail surface. Both of the front and rear portions have been realized in carbon fiber reinforced plastic (CFRP) laminate, instead of the middle portion is sandwich, Nomex-CFRP made. The connections between fuselage and tail and between fuselage and motor-case have been simulated using DOF spring elements with fitted stiffness. The resultant model consists of 2262 elements and 1845 knots. Two load conditions were considered: first, the static load acting on the fuselage when the aircraft is on the ground; in this case the fuselage has been considered fixed to the landing gear constrains. Second, the aerodynamics loads in the worst flight condition; in this case the fuselage has been considered pinned to joint of the wing. The considered loads are:

- the propellers reaction couple;
- the loads (forces and moments) transmitted from the tail;
- the loads (forces and moments) transferred from the wings;
- the motor-group weight;
- the body accelerations due to the worst flight condition.

The result of the static analysis showed the most stressed elements and permitted to size them suitably. Figure 4.10 shows maximum stresses of the laminate. The 8 mm core was elected as the most satisfying for the required strength in the wing connector area. The overall sandwich thickness is 8.6 mm (0.34").

Tail structural analysis

The tail H configuration was thought as a single structural element, mounted on the fuselage by the carbon boom, to which the horizontal tail spars, also made of carbon, are linked. The boom sizing was performed on the basis of the maximum bending stress, transmitted by the tail during the maneuvers; a 40 mm (1.6") diameter pipe, 1 mm (0.04") thick, made of carbon fiber, and with a button lock system, was elected as the optimum solution; the maximum stress it has to bear is a little higher than 50 Mpa (7'250 psi) (See figure 4.11). For the horizontal tail plane, two 8 mm (0.32") diameter, 1 mm (0.04") thick carbon spars were chosen. This solution was preferred to the single-spar one, for the small airfoil thickness (t_{max} = 20 mm, 0.79"). The two spars are located the first at the maximum thickness and the second 8 cm (3.15") aft of it. The vertical planes are linked directly to the two horizontal plane spars by two other identical spars. The maximum bending stress is lower than 200 MPa (29'000 psi). (See figure 4.12).

Landing gear structural analysis

The landing gear was sized on the basis of the maximum bending and shearing stresses generated during the landing phase. It was modeled as a beam with a kwon initial warp, fixed on the lateral fuselage plate for 8 cm (3.15") of its length. The need that the aircraft fits partially mounted in the box, pones a one-foot-limit to the wheel distance. This leads to a low warp, and then to poor flexibility, useful to absorb the impact energy by bending deformations; on the other hand, the legs are mainly loaded axially, and then arise the buckling problem. Therefore, an analytic study was performed to investigate the buckling behavior of the landing gear structure. The results of this study, suggested us to laminate 10 layers of Carbon+Kevlar fabric + 2 layers of unidirectional CFRP. A numerical FE analysis verified this decision. The structure has been simulated with120 elements and 150 nodes FEM model. The Hoffman fracture criterion has been used because of non isotropic material property in 1 and 2 principal directions. In order to simulate the ground impact condition, the connection between the landing gear and the wheel has not been considered infinitely rigid, DOF spring elements with appropriate stiffness but have been used. The load conditions considered in the landing gear sizing, are referred to a landing at a vertical speed of 2 m/s (6.6 ft/s), widely in the range of vertical speed found for the gliding flight phase. The maximum stress, produced in the external carbon layers are nearly 100 Mpa (14'500 psi), while the max failure index is abundantly under 0.06 value. (See figure 4.15).

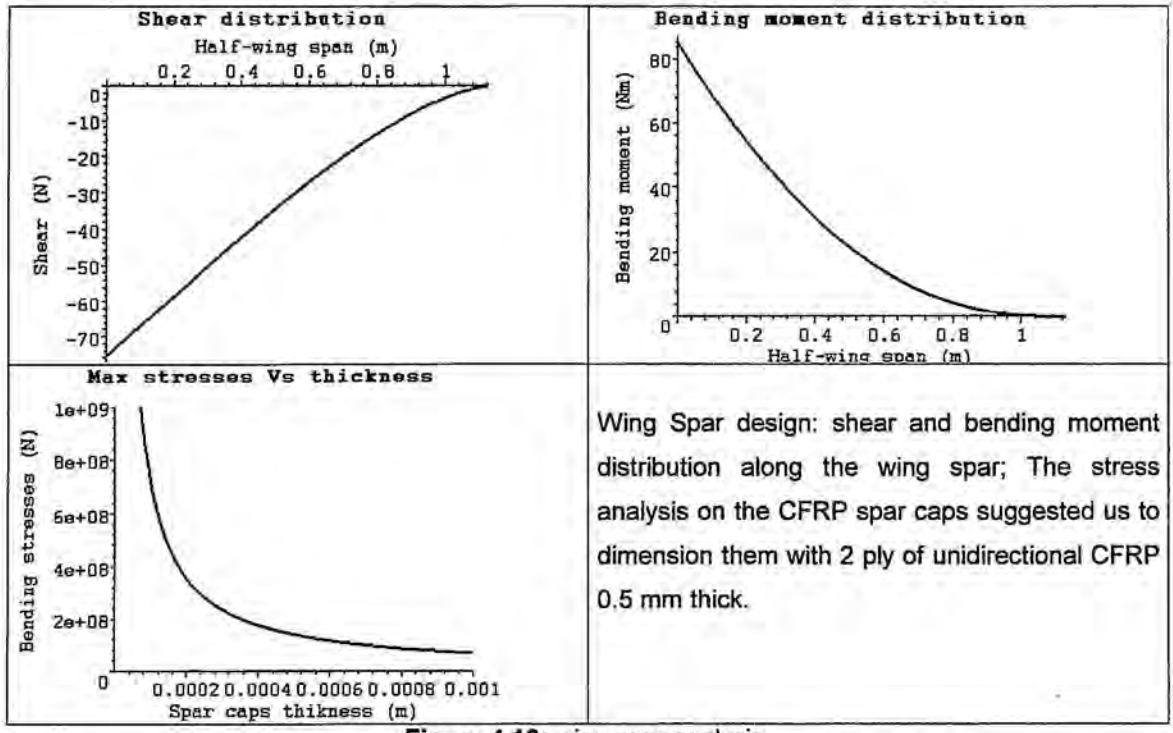

Wing Spar design: shear and bending moment distribution along the wing spar; The stress analysis on the CFRP spar caps suggested us to dimension them with 2 ply of unidirectional CFRP 0.5 mm thick.

Figure 4.10: wing spar analysis.

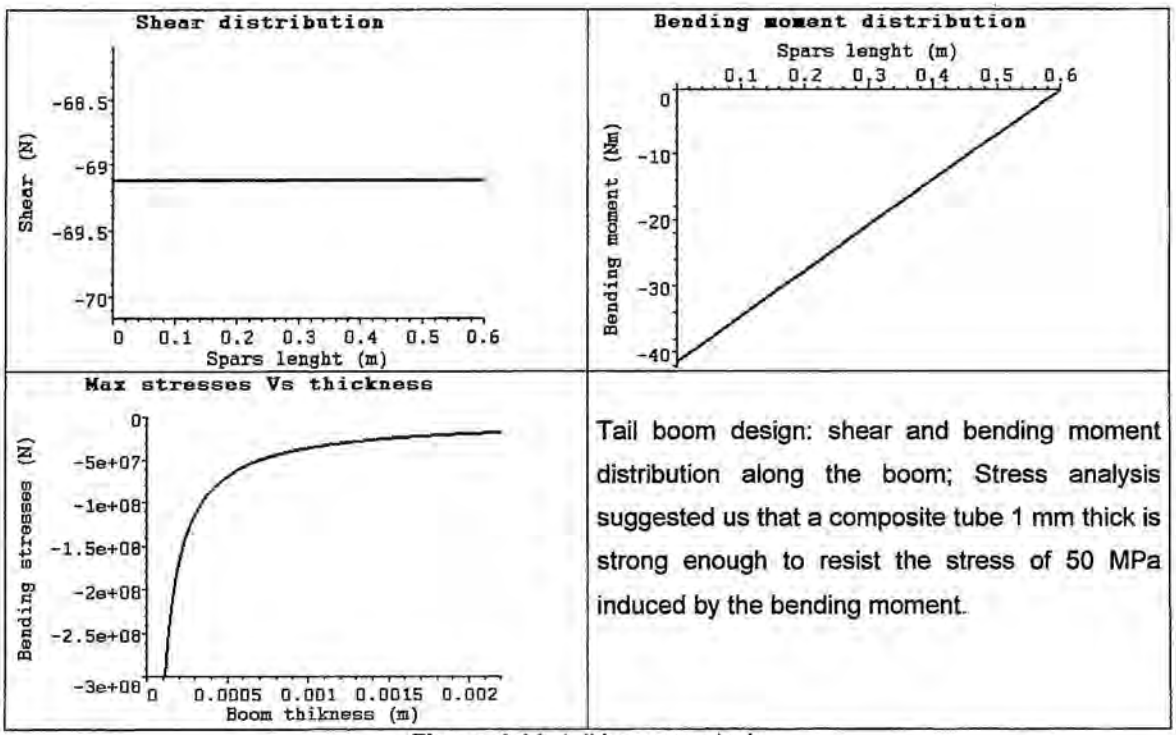

Tail boom design: shear and bending moment distribution along the boom; Stress analysis suggested us that a composite tube 1 mm thick is strong enough to resist the stress of 50 MPa induced by the bending moment.

Figure 4.11: tail boom analysis

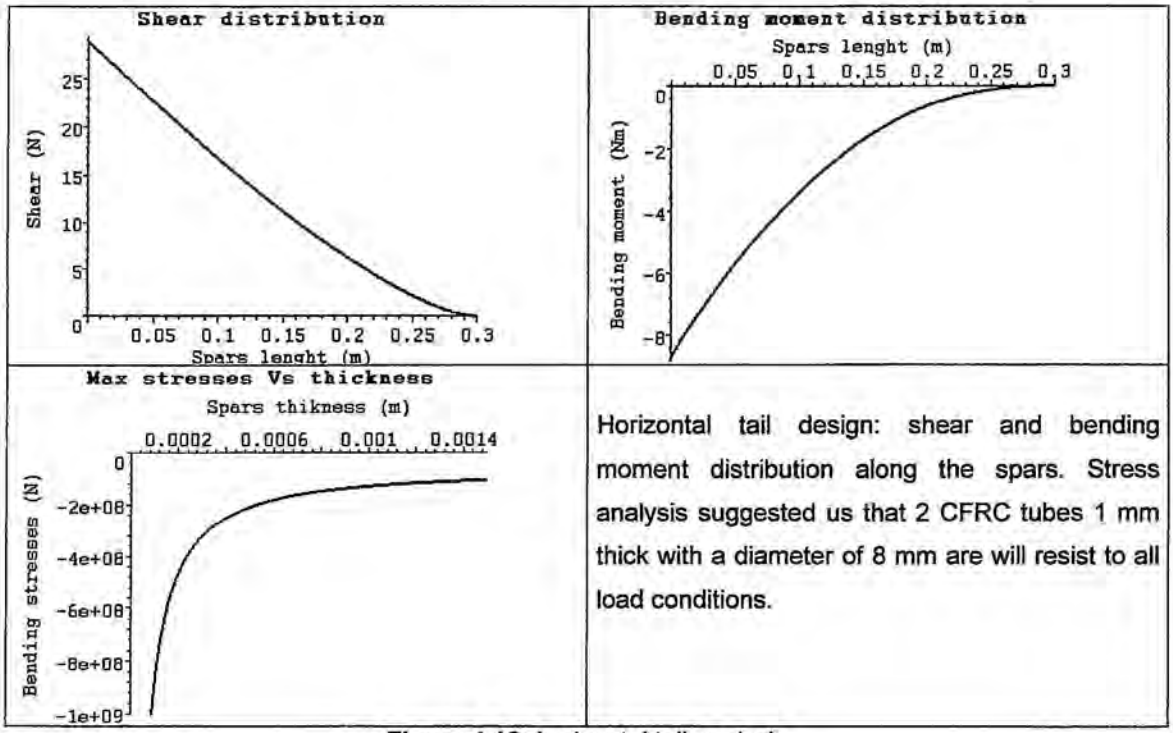

Figure 4.12: horizontal tail analysis

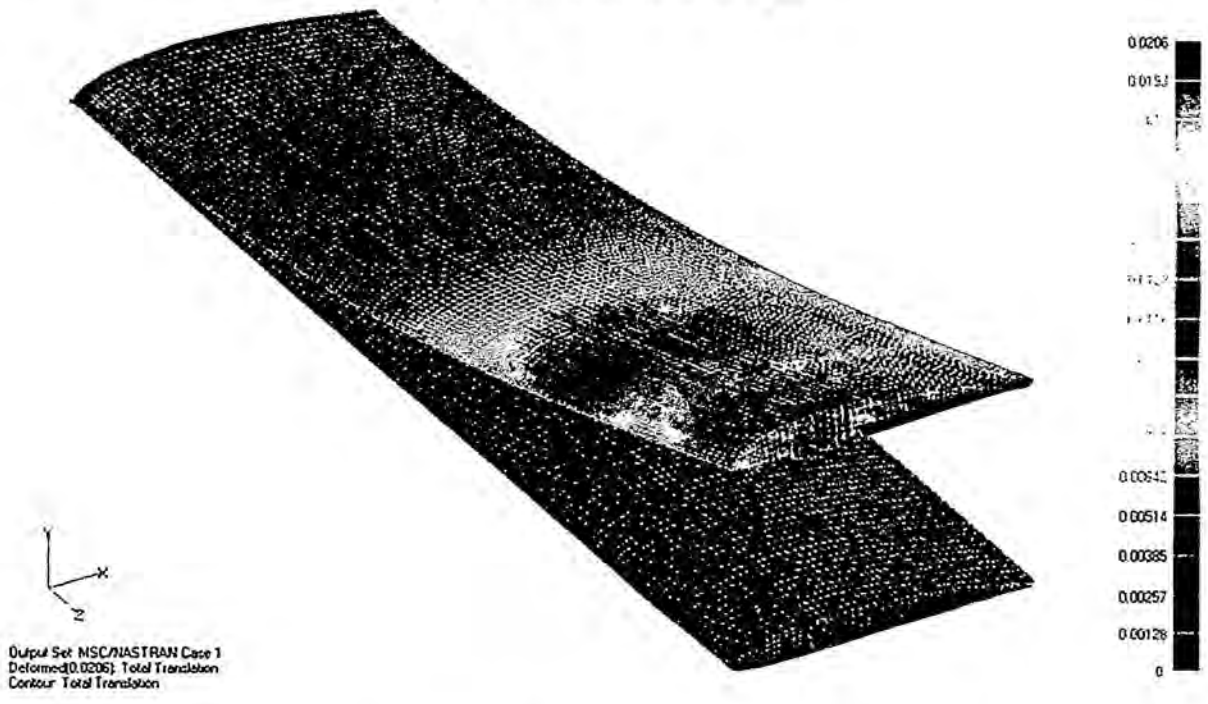

Figure 4.13: half wing: total traslation

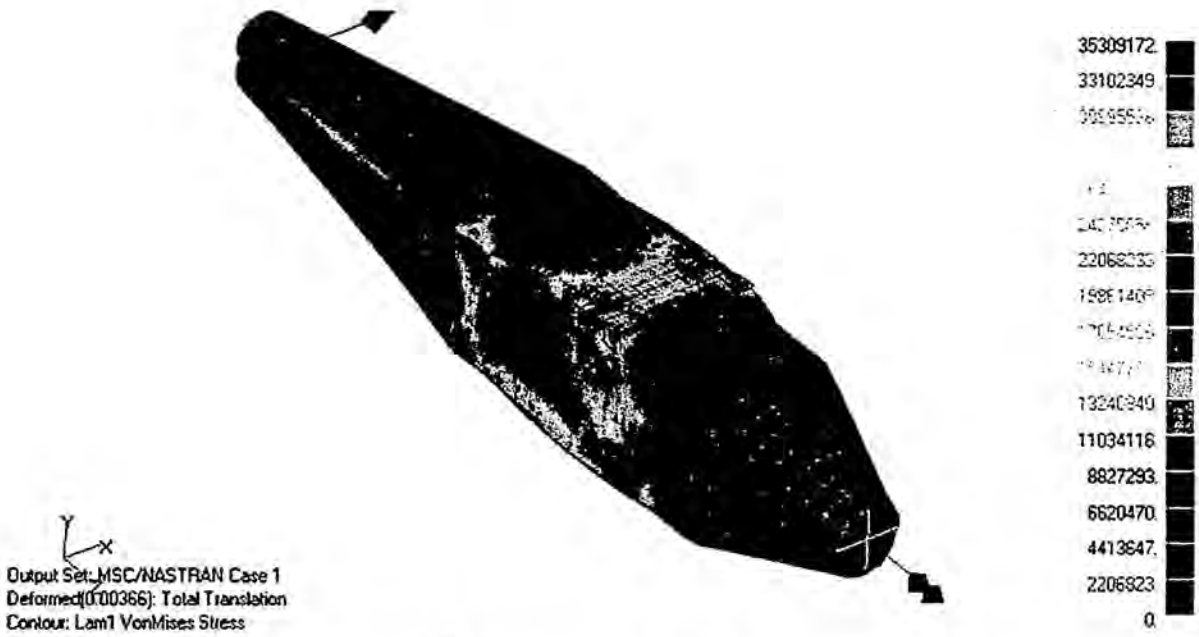

Figure 4.14: fuselage: max Von Mises stresses

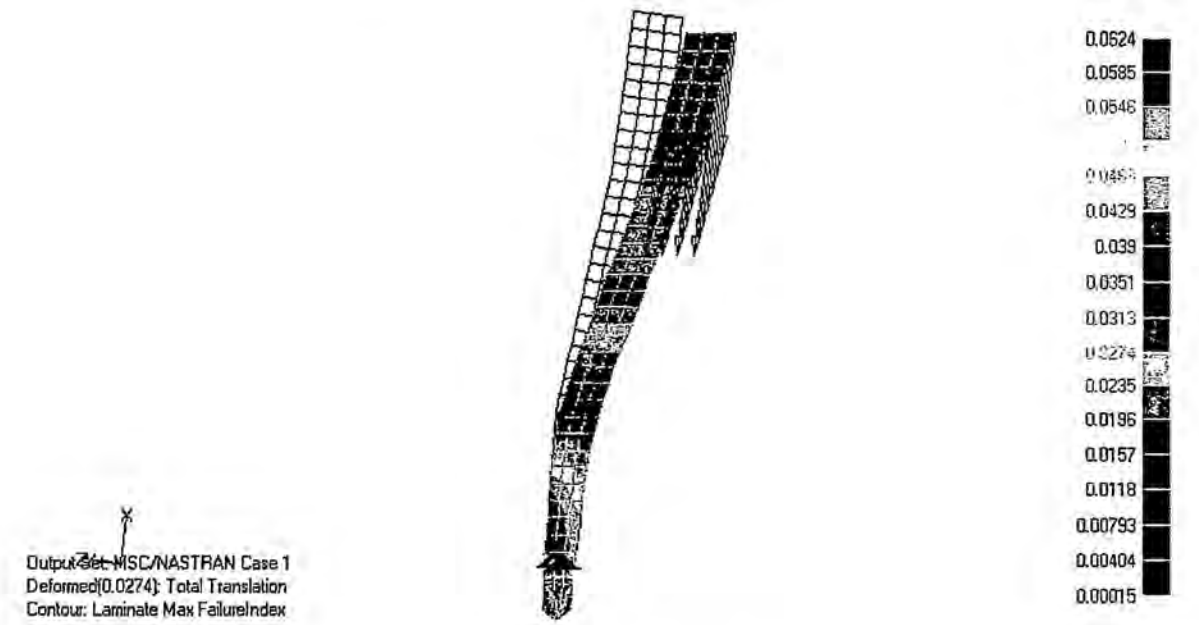

Figure 4.15: maximum failure index distribution, using Hoffman fracture criterion.

5 Detail Design

5.1 Introduction

At the end of the preliminary design stage, we had already sized the main components of our plane. It was known the concept shape, as well as the structural and propulsive subsystem. Moreover, we had identified its predicted performances in various flight conditions. In the next phase of the design process we had to focus attention on that elements we did not have studied yet, and to evaluate with more accuracy the performances we could not estimate in detail before, such as the dynamic behaviour of the plane. Therefore, we proceeded with the sizing of control surfaces, and the analysis of the systems to join the main structural elements. Next we tried to find solutions for the problem of the extendable door for the payload disposal. Finally, we addressed the problem of the cooling system of the propulsive group and the best way to arrange servos and wires.

5.2 Flight Dynamics and Control

5.2.1 Control Surfaces

We had to size the elevator and ailerons mobile surfaces. We decided not to have rudder, because the missions do not include acrobatic manoeuvres and the weather in the contest site should be calm, without wind. For the ground directional control, we introduced a steering nose gear. We sized the control surfaces using the procedure suggested by Raymer.

Elevator: It was sized to produce enough tail load to achieve the take-off rotation at the maximum payload condition. The elevator effect can be considered as the one of a wing flap; then the rotation of this surface does not change the Cl_α but reduces the zero-lift angle. In particular:

$$\Delta\alpha_{0L} = -\frac{\Delta C_L}{C_{L\alpha}} = -\frac{1}{C_{L\alpha}}\frac{\partial C_L}{\partial \delta_E}\delta_E$$

With an iterative method and using empirical curves, giving $\frac{\partial C_L}{\partial \delta_E}$ as a function of the ratio between elevator and the tail chords (c_e/c_t), it was possible to determine the c_e/c_t ratio for the maximum deflection in the range 15-20°. The obtained result is c_e =0.06 m (2.4") for a span b_e =0.48 m (19"), for a maximum deflection of 18°.

Ailerons: For the ailerons sizing we used the same procedure seen for the elevator. The ailerons do not occupy the whole wing span, as the elevator, then we used the balance between the roll moment produced by the ailerons and the roll damping at steady-state roll rate p_{ss}. For p_{ss} =100 deg/sec and maximum deflection δ_A = 17°, from:

$$\frac{p_{SS} b}{2} = \frac{C_{l,\delta A}}{C_{l,p}} V \delta_A$$

we found out: b_a=0.50 m by a chord, c_a =0.07.

Pitching-moment equation and Trim: The pitch moment, about the center of gravity, has to be equal zero. This moment is the sum of the contributes produced by the various aircraft components: wing, fuselage, tail. For a given flight condition, is possible to calculate the single contributes and check if the sum is zero. If this condition is not met, it is possible to vary the tail lift, changing the elevator deflection or the tail incidence, so that the moment vanishes. The change of the tail lift produces a change of the total lift of the aircraft, which should balance the weight. Then, the change of the tail lift causes a change of the angle of attack. To solve the problem an iterative method can be used, or better the graphical solution proposed by Raymer: once the angle of attack α and the elevator deflection δ_E are arbitrarily chosen, we calculate the total pitch moment coefficient:

$$C_{mcg} = C_L(\overline{X_{cg}} - \overline{X_{acw}}) + C_{mw} + C_{mfus} - \eta_h \frac{S_h}{S_w} C_{Lh}(\overline{X_{ach}} - \overline{X_{cg}})$$

where C_{Lh} is the tail contribute, function of the downwash angle and the zero lift angle due to the elevator deflection, found out in the previous elevator sizing. Under the considered hypotheses, it is possible to calculate the total lift coefficient, where the wing and tail lift coefficients are summed, considering the change of the dynamic pressure on the tail. For different angles of attack we calculated the total lift coefficient and C_{mcg}. For C_{mcg} =0, it is possible to find the trim conditions for different elevator deflections.

5.2.2 Handling Qualities

At this point we encountered the problem of studying the dynamics stability of the designed aircraft. That means to predict how the aircraft motion evolves following a perturbation of its equilibrium state. As trim condition we considered a steady state level flight at cruise speed and full weight. The equations of motion were then linearized using the theory of little perturbations. In so doing we obtained, as usual, two sets of decoupled equations for longitudinal and lateral dynamics. The linear equations were written in the space-state. So, we could calculate eigenvalues, damping, and therefore, coefficients and natural frequencies and to analyse the stability of the system. Then we studied the response of the system to inputs of 1 deg for elevator (longitudinal dynamics) and for ailerons (lateral dynamics). To follow this procedure we needed to calculate stability and control derivatives (non dimensional and dimensional). To this end, the method proposed by Roskam was used.

$C_{L,\alpha}$	$C_{D,\alpha}$	$C_{M,\alpha}$	$C_{L,q}$	$C_{M,q}$	$C_{L,\dot{\alpha}}$	$C_{M,\dot{\alpha}}$
4.6261	negligible	-0.8298	4.5669	-5.3245	negligible	negligible

Table 5.1. Longitudinal non-dimensional derivatives

C_{L,δ_E}	C_{D,δ_E}	C_{M,δ_E}
0.9704	negligible	-2.0935

Table 5.2. Longitudinal control derivatives

$I_{yy}[kgm^2]$	X_α	M_α	$M_{\dot{\alpha}}$	M_q
1.8318	5.7115	-23.95272	0	-2.30543

Table 5.3 Longitudinal derivatives and moment of inerzia about Y body axis

$C_{y,\beta}$	$C_{l,\beta}$	$C_{n,\beta}$	$C_{y,p}$	$C_{l,p}$	$C_{n,p}$	$C_{y,r}$	$C_{l,r}$	$C_{n,r}$
-0.4918	-0.0125	0.2907	-0.0035	-0.4710	-0.0444	0.6127	0.1237	-0.5649

Table 5.4 Lateral-directional non-dimensional derivatives

C_{l,δ_A}	C_{n,δ_A}	C_{y,δ_A}
1.82178	-1.40612	negligible

Table 5.5. Lateral control derivatives

$I_{xx}[kgm^2]$	$I_{zz}[kgm^2]$
1.2983	3.0745

Table 5.6 Moment of inertia about X and Z body axes

Y_β	L_β	N_β	L_p	N_p	L_r	N_r
-4.3341	-5.28768	3.1102	-11.95439	-1.1269	3.1396	-28.6753

Table 5.7 Lateral-directional dimensional derivatives

Once the aerodynamic derivatives and the reference flight condition were calculated, we had the components of the state and control matrices. Then, two simple codes were developed in commercial software Matlab to calculate eingenvalues, damping coefficients and frequency for the longitudinal (phugoid and short period) and lateral-directional modes (roll, spiral and ducth roll).

Longitudinal dynamics

From table 5.8 we observe that the real part of the eingenvalues is negative, positive damping so that both modes are stable. Furthermore, the results show how the short period damping is nearly ten times that of the phugoid. The same frequencies, calculated with the approximate models (second-order) of phugoid and short period, are respectively: ω_{PH} = 0.6937 rad/sec, e ω_{SP} = 10.21rad/sec.

Mode	**Eingenvalue**	**Damping**	**Frequency [rad/sec]**
Phugoid	-0.0348 ± 0.611i	0.0569	0.612
Short Period	-5.22 ± 9.87i	0.471	11.1

Table 5.8. longitudinal modes

These values are quite close to the ones obtained as output of the Matlab program.

Next we evaluated the response of the plane model to a single nose down impulse command of 1 deg elevator. By analysing figure 5.1, we can deduce that in the first seconds, when the short period is excited, we find the biggest variation of angle of attack and pitch rate. Then, at later time, when the phugoid mode is the dominant one, we can see the biggest variation of airspeed and pitch attitude.

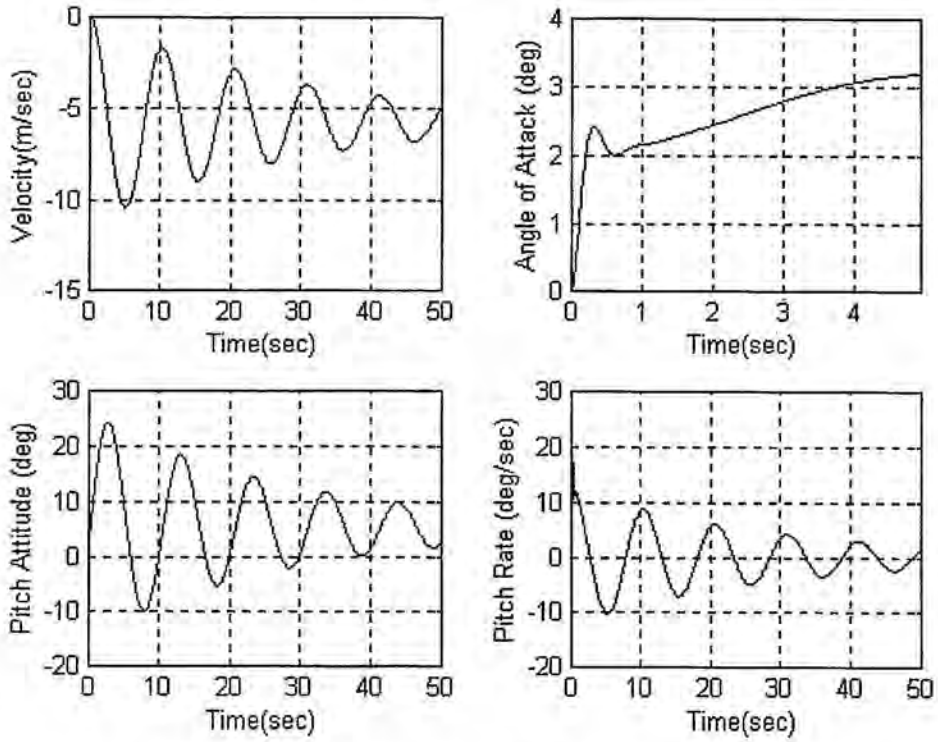

Figure 5.1. longitudinal response to a 1-deg elevator impulse input

Lateral-directional dynamics:

The Matlab program gave the eingenvalues, damping coefficients and frequencies shown in table 5.9 for the roll, spiral and dutch roll modes.

Mode	Eingenvalue	Damping	Frequency [rad/sec]
Spiral	0.00202	-1	0.00202
Dutch Roll	-2.6 ± 5.84i	0.407	6.4
Roll	-14.6	1	14.6

Table 5.9. lateral-directional modes

Results show a slightly unstable spiral mode. It is associated with a real eingenvalues which mainly represents the variations in roll attitude $\Delta\phi$ and depends mostly on the $C_{l,\beta}$. Anyway, spiral mode is typically associated with a slow dynamic. This is our care, actually: in fact the time constant is low so that the pilot has time to react. The dutch-roll is an oscillatory mode with significant component in the yaw Δr and the roll $\Delta\phi$ variables. Table 5.10 shows that it is stable. The roll mode is associated with a real root and the motion is predominantly in roll rate Δp .Next we analysed the response to a single 1 deg impulse on the ailerons, positive (i.e.: right aileron upwards).

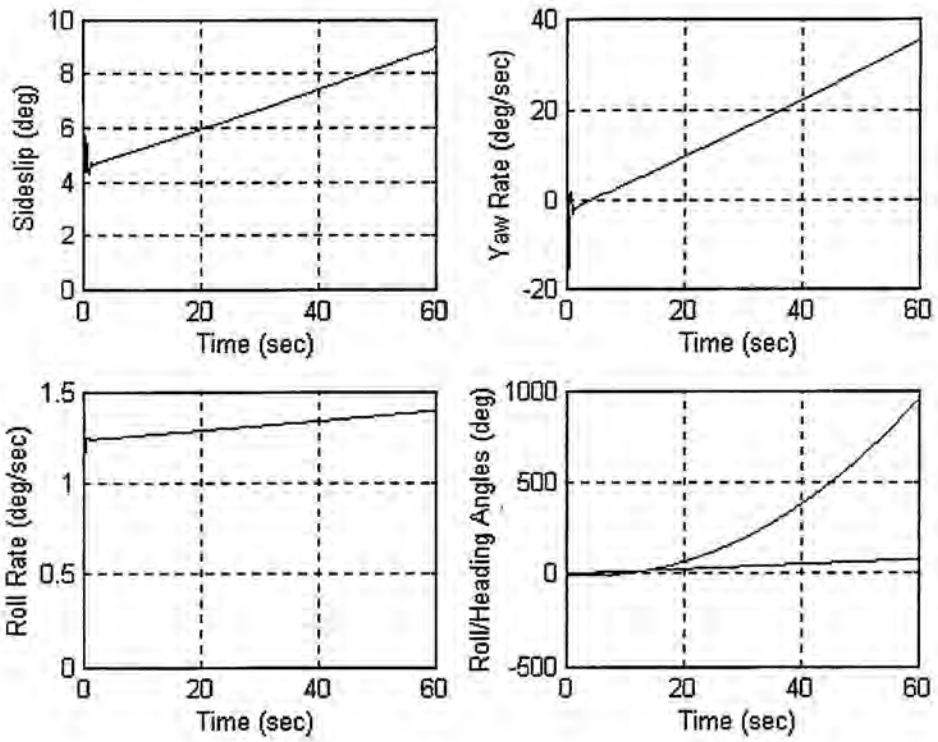

Figure 5.2. lateral-directional aircraft responses to a 1-deg aileron impulse input

5.3 Structures

After the structural sizing of the major elements of the UAV we performed in the preliminary phase, their integration and detailed description was faced in detail design. This aspect of the design process has a strategic role for the entire project. New rules ask to contain the airplane in a specific size box that makes expected to disassemble the model in different parts. Besides, the time needed to extract and to assemble the model will influence the final score. Few elements and easiness to join is a prior task .

5.3.1 Fuselage Structural Details

Fuselage was designed around the payload to limit the frontal surface, caring to not expose sharp angles to the flow of the propeller. It consists in two volumes between three bulkheads and two longitudinal plates sandwich made where all other structures join. The main bay contains the payload, while a smaller volume behind contains the receiver and its cell and a tube to join with the tail section. An opening ensures access to it. Cargo bay has two doors on the bottom where payload is expelled from. The doors open for the weight of the payload and after the deployment it close for the action of two torsion spring. A servo placed outwardly in one of the doors commands the opening. It acts on a pin that works as a bolt. Wing junction is realized by an hand made CFRP T tube where wing booms and antenna join. Wings are prevented to slip from tube thanks to two screw fixed on the aligning little spars. The tail section is fixed to the central section of the fuselage by a CFRP tube constrained between the two aft bulkheads. A blocking

system prevents the tail section to rotate or translate. On the front bulkhead a GFRP pocket is glued to contain the cells' pack. Polystyrene fairings bring the desired aerodynamic shape.

5.3.2 Wing Structural details

The wing is formed by two parts, joining the fuselage. Each half wing is shaped on a polystyrene core and covered with a single ply of GFRP skin. A spar with two caps of CFRP integrated in the maximum airfoil thick provides the required bending strength. The polystyrene core transmits loads to the composite structures. Two balsa ribs are placed at the root and wing tip. A third rib 39 cm far from the root rib allows to align the wing boom joining the fuselage. The ailerons' servos are drowned into the core and fixed to the wing skin by a lime wood thin plate.

5.3.3 Tail Structural Detail

The H tail follows the same building philosophy of the wing: polystyrene core with composite strength element. Loads resistance is provided by two carbon tubes drowned into the core; with the GFRP skin, they constitute the tail structure. The tail's aerodynamic surfaces are glued on the boom that joins with the fuselage main section. The fuselage tail section is a polystyrene shell covered by a thin GFRP and it smooth the shape of the fuselage from the largest section of the cargo bay by an axialsymmetric low drag geometry. The disassembled configuration of the model in the box expected the tail to be set in the fuselage, but it is rotated by 90° to get the horizontal surface to be parallel to the two feet long side of the box. Assembling is obtained by spinning the tail until a blocking system forbid further movements.

5.3.4 Landing Gear Structural Details

The tricycle landing gear consists of a fore leg and a couple of after legs positioned behind the center of gravity of the plane. The froe leg is made of a carbon fiber reinforced plastic tube jointed with a couple of hinges to the foe frame of the fuselage. The main gear is constituted by a couple of legs realized by a manual lay up of carbon-kevlar fabric with epoxy resin cured at environmental conditions and controlled pressure. The latter are jointed directly to the lateral frames of the fuselage box. A servo is positioned on the upper side of the fuselage and moves directly the fore leg to allow driving the plane while on the ground (taxi, rull-out). The need to place the fuselage inside the box with the landing gear already mounted imposed a severe limit to the wheel-truck; in fact the distance within the wheels must be lower than the minimum dimension of the box, that is 1 foot. As a result the curving slope of the two main legs is very little, and its sizing calculations had to considered the possibilities that buckling phenomena would occur. The junction of the main legs to the sandwich frames of the fuselage has been realized using epoxy resin as structural glue. Locally the junction has been reinforced with a manual lay up of carbon fiber reinforced fabric. In fact this junction is severely loaded by huge shear stresses given by the legs at touch down, because of the little energy dissipation the leg can provide with its little flexural deformability. At the moment of sending this paper we have already performed some flight tests on the prototype. As a consequence of that, we are valuating the possibility to adopt a different solution for the after legs. In fact the very little wheel-truck comport stability problems at landings. So we are considering to realize a demountable carriage which would be more reliable, even if it would comport a bigger time for assembly.

5.3.5 *Radome Structural Detail*

Radome is made with polystyrene foam covered with CFRP. The enclosed volume contains the motor and the cells' pack. It transmits the trust to the plane by a connection on each of the two longitudinal plates of the cargo bay. The connections are obtained by two slides of aluminum and four screws for each slide. The junction is intended to be permanent because the two section of the UAV will lay joined into the container box. Two frontal inlets will supply the right cooling of the motor and cells pack.

5.4 Propulsion System

The propulsion system had already been fully designed at the end of preliminary design phase. The propulsive group had selected the proper motor and gear-box. It planned to perform a series of wing tunnel and flight test to choose the propeller and number of cells which would enhance aircraft performances. At this stage of the design the propulsive group considered the various possible cooling systems. It decided a simple air intake would be enough just properly disposing motor, controller and cells inside the radome. The inlet was sited so to guarantee a sufficient airflow not to cause the temperature of the system reaching values so high to endanger the safety of the system.

5.5 Final Aircraft Table

Geometry		
Length	1.18 m	3.87 ft
Span	2.4 m	7.87 ft
Height	0.52 m	1.71 ft
Wing area	0.72 m^2	7.75 ft^2
Aspect ratio	8	
Control volume	0.35	

Weight Statement		
Airframe	2.937 kg	6.475 lb
Propulsion System	1.575 kg	3.472 lb
Control System	0.698 kg	1.539 lb
Payload System	2.268 kg	5 lb
Antenna	0.522 kg	1.151 lb
Empty Weight	5.21 kg	11.4 lb
Gross Weight	8 kg	17.637 lb

Performances			
C_{LMax}		1.14	
L/D Max		14.32	
Static Margin		0.16	
Rate of Climb	Empty	7.22 m/s	23.7 ft/s
	Gross	4.46 m/s	14.7 ft/s
Stall Speed	Empty	11 m/s	36 ft/s
	Gross	12.65 m/s	41 m/s
Max Speed	Empty	29	95
	Gross	25	82
Takeoff Run	Empty	12.53 m	41.11 ft
	Gross	27.57 m	90.45 ft

System	
Radio	Futaba FP8 UPS
Servos	Futaba S9402
Battery Configuration	17 cells, serial
Motor	GraupnerUltra 930-8 12 V
Propeller	20" x 10"
Gear Ratio	3.7:1

Table 5.10: final aircraft table

5.6 Rated Aircraft Cost

In the following table the final competition aircraft RAC is determined according to the supplied cost model: RAC=(A*MEW+B*REP+C*MFHR)/1000 = **8.017** thousand $

Coefficients calculation

Coefficient	Description						Value
A	Manufacturers Empty Weight Multiplier						**$100**
B	Rated Engine Power Multiplier						**$ 1500**
C	Manufacturing Cost Multiplier						**$20**/hour
MEW	Manufacturers Empty Weight						**11.46** lb
REP	Rated Engine Power	# of Motor	# of Cells	Battery Weight			**2.24**
		1	17	2.24 lb			
MFHR	Manufactoring Man Hours	***Wing***	Span	Man Hours/Unit	WBS	***76.87***	**175.57**
			7.87 ft	8 hour/ft	63		
			Chord	Man Hours/Unit	WBS		
			0.98 ft	8 Hour/ft	7.87		
			# of control Surface	Man Hours/Unit	WBS		
			2	3 Hour/ft	6		
		Fuselage	Lenght	Man Hours/Unit	WBS	***38.7***	
			3.87	10	38.7		
		Empenage	# of vertical Surface with no control	Man Hours/Unit	WBS	***20***	
			2	5	10		
			# of Horizontal Surface	Man Hours/Unit	WBS		
			1	10	10		
		Flight System	# of servos	Man Hours/Unit	WBS	***30***	
			6	5	30		
		Propulsion System	# of motor	Man Hours/Unit	WBS	***10***	
			1	5	5		
			# of propeller	Man Hours/Unit	WBS		
			1	5	5		

Table 5.1: final RAC

5.7 Drawing Package

The following pages contain the CAD drawing package.

6 Manufacturing Plan and Processes

Before we began the aircraft manufacturing, we performed a study to find out which techniques were more suitable to build the different components. We identified FOMs measuring the effects of some fundamental parameters on the decision of the manufacturing processes. These parameters are: cost, required skill, availability and the build time.

6.1 Manufacturing Processes Selected

The extensive use of composite materials, allows different production procedures for each components: manual lay up; propylene, wood or metal moulds; curing cycles in autoclave, oven or at room temperature. Various techniques lead to excellent surface smoothness, at the cost of high costs and required skill, or to rougher surfaces, with much lower costs. With the previously introduced FOMs the manufacturing techniques for each aircraft component were selected: manual lay up of GFRP and CFRP over the polystyrene core for the wing and tail surfaces, wooden mould and manual lay up for the main landing gear, manual lay up of GFRP and CFRP over polystyrene shell for the radome and sandwich plates fixture for the boxed main fuselage section.

6.1.1 Fuselage Manufacturing and Tooling

The fuselage is the main aircraft component; it is also the hardest to build. It has to have an aerodynamic shape, with a low drag, it has to carry the payload and and the coupling systems for the other components. The sandwich boxed structure allows to have tough and easy to build coupling systems for the half-wings and the main gear. The necessary aerodynamic shape is obtained with polystyrene fairings, cut with hot wire system. The surface smoothness and the dimensional control obtained this way are obviously lower than the ones obtaining with a composite shell shaped with mould and counter mould, but the costs are far lower. The fuselage building started from the sandwich sheet (nomex honeycomb and prepreg carbon skins), cured in autoclave. From it we obtained the two lateral plates and the three bulkheads. Then these pieces are manually glued. The polystyrene aerodynamic fairings are fixed on the boxed structure obtained. This process is fast and does not require high skill levels, except that for the sandwich preparing.

6.1.2 Wing Manufacturing and Tooling

The lifting surfaces were built laying up manually a GFRP skin on the polystyrene core. For the wing two layers of uniaxial carbon were layed up below the skin on the lower and upper surface of the core, at its maximum thickness zone. 0.5 mm deep tracks were drawn in the polystyrene, to host the carbon fiber. The used epoxy resin polymerizes at room temperature in 24 hours. Once layed, the half-wing is wraped in a plastic sheet, and put inside a mould under controlled pressure. This process has a low cost, but requires previous experience. The surfaces obtained are quite smooth.

6.1.3 Tail Manufacturing and Tooling

The tail surfaces were manufactured the same way, but without the carbon strengthening. Carbon pipes, sank in the polystyrene core, were used as spars.

6.1.4 Landing Gear Manufacturing and Tooling

The composite main landing gear was made laying up carbon-kevlar fabric and uniaxial carbon fibre for the outer layers. The double bent shape was obtained with wooden mould and counter-mould, shaped with a numeric-controlled cutter and CAD drawings templates.

6.2 Analytic Methods

Estimation of manufacturing and tooling costs projects a limited cost for fibers and resins purchase, polystyrene cutting and wood moulds preparation, while a large amount of funds will be allocated for the

sandwich fabrication and propulsion equipment. Particular emphasis is to be set to the high costs of team travel to USA that reduces the funds available for the materials and construction, so cost is the mean FOMs we considered to select the manufacturing and tooling processes.

Skill Matrix

The skill matrix is a mean to select team members to assign to each manufacturing processes. It evaluates the skill required to perform tasks needed to complete the selected manufacturing processes, so that the most efficient members could work on their specific tasks. High values means high skills required.

Aircraft Components	Foam cutting	Wood working	Mould preparation	Composite layup	Radio and electrical installation	CAD Modelling
Fuselage	3	1	0	1	2	3
Wing	2	2	0	3	2	2
Landing gear	0	0	2	2	1	2
Tail	2	2	0	3	2	2
Radome	3	0	2	3	2	3
Propulsion	0	0	0	1	2	1

Table 6.1: skill matrix

6.3 Manufacturing Milestone Chart

Aircraft consists in six separate sections: radome, main fuselage section, tail fuselage section, tail, wing and landing gear. A milestone chart was developed to plan and to coordinate the construction.

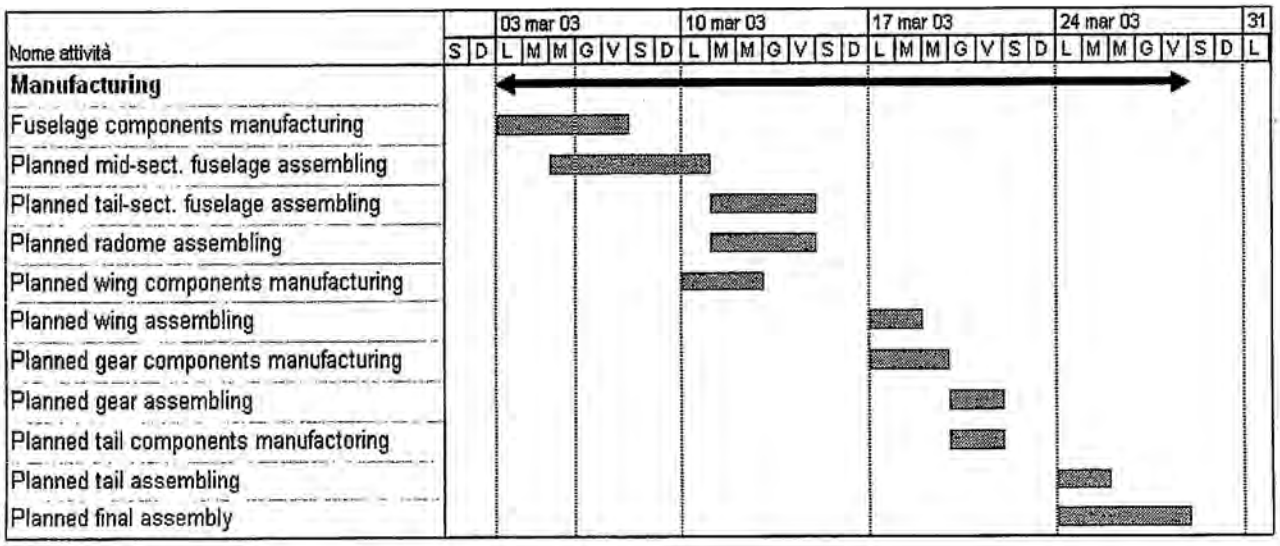

Figure 6.1: manufacturing scheduled timings

7 Testing Plan

Since the first stage of the work, we planned to perform several testing sessions. They would have run parallel to the design process, supplying designers with the needed information about the actual behavior of the various subsystems, and to verify the goodness of the choices made. More, they would have supplied the basis for an iterative optimization process of each single subsystem and of the integrated aircraft.

7.1 Structural Tests

Despite the successes of FE methods, limitations with the constitutive material models available in the numerical codes, particularly for composites, has meant that the days of conducting experimental tests are far from over. Instead, a shift in emphasis such that the experimentalist can maximize the usefulness of a single test has been promoted. It is therefore essential that both numerical and experimental disciplines be used to promote and support each other. This was the driving idea we had to follow in planning our work. In fact, to build our model, we identified a technology that could allow us to produce in a little time several prototypes of each structural element, but we did not have enough confidence with it. It means the results we could have from a numerical design could be very far from the actual characteristics of the structure we could realize. The first step in assessing the performance of any new material/structure normally involves the testing of standard coupons. Although coupon data is a valuable starting point, the results obtained may not be representative of the final structure, due to the actual conditions it will experiment in its life. Better, it is essential to understand how the individual components behave within a complex structure. Resolution of this situation can be limited to the production of sub-structures which can give the designer confidence in using new materials / technologies in a given configuration. We could early produce some benchmarks of our sub-structures (wing, fuselage, ...), and test them by carefully reproducing the boundary and loading conditions of the given configuration, without the problem of the scalability involved in testing scaled structures. So, we thought that by integrating the disciplines of numerical and experimental analysis it was possible to enhance the FE modeling further, whilst reducing the number of experiments that need to be performed. In so doing, we could bridge the gap between coupon testing and the real structure in a time enough short as the one of this competition. So, quite early in the design process we planned a series of structural tests, beginning with the ones on standard coupons and ending by testing entire sub-structures to characterize their performances in the real condition.

7.1.1 Testing ASTM standard specimen

For engineering design purpose it s important to know the mechanical properties of the materials used to manufacture the real object. We said we early thought to use composite materials to manufacture many structural components of the aircraft. After last year experience, we had a sufficient know-how in a self-made technology consisting in a manual lay-up of fiber fabric and a resin curing process in ambient temperature and controlled pressure. However, lesson learned last year suggested extremely care must be taken to secure maximum degree of uniformity in details preparation, treatment an handling, since the method of preparation is directly linked to the final properties of a composite material. Because of the high degree of sensitivity exhibited by many plastics to rate of straining, environmental conditions and - most of all - preparation procedure, data furnished by the product sellers often could not be considered satisfactory in a design process. This is particularly true for our applications involving a self-made technology of curing composites. Thus, to predict the behavior of structural components realized with our method of lay-up and curing, we needed to directly test the materials as they actually appears after the manufacturing process, in

the real condition of operation. So, quite early in the design process we planned a series of test to characterize a few materials we would produce with the dry fabric and resins we could find from our suppliers. We considered the standard test methods as they are described by ASTM rules. In particular, we referred to the rules ASTM C 393-94 for flexural properties of sandwich construction, ASTM D 638M-84 for tensile properties of plastics; ASTM D 790-86 for flexural properties of unreinforced and reinforced plastics.

7.1.2 Static and Dynamic Wing Tests

If standard coupon tests were important to supply the structural design process with the data about materials properties, testing the various structural elements of the real plane would be essential to evaluate the performances of the actual structure in the operation conditions. In particular, we planned to perform experimental analyses on the wing, to establish its load carrying capabilities and its dynamic behaviour. We planned also to perform tests on the structural subsystems which are located within the fuselage, such as the bayonets for joining wing and tail booms and the carriage. Testing the assembled half-wing had the scope to estimate the real stiffness and strength with respect to the nominal data obtained with analytical and numerical studies. We manufactured 3 half wings and collocated an electric strain-gauge (S/G) near the root section, at the point of maximum airfoil thickness (where is the spar), to measure strains on the skin. Then we simulated the static inspection condition, i.e. we fixed the root section of the wing as a cantilever beam and applied to the tip an increasing load. The S/G works like a Wheatstone bridge. It uses the variation of the resistivity of conductor when it is deformed by mechanical stress. We used a half-bridge configuration to obtain bridge amplification on the signal, to avoid the effects of temperature and of unwished tensile or compressive forces applied on the wing. The S/G was glued by a phenolic resin on the wing upper surface, 8 cm from root section upon the upper spar cap. We managed data acquisition and setting of the device by the HBM software supplied with the SCOUT 55 amplifier. To load the wing we used weight of different sizes; analysis data for the three specimens are summarized in table 7.1. An unexpected result was the difference within the loads breaking the wings. Inspecting the wing 1 fracture area, we could notice in the crack region (on the lower surface) that carbon fibres were not properly impregnated of resin. So the failure was due to the buckling of those fibres. On the other side Wing 3 broke showing a clear delamination within the fibres and the core (fig. 7.1). We noticed that this delamination began from servo seat, a point of stress concentration. By plotting the experimental diagram σ–ε for the first wing, we deduced a value of the elastic modulus equals 20 GPa, exactly the one we used in the sizing study, averaging the results supplied by standard coupon tests we had performed. This result validate our first impression about the flexural strength of the broken wing: the offset from nominal behaviour of the material is certainly due to local manufacturing faults. Testing the dynamic behaviour of the half-wing has been performed to compare experimental data, upon natural frequencies and mode shapes, with the ones output by numerical FE codes. We felt useful to compare also this kind of data, to estimate the correspondence within predicted and actual behaviour of the structure. We could predict the actual wing would show lower frequencies with respect to the ones found by using FEM codes, because of the imperfect manufacture and the difficulty of simulating a proper constraint condition. We used an impact hammer. An accelerometer (shock limit of 500 g) was placed on the hammer's head (PCB 356B18), while the measurement accelerometer (PCB333B30) had a 50g shock limit with a voltage sensitivity of 100 mV/g. The acquisition system was made of a 16 bit National board NI DAQ Card AI 16XE 50, with 16 channels and a scan rate of 20000 samples per second. To properly constrain the wing at

its root, trying to represent its real condition of operation,: we clamped the cylindrical spar to a steel support. Along the wing span (1,110 mm) we identified 11 key-points of measure (with a step of 100 mm).

Applied load	Wing 1	Wing 2	Wing 3
[kg]	strain[μm/m]	strain[μm/m],	strain[μm/m]
1	64,2	63,2	59,6
2	143,1	129,5	135,6
3	197,6	188,7	190,9
3,5	229,9	212,4	222,1
4	the wing broke	240,9	243,8
4,5		259,9	263
5		296	294
5,5		325	319
6		the wing broke	331

Table 7.1: static test on the half-wing

	FEM analysis output	Experimental results
ω1	25,04	9,9 Hz
ω2	69,17	72,7 HZ
ω3	130,77	138,4 Hz

Table 7.3: dynamic test

Data recording and processing was done by software we developed in ambient LabVIEW™. We could identify the first 3 natural frequencies of the structure. Table 7.3 shows the comparison between experimental and numerical results. Figure 7.1 illustrates a typical FRF (frequency response function) acquired and the comparison between experimental and analytical calculation of the first modal shape.

7.2 Aerodynamic Tests

We perform two sessions of aerodynamic tests. First we studied a complete semi-model (i.e. a model of the whole airplane, split up by its plane of symmetry) to estimate the interaction among the parts of the airframe (wing, fuselage, tail). Then we tested the assembled fuselage, to measure the effect of the propeller twisted airflow. While the first session was planned to be performed after the end of the preliminary design phase, for testing the interaction propeller-aircraft body we had to wait the the prototype had been realized.

7.2.1 Tests on the semi-model

The model is in 1:2 scale, so to work in dynamic similitude at a wind speed of about 40 m/s (130 ft/s). It is 60 cm (23.6") wide and 60 cm long, made of polystyrene foam and wood, with reinforces in aluminum and glass fiber. (figure 7.2). There are also weights to make the models more stable in the airflow at the higher speeds. In the tests on the half-model, one screen were used to achieve the symmetry condition. In the first day spent at the tunnel we calibrated the balance, i.e. we weighted note masses to find the constants of the linear law that link the output voltage with the load. Then we mounted the half-model, with its screen, and measured drag and lift at various angles of attack. The results, shown in figure 7.2, display a very good match with the analytical data used in the preliminary and detail design. This year we did not consider necessary to test a wing section, to achieve real data on the selected airfoil, because in previous years we already led test on this airfoil, finding a very good match between the experimental data and the ones the ones supplied by Selig (see figure 7.2, lower line).

7.2.2 Testing the propeller mounted on the fuselage

We led test on the assembled fuselage to measure the effect of the propeller twisted airflow. It was not possible to simulate in the wind tunnel the propeller induced velocities (we should mount a complete model with motor and propeller, all in dynamic similitude!). So we performed the test outside the tunnel. With a load

cell we measured the global force on the fuselage. Being known the propeller traction, the difference in the acting force, was the additional drag due to the interference between fuselage and propeller wake.

7.3 Propulsive Tests

In order to estimate the real performances of the propulsive configuration we chose, we planned a second wind tunnel session to test the adopted system motor-gear box-propeller We need to know propulsive performances at various air speed values, so we thought to perform experiments at the bench (in motionless air) and inside a wind tunnel. Tests' results would also be important as comparison data with the output of the numerical simulation codes we used in the design phase. So to eventually update the simulation algorithms, enhancing their capabilities to predict performances in that operation ranges we could not test directly. For the reasons mentioned, it was important to test the motor with a series of different propellers. In so doing we would have enough data to optimise the propulsive configuration to best fit the requirements of the competition. Since we did not have the possibilities to dispose of many motors to be tested, we planned to perform this kind of experiment once the motor had already been chosen.

7.3.1 *Instruments and tests organization*

The measurement system is composed by two blocks linked together by wires for signal transmission and electrical supply. The first block (figure 7.2) includes structures and tools which stay inside the wind tunnel (sensors, structures needed to carry the whole system and a dynamometer connected to the motor). The second block is completely outside the wind tunnel. It includes the power pack for supplying energy, the signal acquirer "Keithley" and the PC that manages it. Figure 7.2 shows an overview of the system.

- Tests' conditions: tested propellers: Menz 17x10, 18x10, 18x12, 19x10, 19x12, 20x10
  tested airspeed: 0, 5, 8, 12, 16, 21 m/s.
  measured data: thrust, propellers' rounds per minute, power absorbed
- Wind tunnel airspeed measures: even if the wind tunnel controls are well calibrated, we decided to put in the flow a Pitot tube to measure the exact air speed. The Pitot tube was put in front of the propeller, immediately after the beginning of the measure room.
- Thrust and propeller RPM measures: the motor was able to roll by its axis (horizontal) thanks to an axial bearing; it was mechanically connected to a vertical cantilever beam. The latter was subjected to a bending moment caused by the tensile loading of the propeller. Measuring the strain near the constraint point of the beam allowed determining thrust. To measure such strain we used electrical strain-gauges. Double precision has been achieved using a variable electrical resistance to evaluate the horizontal displacement of the beam tip. The propeller angular speed was measured with a little invasive optical tachometric probe. The system was calibrated before starting testing.
- Motor input power measures: it was obtained measuring separately voltage and current supplied.

7.3.2 *Measurements procedures and results*

Once fixed the wind tunnel airspeed (v) and the supply voltage at a constant value (16V), we changed the supply current until the RPM measured by probe (n) gave the desired value of the propeller's working ratio. $y=v / (n*D)$. After a time interval, when the system reaches a steady state regime, we could record values of voltage an current input to the motor, thrust and RPM. Varying current and airspeed we could measure, for each propeller, the values of thrust, absorbed power and torque as functions of the working ratio. The results we obtained were comparable with the ones predicted by the softwares Motocalc and Motor1-testprop. It seemed the design of the propulsion system had been performed on the base of reliable data and tools. Only

a real flight test would have said if it could guarantee the performances needed to best fit mission requirements. Table 7.2 reproduce the work sheet used to record data related to a measurement session in the wind tunnel. The software used to manage data recorded by the Keithley system is XLINX 2700.

Propeller size		19x10		
Shunt resistance [W]		0,0008		
Airspeed	Current	Voltage	Thrust	RPMx1000
[m/s]	[A]	[V]	[N]	
0	39,36722	15,72153	28,456	3,992
5	39,14729	15,72211	25,345	3,975
8	38,26821	15,71335	23,543	3,982
12	37,14954	15,71458	19,623	4,198
16	33,7544	15,71824	14,715	4,56
21	24,56729	15,72437	10,115	5,037

Table 7.1: wind tunnel test of motors and propeller

7.4 Flight Tests

We had planned to build quite early a prototype, and fly it, so to directly verify the actual behavior of the selected configuration and so to have enough time to optimize it on the basis of an exact estimation of its performances. When the prototype flew we implemented on it a system able to detect some flight parameters. The scope was to verify actual performances, in comparison with the ones predicted by earlier analyses. We mounted the following items: an altimeter, a Pitot tube to detect the speed in the different phases of the flight, a couple of inclinometers to measure roll and pitch angles. We monitored the values of the control surfaces angle and of the motor throttle. We used commercial sensors connected to a system for data managing realized for embedded acquiring of tension signal. The architecture of the system basis upon a controller (8 bit) which manage a real time clock; a 12-bit analog-digital converter, with a sample time of 10 μs; an eight channels multiplexer; an internal voltage reference generator, for the AD conversion; a coupling circuit for the serial line; an E^2PROM rewritable, non volatile memory; four conditioning modules (one for each channel connected to the sensors). This system, is capable to acquire on four channel, with a scan rate up to 0,1 sample/sec. To program the acquisitions and read the data, it has to be connected to a PC by the serial port. The system is managed by means of programs realized in LabVIEW™ ambient. Since we wanted to acquire 7 signals (altitude, speed, pitch, roll, throttle, elevator and ailerons), we needed to load in the aircraft cargo bay two acquisition systems. The overall instruments weight and volume was not higher than the contest payload, figure 7.4. About the data collected during the flight, the most interesting fact is that speed in the various flight phases is higher than the predicted one. Particularly, the maximum predicted speed was about 20 m/s, while the actual one is 22 m/s. Figure 7.3 show the prototype during flight.

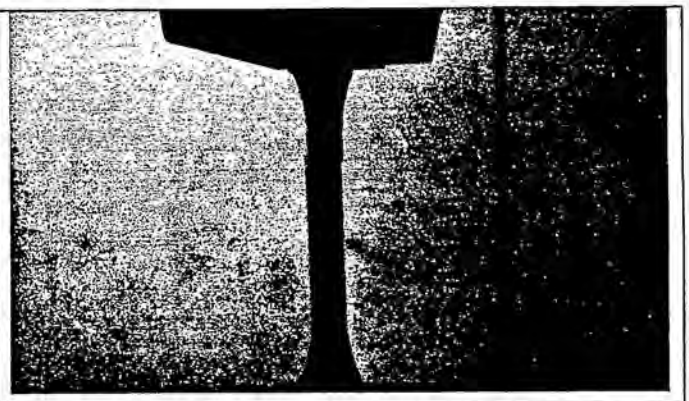

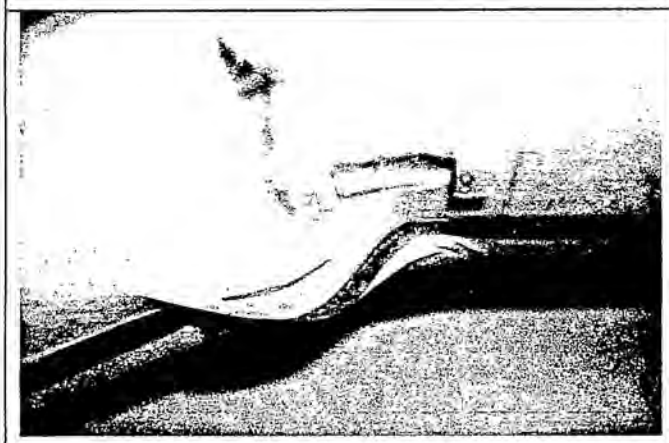

static test on the half-wing: zoom on the failure area

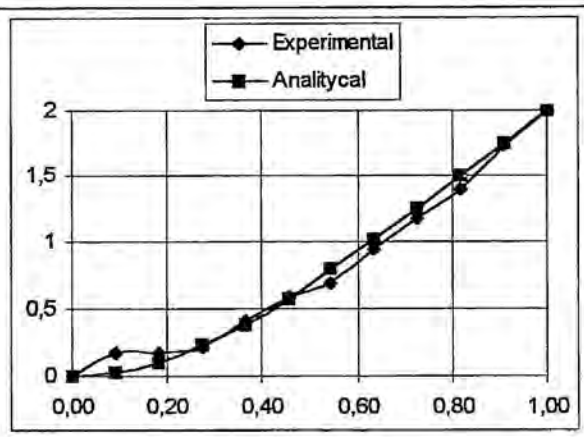

dynamic tests on the half wing: first mode shape

dynamic tests on the half wing: FRF modulus

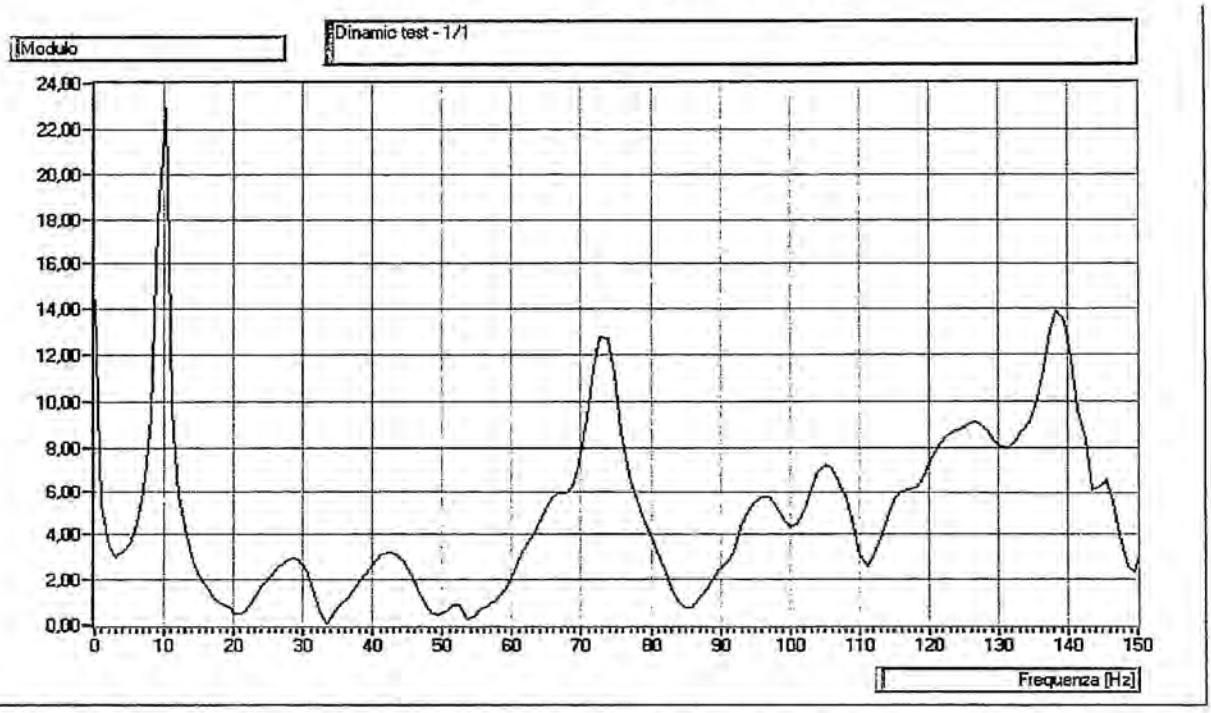

Figure 7.1 structural tests

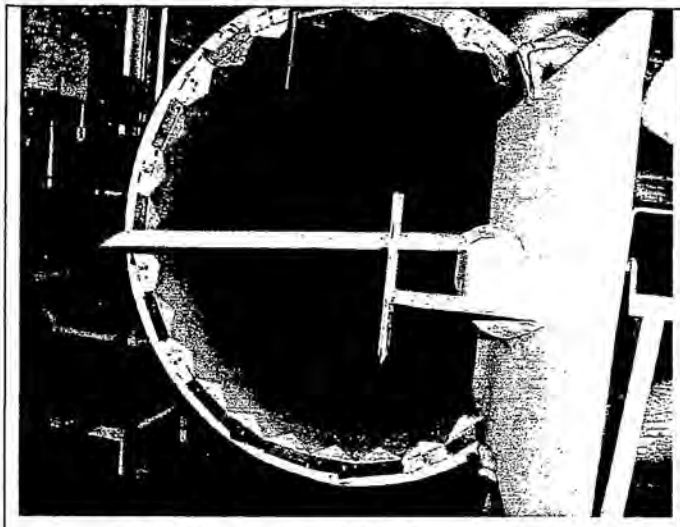

7.2.A: the semi-model in the wind tunnel

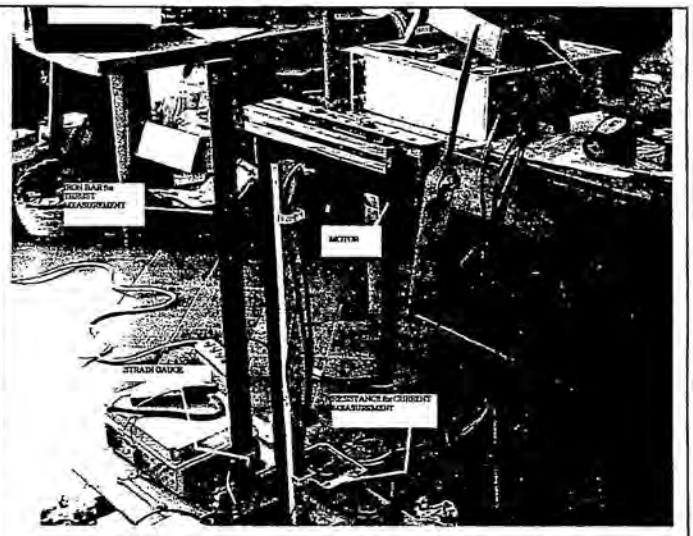

7.2.B: measure system for propulsive tests

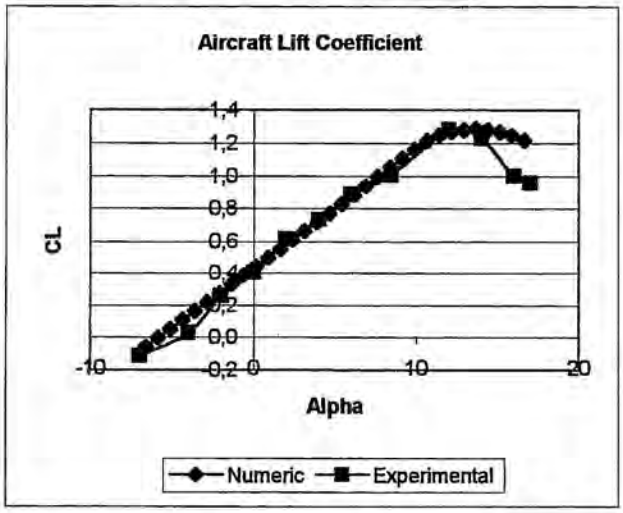

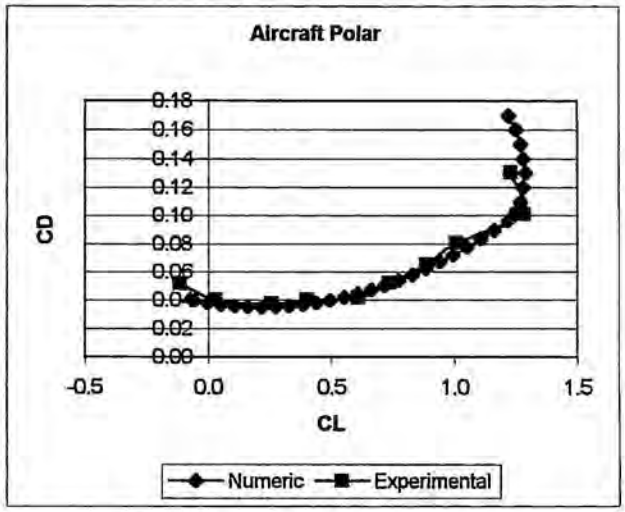

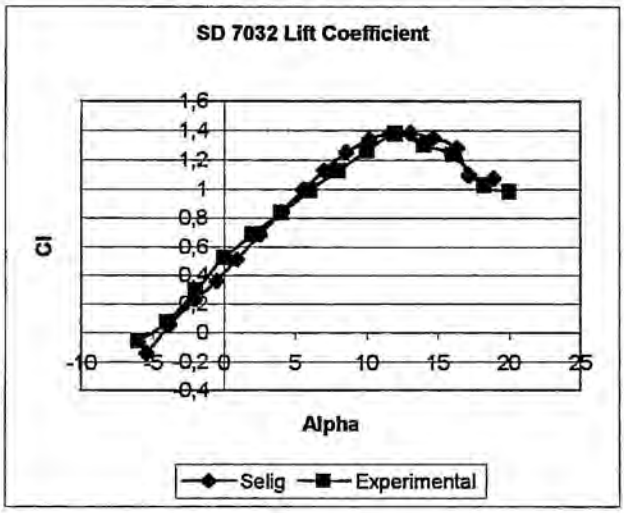

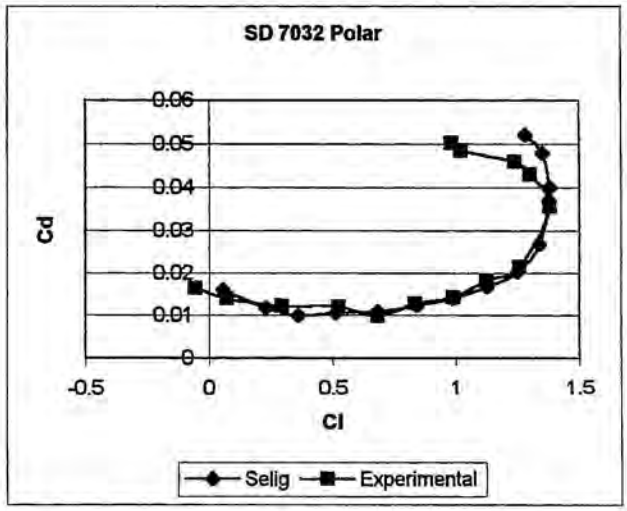

Figure 7.2: wind tunnel and propeller tests

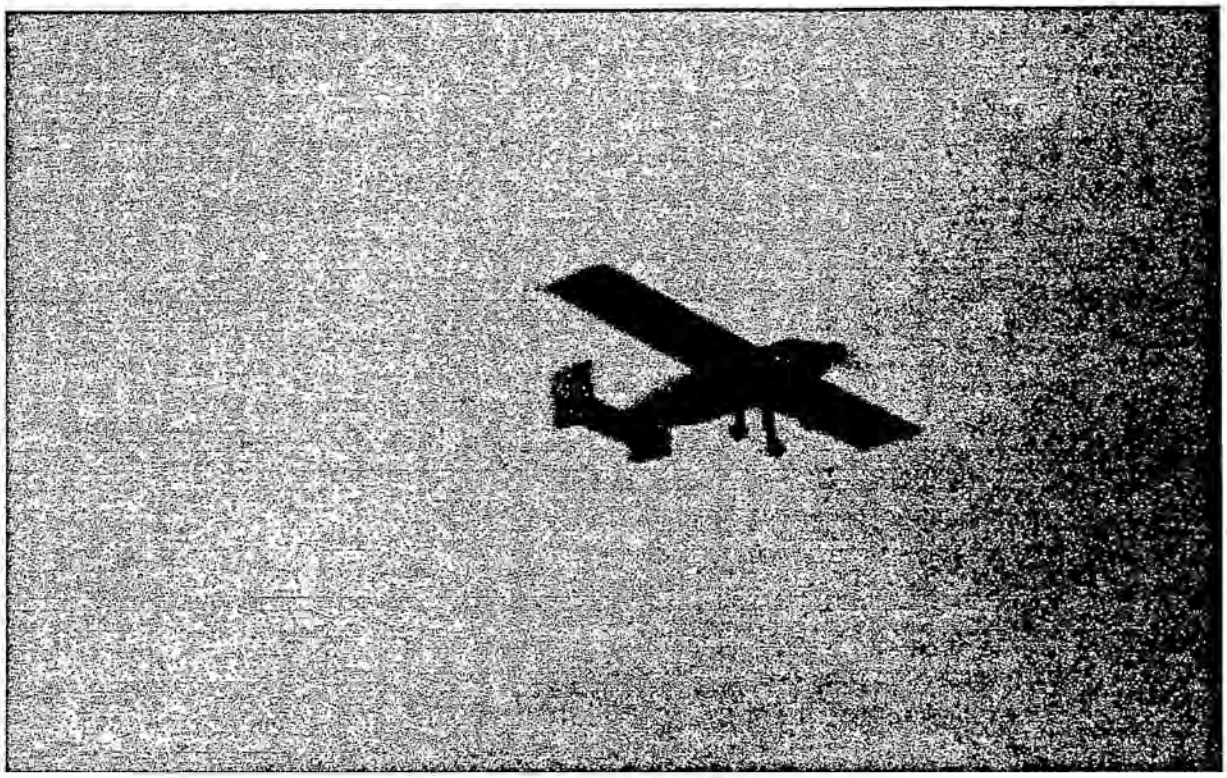

Figure 7.3: the flight of the prototype

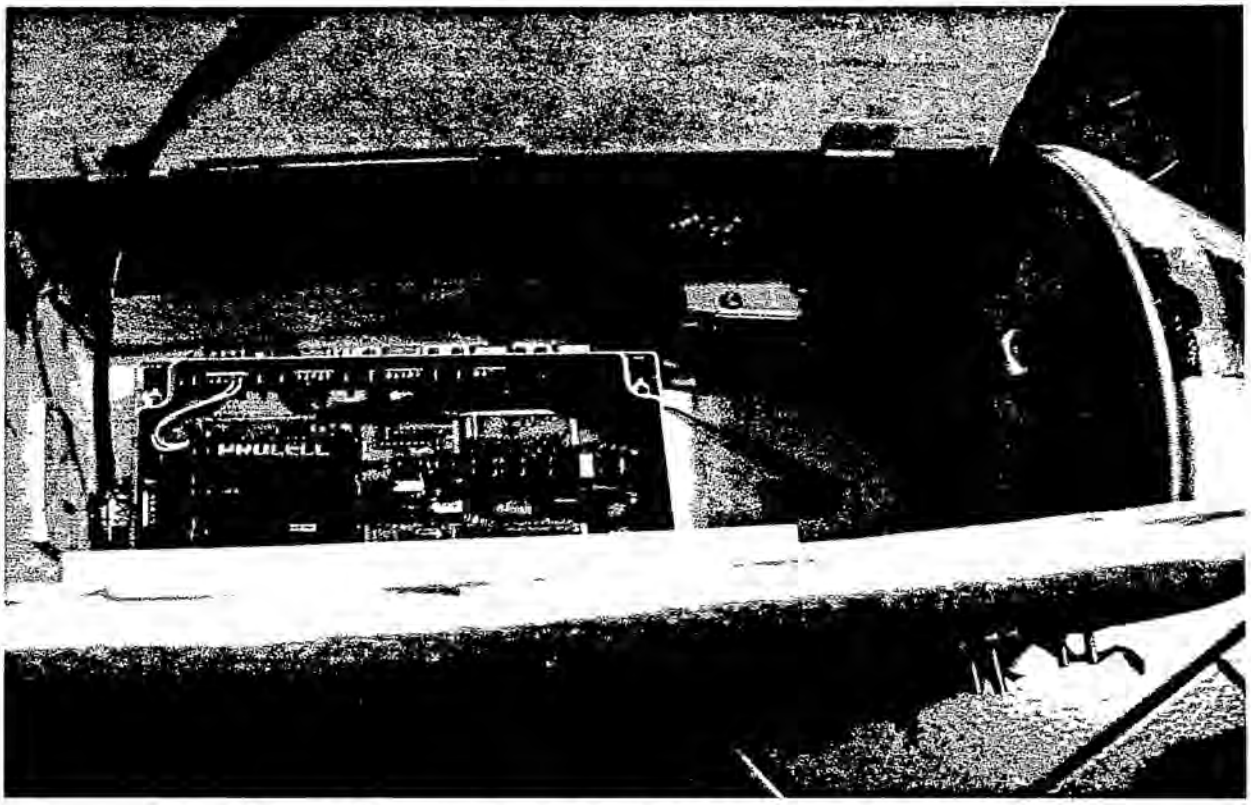

Figure 7.4: measure system inside the fuselage of the prototype